LEVEL STRUCTURE OF SOME A=87 AND A=88 NUCLEI

LEVEL STRUCTURE OF SOME A=87 AND A=88 NUCLEI

by

HEINZ LYCKLAMA a' NYEHOLT, B.Engin.

A Thesis

Submitted to the Faculty of Graduate Studies

in Partial Fulfilment of the Requirements

for the Degree

Doctor of Philosophy

McMaster University

July, 1969

DOCTOR OF PHILOSOPHY (1969)
(Physics)

McMASTER UNIVERSITY
Hamilton, Ontario.

TITLE: Level Structure of Some A=87 and A=88 Nuclei

AUTHOR: Heinz Lycklama a'Nyeholt, B. Engin. (McMaster University)

SUPERVISOR: Dr. T. J. Kennett

NUMBER OF PAGES: x , 256, A9

SCOPE AND CONTENTS:

The level structures of some single closed shell nuclei ($^{87}_{37}Rb_{50}$ and $^{88}_{38}Sr_{50}$) and nearly closed shell nuclei ($^{87}_{38}Sr_{49}$ and $^{88}_{37}Rb_{51}$) have been determined by means of the beta decay processes of ^{87}Kr, ^{88}Kr and ^{88}Rb to final states in ^{87}Rb, ^{88}Rb and ^{88}Sr respectively, and by means of the thermal neutron capture reaction on strontium ($^{86}Sr(n,\gamma)^{87}Sr$ and $^{87}Sr(n,\gamma)^{88}Sr$). The gamma radiation was studied using a Ge(Li) spectrometer and a Ge(Li)-NaI(Tl) coincidence spectrometer. Beta groups were identified using a plastic scintillator and a plastic-NaI(Tl) coincidence spectrometer. Spins and parities were determined for some of the levels from the deduced decay schemes.

ACKNOWLEDGEMENTS

I wish to thank the members of my supervisory committee, Dr. T. J. Kennett, Dr. G. L. Keech and Dr. D. G . Burke for their advice and constructive criticism throughout the course of this work. I am greatly indebted to my Research Director, Dr. T.J. Kennett who demonstrated to me the challenges and rewards of research and offered guidance and suggestions helpful in carrying out the work for this thesis.

This work would not have been possible without the assistance of many of my research associates. I would like to thank L. Nichol for the fabrication of the good resolution Ge(Li) detectors used to collect the data. A. H. Colenbrander simplified many of my tasks by providing some computer programs to handle the vast quantity of data collected. My special gratitude is due to Dr. N. P. Archer for his help in producing the rare gas samples required and for his aid in providing and running the beta analysis programs.

I am very grateful to Mrs. Helen Kennelly whose speed and accuracy in the typing of this manuscript have been of great value in the completion of this work.

Finally I wish to thank my wife and family for their understanding and patience during the entire length of time taken to complete this thesis.

This work has been supported financially by the National Research Council of Canada and by the Ontario Provincial Government.

TABLE OF CONTENTS

LIST OF TABLES

LIST OF ILLUSTRATIONS

CHAPTER I

INTRODUCTION

Four fundamental forces are known to exist in nature, namely the gravitational, weak, electromagnetic and the strong interaction forces, in order of increasing strength. Of these the last three are amenable to study in detail in the field of experimental nuclear physics. Theories for the weak and electromagnetic interactions are well advanced and in general agree with experimental details. However the strong interaction has proven to be most difficult to comprehend on any theoretical basis and has thus led to a concentrated effort in the pursuit of more knowledge, both in the low and high energy branches of nuclear physics. Knowledge of the weak and electromagnetic interactions provides one of the necessary tools in learning the nature of the strong interaction. The other major tool in studying the strong interaction is provided by nuclear particle reactions in which a nuclear projectile probes the sub-atomic nuclear region of the target nucleus.

1-1 Beta Decay

Beta-decay is the experimentally observable process resulting from the weak interaction in low energy nuclear physics. The process of beta-decay consists of a parent nucleus ${}_{Z}A_{N}$

emitting an electron having a continuous energy distribution from zero to some maximum energy and an anti-neutrino[1] with the remainder of the available energy,

$$ {}_{Z}{}^{A}{}_{N} \rightarrow {}_{Z+1}{}^{A}{}_{N-1} + e^{-} + \bar{\nu}. $$

The anti-neutrino serves the purpose of conserving spin, lepton number and the total energy of the process. The ejection of the electron-neutrino lepton pair results in a rearrangement of the nuclear charge and internal structure of the nucleus.

Fermi[2] provided the first adequate mathematical description of the beta-decay process. Letting ψ_i and ψ_f represent the initial and final nuclear wave functions and ϕ_i and ϕ_f the initial and final lepton states, the probability of the beta decay process is given by,

$$ |\langle \psi_f \phi_f | H_w | \phi_i \psi_i \rangle|^2 \rho_f(E) $$

where H_w is the weak interaction Hamiltonian and $\rho_f(E)$ is the density of final states. The transformation of the expression into an energy distribution N(E) with a probability per unit time of emission of a particle into energy interval dE is given by[3],

$$ N(E) = \frac{1}{2\pi^3} pE(W_o - E)^2 F(Z,E) S_n(W_o,E) \ . $$

Here, p - the beta-particle momentum

W_o - the maximum beta energy available

F(Z,E) - the electron screening function (Fermi

function) allowing for the effect of the Coulomb field of the nucleus on the emerging electron

and $S_n(W_o,E)$ - the shape factor which depends on the order of forbiddenness, n, of the transition.

The beta-decay process must be treated relativistically involving four component spinors. As the Hamiltonian must be a scalar, the spinors can be combined in various ways to form a final scalar. Experimentally[4], the vector (singlet) and axial vector (triplet) combinations have been found to occur in nature. The total lepton spin change ΔJ and parity change for transitions between the initial state with spin and parity (J_i,π_i) to the final state (J_f,π_f) follow the selection rules given by

$$|J_i - J_f| \leq \Delta J \leq J_i + J_f$$

$$\Delta\pi = \pi_i\pi_f.$$

The beta-decay transition type is defined by the values of ΔJ and $\Delta\pi$ measured experimentally. Table 1-1 lists the selection rules obeyed by most beta-decay transitions.

Table 1-1

Selection Rules for Beta Decay[5]

Interaction	Allowed		First Forbidden		Second Forbidden	
	$\pi_i\pi_f$	ΔJ	$\pi_i\pi_f$	ΔJ	$\pi_i\pi_f$	ΔJ
Vector	+	0	-	1	+	2
Axial Vector	+	1	-	0,1,2*	+	2,3*

The entries marked with an asterisk have a spin change of one more than the degree of forbiddenness of the transition and are referred to as "unique" transitions. For allowed transitions the shape factor $S_o=1$ and is independent of the beta-particle energy. For first forbidden transitions the shape factor $S_1 \doteq 1$, having a very small energy dependence. But for first forbidden unique transitions the shape factor is proportional to the energy dependent term (q^2+p^2) where q is the neutrino momentum.

A useful experimental quantity which can be calculated is the beta-decay rate given by,

$$\lambda = \int_o^{W_o} N(E)dE$$

$$= \frac{\overline{S_n}}{2\pi^3} f(Z,W_o)$$

where

$$f(Z,W_o) = \int_o^{W_o} F(Z,E)\ pE(W_o-E)^2 dE$$

and $\bar{S}_n$ is the average value of $S_n(W_o,E)$.

The comparative half-life for the transition is given by the quantity,

$$ft_{1/2} = \ell n 2\ (\frac{f(Z,W_o)}{\lambda})$$

and produces an indication of the type of transition involved.

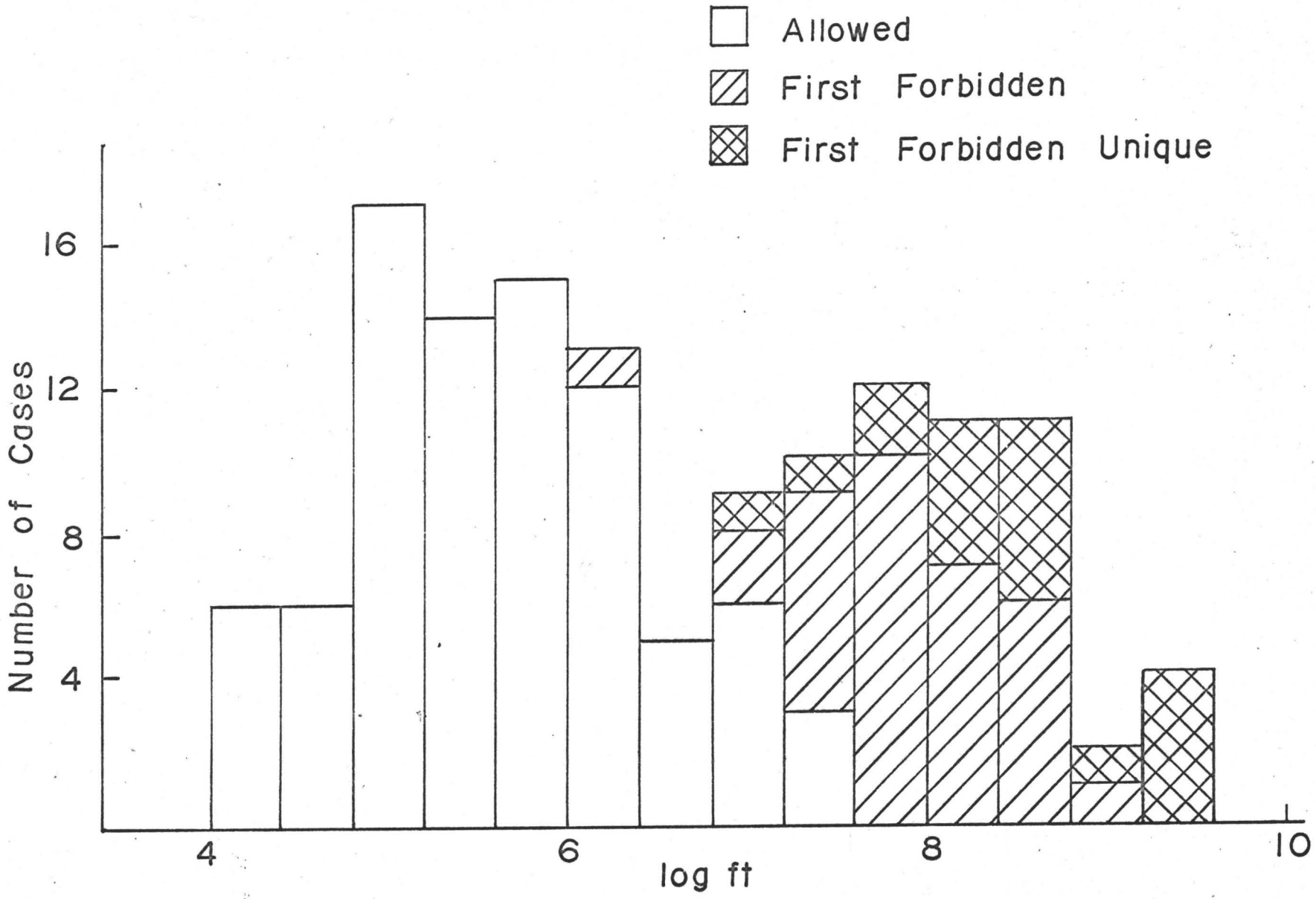

Distribution of log ft values for Mass Region $76 \leq A \leq 100$

FIGURE 1-1

As the value of $ft_{1/2}$ varies by many orders of magnitude it is usual to calculate the log ft value for the beta-transition. Feenberg[6] has tabulated the log ft values for beta decays in which the type of transition is known. Allowed transitions have a log ft value distributed about a mean of ~ 5 whereas the mean value of log ft for first forbidden transitions is about 7. First forbidden unique transitions are inhibited by two more orders of magnitude, having a mean log ft value of about 9.

As this thesis involves beta decay in the mass region A = 87,88 it is appropriate to tabulate the distribution of log ft values for the mass region $76 \leqslant A \leqslant 100$. These distributions are depicted in Figure 1-1. In this mass region the average value of log ft for allowed transitions is about 5.6 while the average value for first forbidden transitions is 7.9. The average log ft value for first forbidden unique transitions is only slightly higher, being 8.5. Thus it is almost impossible to distinguish between the first forbidden and first forbidden unique on the basis of log ft values. Fortunately the shape factors provide a better distinction between these two transition types.

1-2 Gamma Decay - The Electromagnetic Interaction

The spins, parities, energies and matrix elements for the states of a nucleus can be obtained from gamma-ray transi-

tion rates and energies. Theoretically the probability of photon emission from a nucleus is of the order $e^2/\hbar c = 1/137$ (the fine structure constant) times smaller than that for heavy particle emission. However de-excitation by an electromagnetic process does occur in nature if the excited nucleus is stable against nucleon emission because of a quantum mechanical barrier such as Coulomb or centrifugal or if particle emission is inhibited by some selection rule.

First order time-dependent perturbation theory can be used to show that the transition probability between an initial nuclear state ϕ_i and a final state ϕ_f is given by,

$$T_i^f = 2\pi |\langle \phi_i | O | \phi_f \rangle|^2 \rho_f(E)$$

where $\rho_f(E)$ is the density of final states, and O is the electromagnetic interaction operator. A simplified picture can be drawn of the interaction by realizing that the wavelength of photons is usually much larger than the dimensions of the nucleus. For instance for A=88, the nuclear radius, $R=5.5\times10^{-13}$ cm., while the wavelength of a photon, given by

$$\lambda = hc/E_\gamma$$

is 4×10^{-11} for E_γ = 511 keV and 2.5×10^{-12} cm. for E_γ = 8 MeV. Electric radiation is due to the coupling between the charges of the particles in the nucleus and the electromagnetic field. Therefore one can ignore the variation of the electric field of the radiation across the nucleus. Then to a first approxi-

mation one can write the interaction energy as εeZ. The associated matrix element which is proportional to

$$\int_z \phi_i \, Z \, \phi_f \, dZ$$

is non-zero only if there is an angular momentum change, L=1, between the initial and final states as well as a change in parity. In order to conserve angular momentum and parity, the following selection rules must be obeyed,

$$|J_i - J_f| < L < J_i + J_f$$

$$\Delta\pi = \pi_i \pi_f = -1.$$

As the electric field is actually not a constant over the nucleus, correction terms of the form $(Z/\lambda)^L$ must be considered in the integrand of the matrix element for higher order multipole radiation when the lower order multipole radiation is prohibited by selection rules. The contribution from each successive term varies as $(R/\lambda)^{2L} << 1$ since the transition probability varies as the square of the matrix elements. The parity change for each transition is given by,

$$\pi_i \pi_f = (-1)^L .$$

These transitions are then referred to as electric or EL radiation emitted by a vibrating electric 2^L-pole where L indicates the multipolarity.

The other kind or radiation possible between states

in a nucleus is the magnetic radiation emitted by a vibrating magnetic 2^L-pole. This radiation is due to the coupling between the electromagnetic field and the distribution of magnetization in the nucleus arising from the circulation of charges and the intrinsic magnetic moments. Magnetic radiation splits into multipoles and has the same spin selection rules as electric radiation but the associated parity change is $(-1)^{L+1}$. In general magnetic radiation is weaker than electric radiation of the same multipolarity by $(V/C)^2 \doteq 0.05$ since the current density is smaller than the charge density by the factor (V/C) where V is the speed of the charges.

As the photon has one unit of angular momentum associated with it, no transition of multipole order zero can occur, i.e.,

$$J_i \neq J_f \quad \text{where} \quad J_f = J_i = 0.$$

In this case if the energy difference between the two states is greater than $2mc^2$, pair emission is possible (i.e. creation of a negative and positive electron pair). However for lower energy transitions the only possibility is internal conversion in which an orbital electron emerges and carries away the energy of de-excitation. Internal conversion also competes with photon emission for lower energy transitions not involving a 0→0 transition. The internal conversion coefficient for an orbit is defined as the ratio of the probability of emission of an electron to the emission of a photon, i.e. for the L electron shell,

$$\alpha_L = N_{e_L}/N_\gamma \ .$$

Knowing the electronic wave functions involved, the conversion coefficient can be calculated very accurately on a theoretical basis. The coefficient depends only on the energy, multipolarity and parity change of the transition and on the value of Z for the nucleus and not on the nuclear wave functions. Therefore the values of the coefficients are independent of any nuclear model invoked. Theoretical values of internal conversion coefficients have been calculated and tabulated by Sliv and Band[7] as a function of Z, E and L.

Gamma ray transition probabilities depend on the multipolarity, the energy E_γ of the transition and the wave functions of the nuclear states involved in the transition. These probabilities are usually expressed in terms of their mean lifetime τ or the radiative width of the level emitting the radiation, Γ_γ. These two quantities are related through the uncertainty principle, $\Gamma_\gamma \tau_\gamma \simeq \hbar$. Assuming an extreme one-particle nuclear model, Weisskopf[8] has calculated values of $\tau_\gamma^{-1}(EL)$ and $\tau_\gamma^{-1}(ML)$ given by,

$$T_i^f(EL) = \frac{4.4(L+1)}{L[(2L+1)!!]^2} \left(\frac{3}{L+3}\right)^2 \left(\frac{E_\gamma}{197}\right)^{2L+1} R^{2L} \times 10^{21} \ \text{sec}^{-1}$$

and

$$T_i^f(ML) = \frac{1.9(L+1)}{L[(2L+1)!!]^2} \left(\frac{3}{L+3}\right)^2 \left(\frac{E_\gamma}{197}\right)^{2L+1} R^{2L-2} \times 10^{21} \ \text{sec}^{-1}$$

where R is the nuclear radius in fermis (10^{-13} cm.) and E_γ is the energy of the transition in MeV. Here the factor $10(\frac{\hbar}{McR})^2$ is used to relate the magnetic transition probability to the electric transition probability. This factor is obtained by using the uncertainty principle to estimate

$$\frac{V}{C} = \frac{\hbar}{McR}$$

and by taking into consideration the fact that the intrinsic magnetic moment of a nucleon is about 2 Bohr magnetons. Assuming that $R = r_o A^{1/3}$ where $r_o = 1.3$ fm, the Weisskopf estimates for the lowest order transition probabilities are,

$$T_{\gamma W}(E1) = 2.0 \times 10^{-1} A^{2/3} E_\gamma^3$$

$$T_{\gamma W}(M1) = 6.3 \times 10^{-2} E_\gamma^3$$

$$T_{\gamma W}(E2) = 2.7 \times 10^{-7} A^{4/3} E_\gamma^5$$

$$T_{\gamma W}(M2) = 7.5 \times 10^{-8} A^{2/3} E_\gamma^5 \quad .$$

Moszkowski[9] has calculated better estimates for the magnetic transition probabilities by taking into account the orbital magnetic moment of the radiating particle. He simply replaced the factor 10 which is used in coupling the magnetic to the electric transition probability by the factor,

$$[\frac{L+3}{L+2} (\mu_p L - \frac{L}{L+1})]^2$$

where $\mu_p = 2.79$ is the proton's intrinsic magnetic moment. This increases the magnetic transition probability as L^2. Another factor which has been ignored in the Weisskopf estimates of both electric and magnetic transitions is the statistical coupling factor $S(J_i,L,J_f)$ which takes into consideration the spins of the initial and final nuclear states. However for simplicity, transition strengths are usually stated in terms of Weisskopf units. The measured transition probability, T_γ, is said to have strength $|M|^2 = T_\gamma/T_{\gamma W}$ Weisskopf units where $|M|^2$ is a measure of the transition relative to that of the extreme single particle transition. This in turn gives one information about the nuclear wave functions which represent the initial and final states since the transition probabilities are strongly dependent on the nuclear wave function.

The transition probabilities can also be expressed as,

$$T(\sigma,L) = \frac{8\pi(L+1)}{L[(2L+1)!!]^2} \frac{1}{\hbar} \left(\frac{W}{c}\right)^{2L+1} B(\sigma,L)$$

where σ represents either the electric (E) or magnetic (M) transitions. $B(\sigma,L)$ is called the reduced matrix element of the transition and involves the electromagnetic operator and a knowledge of the initial and final nuclear wave functions. Theoretical values of this matrix element can be calculated using nuclear wave functions obtained from a particular nuclear model.

Wilkinson[10] has summarized some of the empirical data available on the strengths of the electric and magnetic transitions observed in nature. In general it is found that the distributions of $|M|^2$ for E1 and M1 transitions are centered at a few orders of magnitude less than for the single particle estimates. Thus the E1 and M1 transitions are strongly hindered. The M2 transitions are not hindered by such a large factor and the E2 transitions are usually in fact strongly enhanced.

1-3 Nuclear Forces - The Strong Interaction

The strong interaction force acts between the nucleons in a nucleus. It is best studied by means of the simple two nucleon scattering experiment as the experiment can be understood in terms of the two-body problem. A nucleus containing more than two nucleons becomes very complex as one is now dealing with a many-body problem which is one for which physicists have not yet provided an adequate solution. However Brueckner[11] has proposed the application of potentials suggested by scattering-experiment results to the many-body problem and has had some success in the problem of nuclear matter. The many body problem has also been approached by various other techniques which were developed in other fields of physics, e.g. the Hartree Fock theory as used in atomic structure and the pairing force theory as developed to explain the state of superconductivity.

Nuclear systems are described mathematically by means of a solution to the Schrodinger equation,

$$H\psi_n = E_n\psi_n.$$

Here ψ_n represents a set of eigenstates for the system and E_n is the corresponding set of energy eigenvalues for the system. The set of energies E_n gives the energies of the excited states of the system while E_o gives the ground state energy of the system. The Hamiltonian operator characteristic of the system, H, containing both kinetic and potential energy operators, determines the nature of the wavefunction, ψ_n. Mathematically the complete description of the nuclear structure of the system is contained in the correct total wave functions of the nuclear excited and ground states. In order to obtain a realistic set of wave functions, one must choose a "model" to determine the nature of the potential well to be used in the Hamiltonian. Certain facts about the forms of the potential are known from experimental data. The high degree of polarization evident in scattering experiments requires the presence of a force component of the form $V_{LS}(r)\bar{L}\cdot\bar{S}$. The fact that the binding energy of a nucleus is not proportional to the number of nucleons in the nucleus, requires that nuclear forces saturate. The nature of the wavefunctions of the states in a nucleus can often be obtained from the weak interaction and electromagnetic interactions making it easier to predict the

nature of the nuclear model to be used to explain the experimental facts.

No one nuclear model can predict all the properties of a single nuclide although progress has been made in describing a "unified" model[12] to account for most properties of all nuclides. An attempt will be made here to describe the salient features of the nuclear models currently in use which will help to unravel the nuclear structure inherent in the mass region under study in this thesis.

1-4 Shell Model

The single particle model proposed by Mayer[13] in 1949 considers the individual nucleons in stationary orbits paired off so that the nuclear parameters are determined by the single unpaired nucleon. The basic assumptions of the model are that the Pauli exclusion principle holds for both protons and neutrons independently and that there are no correlated or collective motions of several particles. The form of the potential energy operator for the shell model was taken to be,

$$U(r) = V(r) + f(r)\ \bar{L}\cdot\bar{S}$$

where

$$V(r) = -\frac{V_o}{1 + e^{(r-R)/a}}$$

and

$$f(r) \propto \frac{1}{r}\frac{dV(r)}{dr} .$$

Here $f(r)\bar{L}\cdot\bar{S}$ is the spin-orbit coupling term and the central potential V(r) corresponds to a form intermediate between a square well and a harmonic oscillator. The spin-orbit force has the effect of removing the degeneracies inherent in the orbital angular momentum, ℓ, of a state and causing a splitting between levels with the same ℓ value into two levels with $j=\ell-s$ and $j=\ell+s$ with the latter being lower in energy. The energy gaps in the level order of single particle states occur at the "magic" numbers as revealed in experimental data. The order of energy levels of the first 126 neutrons in the simple shell model is given by Preston[14]. The shell model has been successful in predicting many experimental facts, e.g. the ground state spins and parities of odd-A nuclei, the spins and parities of the first few excited states and the occurrence of magic numbers.

1-5 Coupling Model-Extension of Single Particle Model

The shell model assumes that an even number of particles in the same shell always couple their angular momenta to zero even in excited states. This assumption however is only true if a shell is almost completely filled or filled with one pair outside the major shell. In regions where there are more than just one or two pairs of nucleons beyond a filled shell one must consider the formation of excited states by re-coupling the angular momenta of the nucleons beyond the closed shell to obtain resultants other than those given by the

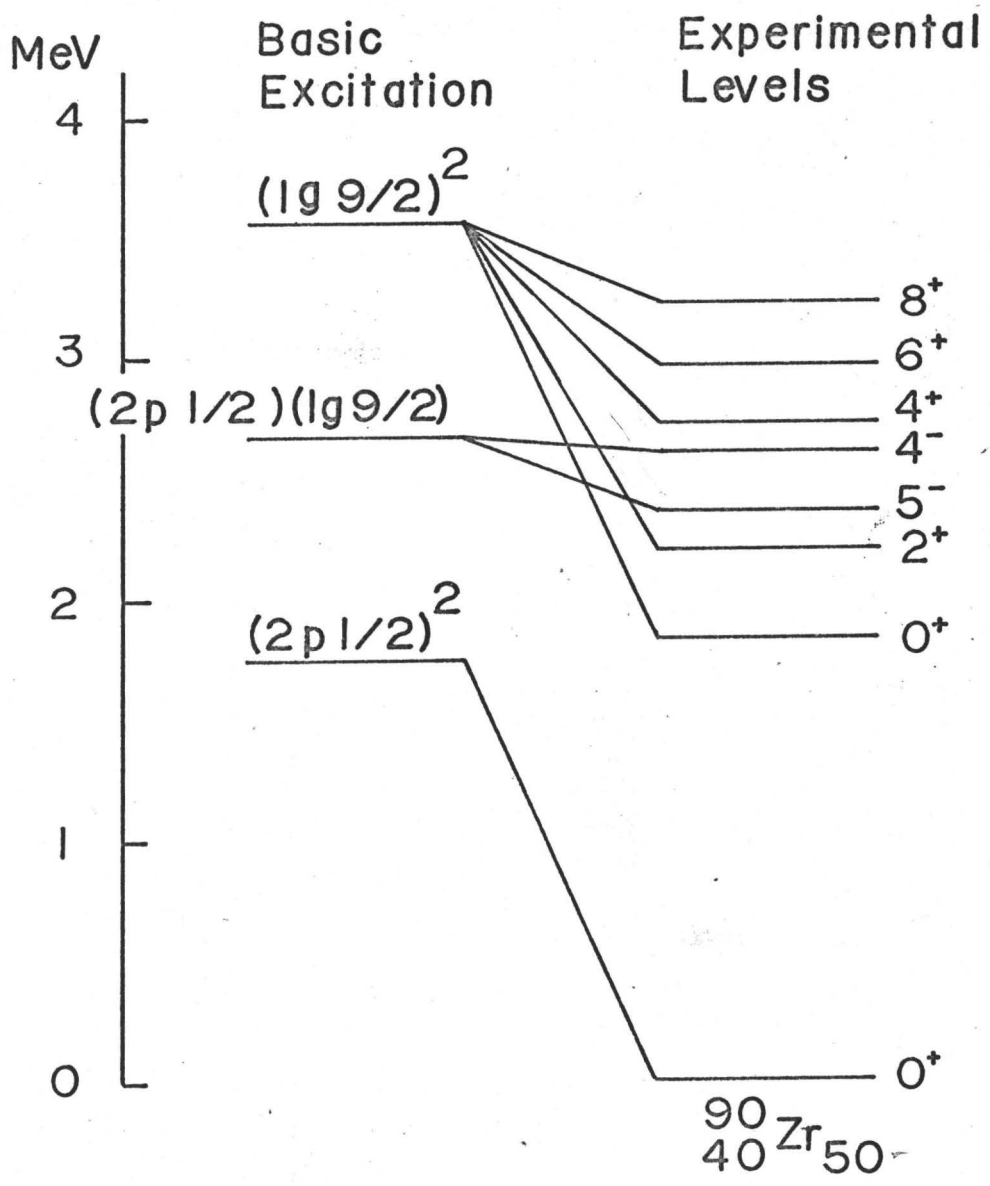
MeV
Basic Excitation
Experimental Levels
4
3
2
1
0
$(1g\ 9/2)^2$
$(2p\ 1/2)(1g\ 9/2)$
$(2p\ 1/2)^2$
8^+
6^+
4^+
4^-
5^-
2^+
0^+
0^+
$^{90}_{40}Zr_{50}$

FIGURE 1-2

assumption of a single-particle model. The simplest case to consider is the coupling of two angular momenta j_1 and j_2 to form a resultant,

$$J = j_1+j_2,\ j_1+j_2-1,\ \ldots\ ,\ |j_1-j_2|.$$

For nucleons in the same shell model orbit, the possible states are given by J=0, 2, 4, ... (2j-1). The parity of the states is always given by $(\ell_1+\ell_2)$. An example of such coupling in the mass region of interest is given by the first few levels of $^{90}_{40}Zr_{50}$ which is a single closed shell nucleus with N=50. Thus the states should be the result of the coupling of two protons. The single-particle energy separation between the $2p_{1/2}$ level and the $1g_{9/2}$ level is about 0.9 MeV in this mass region. The ground state configuration is $(2p_{1/2})^2$ with the excited states arising from the coupled configurations $(2p_{1/2})(1g_{9/2})$ with basic excitation energy of 0.9 MeV and $(1g_{9/2})^2$ with basic excitation of 1.8 MeV. Figure 1-2 shows the experimental states observed in ^{90}Zr [15] and their explanation due to the coupling of two protons is clear.

1-6 Collective Model

The collective properties of a nucleus are clearly demonstrated by the occurrence of 2^+ states in even-even nuclei with large B(E2) values of the ground state transitions. These properties can only be explained by the cooperative effects of many particles. The analysis of the moments of

inertia led to the recognition of two distinct types of correlation in the nucleonic motion. Particles tend to orient their orbits with respect to the axis of the deformed field and the residual forces tend to correlate the particles in a state with a spherical density distribution. This provides competition giving rise to two types of nuclear collective spectra. In spherical nuclei closest to the closed shells the residual forces dominate creating vibrational spectra. Further from closed shells the tendency towards deformation becomes dominant (e.g. rare earth region) giving rise to rotational spectra. This competition between nuclear forces is also evident in particle coupling. The field producing forces cause the core particles to attempt to align their orbits with the deformed field of the odd particle which in turn polarizes the core causing a non-equilibrium shape. The short range pair coupling forces on the other hand tend to scatter the particles isotropically and hence stabilize the spherical shape. In even-even nuclei the energy gap corresponds to the energy required to break a J=0 pair below which only collective states appear. The strength of the pairing force, $G \doteq 22/A$ MeV is such that it overlaps different j-subshells but does not overlap any major shells which are separated by about 10 MeV. Near the middle of a major shell there is a sudden flip from prolate to oblate shape, i.e. holes now align their

orbits along the polar axis. Near the end of the shell, pairing of holes restores the spherical shape. The pairing force is thus essential in determining the equilibrium shape but it destroys the independent particle structure which is a feature of field forces and causes a diffuseness of the Fermi surface. This difficulty is overcome by introducing the concept of "independent quasi-particles" which are partly particles (with probability amplitude V_ν) and partly holes (with probability amplitude U_ν) as depicted in figure 1-3a. The quasiparticle can actually be considered as a conjugate pair (j,m) and (j,-m), i.e. a mixture of a nucleon in state (j,m) and a hole in state (j,-m).

1-7 Pairing Model

The discussion of quasi-particles leads directly to the pairing model. In analogy with the superconductivity problem solved by Bardeen *et al*[16] for metallic conductivity at low temperatures, Bohr, Mottelson and Pines[17] introduced their idea of an energy gap into nuclear physics. The BCS wave function for the ground state of an even-even nucleus can be written as,

$$\phi_o^{BCS} = \prod_\nu (U_\nu + V_\nu \, a_\nu^+ \, a_{\bar{\nu}}^+) \, |0\rangle$$

where $|0\rangle$ is the vacuum state

ν represents a (j,m) particle

$\bar{\nu}$ represents a (j,-m) hole

and a_ν^+ is a particle creation operator.

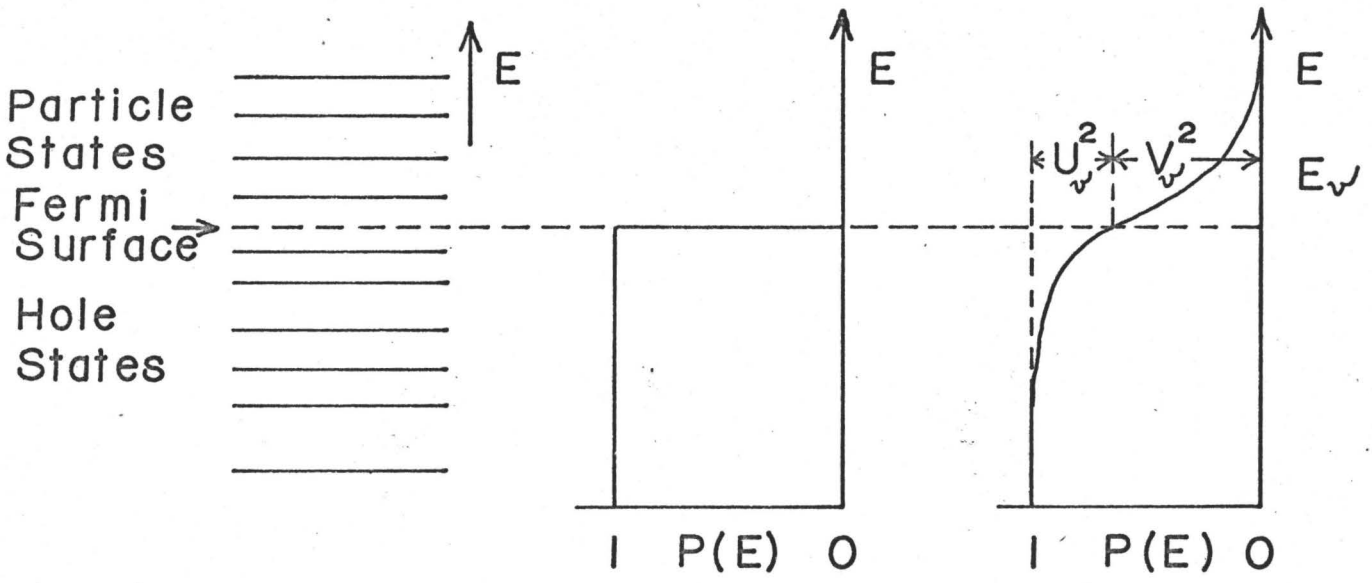

Shell Model Single Particle Energy Levels

Unperturbed Shell Model

Shell Model with Short Range Residual Interactions

FIGURE I-3a

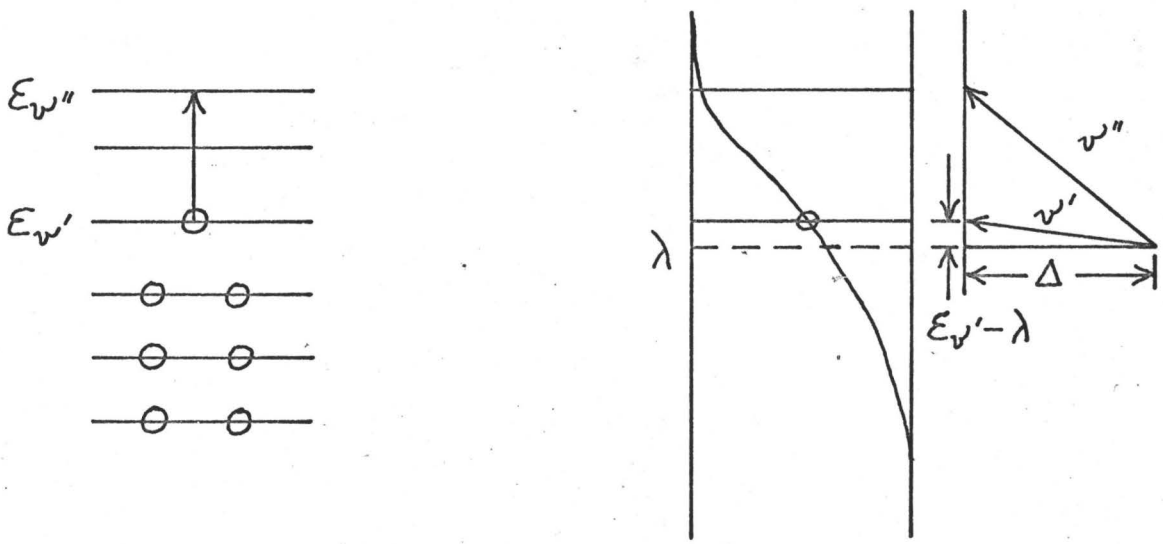

Single-particle Excitation

One quasi-particle Excitation

FIGURE I-3b

The coefficients U_ν and V_ν are subject to the constraints,

$$U_\nu^2 + V_\nu^2 = 1$$

and

$$\sum_\nu 2\Omega_\nu V_\nu^2 = N$$

where N is the total number of nucleons in the state and $\Omega_\nu = j + \frac{1}{2}$ is the number of degenerate pairs of type j. The strength of the pairing interaction is given by G = 22/A MeV and the energy gap Δ is then defined by,

$$\Delta = G \sum_\nu \Omega_\nu U_\nu V_\nu .$$

Defining λ as the average Fermi energy and ε_ν as the single particle energies, the solution for U_ν^2 and V_ν^2 are obtained as,

$$U_\nu^2 = \frac{1}{2}\left[1 + \frac{\varepsilon_\nu - \lambda}{\sqrt{(\varepsilon_\nu - \lambda)^2 + \Delta^2}}\right]$$

$$V_\nu^2 = \frac{1}{2}\left[1 - \frac{\varepsilon_\nu - \lambda}{\sqrt{(\varepsilon_\nu - \lambda)^2 + \Delta^2}}\right] .$$

One can now introduce quasi-particle creation operators in terms of the particle creation operators as[18],

$$\alpha_\nu^+ = U_\nu a_\nu^+ - V_\nu a_{\bar{\nu}}^+$$

$$\alpha_{\bar{\nu}}^+ = U_\nu a_{\bar{\nu}}^+ + V_\nu a_\nu^+ .$$

Then the excited states in BCS formalism are the quasi-particle excitations, $|>, \alpha^+\alpha^+|>$, etc. for an admixture of an even number of real particles and $\alpha^+|>, \alpha^+\alpha^+\alpha^+|>$, etc. for an admixture con-

taining an odd number of real particles. The energy of a ν quasi-particle state is then obtained from the matrix element,

$$H_{11} = \sum_{\nu} E_{\nu}(\alpha_{\nu}^{+} \alpha_{\nu} + \alpha_{\bar{\nu}}^{+} \alpha_{\bar{\nu}})$$

where $E_{\nu} = \sqrt{\Delta^2 + (\varepsilon_{\nu}-\lambda)^2}$ is the quasi-particle energy. Thus the minimum excitation energy of an unperturbed two quasi-particle state is 2Δ which is called the energy gap. A comparison of the resulting level densities in the independent-particle case and the one quasi-particle case is shown in Figure 1-3b. The energy difference between the states with odd particles in the ν" and ν' orbitals is $(\varepsilon_{\nu}'' - \varepsilon_{\nu}')$ for the single particle excitation but $(E_{\nu}'' - E_{\nu}')$ for the quasi-particle excitation.

The pairing model has been very successful in explaining the properties of nuclear structure. Basically it explains why even-even nuclei have spin zero ground states and very few low-lying states, why odd nuclei for which low-lying states are one quasi-particle states have a more complex structure and why odd-odd nuclei for which low-lying states are a proton quasi-particle coupled to a neutron quasi-particle have very complex structures. The pairing model also explains the odd-even mass difference which corresponds to a single quasi-particle state with a minimum energy of Δ. Apart from a few collective states, whose energies are depressed by the residual field interactions no excited states are expected or seen for spherical even-even nuclei below the minimum two quasi-

particle energy 2Δ. Electric matrix elements are expected to be reduced substantially in odd nuclei between one quasi-particle states. The hindrance factor is of the order,

$$F_1 = (U_\nu U_{\nu'} - \tau V_\nu V_{\nu'})^2$$

where $\tau = +1$ for electric transitions. As $\tau = -1$ for magnetic transitions, the rates for these transitions will not be affected much. However for two quasi-particle transitions the hindrance factor given by,

$$F_2 = (U_\nu U_{\nu'} + \tau V_\nu V_{\nu'})^2$$

indicates a large hindrance factor for magnetic transitions and not much change for electric transitions. Beta decay rates are also influenced by pairing. For instance in a beta decay which leaves the number of proton and neutron pairs unchanged, the rate should be the single particle rate times the probability U_ν^2 for finding the state ν not occupied by a pair. Information on the pairing interaction can also be obtained from measurements of the cross-section for stripping and pick-up reactions. The spectroscopic factors in the stripping and pick-up reactions are directly proportional to U_ν^2 and V_ν^2 respectively[19].

1-8 Vibrational Model

Vibrational spectra originate in spherical nuclei due to their shape oscillations. The nucleus can support shape oscillations analogous to those of a liquid drop. The shape of

a nucleus at some time, t, can be described mathematically by the radius at any angle θ,

$$R(\theta) = R_o[1 + \sum_{\lambda\mu} \alpha_{\lambda\mu} Y_{\lambda\mu}(\theta)] + O(\alpha^2).$$

Here $\alpha_{\lambda\mu}$ is the shape parameter for the angular momentum value λ and projection μ. $Y_{\lambda\mu}(\theta)$ is the usual spherical harmonic function. For small amplitude oscillations, one can postulate a surface Hamiltonian,

$$H_s = \frac{1}{2} \sum_{\lambda\mu} B_\lambda |\dot{\alpha}_{\lambda\mu}|^2 + \frac{1}{2} \sum_{\lambda\mu} C_\lambda |\alpha_{\lambda\mu}|^2$$

which has the classical solution,

$$\alpha_{\lambda\mu} = \varepsilon_{\lambda\mu} \cos \omega_\lambda t$$

$$\omega_\lambda = \sqrt{C_\lambda / B_\lambda}$$

$$E = \sum_{\lambda\mu} \frac{1}{2} \varepsilon_{\lambda\mu} \omega_\lambda^2 B_\lambda.$$

The different angular momentum components can be described physically as follows:

λ=0 contributes to the spherical field

λ=1 corresponds to a centre of mass displacement such as the dipole displacement of protons against neutrons in the giant dipole resonance

λ=2 corresponds to a quadrupole deformation

and λ=3 corresponds to an octupole deformation.

The energy levels expected from a degenerate harmonic oscillator are shown in Figure 1-4a. The degenerate levels are

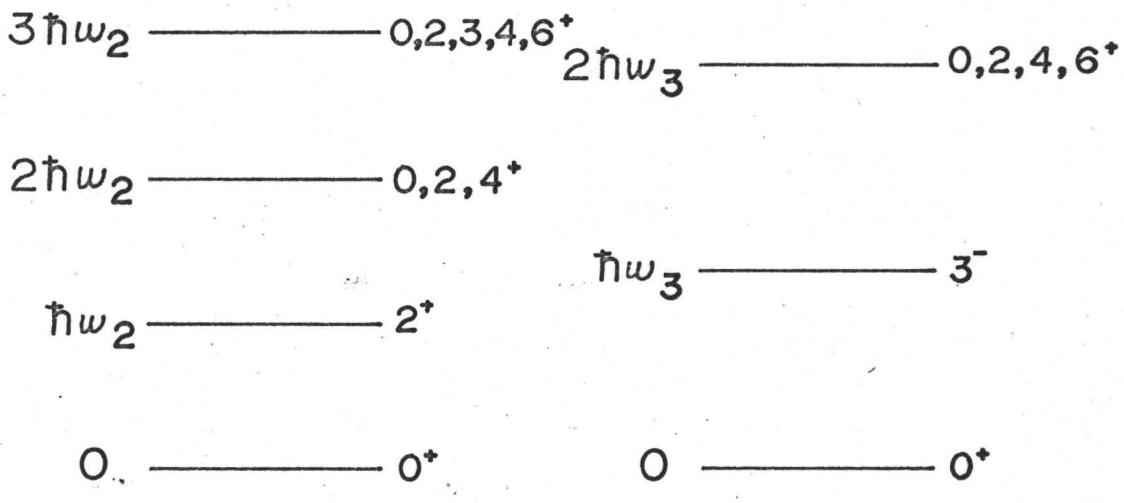

Degenerate Harmonic Oscillator

FIGURE 1-4a

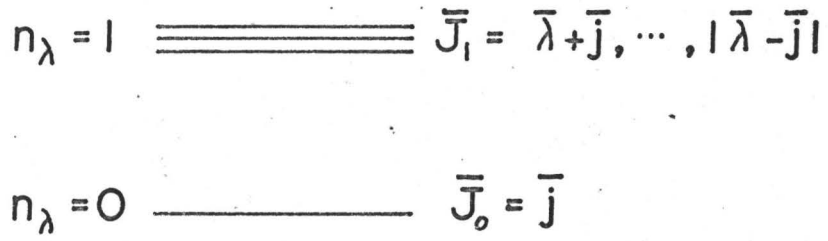

Vibrational States built on a Particle State

FIGURE 1-4b

actually split in realistic nuclei due to the anharmonic nature of the collective Hamiltonian. The magnitude of the vibrational parameters B_λ and C_λ are expected to fluctuate rapidly in certain mass regions because of shell effects.

The vibrational model leads to some very stringent selection rules. The electromagnetic transitions to first order in α obey the selection rules $\Delta n_\lambda = \pm 1$, i.e. the cross-over two phonon transitions are forbidden. Thus one expects the cross-over transitions from the second 2^+ state to the ground state to be strongly inhibited. The M1 component of the $2_2^+ \rightarrow 2_1^+$ gamma-ray transition should be very weak and in most cases is inhibited by factors of the order of 100. This inhibition factor can be explained directly by the fact that the deformation of a uniformly charged fluid induces no magnetic moment and so the model predicts zero magnetic transition. Another important selection or intensity rule for transitions in vibrational nuclei is given by the relation between the reduced transition rates between the second set of vibrational states and the first 2^+ state and between the first 2^+ state and the ground state,

$$B(E2, 0_2^+, 2_2^+, 4_1^+ \rightarrow 2_1^+) = 2\, B(E2, 2_1^+ \rightarrow 0_1^+).$$

This follows from the general intensity sum rule for vibrational transitions,

$$\sum_f B(E\lambda, n_\lambda, I_i \rightarrow n_\lambda - 1, I_f) = n_\lambda B(E\lambda, n_\lambda = 1 \rightarrow n_\lambda = 0).$$

There are no interactions between the different vibrational quanta or between the quanta and quasi-particles in the harmonic approximation of the vibrational model. Thus particles in an odd mass nucleus should move unaffected by the oscillatory field set up by the vibrations and the resulting spectrum will consist of the intrinsic excitations of quasi-particle states and a series of vibrational spectra associated with the intrinsic states. The combination of a particle state with angular momentum $\bar{j}$ with a vibrational state of angular momentum $\bar{\lambda}$ will give rise to a multiplet of states of total angular momentum,

$$J = \lambda+j,\ \lambda+j-1,\ldots,|\lambda-j|$$

as shown in Figure 1-4b. The energy of the multiplet relative to the intrinsic state is approximately equal to the corresponding phonon energy in the neighbouring even-even nucleus. The reduced transition probability for the transitions to and from these vibrational states are related to those for even-even nuclei by a simple geometric factor,

$$B(E\lambda, J_1 \rightarrow J_o) = B(E\lambda, \lambda_1 \rightarrow \lambda_o)$$

$$B(E\lambda, J_o \rightarrow J_1) = \frac{(2J_1+1)}{(2J_o+1)(2\lambda_1+1)} B(E\lambda, \lambda_o \rightarrow \lambda_1).$$

These transitions obey the selection rule, $\Delta n_\lambda = \pm 1$ with no $\Delta n_\lambda = 1, j \rightarrow j'$ transitions allowed.

In general the low-lying states in odd-A nuclei are strongly mixed quasi-particle and vibrational excitations with each state containing more than one vibrational component. The particle-vibration coupling arising from the vibrational shape fluctuations of the potential well in which the odd particle is moving will split any degeneracies in the levels of the nucleus. If short range pairing forces are taken into account, the Fermi surface becomes smeared out and a given single particle state ν becomes occupied with probability amplitude V_ν. Then the energy separation of the first excited state for the shell model plus residual interactions becomes,

$$E_1 - E_o = E_\nu - E_{\nu'},$$

compared to the $\varepsilon_\nu - \varepsilon_{\nu'}$, without the interaction. This is exactly the same results as that derived from BCS theory when the states ν are described as quasi-particle states due to their dual role of being partly particle and partly hole states.

The low-lying states for odd mass nuclei may be associated with the motion of a single particle in the average field. As a result of pair coupling, the more complicated states (i.e. of seniority 3 or higher) are expected to occur at rather high excitation energies. Seniority is defined as the number of unpaired nucleons in an excited state of a nucleus. For spherical nuclei with both protons and neutrons outside of closed shells there is a strong coupling between the particle

motion and the low-lying vibrations resulting in a number of states of mixed particle-vibrational character.

In summary it can be said that the spectra of spherical nuclei[20,21] are due to three basic nucleonic motions: the motion associated with the quasi-particle degrees of freedom, the motion associated with the vibrational degrees of freedom and the motion due to the polarization modes of the core.

1-9 Other Models

Other nuclear models have been proposed to explain nuclear structure. These include the rotational model with its well-known prediction of energy spectra of even-even nuclei given by,

$$E_J = \frac{\hbar^2}{2\mathcal{J}} J(J+1) \qquad J=0,2,4,...$$

where $\mathcal{J}$ is the moment of inertia. For odd mass nuclei the rotational spectra are perturbed somewhat by means of a decoupling term due to the Coriolis force. Nilsson[22] has proposed using a different shell model potential to describe the motion of deformed nuclei,

$$V = \frac{1}{2} M \omega^2 r^2 + C \bar{\ell}\cdot\bar{s} + D\ell^2$$

with a term added proportional to ℓ^2. The resulting wave functions which are the sum of certain single-particle wave functions describe the spectra in the deformed region very well. However these other models are not applicable to

spherical nuclei and will not be discussed any further here.

1-10 The Neutron Capture Reaction

In the neutron capture reaction, a neutron of energy E_n is captured by a nucleus of mass number A to form the compound nuclear system of mass (A+1) and energy E_o,

$$A+n+E_n \rightarrow (A+1)+E_o \ .$$

The Q-value of the reaction is given by,

$$Q = E_o - E_n \ .$$

The compound nucleus may de-excite either by giving off a neutron (elastic scattering) or by a cascade of m gamma rays to the ground state of the system. The Q-value of the reaction may then be measured experimentally as,

$$Q = \sum_{i=1}^{m} \left(E_{\gamma_i} + \frac{E_{\gamma_i}^2}{2\, M_{A+1} c^2}\right)$$

where the last term is the recoil energy given to the nucleus for each gamma-ray de-excitation in the cascade. Neutron capture reactions are usually studied using thermal neutrons which have a Maxwellian velocity distribution with mean neutron energy, $\bar{E}_n$=0.02 eV, as these are easily obtainable with sufficient intensity in a nuclear reactor. Then the measured Q-value for the reaction corresponds to the binding energy of the last neutron in the (A+1) nucleus. The neutron capture reaction has been the major source for the measurement of accurate neutron binding energies as a function of A.

Thermal neutron capture proceeds almost entirely via s-wave neutrons because of the centrifugal barrier for higher angular momenta. The ratio of s-wave to p-wave penetrabilities for neutrons is given by[23],

$$\frac{P_s}{P_p} = 1 + \frac{1}{(kR)^2}$$

where k is the wave number of the neutron

R is the interaction radius.

The ratio is $\sim 10^7$ for light weight nuclei and thermal neutrons. For medium weight nuclei $kR \to 1$ at about 100 keV neutron energy. The gamma-ray yield from neutron capture in p-wave resonances becomes equal to that in s-wave resonances when the p-wave neutron width is comparable to the radiation width. Some p-wave resonances have been found below 100 eV at A=94[24]. In fact the p-wave neutron strength function has a maximum near A=90. However for a thermal neutron beam, the number of neutrons at energies greater than 100 eV is very small and so p-wave capture is not expected to be of any significance.

The capture of an s-wave neutron forms a compound state of spin $J' = |J \pm \frac{1}{2}|$ and parity the same as that of the target ground state where J is the ground state spin of the target. If the energy of the compound nucleus coincides with that of a compound resonance state, the details of the gamma-decay will be determined by the spin and parity and other properties of this compound state. However if the energy of the compound

nucleus falls between resonances both possible spin states will contribute to neutron capture with a mixture depending on the shape and proximity of levels of the two different J' values. Neutron capture then provides information both on the capture mechanism and on the properties of the bound states populated in the reaction.

The nature of the capture mechanism has been the subject of both experimental and theoretical studies. Experimentally strong groups of gamma rays are observed where the p-state is close to the ground state and the gamma-ray transition probability depends on the shell model configuration of the final states. The similarity between the intensity of neutron capture gamma rays and proton groups in the (d,p) stripping reaction to the same final states is taken as strong evidence for single particle effects in the neutron capture mechanism since the (d,p) reaction is regarded as a good direct reaction[25]. The intensities observed in the two reactions are expected to be correlated if either initial or final states in each reaction can be written as a simple product of wave functions representing the target and incident neutron separately in terms of fractional parentage coefficients. Direct capture occurs when the nucleus undergoes a radiative transition before the neutron has shared its excitation energy with the target nucleons. The amount of direct capture can be comparable to compound nuclear formation when capture occurs

far from resonances in nuclei where the level spacings are large and when radiative transitions can occur to levels which are relatively pure single particle states for the added neutron.

The general capture mechanism has been well explained by Lane and Lynn[26,27] using nuclear dispersion theory where they derived a formulation for the complete capture cross-section in the resonance region. Contributions from a compound nuclear resonance internal part, from capture in the entrance channel caused by modifications in the wave function produced by nearby resonances and from hard sphere potential scattering together with its modification by the "direct" capture induced by distant resonances were included. Potential and channel resonance cross-sections depend on the strength of the single-particle p-wave configuration in the final states and can give rise to strong radiative transitions when the p-wave admixture is large. Even the resonance internal part may give rise to enhanced transitions to pure single-particle p-states if the initial state neutron reduced width is large. Exceptionally large values for k_{El}, the reduced electric dipole gamma-ray width, for primary transitions in nuclei near mass number 90 cannot be explained by the capture model of Lane and Lynn however since these nuclei occur at minima in the s-wave neutron strength function where the enhanced radiation widths are not predicted[25]. Bartholomew[28] has plotted the values of k_{El}

and k_{M1} versus mass number A and found that they are actually relatively constant. According to the theory proposed by Lane and Lynn the partial width for an "enhanced" transition to a single particle p-state following resonance capture is proportional to the reduced neutron width of the resonance. Similarly the reduced radiation widths for the primary gamma-rays should follow the well-known Porter-Thomas[29] distribution, which is a chi-squared distribution with one degree of freedom, as do the reduced neutron widths.

The cross-section for neutron capture in a particular resonance of spin J' and energy E_o is given by,

$$\sigma_\gamma = \pi\lambda^2 \, g \, \frac{\Gamma_n \, \Gamma_\gamma}{(E-E_o)^2+(\Gamma/2)^2}$$

where $g = \frac{(2J'+1)}{2(2J+1)}$ is a statistical factor

λ - wavelength of neutron

and $\Gamma = \Gamma_n+\Gamma_\gamma$ is the sum of the partial neutron and gamma widths.

The emission probability is then $\Gamma_\gamma/\hbar$ per second. Actually Γ_γ is relatively constant for all nuclei, being of the order of 100-200 meV, since the capture level possesses a large number of decay modes. The total gamma-ray width, Γ_γ, is composed of a sum of partial gamma-ray widths,

$$\Gamma_\gamma = \Sigma \, \Gamma_{\gamma_i}$$

which obey the Porter-Thomas distribution. The value obtained for Γ_{γ_i} cannot be compared directly to the Weisskopf estimate for single-particle transitions as the level spacing at the neutron capture energy, D, is much less than the single particle level spacing, D_o, which is about 10 to 15 MeV. Thus in real nuclei one must consider the actual level spacing since the gamma strength is actually shared among many levels. This leads to a value of Γ,

$$\Gamma = \Gamma_W \frac{D}{D_o} \quad .$$

So for El transitions,

$$\Gamma(El) = CE^3A^{2/3} \frac{D}{D_o}$$

and the gamma-ray reduced width is defined as,

$$k_{El} = \frac{\Gamma_\gamma(El)}{E^3A^{2/3}D} \quad .$$

Similarly for magnetic transitions,

$$k_{Ml} = \frac{\Gamma_\gamma(Ml)}{E^3D} \quad .$$

Bartholomew[28] has found that $k_{El} \doteq k_{Ml} \doteq 10^{-2}$ for A=88. The reduced widths are particularly large near neutron closed shells.

Besides providing information on the neutron separation energy, insight into the capture mechanism and details on the gamma-ray transition probabilities, the neutron capture reaction gives rise to characteristic spectral distributions and information on the spins, parities and distribution of

energy levels populated in the bound states of the (A+1) nucleus. The number of gamma rays in the neutron capture spectrum depends on the number of states below the capture state to which transitions can occur. The number of levels available increases rapidly with mass number. Also the spectra of odd-odd product nuclei are much more complex than those of neighbouring even-even or even-odd nuclei because of the difference in level density at the same excitation energy in the various nuclei. The pairing energy depresses the energy of the ground state configuration with respect to the neutron separation energy and must be applied to the nucleus before single-particle excitation can occur. The shell structure also affects the spectral shapes. The simplicity of some spectra is associated with the reduced level denisty near closed shells. The strong high energy primary gamma rays may be associated with transitions of single particle type which leave the target nucleus core undisturbed. Collective properties are apparent in spectra of some off-shell mass regions. These properties are displayed in the form of a group of intense gamma-rays at low energy emitted in transitions between members of rotational bands. Above $A \sim 70$ one can treat the gamma-ray cascade as a statistical process. The spectral distribution and the average number of gamma-rays per capture are then statistical properties as well as the total radiation width of the capturing state.

The spectral distribution depends on the level density of states to be populated,

$$\nu(E) = CE^3 \frac{D(S_n)}{D(S_n-E)}$$

where $D(S_n)$ and $D(S_n-E)$ are level spacings at separation energy S_n and at excitation levels of energy S_n-E respectively for levels of the same spin and parity as the capturing state. Then the expression,

$$\int_0^{S_n} E\nu(E)dE = S_n$$

provides a means of obtaining normalized absolute intensities for gamma-rays following neutron capture. Another commonly referred to property of the spectral distribution is the multiplicity, or the average number of gamma rays emitted per capture,

$$M = \int_0^{S_n} \nu(E)dE.$$

This quantity increases slowly as a function of the mass number A.

Gamma-ray selection rules limit the type of states populated directly from the capture state but most low energy states can be populated via two- or three-step cascades. The decay of the compound nuclear state can be ascertained from energy, coincidence and intensity relationships. One often knows the ℓ_n values for many bound levels from the orbital

angular momentum transferred to the neutron in the corresponding (d,p) reaction. Spins and parities of the levels can often be determined from the branching ratios of gamma transitions. The multipolarities of the gamma rays can be determined from measurements of internal conversion coefficients or from gamma-ray angular correlation measurements. Often half-life measurements of some low-lying states lead to useful information concerning the widths of these levels and hence the nature of the states, collective or single-particle. Finally population of the bound states in a nucleus provides information on level densities at low excitation energies.

CHAPTER 2

SURVEY OF PREVIOUS WORK

2-1 The Nuclides Under Study

The details of the level structure of isotopes with a closed or nearly closed neutron shell of N=50 will be determined in this thesis; in particular of the isotopes $^{87}_{37}Rb_{50}$, $^{88}_{37}Rb_{51}$, $^{87}_{38}Sr_{49}$ and $^{88}_{38}Sr_{50}$. The basic level structures as tabulated in the Nuclear Data Sheets[30] and in the sixth edition of the Table of Isotopes[31] are shown in figures 2-1 and 2.2. Some of the pertinent facts known about these isotopes prior to this study will be outlined here. The most recent measurements of the radioactive isotope half-lives of interest are listed in Table 2-1. The lifetime of the well-known isomeric level in

Table 2-1

Parent Half-lives

^{87}Kr	76	min.[32]
^{88}Kr	2.80	hour[32]
^{87}Rb	5.22×10^{10}	year[33]
^{88}Rb	17.78	min.[34]

^{87}Sr has recently been measured to be 2.83 hours[35]. The

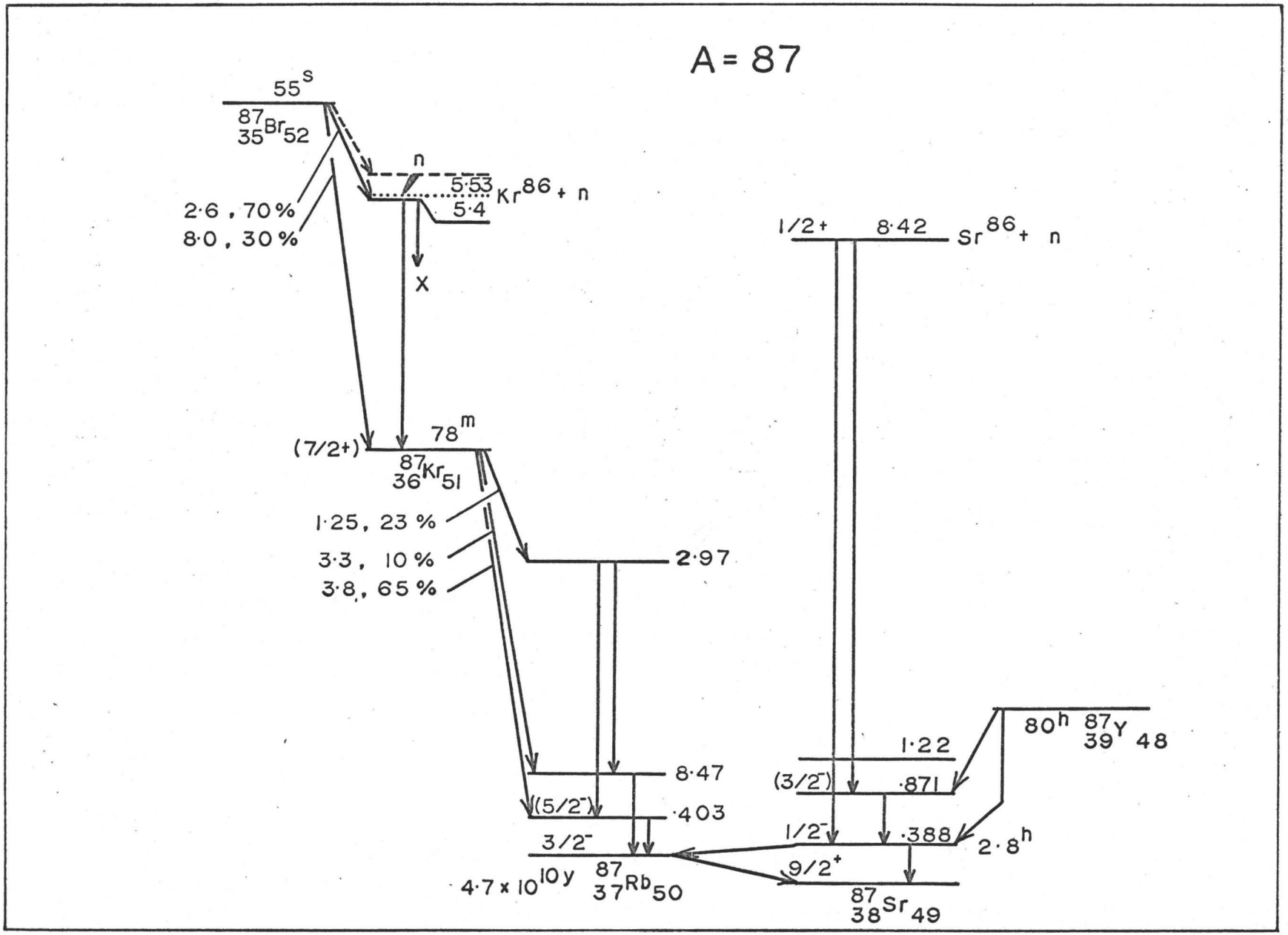
A = 87
55 s
87 35Br52
n
5·53
5·4
Kr86 + n
2·6 , 70 %
8·0 , 30 %
X
1/2+
8·42
Sr86 + n
(7/2+)
78 m
87 36Kr51
1·25, 23 %
3·3 , 10 %
3·8 , 65 %
2·97
8·47
·403
(5/2-)
3/2-
4·7 x 10 10y
87 37Rb50
1·22
(3/2-)
·871
1/2-
·388
2·8 h
80 h
87 39Y 48
9/2+
87 38Sr49

FIGURE 2-1

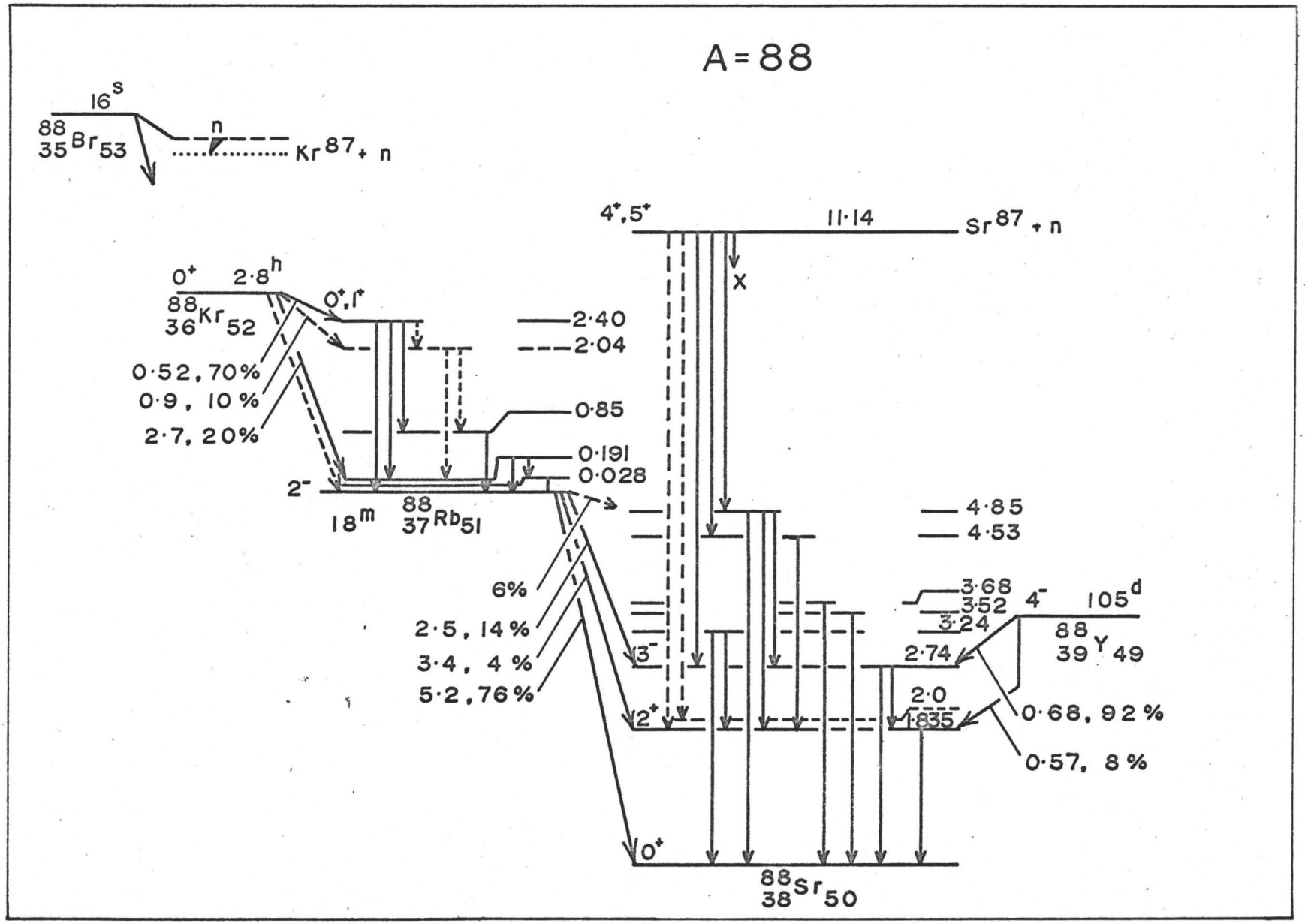
A=88
16^s
88 35 Br 53
n
Kr 87 + n
4+,5+
11·14
Sr 87 + n
X
0+
2·8^h
88 36 Kr 52
0+,1+
2·40
2·04
0·52, 70%
0·9, 10%
2·7, 20%
0·85
0·191
0·028
2-
18^m
88 37 Rb 51
4·85
4·53
6%
2·5, 14%
3·4, 4%
5·2, 76%
3·68
3·52
3·24
4-
105^d
88 39 Y 49
3-
2·74
2·0
2+
1·835
0·68, 92%
0·57, 8%
0+
88 38 Sr 50

FIGURE 2-2

krypton and rubidium isotopes have generally been obtained from the products of the fission reaction on uranium as discussed in section 2-5.

There are four stable strontium isotopes present in nature. Therefore in a neutron capture reaction one must consider the percentage capture in each isotope. The total thermal neutron capture cross-section for natural strontium has been measured to be 1.16 barns by pile oscillator methods[36]. Since the percentage isotope abundance of all four stable isotopes are well known[37] and the neutron capture cross-section for three of the isotopes (84,86,88) have been measured[38] it is possible to calculate the percentage capture contribution for each isotope. Table 2-2 summarizes the results.

Table 2-2

	% Abundance	σ_c	% Capture Contribution	Q(n,γ) (MeV)
^{84}Sr	0.55	0.8	0.38	8.24
^{86}Sr	9.87	1.3	11.0	8.42
^{87}Sr	7.02	∿14.6	∿88.2	11.11
^{88}Sr	82.56	0.006	0.42	6.40

The Q-values[39] listed for the (n,γ) reaction refer to the neutron binding energies for the compound system consisting of target plus neutron. It is seen that the only significant thermal neutron capture contributions come from the $^{86}Sr(n,\gamma)^{87}Sr$

and the $^{87}Sr(n,\gamma)^{88}Sr$ reactions.

The ground state spins of all the isotopes of interest have been determined and are summarized in Table 2-3. The 5/2+ spin-parity assignment of the ground state of ^{87}Kr is based on

Table 2-3

Isotope	Spin	Reference
^{87}Kr	5/2+	37
^{87}Rb	3/2-	38,41
^{87}Sr	9/2+	38
^{88}Kr	0^+	-
^{88}Rb	2^-	39
^{88}Sr	0^+	-

the $^{86}Kr(d,p)^{87}Kr$ reaction studied by Sass *et al*[40] who determined the ground state to be a d-state. The shell model predicts that the ground state should be a neutron in the $d_{5/2}$ configuration for the 51^{st} neutron. A neighbouring nuclide with 51 neutrons, $^{91}_{40}Zr_{51}$, has a measured ground state spin and parity of 5/2+ as well. Many other odd-A nuclei with an odd number of neutrons outside the N=50 shell also have ground state spin of 5/2+, including $^{97}_{42}Mo_{55}$ with five neutrons in the $d_{5/2}$ shell[42]. Thus it can be taken quite conclusively that the ground state spin of ^{87}Kr is 5/2+. The ground state

of ^{87}Rb has been assigned the $p_{3/2}$ configuration based on a measured spin of 3/2 by the atomic beam method[41]. This corresponds to an inversion of the shell level order of fitting for neutrons since for 37 neutrons and an even number of protons one would expect the hole in the $f_{5/2}$ shell to determine the ground state spin. However for protons a hole in the $p_{3/2}$ subshell determines the spin for 37 protons in the case of ^{87}Rb although for $^{83}_{37}Rb_{46}$ the 3/2- level lies 40 keV above the 5/2- ground state demonstrating that the order of filling of the subshells cannot be predicted accurately by the shell model. The ground state spin of ^{87}Sr has been measured to be 9/2+ and can be assigned the $g_{9/2}$ configuration due to a hole in the $g_{9/2}$ subshell. The ground state spins of ^{88}Kr and ^{88}Sr of course are both 0+ being even-even nuclei. The ground state spin and parity of $^{88}_{37}Rb_{51}$ has been measured to be 2^- using atomic beam techniques. Assuming the proton configuration to be the same as that of ^{87}Rb the addition of the 51^{st} neutron would lead to the ground state configuration for ^{88}Rb of $\pi(p_{3/2})^{-1}\nu(d_{5/2})$ which could result in a spin of 1^-, 2^-, 3^- or 4^-. However the value has been well established experimentally to be 2^-. In fact all odd-odd rubidium nuclei from mass number 84 to 90 have ground state spins of 2^-. Vanden Bout et al[43] have recently confirmed the ground state spin-parity assignment of ^{88}Rb using the atomic beam magnetic resonance technique.

2-2 Beta-Decay Studies

The first significant work on the beta decay of the krypton and rubidium radioactive isotopes of mass 87 and 88 was carried out by Thulin[44,45] using electromagnetically isotope separated samples. The krypton samples being inert gases are easily separated chemically from the other products of ^{235}U thermal fission. Rubidium is produced as the daughter product of the krypton gas.

In his work on the beta decay of ^{87}Kr in 1952 Thulin managed to strip off two beta components with energies 1.27 and 3.63 MeV and intensities 25 and 75% respectively using a magnetic beta-ray spectrometer. However later with better instrumentation and beta-gamma coincidence results, Thulin[46] determined three beta components in the decay of ^{87}Kr as shown in Figure 2-1. Using a NaI(Tl) scintillation spectrometer, four gamma-rays of energy 2.57, 2.05, 0.847 and 0.403 MeV were detected and placed in the decay scheme based on beta-gamma coincidence results. Based on this decay scheme, Thulin postulated the ground state of ^{87}Kr to be 7/2+ as no ground state beta group was observed and measured the Q-value for the reaction to be 4.2 MeV. Using the improved nuclear instrumentation available today, Holm[47] studied the decay of ^{87}Kr employing the isotope preparation technique as outlined by Thulin[48]. He employed a germanium lithium detector and scintillation coincidence techniques to establish a level scheme

with states at 0, 403, 845, 1578, 1741, 2416, 2557 and 3310 keV. A beta transition to the ground state was detected and this is plausible on the basis that the ground state of ^{87}Kr has meanwhile been measured to be a $d_{5/2}$ state. A Q-value of 3.9 MeV has been obtained for this beta-decay reaction. Gamma-gamma coincidences were performed using two NaI(Tl) counters. The first excited state in ^{87}Rb has definitely been established to be an $f_{5/2}$ state based on the angular distribution measurements of Alkhazov et al[49] using Coulomb excitation of the first excited state by means of 16.1 MeV nitrogen ions.

The half-life of ^{87}Rb is 5.22×10^{10} years and the isotope decays only via beta-emission to the ground state of ^{87}Sr with an end-point energy of 274 keV[50]. Thus this radioactive decay can yield no information on the excited levels in ^{87}Sr. However the two first excited states in ^{87}Sr at 388 and 871 keV have been established by the study of the 80 hour positron decay of ^{87}Y[51].

The beta-decay of ^{88}Kr to its daughter ^{88}Rb has been studied at two different times by Thulin[44,46]. To obtain good ^{88}Kr beta- and gamma-ray spectra, the spectra of pure ^{88}Rb were subtracted from the corresponding combination of ^{88}Kr and ^{88}Rb spectra. Eight gamma-rays were detected with an NaI scintillator and three beta-components with end-point energies 520, 900 and 2700 keV and intensities 70%, 10% and 20% respectively were observed. With the aid of beta-gamma and gamma-

gamma coincidence results the decay scheme in Figure 2-2 was constructed by Thulin. He also detected the 28 keV conversion electrons in coincidence with the 160 keV gamma-ray and measured the K/(L+M) ratio for this transition to be 8 thus classifying it as an M1 transition. The beta-decay Q-value for ^{88}Kr was measured to be 2.9 MeV.

The first work on the beta-decay of ^{88}Rb to levels in ^{88}Sr was done by Bunker et al[52] using a scintillation spectrometer to detect three gamma-rays of energy 0.908, 1.853 and 2.76 MeV. Thulin detected two more gamma rays of energy 2.18 and 4.2 MeV giving rise to three excited levels in ^{88}Sr at 1.84, 2.76 and 4.1 MeV. Three main beta groups with end-point energies 5.3, 3.5 and 2.5 MeV and intensities 77%, 13% and 9% respectively were determined by Thulin leading to a beta Q-value for this radioactive decay of 5.3 MeV. Directional correlation measurements have definitely established the spin and parity of the first two excited states to be 2^+ and 3^-[53,54] and the intensity ratio of the M2 to E1 components of the 0.908 gamma-ray transition to be $\sim 10^{-4}$. The ^{88}Rb source was prepared by means of electrostatic precipitation from the krypton fission gas.

Lazar et al[55] restudied the low-lying levels of ^{88}Sr via the beta-decay of ^{88}Rb and the positron decay of ^{88}Y. The ^{88}Rb activity was produced by the neutron bombardment of natural rubidium. The ground state beta transition was measured to be

75.9 ± 5% by comparing the total beta activity to the gamma-radiation from the 1.85 MeV level. Using a 3" by 3" NaI crystal ten gamma-ray energies were measured and fit into the decay scheme as shown in Figure 2-2. With the help of gamma-gamma coincidence results, new levels were determined at 3.24, 3.52, 3.65, 4.53 and 4.87 MeV. From the decay scheme the intensities of the beta groups to the first two excited levels in ^{88}Sr were calculated as 4.3% and 13.6% to the 1.85 and 2.76 MeV levels respectively as summarized in Table 2-4.

Table 2-4

	E_β	%	E_β	%	E_β	%
Bunker et al	5.13 ± .03	66	3.39 ± .10	19	2.04 ± .015	15
Thulin	5.30 ± .05	77	3.6	13		9
Lazar et al		79.5 ± 5		4.3		13.6
Ragaini et al	5.199 ± .004	76.2 ± 4	3.363	4.7	2.465	13.8

Recently Ragaini and Knight[34] studied the beta decay of 17.8 minute ^{88}Rb in order to supplement their nuclear reaction studies of the level structure of ^{88}Sr. They used Ge(Li) and NaI(Tl) gamma-ray detectors and a gamma-gamma coincidence spectrometer to observe and place fourteen gamma-rays into the decay scheme. The sample was obtained by neutron activation of ^{87}Rb. By a direct-comparison of the total beta-ray activity with the intensity of the 1836 keV gamma-ray, they determined the ground state beta group to have 76.2 ± 4% of the total beta

intensity. A value of Q_β for the reaction of 5.199 $\pm$ 0.004 MeV was calculated based on the ^{88}Sr neutron binding energy (11.1135 $\pm$ 0.0015 MeV from Irigaray *et al*[56]), the ^{87}Rb Q_β value (0.274 $\pm$ 0.003 MeV from Beard and Kelly[50]), and the ^{88}Rb neutron binding energy (6.188 $\pm$ 0.002 MeV from the rubidium neutron capture data of Rasmussen *et al*[57]).

The decay of ^{88}Y by electron capture to ^{88}Rb has been well studied over the years. It has been found to decay mainly to the 2.76 MeV level in ^{88}Sr[31] which is then de-excited by the 0.908 and 1.853 MeV gamma-ray cascade and the 2.76 MeV cross-over transition. More recently Shastry and Bhattacharyya[58] restudied the decay of ^{88}Y and found that two levels at 3.22 and 3.52 MeV were also weakly populated in ^{88}Sr.

2-3 Neutron Capture Studies

Thermal neutron capture on natural strontium has been investigated previously by various researchers. As there are no strong resonances close to the neutron capture state in the isotopes of interest[59] neutron capture has a very low cross-section.

The first study was undertaken by Kinsey and Bartholomew[36] using a pair spectrometer to detect the high energy gamma rays from thermal neutron capture in natural strontium in the form of $SrCO_3$. They detected the twelve gamma rays listed in Table 2-5 and were able to measure the absolute

Table 2-5

E_γ	I_γ	A of Final Isotope
9.22	0.06	88
9.06	0.1	88
8.376	1.3	88
8.045	1.1	87
7.530	5	87
6.95	5	
6.87	6	
6.671	6	
6.268	5	
6.10	4	
5.82	2	
5.43	2	

gamma-ray intensities per 100 neutrons captured. The intensities were obtained by the "approximate" method in which the sample is assumed black to neutrons. However the technique may have errors of $\pm$ 50%. Isotopic assignments were made for only five of the lines listed. The neutron binding energy was determined to be 11.120 MeV.

Not until 1966 was the study of thermal neutron capture in strontium attempted again, this time by Schmidt et al[60] using a 2 cc. lithium-drifted germanium counter. Bragg reflection from a lead single crystal was used to obtain a pure

thermal neutron beam and the target again was natural strontium in the form of $SrCO_3$. A total of 146 gamma lines were observed with an average error of 8 keV. Of these twenty-three were assigned to the ^{88}Sr and three to the ^{87}Sr decay scheme by means of double coincidence and triple sum coincidence results. The coincidence measurements were performed using NaI(Tl) counters. The 146 gamma-ray lines detected by Schmidt et al are listed in Table 6-2 of this thesis. Several new levels up to 5424 keV were postulated in ^{88}Sr on the basis of the strong high energy gamma-rays.Schmidt et al found no evidence for a 9.22 MeV gamma-ray seen by Kinsey et al[36] and assigned the line at 7.530 MeV to ^{88}Sr rather than ^{87}Sr on the basis of energy differences and intensity considerations. The neutron binding energy of ^{88}Sr was measured to be $11.111 \pm .004$ MeV on the basis of the proposed decay scheme.

In the next year Rasmussen et al[57] published a list of neutron capture gamma-ray lines for most of the elements. The gamma-ray spectra were obtained using a Ge(Li) counter and were analyzed using a computer program[61] to obtain the energies and intensities of all lines in the spectrum. For natural strontium, 188 gamma-ray lines were listed along with their intensities per 100 neutron captures. However the isotopic identification of the lines was not attempted nor was a decay scheme for ^{87}Sr or ^{88}Sr proposed on the basis of this information. As no exhaustive check of the computer generated list

was attempted, the list may well contain some erroneous information such as background lines or gamma-ray lines missed due to strong background lines.

Irigaray et al[56] investigated the neutron capture gamma-ray spectrum of natural strontium again using a 40 cc Ge(Li) spectrometer. They observed 144 gamma-ray lines with an average error of about 3 keV and measured the intensities of the strongest gamma-ray lines by normalizing their intensities to the 5.82 and 7.53 MeV lines observed by Kinsey et al[36]. The errors on their intensity measurements were quoted as of the order of $\pm$ 15%. A total of 25 gamma-ray lines were assigned to the ^{88}Sr decay scheme whereas three gamma-ray lines were assigned to the ^{87}Sr decay scheme. The proposed level structures of ^{87}Sr and ^{88}Sr remained much the same as those proposed by Schmidt et al[60]. On the basis of the decay schemes the neutron separation energies were determined to be 8428.5 $\pm$ 2.5 keV for ^{87}Sr and 11113.5 $\pm$ 1.5 keV for ^{88}Sr. The lists of the energies and intensities of the gamma-ray lines observed by the latter three groups of researchers are tabulated in Table 6-2 for comparison with the results obtained in the present investigation.

2-4 Other Reaction Data

The neutron capture reaction cannot always be relied upon to determine the energies of the low-lying levels in a nucleus as these levels may not be populated by primary gamma-

ray transitions from the capture state. In fact the interpretation of the gamma-ray spectrum from thermal neutron capture often depends on knowing the level positions in the final nucleus from other reactions proceeding to the same final states. Level energies can be determined from particle-particle reactions,

$$A + a \rightarrow B + b + Q$$

since a measure of the Q-value of the reaction together with the kinematics of the reaction will determine the level in the final nucleus.

The first two levels in ^{87}Sr have been determined from the electron capture decay of 80 hour ^{87}Y [51]. Levels up to 3.65 MeV have been populated in ^{87}Sr by the (d,α) reaction on ^{89}Y [62]. This reaction will populate predominantly neutron hole states. The (d,p) reaction, which is a very selective reaction in that it populates predominantly single particle neutron states, has been performed on ^{86}Sr in order to study levels in ^{87}Sr [63]. As ^{86}Sr is an even-even nucleus, the (d,p) reaction should populate good single particle states. Levels up to 4.45 MeV have been observed and the ℓ values of most of these levels have been determined from the angular distributions of the out-going protons. Table 2-6 lists the levels in ^{87}Sr populated by the (d,p) and (d,α) reactions.

The (d,p) reaction has also been performed on ^{87}Rb recently [64] to obtain levels in ^{88}Rb up to 2.8 MeV. The

levels populated by the (d,p) reaction and some ℓ-values and spins of the low-lying states have been listed in Table 2-7 for reference in the beta-decay work discussed in chapters 5 and 7 of this thesis.

By far the most experimental work has been done on the level structure of ^{88}Sr. Various inelastic scattering experiments have been performed to excite the collective states of the nucleus. The inelastic neutron scattering experiment was successful only in exciting the first two states in ^{87}Sr and ^{88}Sr each[65,66] so that this reaction did not add much new information as far as level energies are concerned. McDaniels et al[67] first used the inelastic α-particle scattering reaction to excite the collective levels in the strontium isotopes. Later Alster et al[68] used 42 MeV alpha particles to excite the first three levels in ^{88}Sr to test the validity of the weak coupling core-excitation model for this nucleus. The (α,α') reaction is a powerful tool for studying the low-lying collective levels since it is possible to get the spin and parity assignments as well as the transition strengths. These strengths can be related to the electromagnetic transition rates from the shapes and magnitudes of the angular distributions. The 0^+, 2^+, 3^- and 2^+ states at energies 0.0, 1.84, 2.74 and 3.21 MeV respectively were excited. The values of the B(EL) transition strengths were measured to be 5, 6.2 and 0.4 times the single-particle values for the 1.84, 2.74 and 3.21 MeV states respec-

Table 2-6

Low-Lying Levels in ^{87}Sr

ℓ	(d,p)	(d,α)	Spin
4	0		9/2+
1	389	360	1/2-
1	876	850	3/2-
2	1231	1220	5/2+
2	1779	1700	
0	2175	2100	
		2390	
2	2681	2610	
	2819		
	2922		
0	2942		
		3020	
0	3125		
2	3154		
2	3168		
2	3261		
2	3279		
		3320	
2	3387		
	3434		
(2)	3549		
(2)	3592		
	3603		
(2)	3672	3650	
2	3780		
0	3885		
2	3960		
	4013		
	4081		
(0)	4187		
(2)	4199		

Table 2-6 (continued)

ℓ	(d,p)	(d,α)	Spin
2	4240		
	4305		
	4341		
	4357		
	4384		
	4418		
	4453		

Table 2-7

^{88}Rb Levels populated in ^{87}Rb(d,p)^{88}Rb

E_x	ℓ	Spin
0	2+0	2^-
27	2	3^-
196	2+0	1^-
268	2	4^-
362	2	
390	2	
413	2	
862	0	
1142	0	
1212	0	
1245		
1354	0	
1610		
1665	3?	
1794	0+2?	
1860		
1927		
1965		
2094		
2165		
2230		
2257		
2361		

tively. These values are not as large as expected for good collective states. The inelastic scattering of deuterons on strontium was studied by Hamburger[69] with 15 MeV deuterons. States in ^{88}Sr up to 4.27 MeV were populated as summarized in Table 2-8. Stautberg et al[70] used the proton inelastic

Table 2-8

Summary of Inelastic Scattering Results on ^{88}Sr

(e,e')		(p,p')		(d,d')		(α,α')	
E_x	J^π	E_x	J^π	E_x	J^π	E_x	J^π
		0	0^+	0	0^+	0	0^+
1.84	2^+	1.84	2^+	1.835	2^+	1.84	2^+
2.74	3^-	2.74	3^-	2.74	3^-	2.74	3^-
		3.24	2^+	3.20	2^+	3.21	2^+
				3.52			
		3.57	(2^+)				
				3.61			
4.0	$(2^+,4^+)$	4.05	$(2^+,4^+)$	4.02			
		4.34		4.27			
		4.56					
		4.88					
6.5	$(2^+,3^-)$						
7.75							

scattering and the (He^3,d) reaction to populate some collective and single-particle states in ^{88}Sr up to 4.88 MeV. They

were able to determine the spins of some of the states as well, as shown in Table 2-8. Peterson et al[71] studied the structure of ^{88}Sr via the inelastic scattering of 65 and 70 MeV electrons. The purely electromagnetic interaction of the electrons with nuclei leads to an interpretation which is simpler than for strongly interacting particles. The inelastic electron scattering results give the multi-polarity, L, of a transition and the reduced electric radiation transition probability by use of a distorted wave analysis. The results found by Peterson et al[71] are summarized in Table 2-9 where G is the ratio of the transition probability to the single particle transition probability.

Table 2-9

Electron Inelastic Scattering Results

E_x(MeV)	L	G(W.U.)	Spin
1.84	2	8.5	2^+
2.74	3	25.0	3^-
4.0	2	1.6	$2^+,4^+$
6.5	(2)	1.1	$(2^+,3^+)$
7.75	(3)	4.0	

Single particle configurations in nuclei can of course be excited by means of single-particle transfer reactions. One such reaction which has been studied is the (d,He^3) reaction on

^{89}Y and ^{88}Sr to populate final states in ^{88}Sr and ^{87}Rb respectively[72] using 21 MeV deuterons. The (d,He^3) reaction excites preferentially simple proton-hole configurations. The reaction can be described as a direct proton pick-up process so that spectroscopic information can be obtained from a DWBA analysis. The levels excited in the ^{88}Sr and ^{87}Rb nuclei are summarized in Table 2-10 along with the ℓ-values and probable spin values of the states. These are exactly the states one

Table 2-10

Levels populated by (d,He^3)

	E_x(MeV)	Spin	ℓ
^{88}Sr	0	0^+	1
	1.84	2^+	1,3
	3.21	2^+	1,3
	3.48	(1^+)	1
	3.64	(3^+)	3
^{87}Rb	0	3/2-	1
	.403	5/2-	3
	.847	(1/2-)	1

would expect to excite according to simple shell model considerations. Single particle configurations in ^{88}Sr have also been studied via the (t,α) reaction[73] populating states up

to 4.8 MeV.

The best studied single-particle reaction and the one most analogous to the (n,γ) reaction, the (d,p) reaction has been investigated by Cosman and Slater[74] in order to determine the location of the neutron particle-hole states in ^{88}Sr built on a single $g_{9/2}$ hole in the N=50 core. The $^{87}Sr(d,p)^{88}Sr$ reaction transfers a single neutron to the ^{87}Sr target with J^{π} = 9/2+ in contrast to the (d,He^3) reaction which strips off a single proton exciting proton-hole states. Using 7.5 MeV deuterons and a multi-gap spectrograph, 73 levels below 8.516 MeV excitation were observed of which 32 displayed direct-stripping angular distributions. The transferred angular momentum, ℓ_n, and spectroscopic strengths $(2J+1)S_{\ell_n,J}/(2J_o+1)$ were determined for those states which displayed a direct-stripping distribution. Here J_o is the spin of the target and J is the final state spin. The J_o=9/2+ value of the target spin caused a resultant decrease in yield by a factor of 10. It was found that the levels excited in ^{88}Sr consisted of one cluster of ℓ_n=0 states and two clusters of ℓ_n=2 states and that these clusters could readily be interpreted as resulting from coupling of a $1g_{9/2}$ neutron hole to the $s_{1/2}$, $d_{5/2}$ and $d_{3/2}$ states in ^{89}Sr. No ℓ_n=3 transitions were observed while only two weak ℓ_n=1 transitions were observed indicating that very few neutrons were transferred into the $2p_{3/2}$ and $1f_{5/2}$ orbits.

Recently some two quasi-particle configurations have been studied in ^{88}Sr by means of the (t,p) reaction on ^{86}Sr[75]. However only twelve levels have been reported so far as listed in Table 2-11 and these two quasi-particle levels are not expected to be populated directly either in beta-decay or the neutron capture reaction. Table 2-11 also summarizes the results of the one-particle reactions leading to final states in ^{88}Sr. The (d,p) stripping strengths and ℓ_n values are listed for the first 24 levels only as the higher energy levels populated are not of much interest as far as comparison with levels populated in the (n,γ) reaction is concerned. Table 2-8 summarizes the results of inelastic scattering experiments on ^{88}Sr.

2-5 Fission Products

The fission process, consisting of the splitting of a nucleus into two nuclei of lighter mass and two or three neutrons was first discovered by Hahn and Strassman[76,77]. The probability of a nuclide of mass A being formed in fission plotted as a function of A is referred to as the fission yield curve and as such was first studied by Anderson *et al*[78]. A typical fission yield curve is a doubly-peaked curve on a semi-log plot with sharp peaks at mass numbers A≃90 and A≃140 for the thermal fission of ^{235}U. The positions of these peaks, especially the one at the lower value of A, have a strong depen-

Table 2-11

Summary of Single-Particle and Two-Particle Reaction Results on ^{88}Sr

(d,p)			(d,He^3)		(t,α)		(t,p)	
E_x	ℓ_n	$(\frac{2J+1}{2J_o+1})S_{\ell n,J}$	E_x	J^π	E_x	J^π	E_x	J^π
0	4	1.20	0	0^+	0	0^+	0	0^+
1.839	2	0.126	1.84	2^+			1.836	2^+
2.738	ns				2.734	3^-	2.734	3^-
3.208	ns		3.21	2^+	3.156	0^+	3.152	0^+
					3.221	(2^+)	3.221	(2^+)
			3.48	(1^+)	3.489	(1^+)		
(3.590)	(ns)							
			3.64	(3^+)	3.636	(3^+)		
4.035	2	0.279			4.030	(2^+)	4.030	(2^+)
4.294	2	0.376			4.287	$(2,4^+)$	4.292	$(2,4^+)$
4.408	2	0.875						
4.450	2	0.083						
4.464	(ns)							
							4.485	0^+
4.514	2	1.08						
4.551	?							
					4.607	(+)		
4.636	2	0.564						
4.748	2	0.805						
					4.768		4.712	
4.789	?							
							4.837	(3^-)
4.876	0	0.230						
4.920	ns							
5.101	2	1.04						
5.133	?							
5.157	(ns)						5.163	2^+
5.199	(ns)							
5.418	0	0.105						
5.463	0	0.563					5.459	
5.506	0	0.027						
5.665	(1)	0.029						

dence on the mass of the fissile material. Mass number 235 has been found to be suitable for producing good yields at product masses A=87 and A=88. For a given A the probability of producing a specific Z is given by,

$$P(Z) = \frac{1}{\sqrt{2\pi\sigma^2}} e^{-\frac{(Z-Z_p)}{2\sigma^2}}$$

where Z_p is the most probable charge for a given mass chain and σ the variance of the distribution is $\sim$0.59 as measured by Wahl[79]. It is evident from the fission yield curve that the most probable products of fission are distributed around those with filled neutron shells of N=50 and N=82. However, initially the fission products are neutron rich and therefore undergo beta decay.

The rare gases krypton and xenon are high yield fission products and because of these properties many attempts have been made in the past to collect and separate them. Gas sweeping techniques using either a carrier gas such as helium or the gas itself of which a radioactive sample is to be collected, have been performed. These techniques depend on using highly emanating components for the fissile material. The emanating power of a substance refers to the fraction of the radioactive inert gas which escapes from the substance before radioactive decay occurs. Wahl and Bonner[80] determined the fractional cumulative yields of short-lived krypton isotopes by the use of highly emanating stearate compounds.

However Archer[81] found that uranium stearate although having a good emanating power, disintegrated quickly after a number of long irradiations with a loss in emanating power. He found that hydrous zirconium oxide had a high emanating power of 95 $\pm$ 5%, was resistant to radiation damage in a high neutron flux of $\sim 10^{13}$ n/cm^2/sec. and had a low cross-section for the neutron capture reaction. In fact the emanating power of hydrous zirconium oxide decreased with a half-life of 75 megawatt-minutes irradiation compared to a half-life of less than 10 megawatt-minutes for the uranium stearate.

Gas chromatography using activated charcoal to separate the xenon and krypton gas fractions was first used by Koch and Grandy[82]. They found that with a charcoal column at room temperature a good xenon-krypton separation could be effected in a matter of 10 to 20 minutes. The technique was improved by Ockenden and Tomlinson[83] who dispersed the charcoal as a fine powder on the surface of glass wool at room temperature. A xenon-krypton separation could then be obtained in 10 to 15 seconds. Archer developed a low-temperature gas chromatographic separation technique for preparing xenon samples. Using the fact that the vapour pressure of xenon is 0.0004 mm Hg and that of krypton 2 mm Hg at liquid nitrogen temperatures (77°K), the separation of the krypton and xenon fractions was achieved in a clear empty length of glass tubing kept at 77°K. At this temperature, the krypton sample swept up by the helium carrier

gas does not freeze out in the glass separation columns and goes to exhaust while the xenon condenses on the walls of the separation columns. By warming up the columns after sweeping up the fission gases the xenon gas may be collected in a sample chamber. The details of the irradiation facility and of the gas-sweeping facility which was built in a location distant from the irradiation chamber are well documented in the literature[81,84].

CHAPTER 3

EXPERIMENTAL INSTRUMENTATION AND FACILITIES

3-1 Detector Response to Gamma Radiation

Gamma radiation interacts with material in general by means of the three basic processes, namely photoelectric, Compton and pair production. The interaction cross-sections are energy dependent as well as being dependent on the atomic number (Z) of the material. Gamma-rays are removed from a beam of initial intensity I_o according to the relation, $I = I_o e^{-\mu x}$, where I is the beam intensity after passing through an absorber thickness x and μ is the sum of the three absorption coefficients,

$$\mu = \mu_{photo} + \mu_{Compton} + \mu_{pair}.$$

The absorption coefficient for the photo-electric effect is proportional to $Z^5 E_\gamma^{-b}$ [85] where E_γ is the gamma-ray energy and b, which determines the energy dependence of absorption, depends on the particular absorbing material ($b \simeq 2.0$ for germanium). Thus the photo-electric cross-section increases rapidly with the atomic number of the absorber but decreases quickly with photon energy. Consequently for a detector to be responsive to "full-energy" or photo-electric events, the

material must have a high atomic number.

In the Compton effect, the gamma-radiation undergoes elastic collision with an outer atomic electron which has a very small binding energy. The energy is shared between the scattered gamma-ray and the recoiling electron with the former having energy,

$$E_\gamma' = \frac{E_\gamma}{1+(1-\cos\theta)\frac{E_\gamma}{mc^2}}$$

where θ is the angle of deflection of the gamma-ray

m is the mass of the electron

and c is the velocity of light

and the recoiling electron having energy, $E_\beta = E_\gamma - E_\gamma'$. The recoil electron can have a maximum energy of

$$(E_\beta)_{max} = \frac{2E_\gamma^2}{mc^2+2E_\gamma}$$

corresponding to a back-scattered gamma-ray. The compton absorption coefficient is proportional to the electron density NZ and inversely proportional to the gamma-ray energy,

$$\mu_{Compton} = 1.25\times10^{-25}\,\frac{NZ}{E_\gamma}\,[\log_e\,(2E_\gamma/mc^2) + \tfrac{1}{2}]/cm. \quad (86)$$

Since the Compton effect is of no consequence in gamma-ray energy determination when there is no angular selection, a material of high Z is required to minimize the detection of this effect in a gamma-ray detector.

In pair production, the photon interacts with the

nuclear field of an atom creating an electron-positron pair with total kinetic energy equal to the photon energy less the rest mass of the two particles. Hence for this effect to occur, the gamma-ray energy must be at least twice the rest mass of an electron. The absorption coefficient depends linearly on the photon energy near the threshold, $\mu_{pair} \propto NZ^2 (E_\gamma - 2mc^2)$ [87] but it depends logarithmically on the photon energy at higher energies, $\mu_{pair} \propto NZ^2 \log_o E_\gamma$. [87]

3-2 The Plastic Scintillator

The plastic scintillator is an organic scintillation counter used primarily to measure the energy distribution of beta-rays. The dimensions of a plastic phosphor detector must be large compared to the range of the beta particles of interest but still small enough so that the efficiency for detection of gamma radiation is small. Plastic being a low Z material has a small cross-section for photo-electric events but is quite efficient for the production of Compton interactions. This latter interaction provides the basis for using the plastic scintillator to detect gamma-ray event times on account of the good timing characteristics of plastic.

Electrons emitted in nuclear beta decay are detected through their interaction with other electrons. An energetic electron makes very many inelastic collisions, each resulting in the excitation of atomic electrons. In a certain fraction

of the cases enough energy is transferred to an electron to allow it to escape from the atom creating an electron-positive ion pair. The energy lost per ion pair product ($\sim$ 1000 eV for plastic) is independent of the energy of the incident electron so that the product of the energy lost and the number of ion pairs produced gives a method of determining the incident electron energy. Electrons also lose energy when accelerated in the Coulomb field of a nucleus through radiation bremstrahlung but these effects are negligible in a low Z material such as plastic.Gamma radiation is also detected through the creation of these electron-positive ion pairs which in turn dissipate energy by their conversion to light. The photons created are detected by a light sensitive photocathode which is optically coupled to the scintillator.

Luminescent emission in a phosphor is of two types, fluorescence which is a direct process and phosphorescence which is the delayed emission of radiation. Scintillators must have a short duration of phosphorescence to be useful as detectors. The scintillator must be transparent to its own luminiscent radiation and the spectral distribution of the radiation should match the frequency response curve of the multiplier photo-cathode. Plastic is transparent to its own fluorescent radiation and the decay time of plastic is about 10^{-8} seconds. Of course the rise time of the output pulse is not only

dependent upon the decay of the phosphor but also upon the electron transit time of the photomultiplier. Nevertheless, the fast response of plastic makes this scintillator useful for generating time markers in coincidence experiments. The plastic scintillator has a very linear response to both gamma-ray and beta-ray energies but the energy resolution is of the order of 12% and hence not very satisfactory for gamma-ray spectroscopy.

3-3 The NaI(Tl) Counter

The NaI(Tl) counter consists of an inorganic scintillator (NaI) which is a transparent material made efficient through the use of an "activator", thalium. The main advantage of this detector for use in gamma-ray spectroscopy is its very high photo-efficiency due to the high Z-value of its iodine component. The cross-section for Compton events is relatively small as is the cross-section for pair events which are only significant at energies above a few MeV.

The rise time of the signal pulse is determined almost solely by the decay time of the NaI phosphor ($.25\times10^{-6}$ sec.) and is much longer than that for the plastic scintillator. The energy response of the NaI(Tl) counter is not as linear as that of plastic especially below 0.5 MeV where there is as much as 20% variation[88] in linearity. However the line shapes for different gamma-ray energies have been well determined over the last years[89] for a fixed geometry so that gamma-ray

responses can readily be "stripped" from a spectrum when decomposition is undertaken. An improvement over plastic scintillators is realized by NaI(Tl) counters in the energy resolution obtainable which is generally about 6-7%. The resolution obtained is dependent on many factors in the chain of events leading to the formation of the output voltage pulse which is nominally proportional to the input energy. Some parts of the phosphor may be less transparent than others causing variation in collection efficiency. Also the fraction of light collected may vary depending on where the incident photon entered the phosphor. Variations in the photocathode sensitivity also contribute to deterioration of energy resolution.

3-4 Electronics for Scintillators

A scintillator is optically coupled to a light-sensitive photocathode of a photomultiplier. Light causes the emission of photo-electrons which are accelerated through the photo-tube and create secondary electrons at each of the stages in the photomultiplier. The secondary emission multiplication factor at each dynode increases with the energy of the incident electrons so that the over-all gain of the photomultiplier varies very quickly with applied voltage. The final output current pulse at the photomultiplier anode is proportional to the intensity of the light impulse over a wide range of photomultiplier gain. The resultant current can be integrated

at the anode and then converted to a voltage pulse via a charge-sensitive preamplifier. A time constant, RC, a few times larger than the scintillator decay time constant, τ, is used to integrate the photomultiplier current. This selection is made in order to obtain the maximum pulse height possible and thus the best possible resolution since there is a statistical variance associated with the pulse height which decreases as the size of the pulse increases. The RC time constant must be small enough to obtain narrow pulses yet large enough to prevent any decrease in the signal-to-noise ratio inherent at the photomultiplier anode. The signal-to-noise ratio can be maintained by appropriate choice of the photomultiplier voltage. The voltage must also be chosen to achieve the best dynamic range of the photomultiplier and prevent any saturation.

Other factors must be considered when using the scintillators and their associated electronics. The gain of the photomultiplier is dependent both on the counting rate and any external magnetic fields. Thus analog gain stabilization may be required if counting is carried out over a long period of time or on a time-decaying source. Since one usually has a high counting rate when employing scintillators as gamma-ray detectors, a double-delay line amplifier[90] is frequently used to amplify the voltage pulses from the preamplifier. These amplifiers produce bipolar pulses which eliminate any base-line

shifts. It is impossible to eliminate this effect in an amplifier using mono-polar pulse-shaping.

3-5 The Ge(Li) Detector

The disadvantages of the scintillation counters have been virtually eliminated with the development of the solid state gamma-ray detectors in the last decade. Whereas the energy, ε, required to produce an electron-hole pair in the NaI scintillator is about 110 eV, it is only 2.8 eV for germanium and 3.5 eV for silicon. As a result more pairs are created per incident gamma-ray of energy E and the energy resolution which is proportional to $1/\sqrt{n}$ (for a Fano factor of 1.0) where n is the number of pairs created, is much better for the solid state detectors. Germanium is preferable to silicon for gamma-ray spectroscopy because of its higher value of Z (hence greater efficiency for photo-electric events) and its lower value of ε.

Basically Ge(Li) counters are fabricated by drifting donor atoms of lithium into a p-type piece of germanium. The lithium atoms compensate the acceptor impurities in the drifted region giving rise to a very high resistivity or intrinsic region in the p-type piece of germanium. The final detector then consists of an intrinsic region sandwiched between the original p-type germanium and the low resistivity n-type germanium which was formed by alloying lithium onto the germanium.

By reverse biassing the resulting diode with a large enough field (about 1000 volts per cm.) the electron-hole pairs produced by the gamma-ray interactions in the intrinsic region can be collected.

Ge(Li) detectors are generally fabricated in two different physical configurations - planar and coaxial. Planar detectors consist of an intrinsic region sandwiched between a parallel p-type and an n-type region. However these counters cannot be constructed with a very large active volume. This limitation arises from the fact that the drifting rate varies as $t^{1/3}$ and hence a thickness of 1 cm. which requires some months to achieve is a representative limiting case. Their poor detection efficiency is offset by their uniform collection times making the planar detector useful in experiments in which fast timing is important.

Coaxial detectors are much easier to fabricate with a large sensitive volume than the planar configuration. These counters consist of a central p-type material surrounded by a coaxial section of intrinsic material and then an outer annulus of n-type lithium-diffused material. In this laboratory a different version of the coaxial detector has been fabricated and used almost exclusively. This is the wrap-around configuration[91] which consists of a p-type central region on one side surrounded by a central intrinsic region and an n-type lithium-diffused material on the other five sides. The coaxial

or wrap-around counter is much more efficient than the planar one due to its larger sensitive volume but is not as good for high resolution and fast timing applications. These limitations can be attributed to the nature of the electric field near the n-type region and to certain "dead" regions in the sensitive detector volume.

Ge(Li) detectors are operated at liquid nitrogen temperature in order to reduce bulk currents due to free electrons because of the small band gap in germanium. Both electrons and holes are free to move and be collected by the applied electric field. The holes have a similar mobility to the electrons and hence only a slightly different drift velocity,

$$v_h = \frac{V}{d} \mu_h \quad .$$

Here, v_h - drift velocity of holes

V - applied voltage

d - width of depletion region

and μ_h - mobility of holes.

The time before trapping or recombination is called the lifetime of the carrier (τ) and must be long enough to enable collection of the carriers. The number of charges produced by a gamma-ray of energy E is given by,

$$Q = E/\varepsilon.$$

The number of charges trapped or recombined as a function of

time is then given by,

$$N(t) = Q(1-e^{-t/\tau}).$$

The fraction of charge trapped is directly proportional to the width of the intrinsic region[92],

$$\frac{\Delta Q}{Q} = \frac{d}{\lambda}$$

where λ is the mean trapping length.

As the lifetime of the carriers depends upon the purity of the material, very pure samples of germanium with a minimum of trapping and recombination centres are required. Fast and efficient collection of the electron-hole pairs is obtained both by the good quality of the intrinsic region and by the field strength applied. The voltage applied must be high enough so that complete charge collection is achieved.

One of the limitations of the Ge(Li) counter is associated with the size of the detector. The number of charges collected at any given time after a gamma-ray event is detected has a spread related to the detector thickness as a result of the spatial distribution of the events[93]. There is a spread in pulse shape for different pulses of the same energy and amplitude since the time of arrival of the charges at the detector electrodes depends upon the position of the event in the detector. A minimum collection time of, $\frac{1}{2}\frac{d}{v}$, corresponds to the production of the charge at the center of the intrinsic region. Assuming equal mobility of electrons and holes the

last pair would be collected in a time of d/v when the charge is produced at either electrode. This corresponds to a differential spread in time for the last pair to be collected of,

$$t \doteq \frac{1}{2} \frac{d}{v} = 50 \text{ nsec.}$$

for a detector thickness of 1 cm and a drift velocity of 10^7 cm/sec. The average collection time for all pairs produced by a gamma event would then be approximately 75 nsec.

The limitations placed on the Ge(Li) counter resolution include noise sources such as surface leakage currents, generation-recombination noise and the statistical fluctuation in the number of ion pairs created by a gamma ray of energy E. This latter limitation involves the Fano factor[94] which is the ratio of the variance to the yield. The yield is the number of electron-hole pairs produced by a gamma ray and the variance σ^2 is the mean square variation in this yield. The Fano factor then is given by the expression

$$F = \frac{\sigma^2}{E/\varepsilon} .$$

The incident energy of a gamma ray is divided between ion-pair production and the competing process of energy loss through heating of the lattice crystal structure. Whereas the Fano factor for NaI is rather large ($\sim$ 1), for germanium it is about 0.075[95] which corresponds to small statistical fluctuations in the yield and most of the incident energy being dissipated in ion-pair production. The energy resolution obtained for a

gamma ray of energy E is then given by,

$$R = \varepsilon\sigma = \sqrt{\varepsilon EF}$$

which varies as the square root of the product of the energy and the Fano factor. The full width at half-maximum (FWHM) is given by,

$$FWHM = 2.35\ R\ .$$

The best possible resolution obtainable then is 1.2 keV at 1 MeV and 3.6 keV at 10 MeV.

3-6 Electronics for Ge(Li) System

In order to take advantage of the inherent good qualities of the Ge(Li) detector it has been necessary to make a considerable improvement in the available electronic equipment. The electronic system used for scintillation spectroscopy is not too critical since the resolution is poor and a simple adaptation for solid state devices is not possible.

The Ge(Li) detector is operated at 77°K with a reverse bias of the order of 1000 to 2000 volts applied. The pulse resulting from a gamma-ray interaction in the detector is essentially a current pulse proportional to the number of ion pairs produced in the intrinsic region of the detector. This signal is amplified via a current-sensitive preamplifier which is usually capacitively coupled to the detector. Figure 3-1 depicts the block diagram of a preamplifier with the pulse shapes shown at various stages. Basically preamplifiers are designed

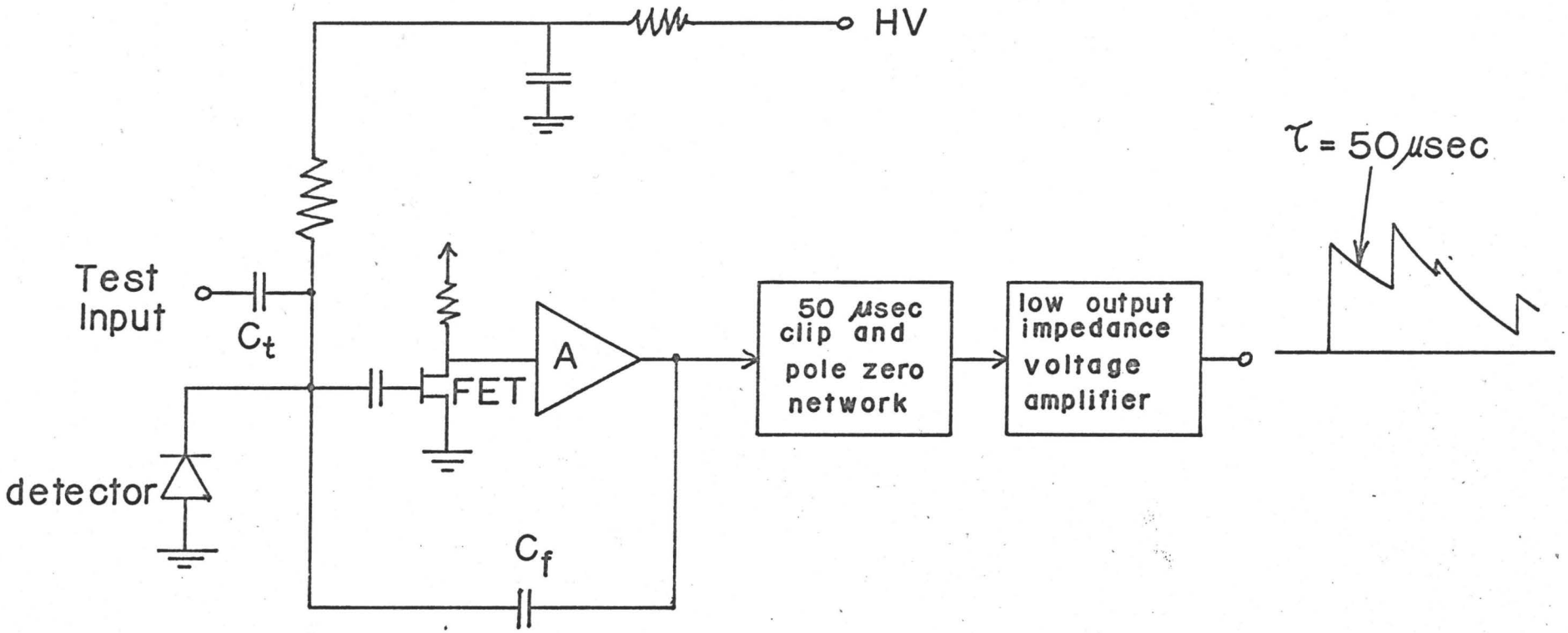

Pre-amplifier for Solid State Detectors

FIGURE 3-1

to provide good energy resolution and a fast speed of response as well as maintaining the good energy linearity inherent in the Ge(Li) detector itself. The charge sensitive preamplifier consists of an extremely high input impedance FET (field effect transistor) in the first stage followed by a high-gain operational amplifier with capacitive feedback C_f, a passive element. The transfer function of this stage is essentially,

$$\frac{AC_f}{C_d + AC_f}$$

where C_d is the detector input capacitance. Thus the output voltage is very insensitive to the detector capacitance variations. It is important that low noise resistors be used in the first stages of the preamplifier in order to minimize noise contributions and thereby retain the inherent signal-to-noise ratio.

At the input of the preamplifier the noise factor is proportional to capacitance. The detector's capacitance is proportional to the sensitive area of the detector and inversely proportional to the effective depletion depth so that it is entirely dependent on the detector dimensions and the applied voltage. The input capacitance can be minimized by connecting the first stage of the preamplifier directly to the counter since capacitive ac coupling usually causes higher noise. This is achieved using sapphire[96] to isolate the detector electrically but connect it thermally to the cold finger in the detector

chamber. This configuration eliminates ground loops or stray pick-up of external electrical signals and has the additional advantage that some cooling of the FET leads to a noise reduction in the input stage of the preamplifier. The coupling capacitor and feed-through connectors are now no longer sources of noise.

The output of the high gain stage is frequently fed into a clipping stage which has pole-zero cancellation built-in with a 50 μsec time constant. Further voltage amplification may then be required before the preamplifier output is fed directly into the main amplifier. The output of the preamplifier is a "non-shaped" fast rise pulse with a long decay time constant of about 50 μsec, long enough so as not to interfere with pulse shaping in the main amplifier but short enough to reduce pulse-pile-up effects. At a reasonable counting rate of say 10,000 counts per second each pulse rides on the tails of the preceding pulses but the energy information in the pulses can still be obtained after pulse-shaping in the main amplifier.

The resolution of a preamplifier is stated in terms of x keV at zero input capacitance with a slope of y keV per pF of input capacitance. In designing a preamplifier system it is important to minimize the input capacitance as well as the slope y keV/pF of the preamplifier in order that the preamplifier be satisfactory for large volume detectors as well as the smaller

detectors. The slope y can often be reduced by the proper choice of the input FET transistor.

The purpose of the main amplifier is to provide pulse shaping of the preamplifier output pulses and to produce a low output impedance pulse of sufficient amplitude to be analyzed by an analog-to-digital convertor (ADC). Pulse shaping is done to prevent overlap of the adjacent or sequential pulses and to enhance the signal-to-noise ratio by filtering out the noise sources in the detector and preamplifier which have a wide bandwidth compared to the useful components of the signal. The pulse-shaping most often used for Ge(Li) detectors is a CR-RC network which consists of a high-pass differentiating filter to cut down on the low frequency components of the waveform and a low-pass integrating filter to attenuate the high frequency components of the waveform. This bandpass filter removes both low and high frequency signal and noise components but enhances the signal-to-noise ratio. The best results are usually obtained for equal[97] CR and RC time constants, τ, in the range 0.5 to 2.0 μsec. An optimum value for the RC time constant must be chosen empirically for each detector-preamplifier configuration in order to compromise between signal-to-noise enhancement and pulse overlap prevention. A relatively long time constant may be adequate for low counting rate systems but a short time constant will be required for high count rates (greater than 10,000 per sec.) to minimize pulse overlap.

The pulse produced by a CR-RC shaping network is a mono-polar pulse with a small component of voltage lingering below 0 volts after the crossover point for positive polarity pulses. This is depicted in figure 3-2. For high count rates subsequent pulses will ride on the tails of the preceding pulses producing an amplitude defect. To partially overcome this defect another differentiating stage is added as shown in Figure 3-2 to produce a doubly-differentiated bi-polar pulse minimizing baseline shifts in the amplifier and decreasing the effective resolving time of the amplifier.

The probability of getting pulse pile-up can be calculated for a paralyzable system with resolving time ρ and an average counting rate of $\bar{n}$ per second. The probability of getting x counts within a time interval ρ is given by the Poisson distribution,

$$P(x) = \frac{(\bar{n}\rho)^{x-1}}{(x-1)!} e^{-\bar{n}\rho} .$$

Thus for a counting rate of 10,000 per second and a resolving time of 2 μsec one would get a pulse pile-up probability of,

$$\sum_{x=2}^{\infty} P(x) \doteq 0.02.$$

For a higher counting rate of 100,000 per second the probability of pulse pile-up increases to about 0.18 for a resolving time of 2 μsec and to about 0.10 for a resolving time of 1 μsec. Thus at high counting rates it becomes important to have pulse widths

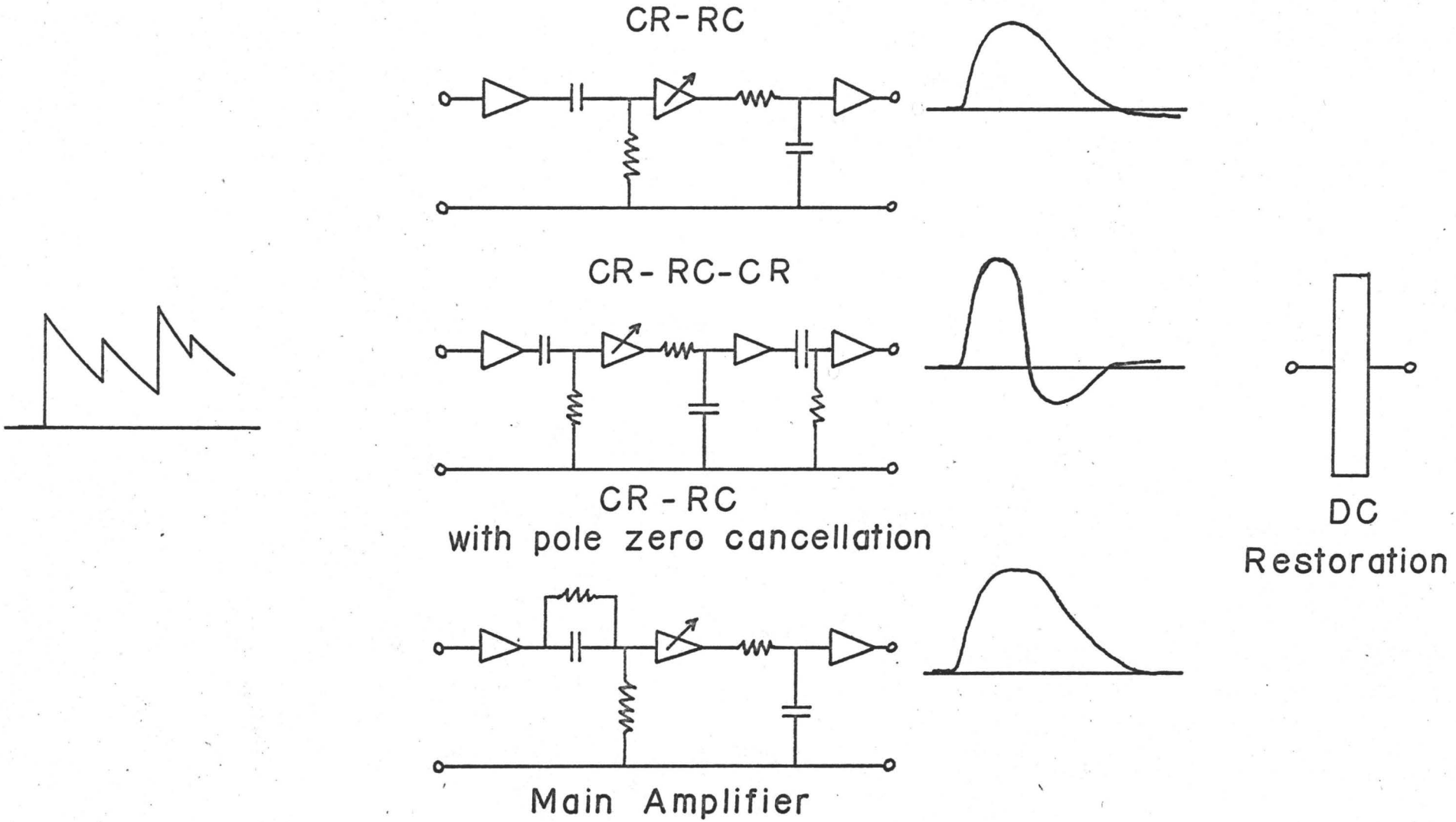
CR-RC
CR-RC-CR
CR-RC
with pole zero cancellation
DC
Restoration
Main Amplifier

FIGURE 3-2

as narrow as possible in order to distinguish between adjacent pulses. Often pulse-shape and baseline discrimination can be used to reject the pile-up pulses.

Two additional improvements have been added in the last few years to maintain good resolution at high counting rates, namely pole zero cancellation and DC baseline restoration. Pole zero cancellation is achieved by adding a resistor in parallel to the capacitors in all CR differentiation circuits in the preamplifier as well as the main amplifier as shown in Figure 3-2. This removes the unwanted undershoot due to multiple time constants inherent in the pulses produced by the CR-RC circuit. Since DC coupling is retained, complete pole zero cancellation is limited by the difficulties of stabilizing the DC output level of a DC-coupled amplifier. Baseline restoration removes any residual undershoots remaining at the amplifier output by forcing the signal to return to the baseline immediately after each pulse.

A properly designed amplifier will not contribute significantly to any loss in the resolution or linearity of the Ge(Li) counter and preamplifier system.

3-7 Electronics for Time Correlation Studies

In order to construct a nuclear decay scheme it is often necessary to look at the time correlation between the decay radiation. This can be done using a two-channel fast-

slow coincidence circuit[98] as shown in Figure 3-3. In order to obtain a time mark denoting the occurrence of a nuclear event one of two techniques is available: leading edge timing at or near the output of the detector or zero cross-over timing determined after the amplifier. In determining the time marker at the leading edge of the pulse a Schmitt trigger circuit set for a low discriminating voltage is used. Taking the output pulse immediately after the detector avoids the noise contributions and bandwidth limitations of the preamplifier and amplifier. When using a Ge(Li) detector in a coincidence experiment the timing marker is obtained by amplifying the energy pulse at the output of the first stage of the amplifier before pulse shaping occurs. The timing information is obtained using the crossover method which requires a double-differentiated bipolar pulse obtained with a DD2 amplifier. When the pulse crosses the baseline the zero amplitude is detected by means of a threshold trigger. Fairstein[99] has shown that the crossover point is almost independent of the energy of the incident radiation. However each method of obtaining a time marker has two basic uncertainties associated with it, namely "jitter" and "walk" . Jitter is the uncertainty in the time mark caused by signal noise or the noise in the discriminator circuit whereas walk which is the main cause of time variation is the variation in the time mark created by different signal amplitudes. Walk is less of a problem with the crossover method than with leading edge timing so that the crossover method is

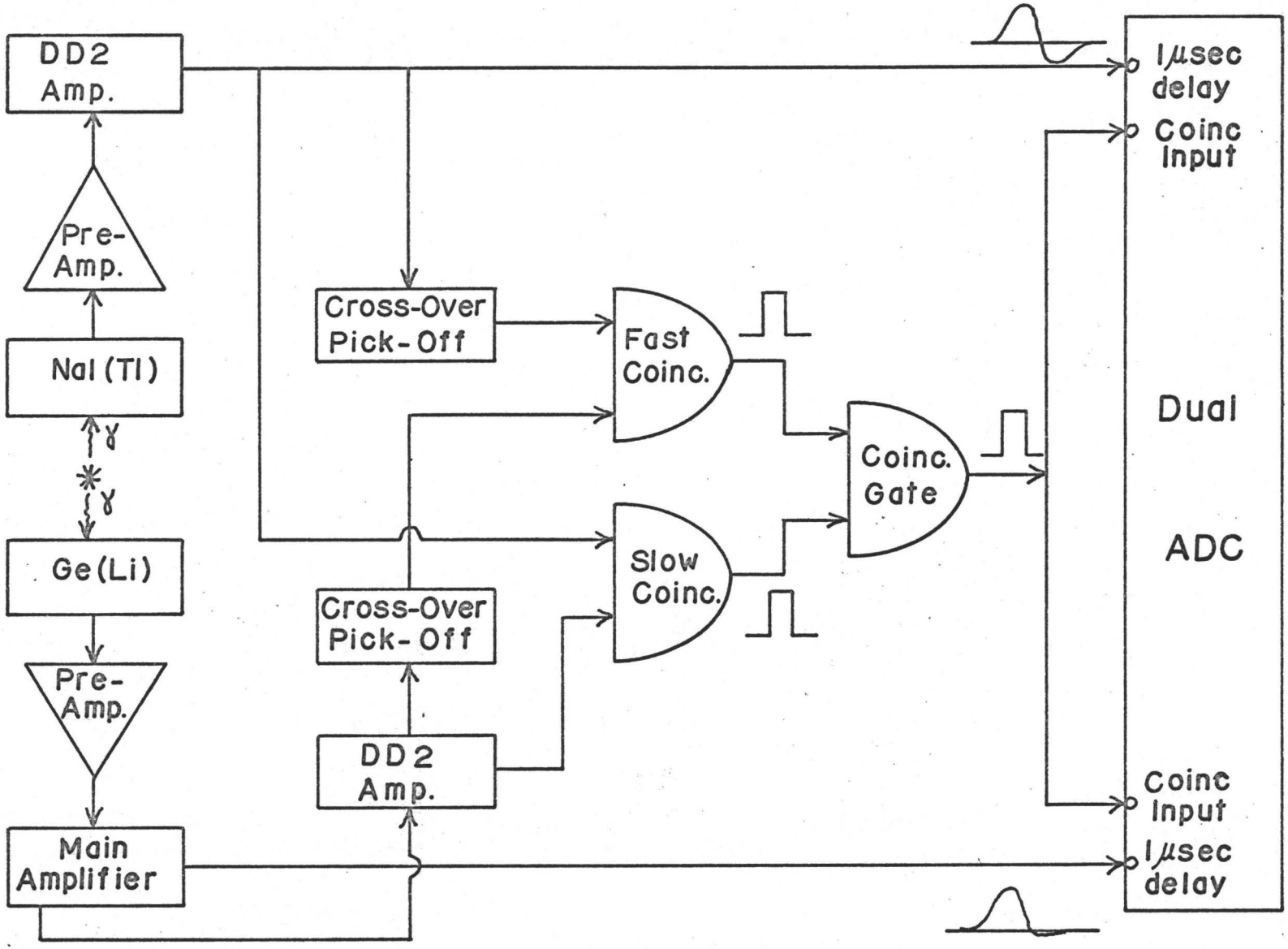

Electronics for Time-Correlation Studies

FIGURE 3-3

a more popular technique.

Ge(Li) detectors characteristically have long collection times (> 30 nsec.) and hence an appreciable amount of walk is inherent in leading edge timing as the walk is directly proportional to the rate of charge collection in a detector. The number of charges collected as a function of time is given by,

$$N(t) = Q(1-e^{-t/T})$$

where T is the collection time constant characteristic of the detector. If a Schmidt trigger is set up to sense a voltage proportional to an amount of charge Q',

$$N(t) = Q' << Q$$

then the corresponding time marker occurs at a time,

$$t = \frac{Q'}{Q} \quad T.$$

As the charge is directly proportional to the energy of the gamma ray producing the charge, the time marker will occur at a time inversely proportional to energy. Figure 3-4 illustrates the walk over an energy range of 0 to 2.75 MeV exhibited by leading edge timing in a good wrap-around Ge(Li) detector. The ordinate in the figures is the average time between detection of a beta-ray emitted in the decay of ^{24}Na by a fast plastic scintillator and detection of the gamma rays de-exciting the populated states in ^{24}Mg by the Ge(Li) counter. The 1/E variation of leading edge timing is evident

Fig. 3-4 Walk in Time Channel as a Function of Energy for Ge(Li) Detector:- The ragged curve is a plot of the centroid of the timing distribution peak in the time dimension as a function of energy. The smooth curve shown is a least squares fit to a hyperbolic function of energy and time. It is to be noted that the "walk" inherent in leading edge timing for Ge(Li) detectors can be quite significant. The spikes observed in the curve correspond to gamma-ray peak locations.

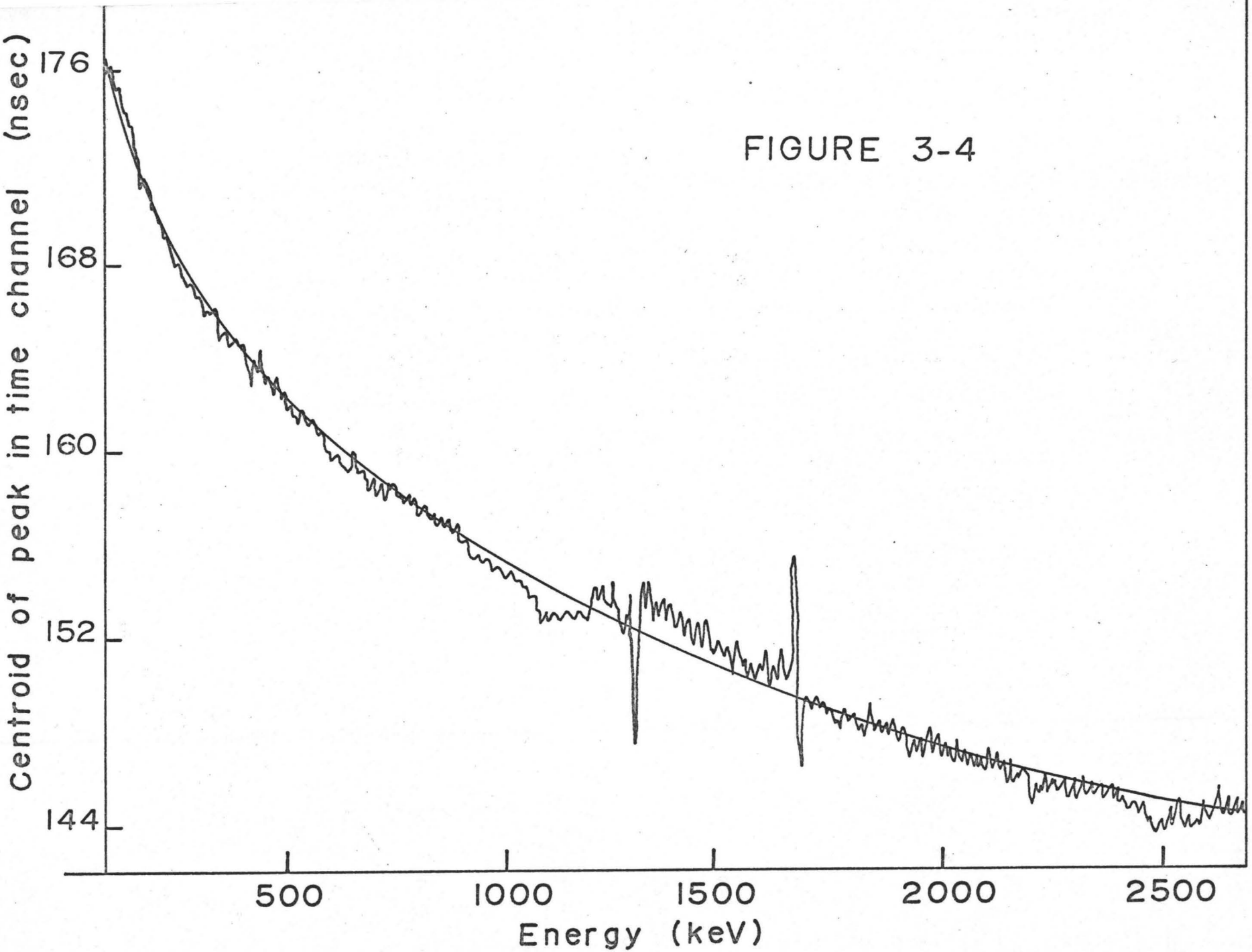
Centroid of peak in time channel (nsec)
176
168
160
152
144
500
1000
1500
2000
2500
Energy (keV)

FIGURE 3-4

from the curve.

A typical two-parameter experimental configuration is shown in Figure 3-3 where coincidence events are detected using a Ge(Li) detector in conjunction with a large NaI(Tl) counter. It has been common to use two NaI(Tl) counters on account of their high efficiency since the number of events detected in a coincidence experiment is very small. However the energy resolution of the NaI(Tl) counters is a limiting factor when the gamma-ray energy spacing is less than the resolving power of the NaI(Tl) counter. In order to use two Ge(Li) detectors, these would have to be very efficient (20-30 cc. active volume) and the singles counting rate in each detector should be fairly high to achieve a suitable coincidence counting rate. A compromise can be arrived at by using a NaI(Tl) counter to obtain good efficiency in one dimension and a large volume Ge(Li) detector to obtain good energy resolution in the second dimension.

Good time definition is obtained by using a DD2 amplifier in each dimension to create time markers of width τ nanoseconds at the time of crossover of the bipolar pulses. These two square pulses of variable width τ are fed into an AND circuit which generates a fast coincidence pulse of width 2 μsec upon overlap of these two timing markers. The circuit is then said to have a coincidence resolving time of 2τ nsec. Each time marker can be delayed with respect to the other and are set so that there is a maximum coincidence counting rate.

The slow coincidence part of the circuit consists of an energy selection on each parameter of the two-parameter experiment achieved by a low level discriminator (baseline) and a variable window width which are set to determine the energy range of the spectrum for each parameter. If the energy pulse satisfies the given energy conditions, a gating pulse is generated. Provided that energy conditions are satisfied on both sides, a slow coincidence pulse is formed. If both the slow and fast coincidence pulses are formed a gate pulse is generated which enables the two analog-to-digital convertors and permits analysis and storage of the information in the two-dimensional array. The energy pulses at the input of the ADC's are delayed for $\sim$ 1 μsec as the coincidence gate is not formed until the crossovers are detected which is about 1 μsec after the start of the energy pulses.

The resolving time of the coincidence circuit is an important parameter which affects the quality of the data collected. The coincidence circuit is efficient in the region where the coincidence counting rate is independent of the relative time delay between the two time markers, i.e. in the flat portion of the time resolution curve. Typical resolving times (width of resolution curve at half maximum) obtainable with an efficient coincidence circuit are of the order of 2τ = 60 nsec for a Ge(Li)-NaI(Tl) coincidence set-up. As the events from de-exciting nuclei are randomly distributed in

time, true coincidence events are not the only ones which have to be considered in a coincidence spectrum. There are also contributions from chance, sum and random summing coincidences although the latter two are not of too much consequence in a Ge(Li)-NaI(Tl) coincidence experiment. Chance events occur when radiation is sensed by both detectors within the time interval 2τ and yet the source is not common. The chance counting rate which is given by,

$$N_{ch.} = 2\tau n_a n_b$$

is proportional to the square of the source intensity. Here n_a and n_b are the singles counting rates in detectors a and b respectively. As the true coincidence counting rate is proportional to the source intensity the true-to-chance ratio is then inversely proportional to the source intensity and the resolving time of the circuit. Thus the source strength must be kept within reasonable limits to obtain a sufficiently high true-to-chance ratio to make the results meaningful.

3-8 The Central Data Handling System

The basic data handling system used to analyze the analog input voltages presented to the ADC's is the Nuclear Data Series 3300 Analyzer System. The system is capable of converting the analog input and of storing and processing the resulting digital information. Figure 3-5 shows a block diagram of all the pertinent components in this system.

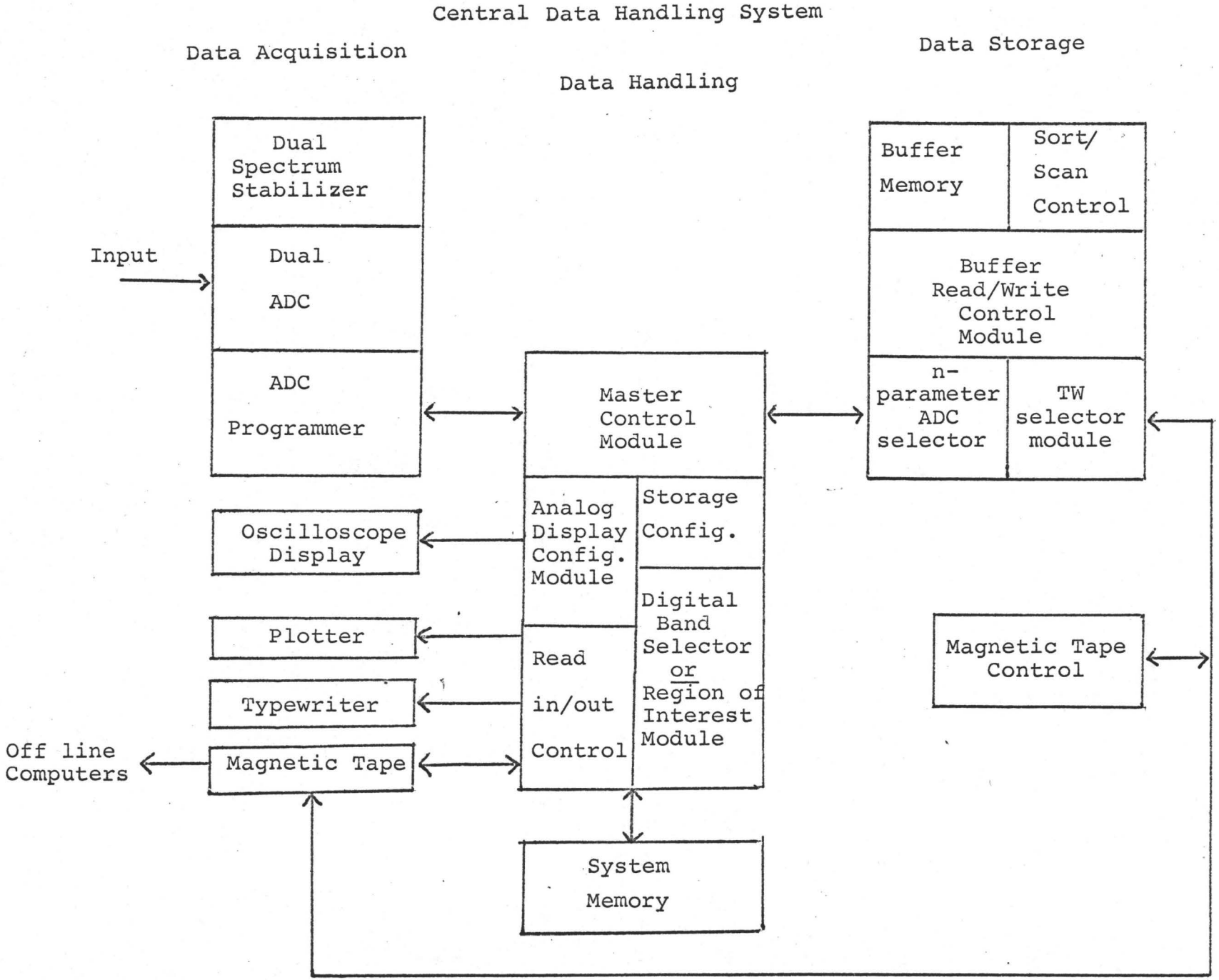
Central Data Handling System
Data Acquisition
Data Handling
Data Storage
Dual Spectrum Stabilizer
Input
Dual ADC
ADC Programmer
Master Control Module
Buffer Memory
Sort/ Scan Control
Buffer Read/Write Control Module
n-parameter ADC selector
TW selector module
Analog Display Config. Module
Storage Config.
Digital Band Selector or Region of Interest Module
Oscilloscope Display
Plotter
Typewriter
Read in/out Control
Magnetic Tape Control
Off line Computers
Magnetic Tape
System Memory

Figure 3-5

The analog voltages are accepted by the ADC's under control of the master processor module and the ADC program module. Each ADC is a Wilkinson type[100] convertor in which a capacitor is charged with the input voltage pulse. As soon as the top of the pulse has been sensed, the capacitor is discharged linearly until the voltage reaches a certain threshold value. The discharge time interval is determined by scaling a gated 16 Mc/s clock. The number of clock pulses counted is the channel number to which the incoming event is assigned. During the analysis of each event the ADC will not accept any further events so that the system is said to be "dead" during this time. The percentage dead-time is a measure of the counting rate at the detector of the nuclear radiation under study but depends upon the analysis time of the convertor. Each ADC has a resolution of 4096 so that when analyzing a typical singles spectrum with energies up to about 8 MeV the gain of the ADC ramp is about 2 keV per channel. This conversion gain is adequate for high energy gamma-rays for which the minimum obtainable line width with present Ge(Li) detector systems is about 6 keV FWHM. The ADC's are quite stable with respect to gain and zero parameters over a relatively long period of time but for long runs of more than one day in duration the gain and zero parameters may be held constant by means of digital spectrum stabilizers.

The analyzer system memory consists of 16,384 words of 18 bits each permitting the storage of 262,143 events per memory location. This permits the acquisition of four singles spectra of 4096 channels each or a symmetric two parameter configuration of 128 by 128 channels. To handle a two-dimensional experiment requiring a larger memory size, a buffer memory is provided permitting the addresses of events to be stored and then written on magnetic tape periodically as the memory buffer fills. Sorting of this encoded information can be done by the use of the digital band selector or the region of interest module in conjunction with the sort/scan module provided the array size is not too many times larger than the memory size. Thus for a 512 by 128 two-dimensional experiment the encoded data can be sorted in four passes of the tape. For larger two-dimensional arrays it is more feasible to use the off-line computers available. The IBM-7040 computer has 20^K of 36-bit words available for data storage. Breaking up each 36-bit word into four 9-bit words allows the storage of an 80^K two-dimensional array compared to 16^K in the analyzer memory. The CDC-6400 computer has 48^K of 60-bit words available for data storage. Breaking up each one of these 60-bit words into six 10-bit words then allows the storage of about 300^K members of a two-dimensional array which is almost twenty times larger than the analyzer memory size available.

The data gathered in the system memory may be output

in various ways as illustrated in Figure 3-5. Analog output is provided in the form of an oscilloscope display or a spectrum plot. Digital output is provided in the form of magnetic tape output or a typed copy of the spectrum in memory.

3-9 Neutron Irradiation Facilities

The basic irradiation facility used for thermal neutron capture studies was the through tube facility[101] in the McMaster nuclear reactor. This facility consists of a vertical aluminum tube passing through the reactor core and in which graphite is placed in order to scatter neutrons from the core. The aluminum tube is lined with lead- and paraffin-filled collimators in order to define a 3/4" neutron beam and remove scattered gamma ray and neutron backgrounds. Loss of neutrons from the collimated beam was minimized by evacuation of the entire system. A flux of about 10^7 neutrons/cm^2/sec. is obtained at the sample position at the top of the evacuated tube. This was found to be adequate for both single and double parameter studies. The sample is usually held in a 3 mm. thick annular column of ^{6}LiF to utilize the large (n,α) cross section of ^{6}Li. This is done both to provide protection for the Ge(Li) counters which deteriorate quickly under neutron irradiation and to minimize any thermal neutron capture in the materials surrounding the counter.

A second neutron beam facility was also available for thermal neutron capture gamma ray studies. This was a horizontal beam tube on the beam port floor of the McMaster nuclear reactor. This beam port consists of an aluminum tube extending up to the reactor core thus allowing a complete spectrum of neutrons produced in the fission reaction to travel up the tube. Gamma-ray background from the reactor core is minimized by placing a foot long plug of bismuth directly between the reactor core and the beam tube. Quartz plugs are used to attenuate the high energy neutron beam. The proper length of aligned quartz plugs attenuates all high energy neutrons and allows thermal neutrons to get through with essentially no attenuation. Collimation of the beam and the use of these quartz crystal plugs also have the effect of reducing the gamma-ray background. When the neutron beam is not in use, all thermal neutrons are easily stopped by means of a 1" thick boron plug.

3-10 Gas Sweeping Facility for Production of Rare Gas Fission Products

The rare gases krypton and xenon are high-yield fission products which can be easily produced in the thermal neutron fission of ^{235}U. The irradiation apparatus and the techniques for obtaining gaseous fission products have been described in detail by Archer[81,84]. The fission chamber used contained uranyl nitrate (94% ^{235}U enriched) dissolved in the efficient emanating material, hydrous zirconium oxide crystals. During

an irradiation the fission chamber is lowered down from its normal position of about 6 feet above the reactor core to a position beside the core in a flux of $\sim 10^{13}$ neutrons/cm^2/sec for a certain period of time. After raising the chamber back to its normal position the sample is allowed to cool for a long enough time to permit short-lived isotopes to decay. The gaseous fission products are then swept from the fission chamber to the chromatographic separator using a helium carrier gas as illustrated in Figure 3-6. Krypton, being the lighter gas, emerges first followed by the much heavier xenon gas. The krypton gas, having a lower condensation point than xenon, passes through the first two stages shown in Figure 3-6 as these two stages are kept at 77°K (liquid nitrogen temperature). The xenon fraction has a low enough vapour pressure at this temperature to be condensed on the walls of the glass U-tubes of the first two stages of the separation apparatus. Krypton passes through into the first sample holder which is a small glass U-tube filled with glass wool and activated charcoal. The krypton is adsorbed onto this charcoal at liquid nitrogen temperatures.

To prepare relatively pure samples of the krypton or rubidium isotope of interest it is necessary to consider the other isotopes produced as well as their precursors. The isobaric beta decay chains of interest are listed in Table 3-1.

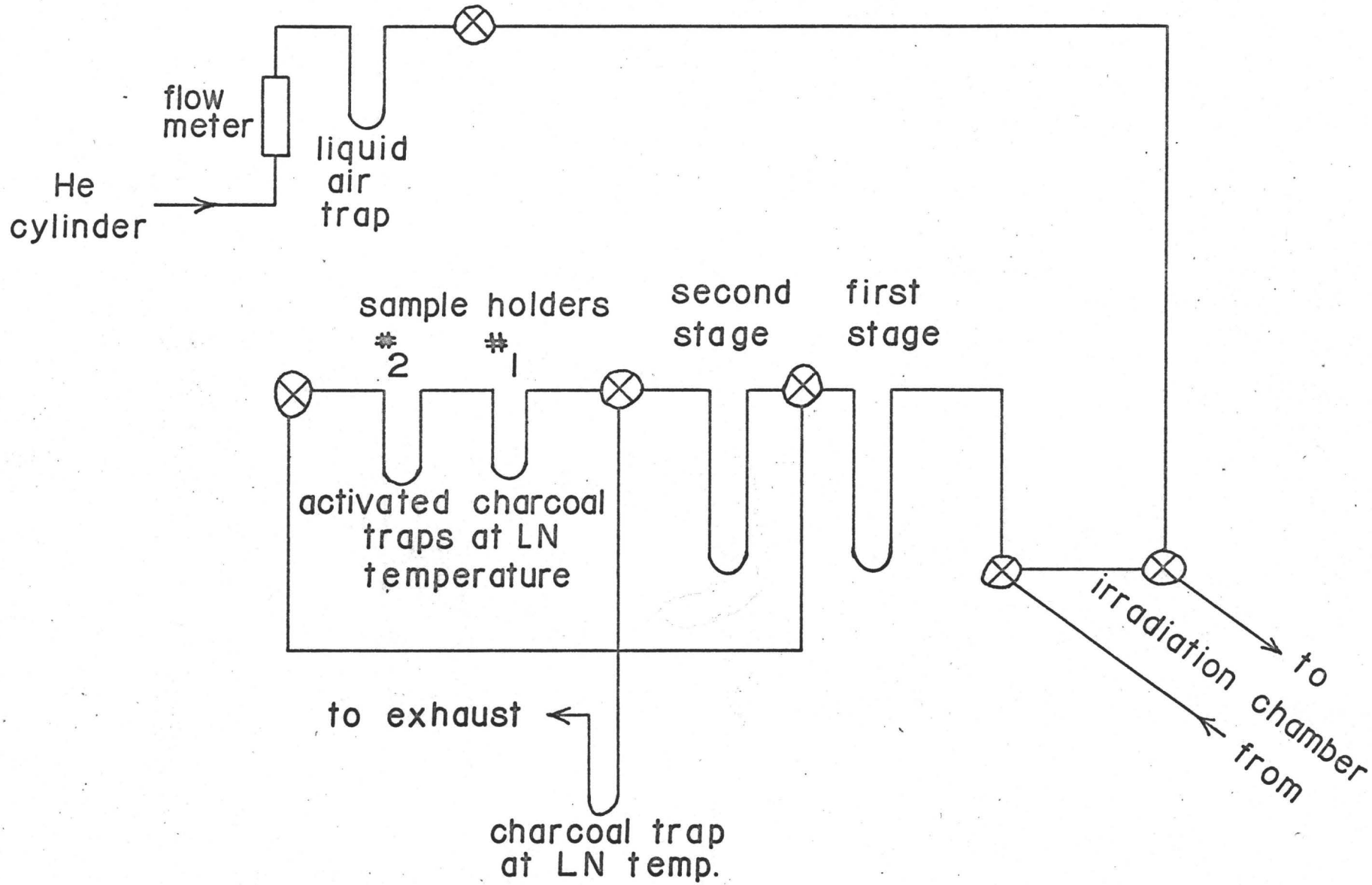

Sample Preparation Apparatus

FIGURE 3-6

Table 3-1

Krypton Beta Decay Chains

$^{91}Br \xrightarrow{\text{short}} {}^{91}Kr \xrightarrow{10\ s} {}^{91}Rb \xrightarrow{72\ s} {}^{91}Sr \xrightarrow{9.7\ h} {}^{91}Y$

$^{90}Br \xrightarrow{1.6\ s} {}^{90}Kr \xrightarrow{33\ s} {}^{90}Rb \xrightarrow{2.9\ m} {}^{90}Sr \xrightarrow{28\ y} {}^{90}Y$

$^{89}Br \xrightarrow{4.5\ s} {}^{89}Kr \xrightarrow{3.2\ m} {}^{89}Rb \xrightarrow{15\ m} {}^{89}Sr$

$^{88}Br \xrightarrow{16\ s} {}^{88}Kr \xrightarrow{2.8\ h} {}^{88}Rb \xrightarrow{18\ m} {}^{88}Sr$

$^{87}Br \xrightarrow{55\ s} {}^{87}Kr \xrightarrow{78\ m} {}^{87}Rb \xrightarrow{4.7\times10^{10}\ y} {}^{87}Sr$

$^{85}Br \xrightarrow{3\ m} {}^{85}Kr \xrightarrow{4.4\ h} {}^{85}Rb$

An enhanced source of ^{87}Kr was produced by the following procedure: an irradiation time of 2 minutes ($\sim$ 2 half-lives of ^{87}Br), a cooling down time of 1 minute ($\sim$ 4 half-lives of ^{88}Br), sweeping of the ^{88}Kr gas produced to exhaust and then waiting for 3 more minutes ($\sim$ 3 half-lives of ^{87}Br) before sweeping the ^{87}Kr gas sample to the first sample holder. The isotope ^{85}Kr appears as an undesirable contaminant but it has only two known gamma-decay lines of energy 150 keV and 305 keV which are easily identified. To produce an enhanced source of ^{88}Kr, an irradiation time of 15 seconds ($\sim$ 1 half-life of ^{88}Br and $\sim$ 1/4 half-life of ^{87}Br) was used. After a cooling time of 30 seconds ($\sim$ 2 half-lives of ^{88}Br and $\sim$ 1/2 half-life of ^{87}Br) the ^{88}Kr gas sample was swept into the cold activated charcoal sample holder. ^{89}Kr and its daughter product ^{89}Rb were major contaminants in such a sample but their effects could be removed

by allowing the sample to decay for 15 minutes (∿ 5 half-lives of ^{89}Kr). The remaining ^{88}Kr gas was then transferred to the second sample holder (at 77°K) by heating the first sample holder and sweeping with the helium carrier gas. The unwanted ^{89}Rb solid decay product was left behind in the first sample holder. The 18 minute ^{88}Rb activity could in turn be obtained by allowing the ^{88}Kr to decay for about two half-lives of ^{88}Rb and then warming up the second sample holder and sweeping with the helium carrier gas leaving the ^{88}Rb activity behind in the second sample holder. In obtaining samples as clean as possible without xenon contamination the first and second separation stages were periodically flamed to remove any contaminants adsorbed to the glass walls.

The samples produced as described above were adequate for single parameter gamma-ray spectroscopy using a Ge(Li) detector. However the need for thin sources for beta-ray studies necessitated a different source preparation procedure. The ^{88}Rb activity was obtained by flushing ^{88}Kr gas into a small brass chamber 2.5" in diameter and 2" in length and electrostatically collecting the ^{88}Rb on a .001" thick, 1/2" diameter brass disc held at -200 volts potential. Collection was continued until the activity was adequate for the beta-singles runs or the beta-gamma coincidence runs. In obtaining beta singles and beta-gamma coincidence results for the two krypton isotopes it was important to remove the rubidium daughter products as

quickly as they are produced. This was done using a travelling charged wire counting chamber as described by Archer[81]. The krypton gas sample was initially flushed into the charged wire counting chamber which consisted of a cylinder made of .001" brass sheet 2-1/2" long and 1/2" in diameter. A window cut in the side of the chamber towards the beta-counter was covered with gold-coated mylar. Rubidium decay products were then removed by means of a .030" tinned copper wire which was moved continuously through the centre of the chamber and charged at -200 volts. This method of removing decay products was $\sim$ 75% efficient.

CHAPTER 4

DATA ANALYSIS

4-1 Ge(Li) Spectrometer Response

The gamma radiation characteristic of an isotope undergoing radioactive decay or thermal neutron capture is initially investigated by collecting a gamma-ray singles spectrum. The information which can be obtained from the singles spectrum is a set of energies and intensities of the gamma rays emitted by this nuclide. To obtain the maximum quantity and quality of data possible, a good resolution Ge(Li) detector is used in conjunction with a linear preamplifier, amplifier and ADC system. The pertinent information can be obtained from the raw data only by a good understanding of the response of a Ge(Li) detector to a gamma-ray of energy E.

The measured spectrum M(x) is a convolution of the true spectrum which can be considered to be an assemblage of delta functions, a_i, and the response function $R(x,y_i)$,

$$M(x) = \sum_i R(x,y_i)a_i \ .$$

Here the response function $R(x,y_i)$ can be considered to be

the convolution of a Gaussian and the complete spectral form arising from the interaction of a gamma ray of energy y_i,

$$R(x;y_i) = \int G(x,x')\ L(x',y_i)dx' \ .$$

The problem with which one is confronted then is to unfold the measured spectrum[102] to obtain the true spectrum of delta functions. Only a complete understanding of the salient features of the function L(x,y) permits one to correctly interpret the complex measured spectra.

The nature of the function L(x,y) is determined by the energy and hence interaction mechanisms of prominence, the detecting material and the detection mechanism, and the geometry and volume of the detector. Whereas a high Z material such as NaI(Tl) favours photoelectric and pair production events, a medium Z material such as germanium enhances Compton events as well. The inefficiency of scintillation counters ($\sim$ 100 eV/photon) results in much poorer resolution than that obtained with solid state detectors ($\sim$3 eV/carrier). The dimensions and configuration of the detecting material considerably affect the nature of the line shape. Large active volumes enhance full energy deposition since multiple interactions can occur. Geometry and volume are important as the collection of all energy present requires the stopping of the electron within the active volume.

Figure 4-1 illustrates the form of L(x,y) for a Ge(Li) counter for a single gamma ray having an energy of $\sim$ 3 MeV. In part (a) of the figure, the photo-peak, Compton distribution and the back-scatter peak are depicted. Part (b) of the figure shows the double escape peak, the single escape peak, the full energy peak and all of the associated Compton distributions. A 511 keV spectrum arises from interactions in the source. The full energy peak results because of the finite probability of detecting the e^--e^+ pair and the two associated annihilation gamma rays simultaneously. Figure 4-1(c) shows the form of the complete line shape L(x,y). Coincident summing events are quite negligible in a Ge(Li) spectrum[103].

The photo peak and double escape peaks being the predominant response peaks are the most useful ones for determining a set of energies and intensities for a spectrum. However for relatively intense gamma rays all three main peaks, namely the double escape, single escape and photo-peaks can be useful for energy calibration purposes as their common energy difference is $m_o c^2$.

In order to obtain the energy of a gamma ray line one must determine accurately the channel positions of the response peaks. The position of a peak depends on many variables which cannot always be controlled by the experimenter. Normally it is expected that the single escape and double escape peaks

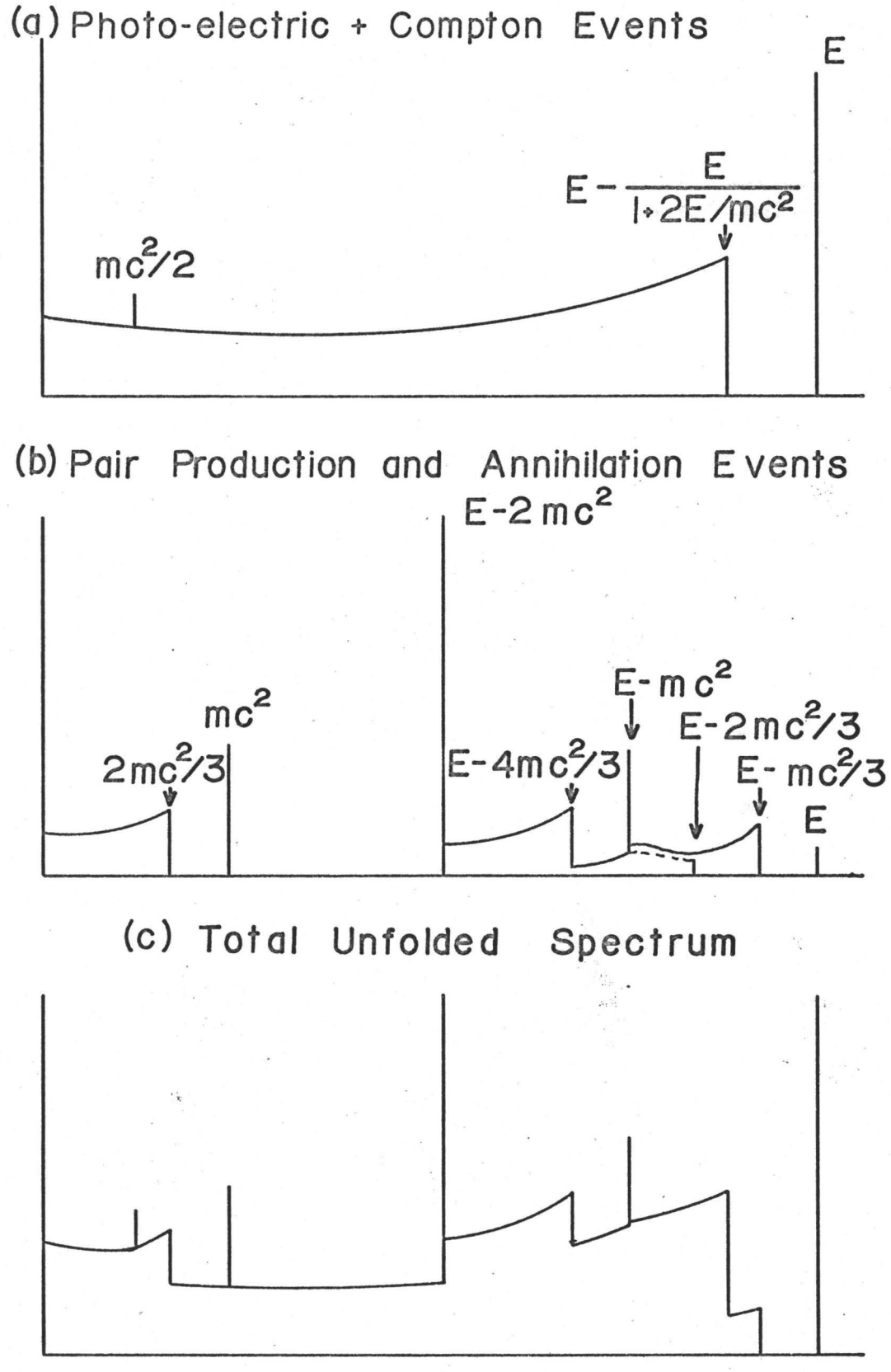

Response of Ge(Li) Detector to Gamma Ray of Energy E

FIGURE 4-1

should have a good Gaussian response shape. However for a large volume counter in which the collection properties are poor there is a large contribution of events near zero energy both for low energy gamma rays and for the 511 keV gamma rays. Hence when the response of a pair event (single escape or double escape) is convolved with the response of one or two 511 keV gamma rays there is a resultant shift in the single escape and double escape peak positions to higher channel numbers and hence apparently high energies. Thus there is no longer a 511 keV difference between the double escape and single escape peaks or between the single escape and photo-peaks. In extreme cases, it has been found that a direct comparison between photo-peak and double escape peak energies may lead to systematic errors of the order of 1 keV[104]. Fortunately this effect is negligible for counters with good collection properties such as small volume wrap-around and planar counters. Poor collection properties in a counter also manifest themselves in the skewness of a peak, usually to the low energy side. This effect may be the result of operation of a counter at insufficient voltage or as a result of the lifetime of the carriers being too short so that all electron-hole pairs created are not collected before being trapped or recombined. On the other hand if too much voltage is applied to a detector the peaks will tend to have poorer

resolution as the leakage current of the detector and connectors will increase creating more electronic noise. Thus it is imperative to determine the optimum operating voltage empirically for each Ge(Li) detector. High count rates will also tend to deteriorate the resolution but this can usually be compensated for by proper pole zero cancellation and DC restoration of the amplifier output. It has been shown recently[105] that the geometry of the source and counter can have a measurable effect on peak position. This effect depends on the fact that photo-electrons are accelerated or decelerated by the application of an electric field depending on the polarity of the field. The resultant shift in photo-peak position depending on geometry is another source of error when comparing double escape peak and photo-peak positions. Photo-peak energy shifts of as much as 0.4 keV[105] have been measured due to this effect.

4-2 Energy Calibration of Ge(Li) Spectrometer

The precision of energy estimates is determined by one's ability to obtain the centroid of spectral peaks. The simplest technique for determination of the peak centroid is through visual observation. Generally one can determine the position of a peak to within a factor of about two of the statistical error associated with fitting the peak shape to a Gaussian peak. One can also calculate the centroid of a

peak by means of the first moment after correction for background interference. However this technique is only reliable if the peak is not skewed. The non-linear least squares Gaussian fit to a peak provides one of the most reliable and accurate methods of finding the peak centroid. Here the peak is fitted to a channel-integrated Gaussian peak, with three unknown parameters,

A - peak area

σ - sigma of peak position

and x_o - peak position

riding on a linear background with two unknown parameters a and b,

$$y_i = \frac{A}{\sqrt{2\pi\sigma^2}} \int_{i-\frac{1}{2}}^{i+\frac{1}{2}} \exp - \frac{(x-x_o)^2}{2\sigma^2} \, dx + \int_{i-\frac{1}{2}}^{i+\frac{1}{2}} (ax+b)\,dx.$$

Here y_i is the number of counts in channel i. The uncertainty in the peak position, x_o, is then $\sigma/\sqrt{A}$. More sophisticated attempts have been made such as the use of a skewed Gaussian model to take account of any asymmetry in the peak shape. However it has been found that the use of extra parameters is usually not warranted since there are too many systematic errors which obscure any noticeable improvements in precision gained by this technique. Another method for peak fitting has recently

been proposed[106] involving fitting of the peak and the linear background to a series of Hermite polynomials,

$$y_i = \int_{i-\frac{1}{2}}^{i+\frac{1}{2}} (ax+b+c_o H_o + c_1 H_1 + c_2 H_2)dx.$$

The Hermite polynomials are functions of the parameters A, σ and x_o. These unknown parameters can be calculated from a first estimate of these parameters using the fact that the polynomials are orthogonal. Provided that the initial guesses at the unknown parameters are realistic, a convergent solution can be arrived at in one iteration. This compares with up to ten iterations required to reach a convergent solution for the non-linear least squares Gaussian fit. In this thesis the "centre of gravity" and the visual methods were used in most cases and found to give very little error. In some cases a non-linear least squares Gaussian fit was employed. However it has been found that although one may be able to determine a peak position with good precision the peak position may still have systematic errors associated with it which are larger than the errors inherent in using any of the techniques outlined above.

Having determined the peak positions one must now determine the transformation from channel position to absolute energies. Ideally this transformation is linear but in practice it never is. The linearity of response of a Ge(Li) detector,

preamplifier and amplifier system is usually very good, the differential linearity being less than .01%. However the ADC is frequently the most non-linear component of the total system. The linearity of a system is often measured using an accurate and calibrated sliding pulser. The pulser must have a non-linearity much less than that of the system to be measured. This technique has the disadvantage that the set of calibrated peaks in the spectrum must be accumulated one at a time. Thus if the gain of the system varies slightly as a function of temperature and time, some peak positions may be shifted somewhat independent of the linearity of the system. A method has been developed in this laboratory[107] for measuring the non-linearity of an ADC, which is independent of the linearity of the pulser and independent of any instabilities in the system. The technique consists of triggering a pulser at a set of n voltage steps in which each step is greater than the previous one by a nominally equal voltage increment. This set of triggering voltages is applied many times for an interval of about one quarter of a second during which counts are accumulated in a series of n peaks. Then a zero offset is applied to the ADC automatically and the pulser repeats the sequence for the same time interval so that during this period counts are accumulated in a series of n peaks which are nominally ΔV volts distant from the previous series. The variation of ΔV versus channel number then provides a measure of the non-linearity of the system.

This technique was accurate enough to measure the differential linearity to a precision of one part in five thousand. Systematic deviations in the differential linearity were easily recognized in this manner so that the form of the transformation of peak position to energy could be determined accurately as a function of channel number. For most 4^K ADC's it was found that the differential linearity could be approximated quite well for the upper 3500 channels by the form, $\frac{dE}{dI} = b + 2cI$ so that the energy was given by

$$E = a + bI + cI^2$$

where I is the channel position of the peak and a, b and c are the parameters to be determined.

In the energy range below 3 MeV it is possible to use the "mixed source" technique to determine the parameters a, b and c and hence the energies of the unknown lines. Using this method the spectra of certain standards and of the unknown source are accumulated concurrently. Then using the strong peaks of the standards as energy calibration points, the parameters a, b and c are determined by linear least squares fitting techniques and hence the energies of the lines of the source being determined can be calculated from the resulting transformation. Energies of the stronger gamma rays have been determined with errors of less than a tenth of a keV below 3 MeV using this technique. The energies of the gamma-ray standards used in this work are listed in Table 4-1.

TABLE 4-1

Calibration Gamma-Ray Energies, 0-3 MeV

Isotope	Energy (keV)	Error (keV)	Reference
^{152}Eu	121.79	0.03	108
^{152}Eu	244.64	0.08	109
^{203}Hg	279.16	0.02	110
^{152}Eu	344.34	0.23	109
Annihilation	511.006	0.002	111
^{137}Cs	661.595	0.076	112
^{208}Tl	583.139	0.023	113
^{54}Mn	834.84	0.07	114
^{56}Fe	846.8	0.6	115
^{88}Y	898.01	0.07	114
^{65}Zn	1115.51	0.07	114
^{60}Co	1173.226	0.040	113
^{22}Na	1274.50	0.07	114
^{41}A	1293.76	0.14	116
^{60}Co	1332.483	0.046	113
^{24}Na	1368.526	0.044	113
^{28}Al	1778.70	0.17	116
^{88}Y	1836.08	0.07	114
$H(n,\gamma)D$	2223.28	0.15	117
^{208}Tl	2614.47	0.10	113
^{24}Na	2753.92	0.12	113

Above 3 MeV gamma-ray energies are not known with the same precision as those listed in Table 4-1. Thus in order to calibrate the spectrum above 3 MeV it becomes necessary to extrapolate beyond the known standard gamma-ray energies. However it is possible to use the fact that the double- and single-escape peaks, and the single escape peak and photo-peak of the gamma-ray response function are separated by 511 keV to determine the slope of the energy versus channel curves in the high energy region. In neutron capture gamma-ray spectra the identification of a cascade and an associated crossover transition can yield an accurate energy difference provided that one of the cascade members has an energy below 3 MeV and hence can be calibrated against accurate standards. The $^{28}Si(n,\gamma)^{29}Si$ reaction provides an excellent means of determining energies in the region above 3 MeV since the capture state of ^{29}Si decays by a few very strong two and three step cascades. The strong silicon gamma rays below 3 MeV were calibrated using the energy standards listed in Table 4-1. The 3.54 MeV line was calibrated by measuring the energy of its double escape peak with respect to the photo-peaks of the 2754 keV gamma ray emitted in the beta decay of ^{24}Na and the 2614 keV gamma ray emitted in the beta decay of ^{208}Tl. A regression analysis was used to determine the value for the high energy gamma-ray transitions. For this analysis an initial estimate of the Q-value was used so that all the gamma-ray energies could be

placed on an energy basis. The best estimate for the value of a high-energy gamma ray is then given by,

$$\bar{E}_j = E_j + \delta$$

where E_j is the energy deduced from the initial Q-value . The parameter δ is the correction to the initial estimate and its value is determined from the regression analysis. The model equation used was,

$$E_j = a + bI_j + cI_j^2 + S(I_j)$$

where $S(I_j)$ is a step function defined as,

$$S(I_j) = 0 \qquad ,I \leqslant I_M$$

$$S(I_j) = \delta \qquad ,I > I_M$$

and I_M is the channel number corresponding to the highest energy gamma ray which was calibrated against a standard. The residuals squares, R^2, was computed for all gamma rays involved in cascades from the capture state for each initial estimate of Q in steps of 0.1 keV. The residual squared is related to Q by the equation[118],

$$R^2 - R_o^2 = (Q-Q_o)^2/C_{mm}$$

where Q_o is the least-squares estimate of the separation energy and C_{mm} the variance in Q_o. This relationship between R^2 and Q is depicted in figure 4-2. From the parameters a value of $Q_o = 8473.8 \pm 0.87$ keV was determined taking the recoil energies of the transitions into consideration. The energies of the strong transitions observed as obtained using the above value for

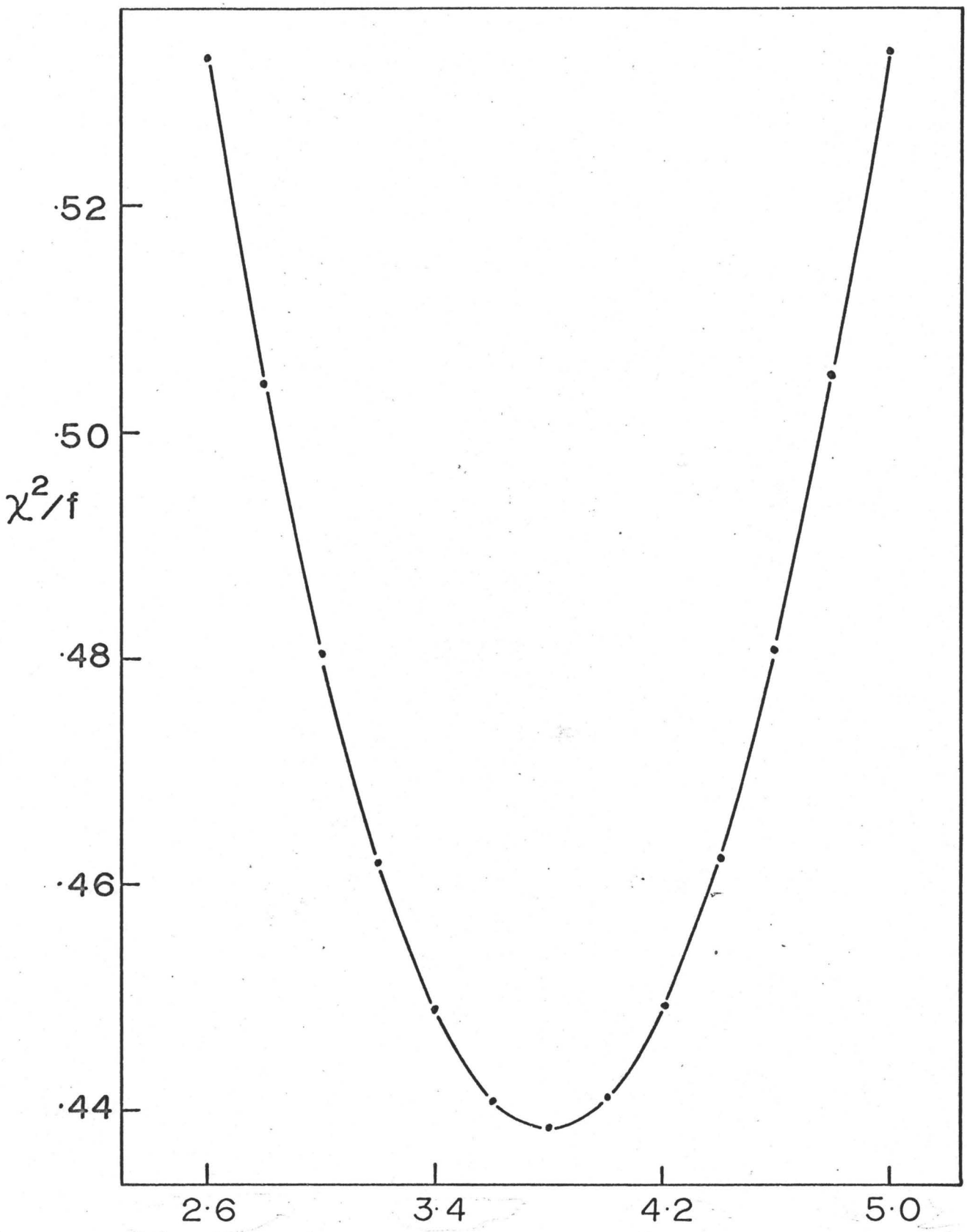

FIGURE 4-2

TABLE 4-2

$^{28}Si(n,\gamma)^{29}Si$ Calibration Energies

Energy (keV)	Error (keV)
8471.8	1.0
7199.8	1.0
6380.9	1.0
5108.3	1.0
4933.9	1.0
3539.0	0.5
2092.0	0.5
1273.0	0.5

the neutron separation energy are listed in Table 4-2. These silicon gamma-ray energies were then used as calibration standards over the whole spectral energy range from 1 to 8.5 MeV.

4-3 Intensity Calibration of Ge(Li) Spectrometer

In order to obtain either the relative or absolute transition probabilities or intensities of the gamma rays emitted by a nucleus it is necessary to calibrate each Ge(Li) spectrometer used for its detection efficiency as a function of energy. The intensities, I_i, are related to the measured areas, $A_i(k)$, of the response peaks by the relationship,

$$A_i(k) = \varepsilon(E,k) I_i$$

where $\varepsilon(E,k)$ represents the detector efficiency as a function of energy and the parameter k refers to the type of response

peak, double escape or photo-peak, as these are the predominant response peaks in any spectrum. The efficiency curves were obtained using well-known standards whose decay modes are known. Table 4-3 lists all the intensity standards used to determine the energy dependence of the efficiency curves. Part (a) of the table lists the set of calibrated gamma ray sources from the International Atomic Energy Agency used to calibrate the photo-peak efficiency below about 1.8 MeV. Among the other sources used as listed in Part (b) ^{152}Eu emits some intense gamma rays over the energy range 122 keV to 1408 keV and thus provides another useful calibration standard in the low energy region. The ^{24}Na source provides a convenient means of extending the photo-peak efficiency curve to 2.75 MeV. The three gamma rays of energy 1836, 2614 and 2754 keV provide a method of relating the low energy portion of the double escape peak efficiency curve to the photo-peak efficiency curve as the areas of the double escape and photo-peaks are of the same order of magnitude in this energy range. The gamma-ray corresponding to the deuteron binding energy is another one that can be used to relate the two curves. Above 3 MeV the double escape peak is the predominant response peak. The gamma rays associated with the neutron capture reaction are sufficiently intense and numerous that they may provide some suitable calibration standards in the energy range above 3 MeV. The $^{28}Si(n,\gamma)^{29}Si$ [104] and the $^{32}S(n,\gamma)^{33}S$ [124] reactions are ideal for this purpose

TABLE 4-3

Intensity Standards used for calibrating Ge(Li) Detector Efficiency

(a) Set of Calibrated Gamma Sources (IAEA)

Source	Activity (μC) as of Jan.1/ 68	Half-life	Energy (keV)	Gamma-rays per Disintegration (%)	Reference
^{57}Co	10.75	271.6 ±0.5d	121.97	85.3 ±1.5	119
			136.33	11.2 ±1.2	
^{203}Hg	21.68	46.57 ±0.03d	279.15	81.55±0.15	120
^{22}Na	11.07	2.602±0.05y	511.006	179.7 ±0.8	31
			1274.52	99.9 ±0.02	
^{137}Cs	10.27	30.6 ±0.4y	661.595	85.9 ±0.9	120
^{54}Mn	11.01	312.7 ±0.3d	834.75	100.00	121
^{60}Co	10.75	5.264±0.005y	1173.24	99.87±0.012	122
			1332.48	100.00	
^{88}Y	9.77	107.4 ±0.8d	511.006	0.50±0.02	123
			897.95	93.5 ±0.7	
			1836.10	99.5 ±0.1	
			2734.05	0.56±0.03	

(b) Other Sources Used

Source	Energy (keV)	Relative number of gamma rays per disintegration	Reference
^{24}Na(15 hr.)	1368.53	100.0	31
	2753.92	100.0	
^{208}Tl	2614.47	100.0	31

(continued next page)

Source	Energy (keV)	Relative number of gamma rays per disintegration	Reference
^{152}Eu(12yr.)	1408.0	22.0	31
	1113.0	14.0	
	1087.0	12.0	
	965.0	15.0	
	869.0	4.1	
	779.0	14.0	
	444.2	4.0	
	411.2	2.2	
	344.4	27.0	
	244.7	8.0	
	121.79	24.5	

(c) Neutron Capture Gamma-Ray Standards

Reaction	Energy (keV)	Relative Intensity	Reference
$^{1}H(n,\gamma)^{2}H$	2223.28	100.0	117
$^{28}Si(n,\gamma)^{29}Si$	8471.8	2.7 ± 0.2	104
	7199.8	10.0 ± 1.0	
	6380.9	14.5 ± 1.0	
	5108.3	4.5 ± 0.4	
	4933.9	61.0 ± 3.0	
	3539.0	64.0 ± 3.0	
	2092.0	20.0 ± 2.0	

(continued next Page)

Reaction	Energy (keV)	Relative Intensity	Reference
$^{32}S(n,\gamma)^{33}S$	8646	2.5 ± 0.5	124
	7804	4.1 ± 0.6	
	5586	1.7 ± 0.0	
	5425	61.0	
	5051	3.5 ± 0.5	
	4874	12.8 ± 1.0	
	4640	1.4 ± 0.3	
	4432	5.0 ± 0.4	
	3726	3.4 ± 0.3	
	3370	5.5 ± 0.6	
	3221	23.5 ± 1.6	
	2931	16.0 ± 1.1	
	2753	4.5 ± 0.5	
	2379	43.9 ± 3.3	
	842	69.5 ± 5.3	

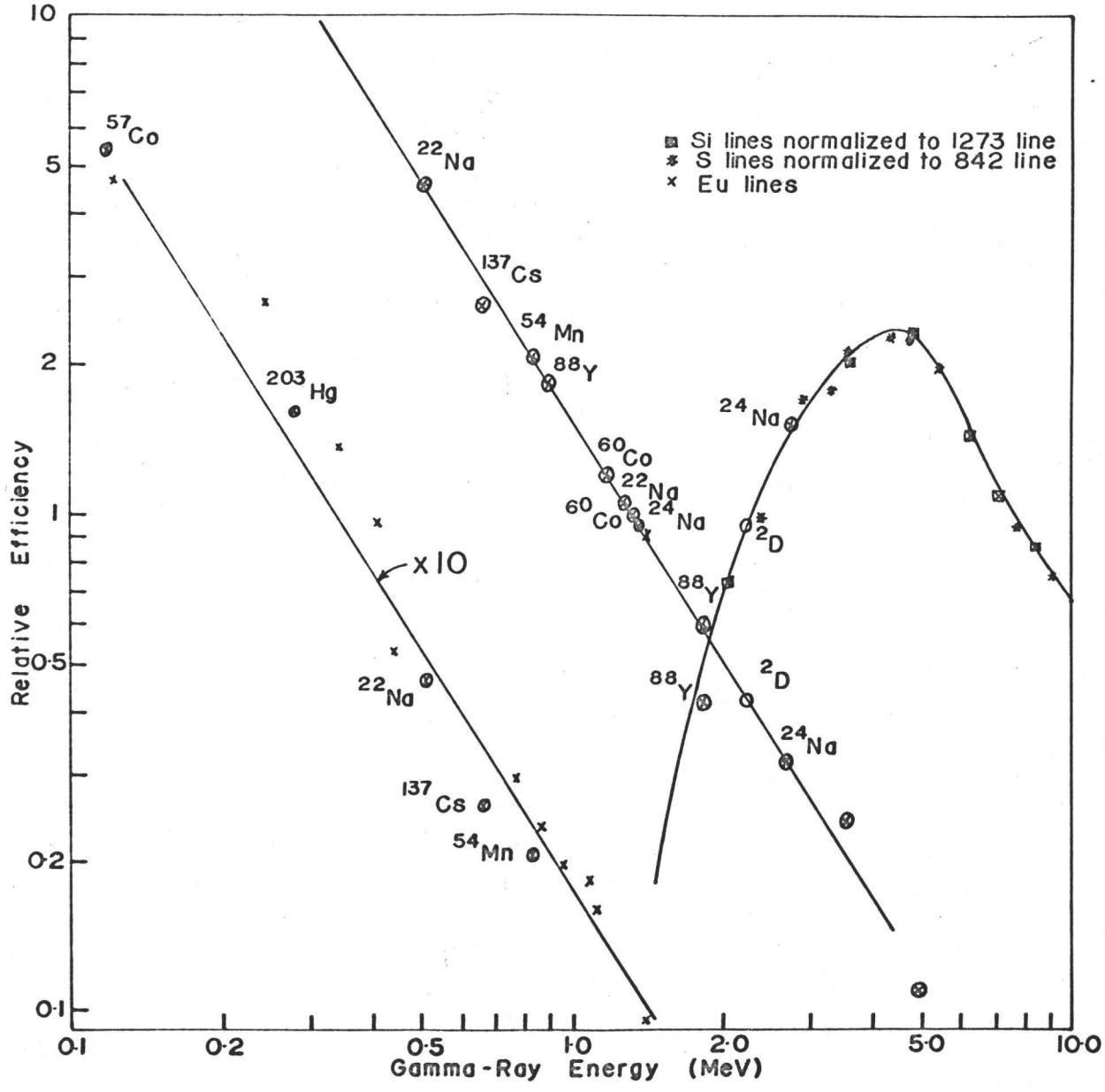
Si lines normalized to 1273 line
S lines normalized to 842 line
Eu lines
57Co
22Na
137Cs
54Mn
88Y
203Hg
60Co
22Na
24Na
2D
x 10
Relative Efficiency
Gamma-Ray Energy (MeV)
10
5
2
1
0·5
0·2
0·1
0·1
0·2
0·5
1·0
2·0
5·0
10·0

FIGURE 4-3

since they each have simple well-known decay schemes and very strong gamma rays in the region 3 to 8.6 MeV as well as some strong low energy gamma rays which can be used to relate the two efficiency curves. The form of the efficiency curves is shown in Figure 4-3 on a log-log plot. It was found that the curves were very well fitted by the following analytical expressions,

$$\varepsilon(E,pp) = a_o E^{-n_o}$$

$$\varepsilon(E,de) = a_1 \exp(-b_1[\ln(c_1/E)]^{n_1}) \quad E < c_1$$

$$= a_2 \exp(-b_2[\ln(E/c_1)]^{n_2}) \quad E > c_1.$$

It should be noted that,

$$\varepsilon(E,se) = \text{constant} \times \varepsilon(E,de)$$

since the probability of detection of a single escape event is the product of the probability of detection of a double escape event and the probability of detection of a 511 keV gamma ray, the latter probability being a constant for a given counter.

4-4 Singles Spectra Collection and Reduction

The procedure used to collect a singles spectrum and to enable easy interpretation of the data varied with the length of run desired and the stability of the system. For short runs of an hour or two the system was usually stable enough to allow

uninterrupted collection of the data without the use of any spectrum stabilization. In collecting a long run there are frequently drifts in the gain and zero of the system corresponding to a shift in a peak position of as many as 3 or 4 channels. This is intolerable if the width of the peak is of this order. One solution is to use the digital spectrum stabilizers but this was rarely done as these tend to contribute to the deterioration of the peak resolution obtainable. Instead long runs were collected in 80-minute successive intervals during which there is no appreciable gain or zero change. After each 80 minute interval the data collected were automatically dumped onto magnetic tape, the 4^K section of memory cleared and the collection of another 80-minute run was initiated. This process was cycled for up to three days at a time. The result was n 80-minute dumps stored on magnetic tape. The procedure used to collect all of the data into one spectrum was to shift the last n-1 dumps so that they all had the same zero and gain settings as the first dump. The zero and gain parameters were determined for each dump by fitting a straight line through the peak positions of two prominent peaks in the spectrum, one at the low-energy end and the other at the high-energy end. The spectrum contained in each dump was then shifted so that each had the same zero and gain parameters as those of the first dump. Having shifted all the dumps properly, the individual spectra were then collected into one

single spectrum which could then be analyzed.

Before analysis of a spectrum it was sometimes desirable to make further adjustments to the spectrum. One adjustment often made was to smooth the spectrum in order to bring any isolated high or low points back into a smoothly varying function. This involves replacing the contents of each channel by weighted fractions of the contents of itself and a few adjacent channels. The usual smoothing function applied was of triangular shape taking a quarter of the contents of the two adjacent channels and one-half of the contents of the channel of interest and putting the results back in the channel of interest, i,

$$C_i = \frac{1}{4} C_{i-1} + \frac{1}{2} C_i + \frac{1}{4} C_{i+1}.$$

This smoothing does not interfere with the resolution of the peaks as their widths are of the order of four or five channels. Peaks appear much more prominent after smoothing has been applied to a spectrum with poor statistics.

After smoothing a spectrum it is sometimes convenient to subtract off all background contributions such as Compton distributions and tails of peaks in order to have a resultant spectrum consisting ideally only of peaks. This was done by calculating a background function over successive intervals of width Δ which are more than four times wider than the energy resolution in the interval Δ. A polynomial was fitted through

the lowest channel contents in four successive intervals. The part of the polynomial function between the middle two intervals was used as a background function in that energy region. Stepping along one interval of width Δ the procedure was repeated to obtain a background function in the adjacent region. The resultant background function was a smoothly varying curve with no discontinuities. The background was then subtracted from the original spectrum leaving a clean spectrum of peaks only. This facilitates spectrum analysis considerably as far as determining peak positions and areas for the purpose of obtaining gamma-ray energies and intensities.

4-5 Two Parameter Data Analysis

The distribution of coincident events as determined by a pair of counters forms a two-dimensional matrix array, one dimension associated with counter A and the other associated with counter B. All coincidence experiments performed in this work used a Ge(Li) detector for counter A and a NaI(Tl) detector for counter B. A Ge(Li) counter was used in conjunction with a NaI(Tl) counter in order to take advantage of the good energy resolution of the Ge(Li) counter in the one dimension and the high efficiency of the NaI(Tl) counter in the other dimension. The use of two NaI(Tl) counters would have resulted in insufficient resolution for the gamma-ray spectra being studied whereas the use of two Ge(Li) counters would have resulted in insufficient counts in the two dimensional array. Using a Ge(Li)

spectrometer in conjunction with a NaI(Tl) spectrometer provided a compromise but presented a problem in data storage. Array sizes up to 16^K could be accumulated in the analyzer memory in real time, i.e. as the events were recorded. This array size was sufficient for low energy coincidence experiments requiring only 128 channels in each dimension or 64 channels in one dimension and 256 channels in the other dimension. However to cover a bigger energy range more channels were required in each dimension. It was then necessary to use address recording and sort the events either in the computer or on the analyzer at a later time as discussed in section 3-8.

As discussed in section 4-1, the measured singles spectrum in each dimension is related to the true spectrum by the relationships,

$$M(E_x) = \int R_A(E_x,E_x')S(E_x')dE_x'$$

and

$$M(E_y) = \int R_B(E_y,E_y')S(E_y')dE_y'$$

in the x and y dimensions respectively. In an analogous fashion the two-dimensional array can be represented by,

$$M(E_x,E_y) = \int R_A(E_x,E_x')R_B(E_y,E_y')S(E_x',E_y')dE_x'dE_y'.$$

In terms of a channel basis the equation can be rewritten as,

$$M(E_x,E_y) = \sum_{i=1}^{n_x}\sum_{j=1}^{n_y} Q_{ij}A_i(E_x)B_j(E_y)$$

where $$A_i(E_x) = R_A(E_x, E_i)$$

$$B_j(E_y) = R_B(E_y, E_j)$$

and n_x and n_y are the number of channels utilized in the x and y dimensions respectively. The purpose of the coincidence experiments then is to determine the coincidence quotients, Q_{ij}. This is difficult to do empirically unless the detector response is known over a wide energy range for both detectors A and B. The line shapes for the NaI(Tl) detector have been well determined[81] but the line shapes for the Ge(Li) detector have been more difficult to determine as they are very sensitive to geometry effects and counter characteristics. Also the large matrix size involved makes regression analysis difficult on all but the largest computers. Therefore one must usually be content with detecting only whether a certain coincidence relationship does or does not exist. This information can still be very useful in determining the decay modes of a nucleus. The absolute values of the coincident quotients are usually not necessary.

The usual technique of examining the coincidence relationships is to examine the spectrum in dimension x in coincidence with a fixed gamma-ray energy E_y in the y-dimension. The spectrum for a given E_y is defined by,

$$\beta_j(E_y) = \sum_{i=1}^{n_x} Q_{ij} A_i(E_x).$$

Similarly the spectrum for a given E_x is defined by,

$$\alpha_i(E_x) = \sum_{j=1}^{n_y} Q_{ij}\, B_j(E_y).$$

This distribution is referred to as the spectrum in coincidence with gamma rays of energy E_x in channel number i. The measured coincidence response surface can be rewritten in terms of these distributions, $\alpha_i(E_x)$ and $\beta_j(E_y)$ as,

$$M(E_x,E_y) = \sum_{i=1}^{n_x} \alpha_i(E_x)A_i(E_x) = \sum_{j=1}^{n_y} \beta_j(E_y)B_j(E_y).$$

In the coincidence experiments performed in this thesis, most of the useful information was obtained by examining the spectra in the Ge(Li) dimension. The diagonal elements of this matrix are a measure of the chance contributions to the coincidence events.

4-6 Beta-Ray Spectral Analysis

The response of a plastic scintillator is very linear for beta rays over the energy range studied in this thesis. In order to put energy on an absolute basis the beta spectra of ^{90}Y, ^{90}Sr, ^{106}Rh, ^{83}Cl and ^{91}Y [125] were used as calibration sources. To determine the end-point energies of unknown beta-ray groups it is necessary to determine the channel intercept of the beta spectrum. However some effects must be taken into consideration in order to estimate the end-point energy accurately. One effect which will tend to extend the end-point of a

beta spectrum is that of beta gamma coincidence summing. This can be minimized by using a thin plastic detector. Random beta-beta summing will also extend the end-point of a beta spectrum. This can be reduced by using a weaker source since the effect is proportional to the square of the beta counting rate as beta-ray transitions are not correlated. A third effect which will extend the beta end-point energy is the Gaussian resolution function which is convolved into the true beta-ray spectrum. This effect can be removed by the unfolding process as discussed below.

The response of a plastic counter to a beta-particle of energy E_o is given by,

$$R(E,E_o) = \int L(E,E')G(E',E_o)dE'$$

where

$$L(E,E_o) = \frac{k_o + \delta(E-E_o)}{k_oE_o+1} \qquad E \leq E_o$$

$$= 0 \qquad E > E_o$$

and

$$G(E,E_o) = \frac{1}{\sqrt{2\pi\sigma_o^2}} \exp\left[- \frac{(E-E_o)^2}{2\sigma_o^2} \right] .$$

Here the parameter k_o is independent of E_o according to Freedman et. al.[126]. The true spectrum for a beta transition of end-point energy W_o is given by,

$$S(E) = C_pE(W_o-E)^2F(Z,E)S_n(W_o,E)$$

where the symbols are defined in section 1-1. The Fermi plot of,

$$\sqrt{\frac{S(E)}{FS_n pE}} = C^{\frac{1}{2}} \ (W_o - E)$$

versus energy results in a straight line with intercept on the energy axis at W_o. However corrections can be made for the resolution function. Using matrix designation of the various measured and response vectors, an initial estimate S^1 can be made of the true spectrum. Then a second estimate can be obtained by means of the following iteration,

$$S^2 = S^1 + M - RS^1$$

where M is the measured spectrum and R is the response matrix. When many iterations are used to remove the Gaussian response the statistical deviations increase rapidly with each iteration. Methods have been developed by Slavinskas et.al.[127] to obtain an estimate of the true spectrum after only one iteration. The full response matrix is written as the product of a triangular matrix representing the tail part of the response and a Gaussian matrix,

$$R = LG.$$

The triangular matrix can be inverted in closed form. Then multiplying the measured spectrum by the inverse triangular matrix due to the tail, the Fermi plot of the spectrum is nearly linear and one has a good initial estimate for S^1. Then with one iteration to correct for the Gaussian response, one can obtain a very good estimate of the true spectrum and hence end-point energy.

To analyze a complex beta-ray spectrum, a stripping procedure was used in which the highest energy component was subtracted off first as only one beta-group contributes to the higher energy portion of the spectrum. In doing a complex analysis it was often helpful to have estimates of the end-point energies and of the intensities of each beta-ray component, since after the subtraction of each successively lower energy component the analysis became more nebulous. It was especially difficult to strip off low energy and low intensity components or two components with nearly equal end-point energies. It was usually only possible to obtain the shape of the first few high energy components as the shape factors are obscured for the low energy components.

In order to analyze a complex beta spectrum it was often easier to perform a beta-gamma coincidence gating experiment on particular gamma rays which are in coincidence with one or maybe two beta-ray components. This made the beta stripping analysis much simpler and more accurate.

Corrections can be made for random summing contributions at high count rates by recording the beta spectrum as a function of time. By plotting the number of counts per channel as a function of time it is possible to calculate the random summing contributions since the random count rate decreases twice as fast as the true singles rate as the random count rate is proportional to the square of the singles count rate.

Corrections for gamma-ray background can be made for each run by repeating the run with an aluminum absorber to stop all beta rays.

The log ft values of the beta transitions are important in determining the spins and parities of the levels populated in the final nucleus. In this thesis log ft values were determined using a nomogram[128]. The log ft value for a beta transition of energy E, total half-life t, and percentage of decay occurring in the mode under consideration p, is given by,

$$\log(ft) = \log(f_o t) + \log(C) - \log(p/100)$$

where $\log(f_o t)$ is determined from the nomogram and log(C) is determined from a graph[128]. The correction term log(C) is a function of atomic number Z and beta end-point energy, E.

4-7 Decay Scheme Construction Through Use of Computer Program

Fitting together a decay scheme can pose quite a chore when the number of gamma rays is large and not very many decay chains are known. Ideally coincidence and intensity relationships should be adequate to fit together a decay scheme but when these are not available one must rely completely on energy relationships. The scope of the problem can be realized when one considers that n gamma rays can be combined in $n(n-1)/2$ possible two-step cascades and in general can be combined in $\frac{n(n-1)\ldots(n-x+1)}{x!}$ possible x-step cascades. When only NaI(Tl)

spectra were available one could possibly have to consider up to 40 gamma-ray transitions in a decay scheme, but with the resolving power of the Ge(Li) spectrometer it has become common to deal with a few hundred transitions. Thus the number of combinations can become quite large and only the use of a fast large memory computer can provide the computational ability to calculate and examine all of the possible combinations.

It is necessary here to distinguish between three basically different decay scheme problems with which one may be confronted. The first type of problem involves a nucleus in which no levels are known and the decay scheme must be constructed from scratch. This is analogous to the problem in atomic spectroscopy which was solved using the Ritz combination principle involving common differences. Hamermesh et. al.[129] attempted to use a variant of this technique to construct a decay scheme for the low-lying levels of ^{198}Au using the energies of the low-energy gamma rays from the thermal neutron capture reaction on ^{197}Au as measured by a bent-crystal spectrometer. A "most probable" level scheme for ^{198}Au was generated containing 25 levels without the constraints provided by high-energy gamma rays from the capture state. However later work by Johnson et.al.[130] on the high energy gamma rays of ^{198}Au proved the "probable"

decay scheme completely erroneous. The reason for this erroneous fit was no doubt that Hamermesh et.al. had no known levels to start with. Thus if the first few levels generated by the program were incorrect all further levels would also be erroneous. Sumbaev et.al.[131] used a technique similar to Hamermesh et.al.[129], for the low lying levels of ^{104}Rh, but employed common sums as well as common differences. The use of common sums tends to reduce errors. Fortunately a few levels were known and a decay scheme consisting of 38 of the 193 low-energy gamma rays measured by a bent-crystal spectrometer were fit into a consistent decay scheme with a good probability of being correct.

The second type of decay scheme construction problem which can be distinguished is that involving the decay of the capture state of a nucleus to the bound levels in a nucleus which are known from another reaction such as the analogous (d,p) reaction. In this case one considers only the possible decay chains de-exciting the capture state which populate known levels. Normally there are many ambiguous chains to consider and it is useful to have a computer to keep track of all the possible chains and remove all the cascades which do not fit between the energy levels. Johnson[132] wrote a computer program to construct a decay scheme given all the energy levels and gamma-ray energies of a neutron capture

gamma-ray spectrum. This program tested all energy and coincidence relationships and formed a unique core of transition assignments. The remaining number of ambiguous chains were reduced by selecting the chains using the following order of criteria,

(1) most coincidence relationships per chain

(2) least number of gamma rays per chain

and (3) the chain with the most intensity.

Having moved this chain to the core transitions, the remaining number of ambiguous chains could be reduced accordingly. The final decay scheme was the one achieved when no ambiguous decay chains remained.

The type of decay scheme construction problem encountered in this thesis is of the third type in which there are some known levels but not enough to account for all of the gamma rays observed. A program DCYSCH was developed to fit gamma-ray transitions to the known excited levels of a nucleus for a thermal neutron capture reaction specifically. A second program COMB was developed to deduce other level energies based on combinations of gamma rays and known levels in the nucleus. A similar program to COMB was successfully used by Helmer and Bäcklin[133] to deduce new levels in ^{149}Pm populated in the beta decay of ^{149}Nd. The programs DCYSCH and COMB were developed specifically for neutron capture decay scheme con-

struction but can easily be modified for beta-decay schemes. Flow charts for these programs are included in Appendix A.

The problem then is to construct a consistent decay scheme given a set of gamma-ray transition energies,

$$\{T_i\} \ , \ i = 1,n$$

with an associated set of errors,

$$\{\Delta T_i\} \ , \ i = 1,n$$

and intensities,

$$\{I_i\} \ , \ i = 1,n$$

and a set of known energy levels,

$$\{L_j\} \ , \ j = 1,\ell$$

and their associated set of errors,

$$\{\Delta L_j\} \ , \ j = 1,\ell.$$

The gamma rays also have associated with them a set of coincidence relationships,

$$\{C_{ik}\} \ , \ i = 1,n),k = i+1,n$$

defined such that C_{ik} is non-zero only if gamma ray T_i has been detected in coincidence with gamma ray T_k. These coincidence relationships provide valuable constraints on the possible gamma-ray assignments in the decay scheme. However it is often difficult or impossible to obtain the non-zero elements of $\{C_{ik}\}$ especially for the weaker gamma rays as counting statistics improve as the square root of counting

time. Therefore it becomes necessary to rely on the energies and intensities of the gamma rays. The intensities are usually difficult to measure with great accuracy and the possibility of missing weak or unresolved transitions makes intensity balance across a level only a rough indication of the correctness of transition assignments. Hence one is forced to rely almost entirely on gamma-ray energy relationships. These relationships are limited entirely by the measurement errors $\{\Delta T_i\}$. For instance the number of chance crossover transitions of the type,

$$T_k = T_i + T_j$$

increases as the measurement error. The number of such crossover conditions was calculated by computer for the 168 gamma rays listed in Table 6-2 and a randomized set of 168 gamma rays as well as a function of the parameter α in the error expression,

$$\alpha(\Delta T_i^2 + \Delta T_j^2 + \Delta T_k^2)^{\frac{1}{2}} \quad .$$

Here α is the number of standard deviations within which the energy difference,

$$T_k - (T_i + T_j)$$

is permitted to close. The number of chance cross-over transitions can also be determined by calculating the fraction of the energy range covered by the errors. The number is then given by,

$$N_c = \sum_{i=1}^{i_{max}} \left[\frac{2\alpha N_i \sum_{j=i+1}^{j_{max}} \Delta T_{ijk}}{(T_n - 2\,T_i)} \right]$$

where N_i is the number of gamma rays in the energy range

$$T_i + T_{i+1} \leq T \leq T_n$$

and

$$\Delta T_{ijk} = (\Delta T_i^2 + \Delta T_j^2 + \Delta T_k^2)^{\frac{1}{2}} .$$

The sum over j is for all T_j satisfying,

$$2T_i < T_i + T_j \leq T_n$$

and the sum over i is for all T_i satisfying,

$$T_i + T_{i+1} \leq T_n .$$

The above formula for N_c is valid for any distribution of gamma rays and thus no a priori distribution need be assumed in order to calculate the number of chance crossovers. The results of the calculation of the number of crossovers by the three different methods as a function of the parameter α are summarized in Table 4-4. It is seen that the number of chance crossovers calculated for a random set of 168 gamma rays and by the formula for N_c agree quite well for corresponding values of α. The number of cross-over transitions calculated for the real set of gamma rays is almost the same as the number for a random set of gamma rays and thus it is impossible to fit together a decay scheme using only information from crossovers in the case of $^{87}Sr(n,\gamma)^{88}Sr$. For a

Table 4-4

Number of Crossovers for 168 Gamma Rays Listed in Table 6-2

α	Real Set	Random Set	N_c
0.25	193	192	195
0.5	411	401	391
1.0	787	784	783
2.0	1585	1590	1566
4.0	3191	3142	3132

value of $\alpha = 0.5$ the number of crossovers generated by the real set is slightly greater than for the random set indicating that most of the real fits are included for this value of α.

CHAPTER 5

BETA DECAY RESULTS

5-1 Singles Spectra of the Gamma Radiation

The gamma-ray energies and intensities for each of the isotopes under study were obtained from a detailed analysis of a series of singles spectra collected using various Ge(Li) counters. The particular counter used to obtain most of the results listed in this chapter was a 5 cc. active volume Ge(Li) detector capable of achieving an energy resolution of 6 keV at 2 MeV gamma-ray energy. The output pulses from the detector were fed into a Tennelec FET pre-amplifier and TC200 amplifier system and thence analyzed using a ND3300 analyzer system with a 4^K ramp ADC. Efficiency curves for this detector were obtained using the intensity standards listed in Table 4-3. The energies of the gamma-ray lines were determined using the mixed source technique. The energy versus channel relationship was obtained using the energy standards listed in Table 4-1. Of course there are also the built-in energy standards of the two ^{88}Rb beta decay lines at energies 898.0±.1 and 1836.1±.1 keV corresponding to the ^{88}Y positron decay line calibration standards[114].

5-1.1 Singles Spectrum of ^{87}Kr

The ^{87}Kr singles spectrum shown in Fig. 5.1 was collected over a period of 10 hours. A new ^{87}Kr source was prepared every two hours. The individual spectra obtained in a two hour period were stored on magnetic tape and then corrected for zero and gain shifts and added up on the McMaster 7040 computer facility. All of the lines belonging to ^{87}Kr are labelled with their respective energy values. The stronger lines from the decay of ^{88}Kr and ^{88}Rb are labelled as such as are the lines of some of the other main contaminants such as ^{135}Xe, ^{138}Xe, ^{138}Cs and ^{89}Rb. It was found to be almost impossible to remove all of the ^{88}Kr and ^{88}Rb isotopes without obtaining only a weak sample of ^{87}Kr. The gamma-ray energies and intensities of the $^{135}Xe(31)$, $^{138}Xe(81)$, $^{138}Cs(81)$ and $^{89}Rb(134)$ lines are well-known so that they pose no great problem in interpreting the spectrum. The ^{85}Kr contaminant is also quite prominent but its decay scheme is very simple. The removal of the ^{89}Rb contamination is possible as outlined in section 3-10 but it was not removed for the sake of maintaining a fairly high count rate.

The ^{87}Kr lines are easily identified by their relative intensities in different runs with sources containing various amounts of contaminants. The energy and

Figure 5-1(a,b) ^{87}Kr gamma-ray singles run. Lines are identified by their energy E, as: E"- double-escape peak, E' - single-escape peak, and E- photopeak.

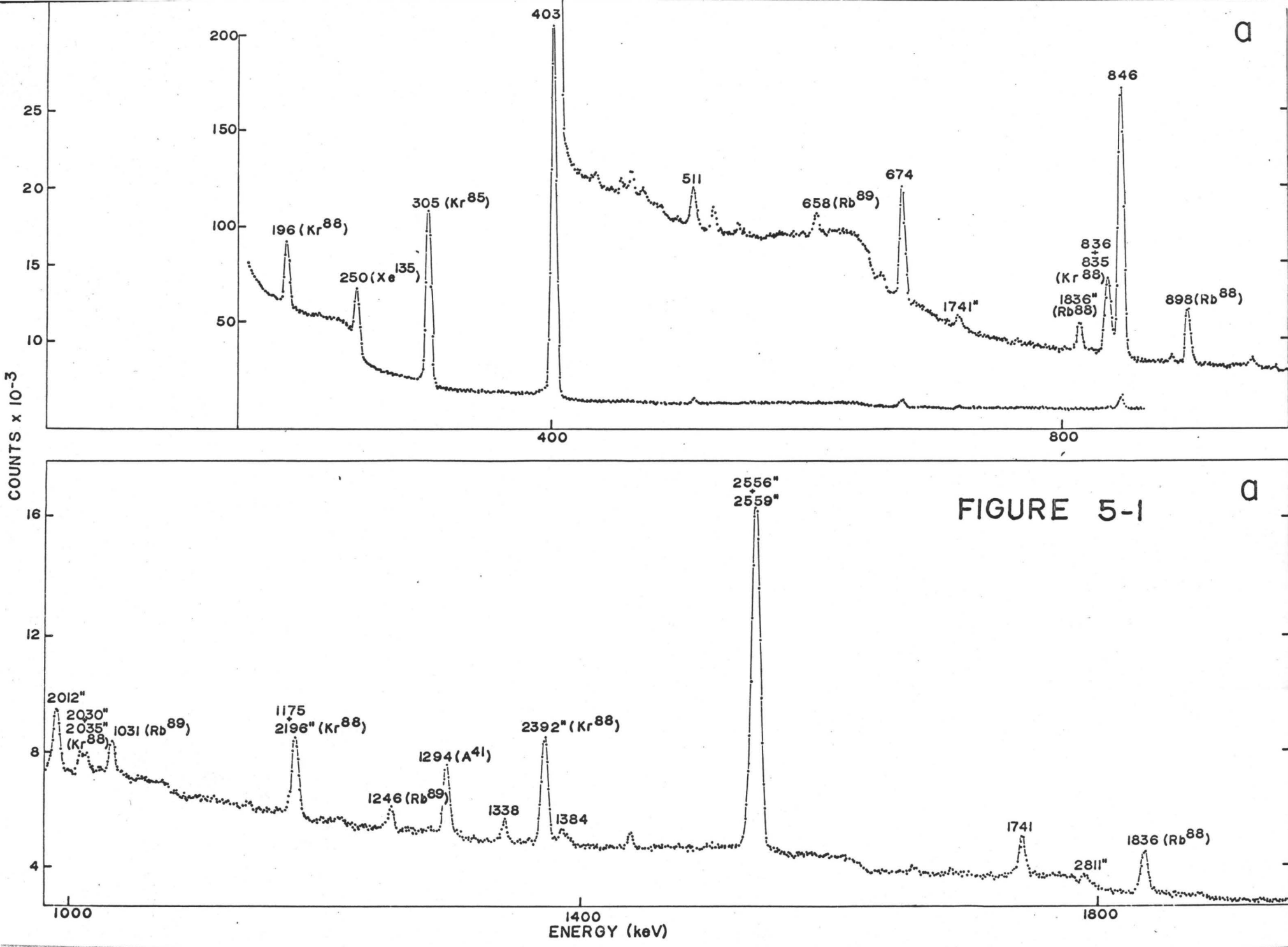
a
403
846
511
674
658(Rb89)
305 (Kr85)
196 (Kr88)
250(Xe135)
836
835
(Kr88)
1836"
(Rb88)
1741"
898(Rb88)
200
150
100
50
25
20
15
10
400
800
COUNTS x 10-3
a
2556"
2559"
2012"
2030"
2035"
(Kr88)
1031 (Rb89)
1175
2196" (Kr88)
2392" (Kr88)
1294(A41)
1246(Rb89)
1338
1384
1741
2811"
1836 (Rb88)
16
12
8
4
1000
1400
1800
ENERGY (keV)

FIGURE 5-1

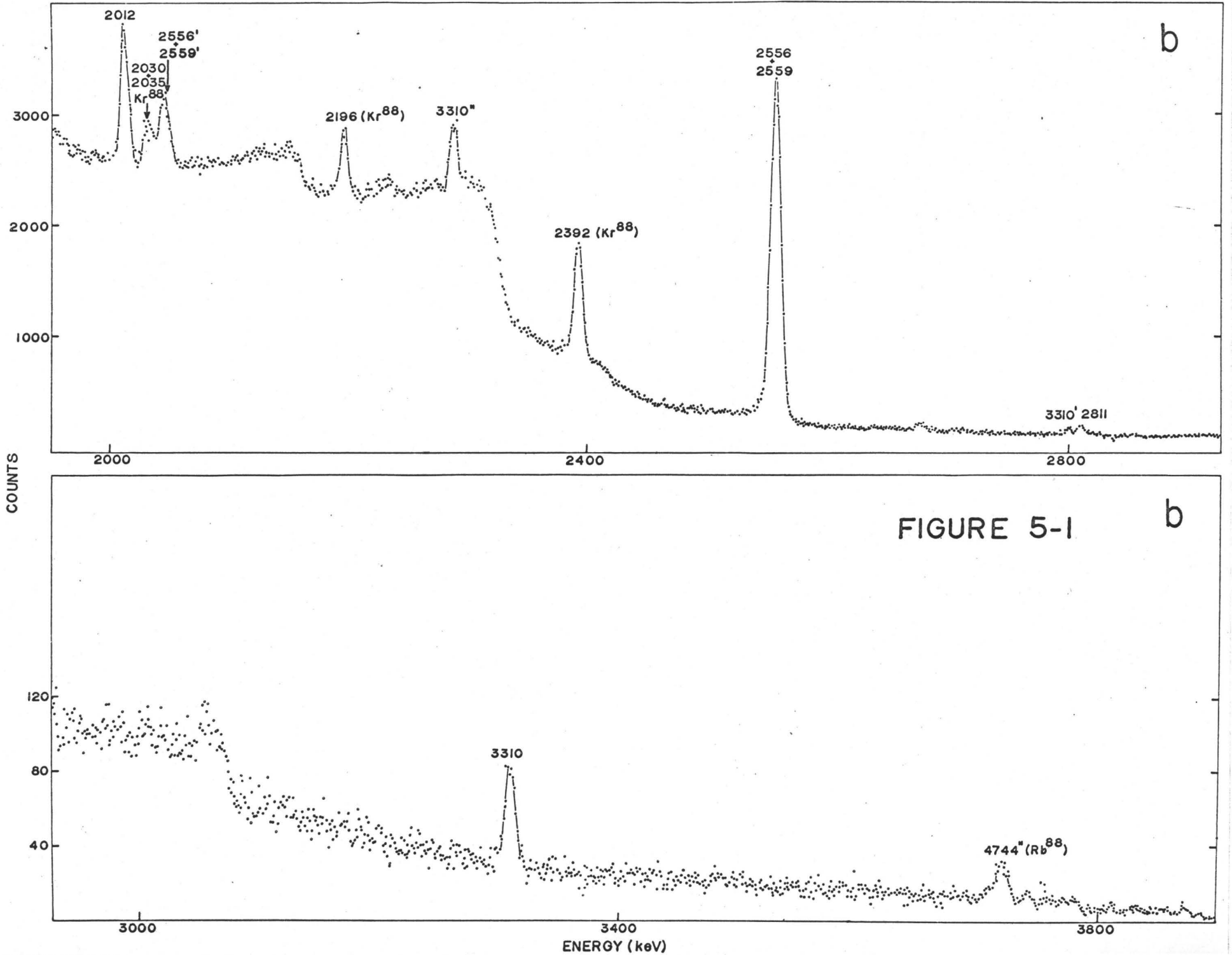
b
2012
2556'
2559'
2030
2035
Kr88
2196 (Kr88)
3310"
2556
2559
2392 (Kr88)
3310' 2811
3000
2000
1000
2000
2400
2800
COUNTS
b
120
80
40
3310
4744" (Rb88)
3000
3400
3800
ENERGY (keV)

FIGURE 5-1

intensity measurements obtained have been verified using slightly different source preparation techniques and various Ge(Li) counters. The list of gamma-ray energies and intensities in Table 5-1 are average values obtained from a few different runs. The dominant line in the spectrum is the 403 keV gamma-ray. The 836 and 1175 keV lines form closely spaced doublets with some ^{88}Kr lines of similar energies. The ^{87}Kr gamma-ray spectrum has a closely-spaced doublet itself at 2556 keV and 2559 keV. This doublet has not been split in the spectrum illustrated in Fig. 5-1 although a broadening of the peak with respect to the 2392 keV peak in ^{88}Kr is evident. The doublet, however, has been split using a better resolution Ge(Li) detector than the one used to obtain the spectrum shown in Fig. 5-1. From this run it was estimated that the energy separation was of the order of 3 keV and that the lower energy component comprised $\sim$ 60% of the intensity of the peak. This intensity ratio was verified in the coincidence run discussed under section 5-2.1.

5-1.2 Singles Spectra of ^{88}Kr and ^{88}Rb

A singles spectrum of ^{88}Kr and ^{88}Rb was obtained with the rubidium daughter in "transient" equilibrium with the parent ^{88}Kr activity. The ^{88}Kr atoms decay according to

$$N_{Kr}(t) = N_{Kr}(o)\ e^{-\lambda_{Kr}t}$$

TABLE 5-1

Gamma-Ray Energies and Intensities of ^{87}Kr Lines

E_γ (keV)	I_γ (I_{403}=100)	I_{abs} (%)*
403.0(0.5)	100	59.7(3.0)
674.3(0.5)	3.4	2.0(0.2)
836.0(0.5)	1.2	0.7(0.1)
845.8(0.5)	13.8	8.2(0.4)
1175.5(1.0)	2.2	1.3(0.1)
1338.0(1.0)	1.0	0.6(0.1)
1384.0(1.0)	1.0	0.6(0.1)
1741.0(1.0)	3.4	2.0(0.2)
2012.0(1.0)	4.9	2.9(0.3)
2556.0(2.0)	~ 16.0	9.5(0.5)
2559.0(2.0)	~ 8.5	5.1(0.3)
2811.2(3.0)	0.5	0.3(0.05)
3309.8(2.0)	1.1	0.6(0.1)

*Calculated using decay scheme in Figure 5-17.

whereas the ^{88}Rb atoms decay according to,

$$N_{Rb}(t) = \frac{\lambda_{Kr}}{\lambda_{Rb}-\lambda_{Kr}} N_{Kr}(o) \left(e^{-\lambda_{Kr}t} - e^{-\lambda_{Rb}t}\right) .$$

Here $N_{Kr}(o)$ is the number of ^{88}Kr atoms at time zero and the disintegration constant for ^{88}Kr, λ_{Kr} is much smaller than that for ^{88}Rb, λ_{Rb}. After a time of about 5 or 6 half-lives of ^{88}Rb the ^{88}Rb decays effectively with the same time constant as the parent activity, ^{88}Kr. The ^{88}Kr and ^{88}Rb singles spectrum shown in Figure 5-2 was obtained by counting after the rubidium daughter was in equilibrium with the parent activity. In this case the individual spectra were obtained in five hour running periods during which each spectrum was stabilized against gain and zero shifts using a ND spectrum stabilizer. The individual runs collected over a period of two days were then added together in the ND3300 system memory. Again there is some xenon and cesium contamination but relatively little ^{87}Kr present in the spectrum. The high resolution run permitted the splitting of the closely spaced 2030 and 2035 keV peaks as well as the separation of the weak lines at 1183 and 1518 keV from their strong neighbouring peaks. The 1518 keV line has not definitely been established in the ^{88}Kr decay scheme, however. The doublet at 2112 and 2119 keV cannot be observed in this run because of the poor efficiency of the counter in the 2 MeV region for both photo-electric and pair production

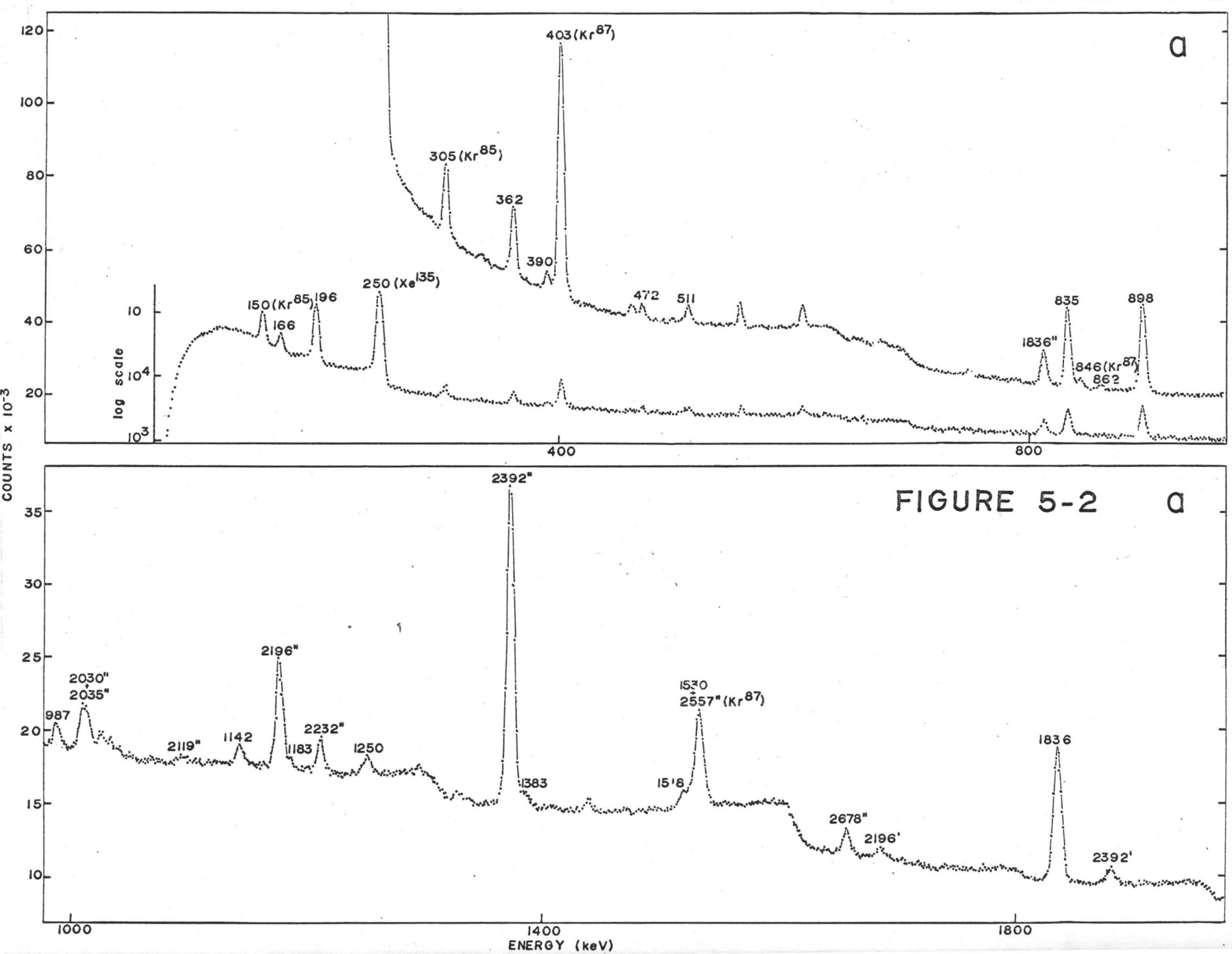
a
403(Kr87)
305(Kr85)
362
390
250(Xe135)
150(Kr85)
196
166
472
511
835
898
1836"
846(Kr87)
862
log scale
10
10⁴
10³
120
100
80
60
40
20
400
800
COUNTS x 10⁻³
2392"
2196"
2030"
2035"
987
2119"
1142
1183
2232"
1250
1383
1530
2557"(Kr87)
1518
1836
2678"
2196'
2392'
35
30
25
20
15
10
1000
1400
1800
ENERGY (keV)

FIGURE 5-2 a

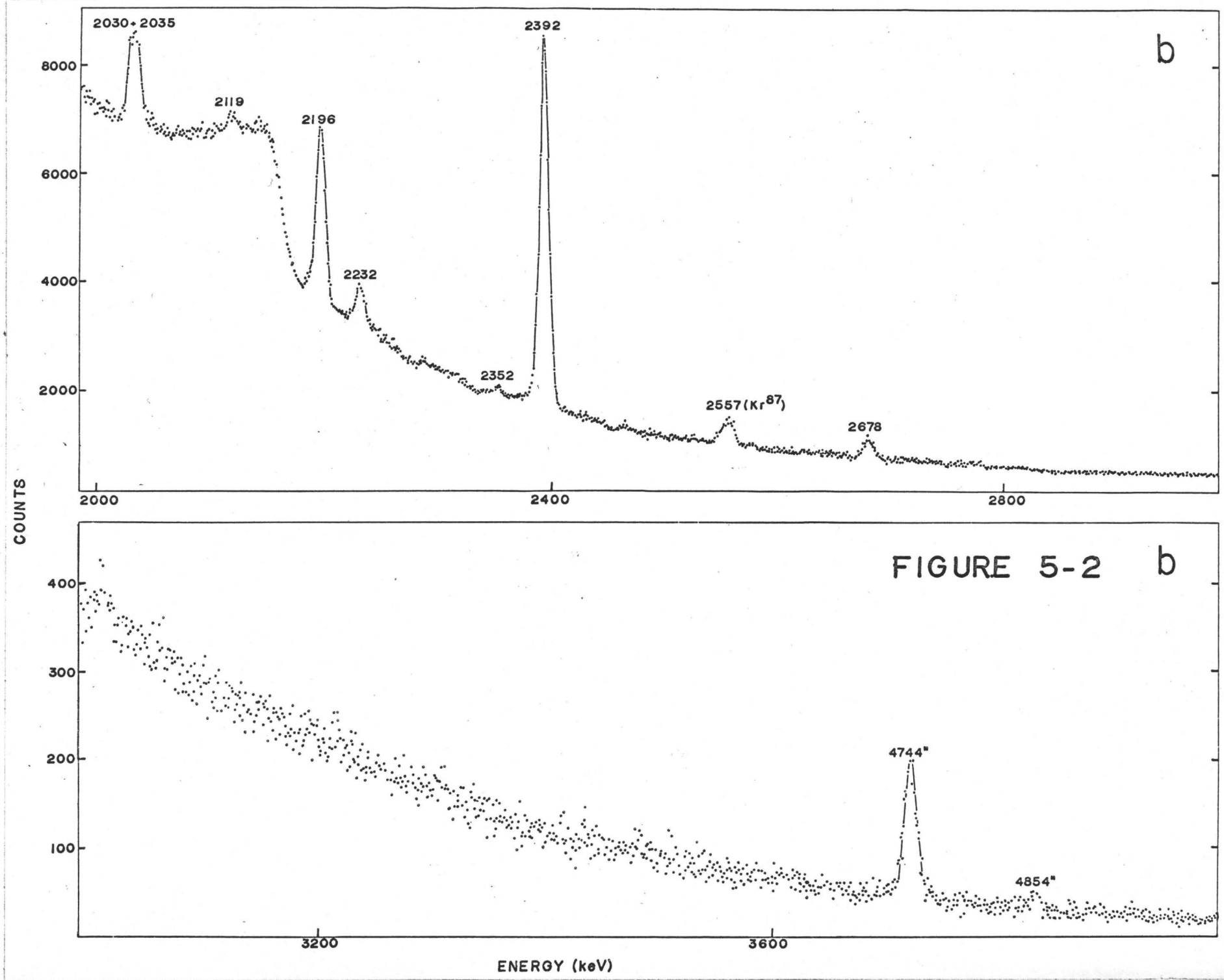
b
2030+2035
2392
2119
2196
2232
2352
2557(Kr87)
2678
8000
6000
4000
2000
2000
2400
2800
COUNTS
400
300
200
100
4744"
4854"
3200
3600
ENERGY (keV)

FIGURE 5-2 b

events.

Some of the weaker gamma-ray lines were not evident in the spectrum shown in figure 5-2. A singles spectrum of ^{88}Rb itself was collected using a 12 cc. active volume Ge(Li) counter. A ND150 1^{K} ADC analyzer system was utilized to collect the spectrum shown in figure 5-3 during a running time of 2 hours. During this time new sources of ^{88}Rb were prepared every half hour. The existence of the weak 1518 and 1535 keV lines has been verified in other runs. The high energy lines are quite prominent in the spectrum. Because of the poorer resolution of the counter used here, evidence for existence of the doublet at 2112 and 2119 keV is not seen in the spectrum.

An additional spectrum of the gamma-radiation following the beta decay of ^{88}Kr and ^{88}Rb was gathered using a 40 cc. active volume coaxial Ge(Li) counter. This detector was capable of $\sim$ 3 keV resolution at 1 MeV and had a very high photo-peak efficiency. Thus it was possible to detect many weak gamma-ray lines in this run which were not seen in the previous runs. Some of the sections of interest are shown in figure 5-4. Here it is evident that the 1183 keV line observed in figure 5-2 is actually a doublet. The line at 1213 keV is postulated on the basis that the double-escape peak of the 2232 keV

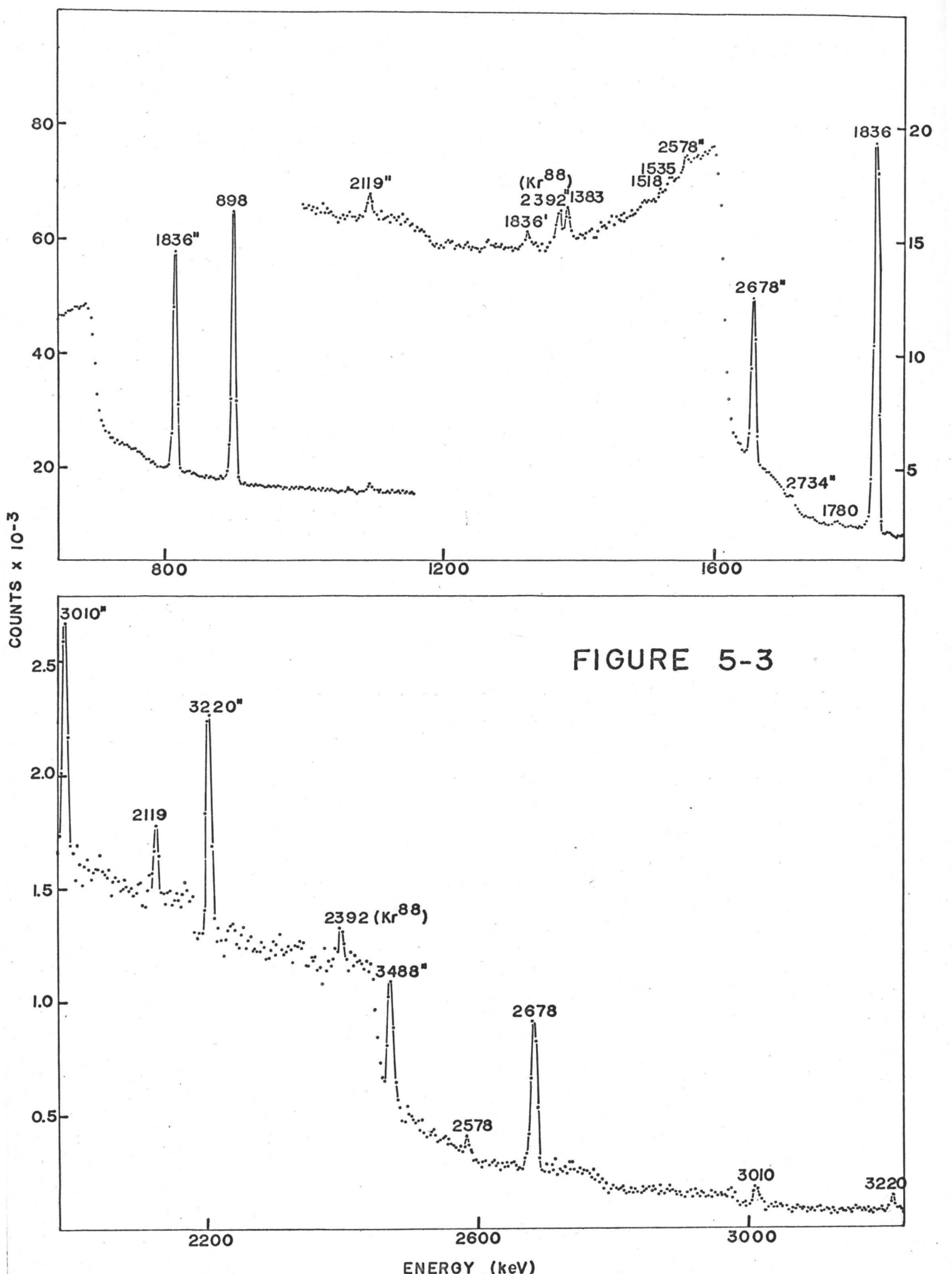
COUNTS x 10-3
80
60
40
20
20
15
10
5
1836"
898
2119"
(Kr88)
2392"
1383
1836'
2578"
1535
1518
2678"
2734"
1780
1836
800
1200
1600
3010"
3220"
2119
2392 (Kr88)
3488"
2678
2578
3010
3220
2.5
2.0
1.5
1.0
0.5
2200
2600
3000
ENERGY (keV)

FIGURE 5-3

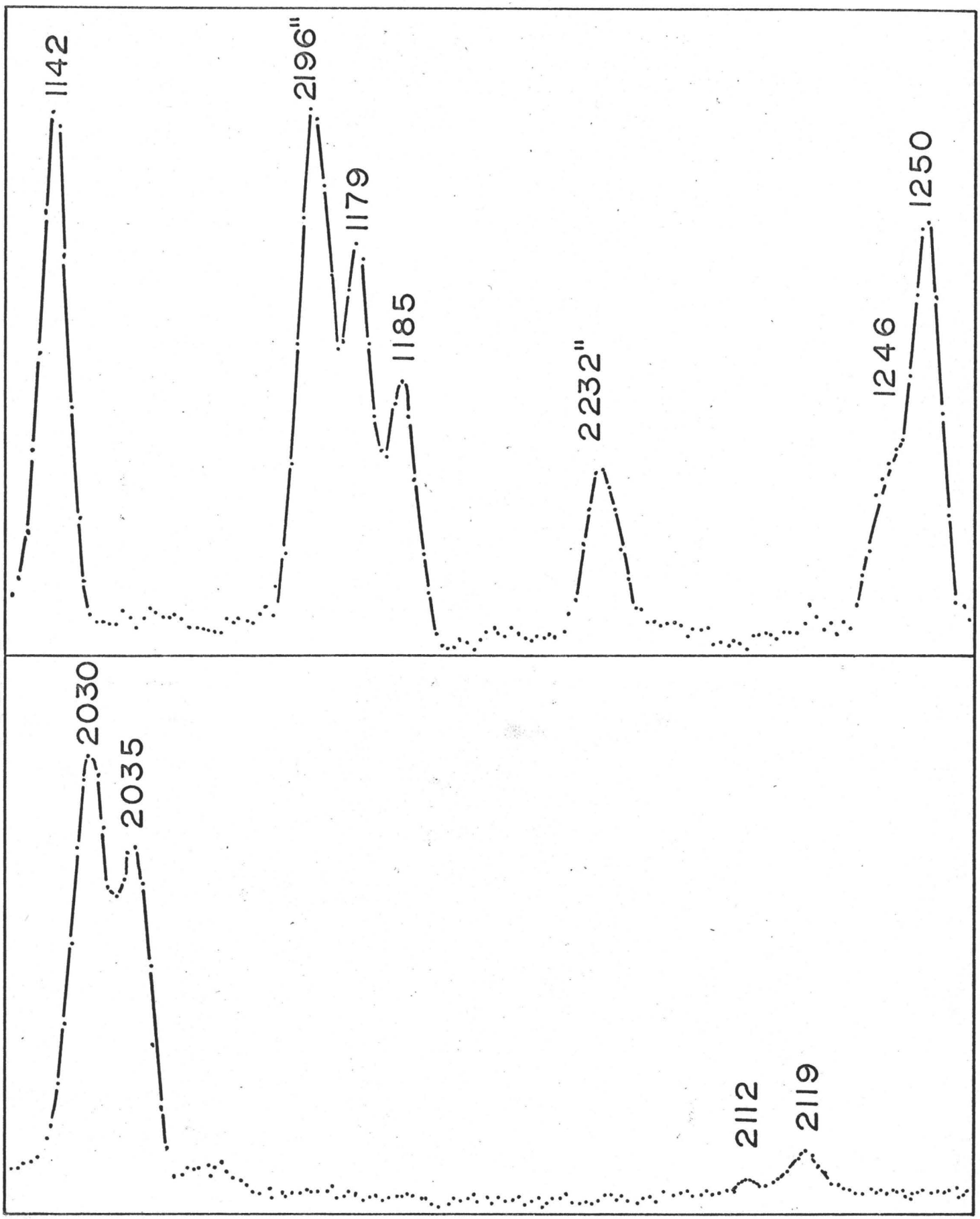
1142
2196"
1179
1185
2232"
1246
1250
2030
2035
2112
2119
Counts
Energy

FIGURE 5-4

line is stronger than expected, broader than neighbouring single line peaks and shows a skewing to the high energy side. The 1246 keV gamma-ray is also evident here. The bottom portion of figure 5-4 displays the two doublets at 2030 and 2035 and at 2112 and 2119 keV. Almost all of the weak lines detected in this run have been assigned to the ^{88}Kr beta-decay scheme as discussed in section 5-4.2. The energies and intensities of the lines belonging to the beta-decay of ^{88}Kr and ^{88}Rb are listed in Tables 5-2 and 5-3, respectively. It should be noted that in the case of all three isotopes, the intensities are relative to the strongest line in each particular decay scheme.

5-2 Gamma-Gamma Coincidence Results

The gamma-gamma coincidence runs were performed using a 3"×3" NaI(Tl) counter in conjunction with a large efficient Ge(Li) detector. The coincidence circuit used was that described in section 3-7. No gain stabilization was required as the runs were of relatively short duration.

5-2.1 ^{87}Kr Gamma-Gamma Coincidence Results

The coincidence run performed on the ^{87}Kr isotope was carried out using an energy range of 0 to 900 keV in the NaI(Tl) dimension and 0 to 3000 keV in the Ge(Li) dimension. The ND3300 analyzer system was set up in a 32 by 512

TABLE 5-2

Gamma-ray Energies and Intensities of ^{88}Kr Lines

E_γ (keV)	I_γ (I_{2392}=100)	I_{abs} (%)*
28.0(1.0)	-	
166.0(1.0)	18.0	6.8 (0.4)
196.1(0.5)	100.0	37.8 (2.0)
240.4(1.0)	0.8	0.3 (0.03)
362.6(1.0)	7.8	3.0 (0.2)
390.4(1.0)	1.6	0.6 (0.1)
472.3(1.0)	1.6	0.6 (0.1)
789.0(1.0)†	1.0	0.4 (0.05)
834.7(0.5)	34.4	13.0 (0.6)
862.4(1.0)	1.4	0.53(0.1)
945.2(1.0)	0.7	0.26(0.04)
962.2(1.0)	0.2	0.07(0.01)
986.7(1.0)	4.2	1.6 (0.15)
1039.6(1.0)	1.0	0.4 (0.05)
1049.5(1.0)	0.3	0.1 (0.02)
1141.7(1.0)	4.6	1.7 (0.15)
1179.5(1.0)	2.0	0.75(0.10)
1185.1(1.0)	1.5	0.57(0.06)
1213.0(2.0)	0.5	0.2 (0.1)
1245.6(2.0)	0.8	0.3 (0.03)
1250.0(1.0)	3.0	1.1 (0.1)
1352.5(1.0)	0.5	0.2 (0.05)
1518.5(2.0)†	4.0	1.5 (0.1)
1529.8(1.0)	30.0	11.3 (0.6)
2029.5(2.0)	12.7	4.8 (0.3)
2035.3(2.0)	12.7	4.8 (0.3)
2186.8(2.0)	0.4	0.15(0.02)

(continued next page)

E_γ(keV)	I_γ(I_{2392}=100)	I_{abs}(%)*
2195.9(0.5)	39.5	14.9 (0.8)
2231.6(1.0)	9.5	3.6 (0.2)
2352.4(2.0)	0.5	0.2 (0.04)
2392.0(0.5)	100	37.8 (2.0)
2409.4(2.0)	0.2	0.07(0.01)
2549.0(2.0)	0.7	0.26(0.04)
2771.8(2.0)	0.1	0.04(0.01)

*Calculated using decay scheme in Fig. 5-18.
†Not placed in decay scheme.

TABLE 5-3

Gamma-ray Energies and Intensities of ^{88}Rb lines

E_γ(keV)	I_γ(I_{1836}=100)	I_{abs}(%)*
898.0	60.0	18.1 (0.8)
1383.5(1.0)	3.5	1.1 (0.1)
1518.5(2.0)†	0.6	0.2(0.05)
1535.5(1.0)	0.6	0.2(0.05)
1779.8(2.0)	1.0	0.3(0.05)
1836.1	100	30.2 (1.0)
2112.0(2.0)	0.4	0.1 (0.02)
2119.5(1.0)	1.8	0.5 (0.05)
2577.8(1.0)	0.7	0.2 (0.05)
2677.8(1.0)	9.5	2.9 (0.15)
2734.1	0.6	0.2 (0.05)
3009.5(1.0)	1.6	0.5 (0.05)
3220.0(2.0)	1.2	0.4 (0.05)
3487.8(2.0)	0.8	0.2 (0.05)
4744.5(3.0)	1.5	0.5 (0.05)
4854.0(3.0)	0.1	0.03(0.005)

*Calculated using decay scheme in Fig. 5-19 .
†Not placed in decay scheme.

two parameter configuration thus utilizing the full 16^K memory available and making real-time analysis possible. The 512 channels in the solid state (Ge(Li)) dimension were sufficient for retaining the energy resolution required for the experiment. A resolving time of 2τ = 60 nsec. was used in the coincidence circuit giving a chance rate of about 15%. All of the coincidence relationships of interest were discernable in the six hour run performed. Figures 5-5a and 5-5b show spectra obtained with the Ge(Li) detector in coincidence with the 674 and 403 keV transitions respectively. In each spectrum the 403 keV line is a major source of random coincidences as it it such an overwhelmingly strong line in the singles spectrum. By comparison of figure 5-5a and 5-5b it is obvious that the 1338 and 1741 keV lines are in coincidence with the 674 keV line. A large number of gamma-ray lines seem to be in coincidence with the 403 keV line from a cursory examination of figure 5-5b. However a comparison of the intensities of the gamma-rays in the coincidence spectrum with the corresponding singles intensities reveals that the appearance of the 846 keV line is due to chance contributions. It is also noted that one or more of the components of the 2556-2559 keV doublet is in coincidence with the 403 keV line but with only about one third of the intensity expected from the singles run. This is interpreted as meaning that only one of the

Figure 5-5a. Ge(Li) spectrum in coincidence with the 674 keV line in ^{87}Kr

Figure 5-5b Ge(Li) spectrum in coincidence with the 403 keV line in ^{87}Kr

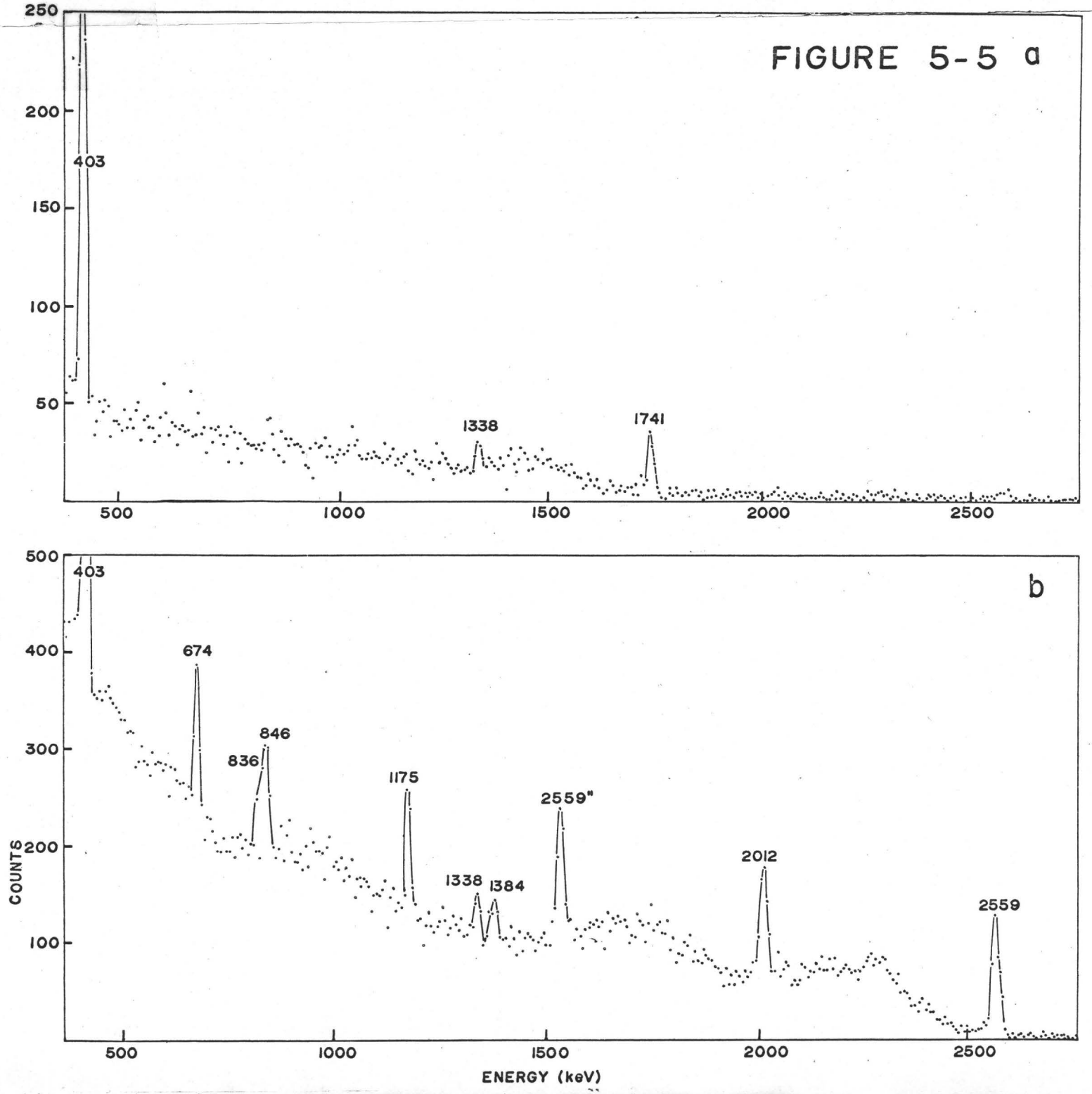
FIGURE 5-5 a
250
200
150
100
50
403
1338
1741
500
1000
1500
2000
2500
b
500
400
300
200
100
COUNTS
403
674
846
836
1175
2559"
1338
1384
2012
2559
500
1000
1500
2000
2500
ENERGY (keV)

components of this doublet is in coincidence with the 403 keV line. Energy considerations and intensity measurements indicate that it is the higher energy component at 2559 keV which accounts for the coincidence results. The results of the gamma-gamma coincidence measurements on ^{87}Kr are summarized in Table 5-4.

TABLE 5-4

^{87}Kr Coincidence Results

Line in NaI Dimension	Lines in Ge dimensionn observed in coincidence
403	674,836,1175,1338,1384,2012,2559
674	1338,1741
836	403,1175
846	-

5-2.2 ^{88}Kr and ^{88}Rb Gamma-Gamma Coincidence Results

A gamma-gamma coincidence run was performed on ^{88}Kr and ^{88}Rb concurrently because of the difficulty of maintaining a relatively pure source of either isotope for a time long enough to obtain sufficient counting statistics. It is necessary to span an energy range of 0 to 3500 keV in both the NaI(Tl) and Ge(Li) dimensions. To retain adequate energy resolution in both dimensions at least 1024 channels were required on the solid state side and 256 channels on the NaI(Tl) side. As this would have required 2^{18}(262,144) memory lo-

cations to record coincidences in real time, address recording was utilized to record the entire coincidence surface concurrently. Writing at 200 bits per inch, it was possible to record about 1.5×10^6 coincidence events of 18 bits each on a 2400 foot roll of magnetic tape. In the ^{88}Kr-^{88}Rb coincidence run, seven such tapes were filled during a continuous running time of ten hours. New sources were prepared every few hours to maintain an average total coincidence counting rate of 300 per second with a chance contribution of about 15%. The coincidence circuit was set for a resolving time of 2τ = 60 nsec.

To sort the collected data, four passes were required for each tape using the IBM 7040 computer facility. The spectra from each tape were adjusted for zero and gain shifts and then summed to obtain the resulting 256 by 1024 two-dimensional array. To simplify analysis of the coincidence data, the large array was reduced in size by adding the NaI(Tl) channel spectra in pairs resulting in a 128 by 1024 array. The coincidence data were then analyzed thoroughly in both dimensions. One method of analysis used was to sum the data in the NaI(Tl)-counter dimension across a peak in the Ge(Li)-counter dimension and then subtract from this spectrum the background under the peak by using a sample from the same number of channels but located on the wings of the peak.

Figure 5-6a. NaI(Tl) spectrum in coincidence with the 472 keV line in ^{88}Kr

Figure 5-6b. NaI(Tl) spectrum in coincidence with the 896 keV line in ^{88}Rb

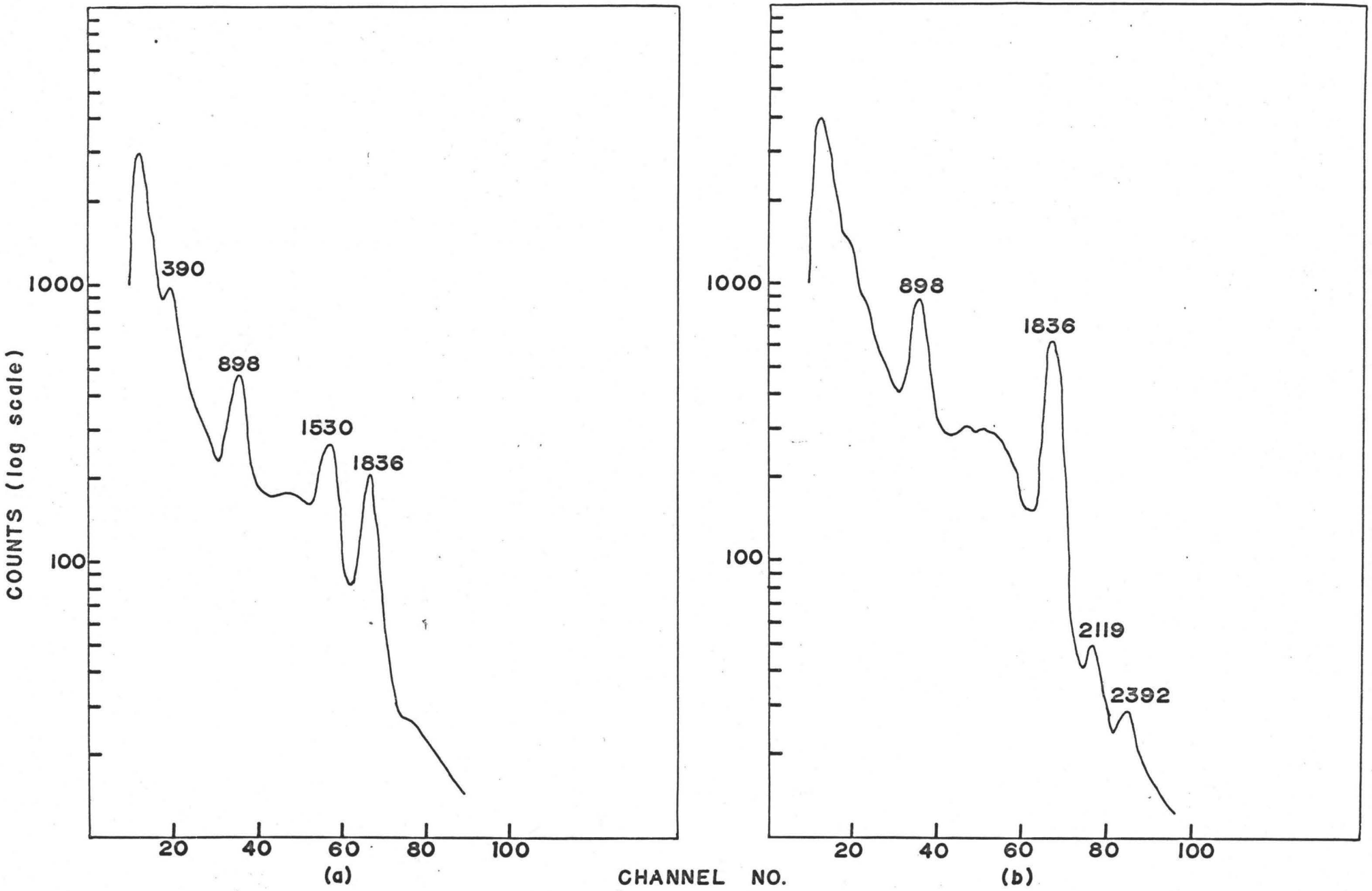
COUNTS (log scale)
1000
100
390
898
1530
1836
20
40
60
80
100
(a)
CHANNEL NO.
1000
100
898
1836
2119
2392
20
40
60
80
100
(b)

FIGURE 5-6

Figures 5-6a and 5-6b depict two such spectra. The first figure indicates that the 390 and 1530 keV lines are in coincidence with the 472 keV line in the Ge(Li) dimension while the second figure demonstrates the coincidence of the 1836 and 2119 keV lines with the 898 keV line in the Ge(Li)-dimension. It will be noted that in these spectra there is a strong chance contribution from the 898 and 1836 keV lines. This was considered quantitatively when analyzing the coincidence spectra. Evidence for a coincidence is best established by comparing the coincidence spectrum under scrutiny with both a singles spectrum and a neighbouring coincidence spectra. The analysis technique as described above was found to be useful in bringing out the stronger coincidence relations. It was found that the most sensitive method for detecting coincidences was to examine the Ge(Li) spectra in the region around a peak in the NaI(Tl) dimension. Figure 5-7 shows four such Ge(Li) spectra in coincidence with the 472, 835, 1142 and 1530 keV lines in the NaI(Tl) dimension respectively. The coincidence of the 1530 keV line with the 472 keV line is concluded from a comparison of figure 5-7a with adjacent spectra and a singles spectrum. The other prominent peaks in this figure appear with about the same intensity ratio as in a singles spectrum. A comparison of figures 5-7a and 5-7b leads to the conclusion that the 1530 keV line is in coinci-

Figure 5-7a. Ge(Li) spectrum in coincidence with the 472 keV line in ^{88}Kr

Figure 5-7b. Ge(Li) spectrum in coincidence with the 835 keV line in ^{88}Kr

Figure 5-7c. Ge(Li) spectrum in coincidence with the 1142 keV line in ^{88}Kr

Figure 5-7d. Ge(Li) spectrum in coincidence with the 1530 keV line in ^{88}Kr

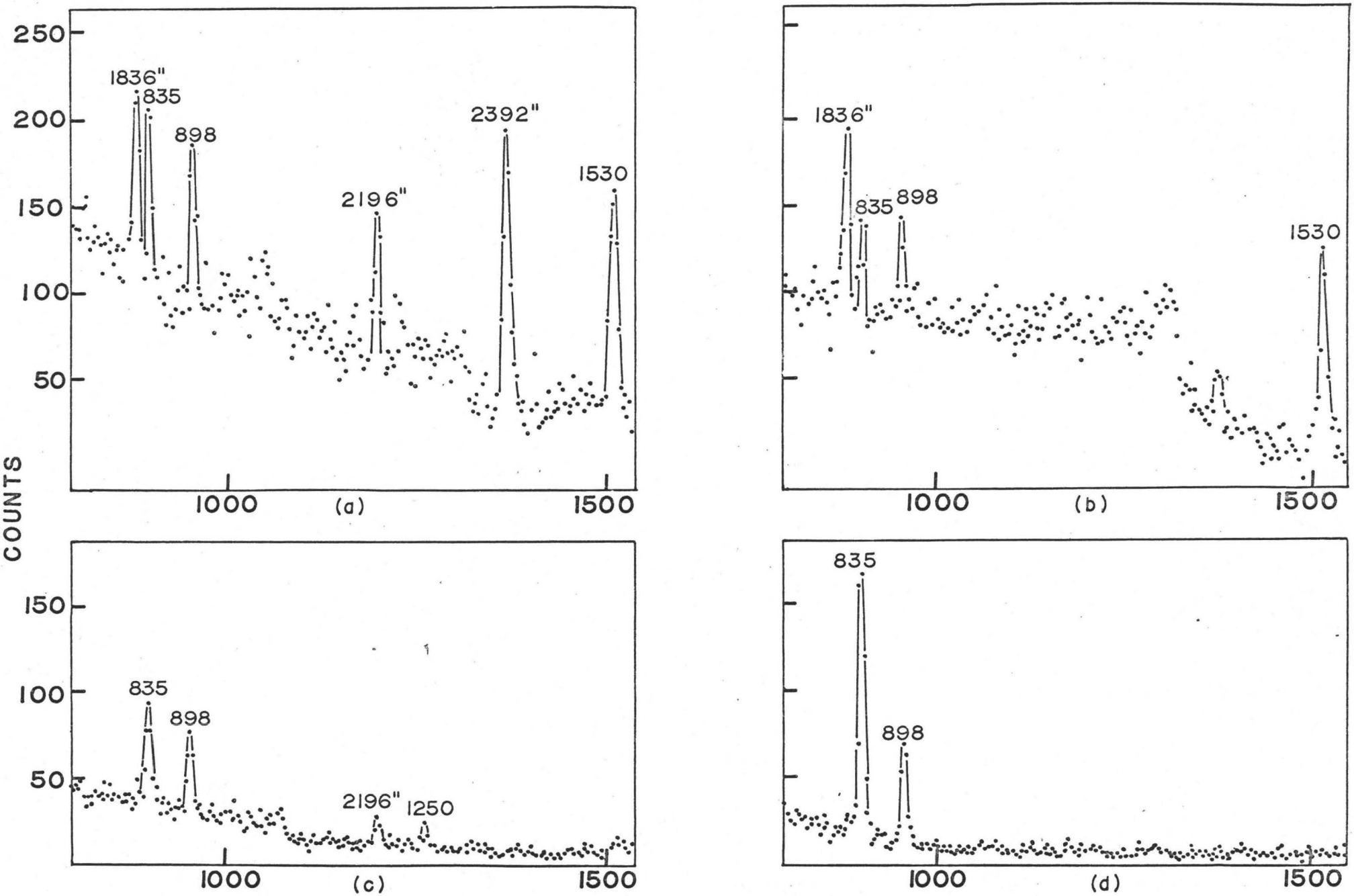
250
200
150
100
50
COUNTS
1836"
835
898
2196"
2392"
1530
1000
(a)
1500
1836"
835
898
1530
1000
(b)
1500
150
100
50
835
898
2196"
1250
1000
(c)
1500
835
898
1000
(d)
1500
ENERGY (keV)

FIGURE 5-7

Figure 5-8 - Gamma-gamma coincidence matrix for ^{88}Kr and ^{88}Rb. Coincidence with a peak in the NaI(Tl) dimension is indicated by an open circle while coincidence with a peak in the solid state dimension is indicated by an X.

NaI \ Ge	166	196	362	390	472	835	862	898	987	1142	1250	1383	1530	1836	2032	2119	2196	2678	3010
166		⊠																	
196	⊠																⊠		
362															⊠				
390					⊠								O						
472				⊠									O						
835													⊠						
898														⊠					
987		⊠																	
1142											O								
1250										O									
1383														X					
1530				⊠	⊠	⊠	O												
1836								⊠				O				O		⊠	O
2032	⊠	⊠	⊠																
2119								X											
2196		⊠																	
2678														O					
3010																			

FIGURE 5-8

dence with the 835 keV line. Even the weak coincidence of the 1250 keV line with the 1142 keV line is evident in figure 5-7c. Figure 5-7d clearly shows the coincidence of the 835 keV line with the 1530 keV line. The complete results of these measurements on ^{88}Kr and ^{88}Rb are summarized in figure 5-8 in the form of a matrix. Coincidence with a peak in the NaI(Tl) dimension is indicated by an open circle while coincidence with a peak in the solid state dimension is indicated by an X.

5-3 Beta Singles and Beta-Gamma Coincidence Measurements

The beta singles for each isotope were obtained mainly to determine the ground state branching ratio of the beta-rays while the beta-gamma coincidence runs were performed to facilitate the assignment of the gamma rays in the decay scheme. The beta singles were obtained using a 2"×2" plastic scintillator system with good linearity and gain stability against counting rate changes.

5-3.1 Beta Analysis of ^{88}Rb

The samples of ^{88}Rb were obtained by means of the charged wire and collection continued until the activity was adequate for the experiment to be carried out. A collection time of about two minutes was sufficient for the singles runs to obtain an initial count rate of 2000 per second in

the beta counter at a range of 1" in air. For coincidence runs a higher counting rate of the order of 4000 counts per second was obtained after collecting for 4 to 5 minutes. In order to check for sample contamination and to ensure that there were no random summing contributions in the beta singles, a series of runs was carried out using one ^{88}Rb sample. After initial calibration of the beta counter with a ruthenium source[135] the series of runs was started. Eight consecutive runs were carried out using 3.5 minute counting intervals with a 0.5 minute interval between runs. During each counting interval the sample spectrum was recorded in a 256 channel group of a 4096 channel analyzer. Immediately following the ^{88}Rb runs the room background spectrum was recorded. Then the plastic scintillator was re-calibrated by recording the beta spectra of ^{106}Ru, ^{90}Sr, ^{90}Y and ^{38}Cl.

The analysis of the ^{88}Rb beta spectra was carried out as follows. The Fermi plots of the ^{106}Ru spectra recorded before and after the experiment were compared to ensure that no gain shift had occurred during the run. Fermi plots of the beta standards were used to obtain an accurate energy scale for the beta spectra. Room background was subtracted from each ^{88}Rb spectrum in the series. To check for the presence of random summing and contaminants in the beta spectra, the series of eight runs was then fitted by least-squares

channel by channel to a decay curve composed of a 17.8 minute half-life component and an 8.9 minute component since random summing is proportional to the square of the counting rate. A chi-squared analysis of the fit for all channels showed that random summing was completely negligible and that there was no noticeable quantity of contaminant present in the sample. The resulting fit was then used together with the weights found in the stripping of the beta-ray spectra to determine the group intensities.

A beta singles run of ^{88}Rb is shown in figure 5-9 with the beta groups stripped off. The highest energy group was found to have the first-forbidden unique shape as expected and an end-point energy of 5080±50 keV. This is to be compared with the value of 5200 keV determined by Lazar et al.[55] The high intensity and large energy separation of the next beta end-point energy permitted an accurate determination of the shape and end-point energy of the ground state beta group. Further stripping off of the beta groups yielded four main beta groups with branching percentages as shown in Table 5-5. The first three beta groups are easily identified as the beta groups to the ground state and the first two excited states in ^{88}Sr respectively but the 1100

Figure 5-9. Beta-singles run for ^{88}Rb with four beta components stripped off

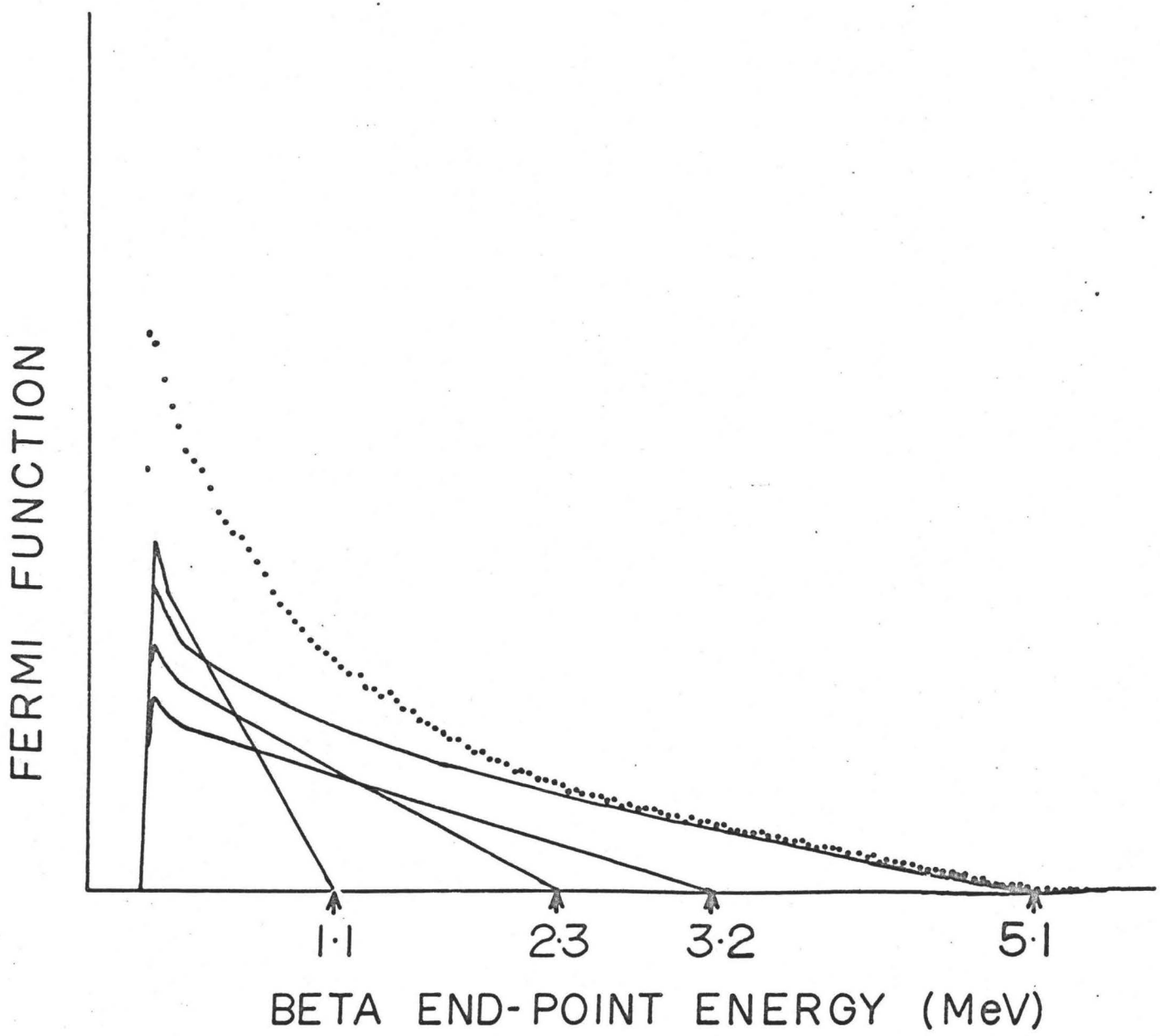

FIGURE 5-9

TABLE 5-5

Beta Transition Groups in ^{88}Rb

Group	End-point (keV)	Branching %
β_1	5080	65.5
β_2	3240	16.0
β_3	2350	12.5
β_4	1100	6.0

keV group cannot definitely be identified as its intensity is low and thus the end-point energy cannot be determined accurately. The beta group, β_4, actually consists of a complexity of weak beta groups with very close end-point energies. This makes the stripping down of this part of the beta spectrum almost impossible.

Two beta-gamma coincidence runs were carried out on ^{88}Rb using the multi-channel analyzer in a 64×64 two parameter configuration. The first run covered the entire beta spectrum and the gamma spectrum from 1.2 to 3.0 MeV. In a 30 minute run, 74,000 coincidence events were collected. The second beta-gamma coincidence run covered the entire beta energy range and the gamma-ray energy range from 0 to 2.0 MeV. An analysis of the beta-ray spectra from these runs was carried out using Fermi-plot stripping techniques as done for the beta-ray singles spectra. Plots of the intensity of beta groups obtained as a function of gamma-ray energy,

Figure 5-10. Beta spectrum in coincidence with 898 keV line in ^{88}Rb

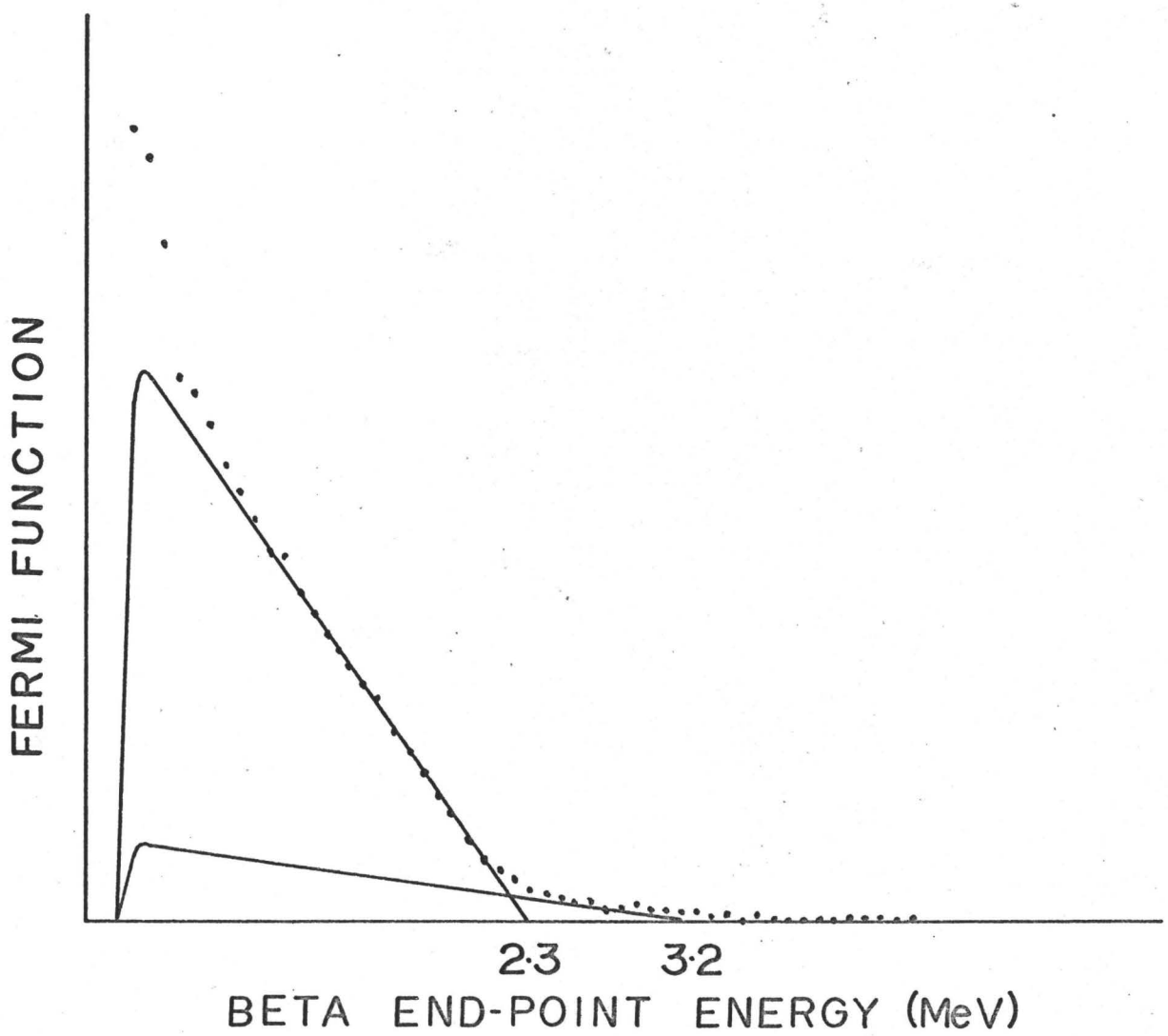

FIGURE 5-10

Figure 5-11. Beta spectrum in coincidence with 1836 keV line in ^{88}Rb

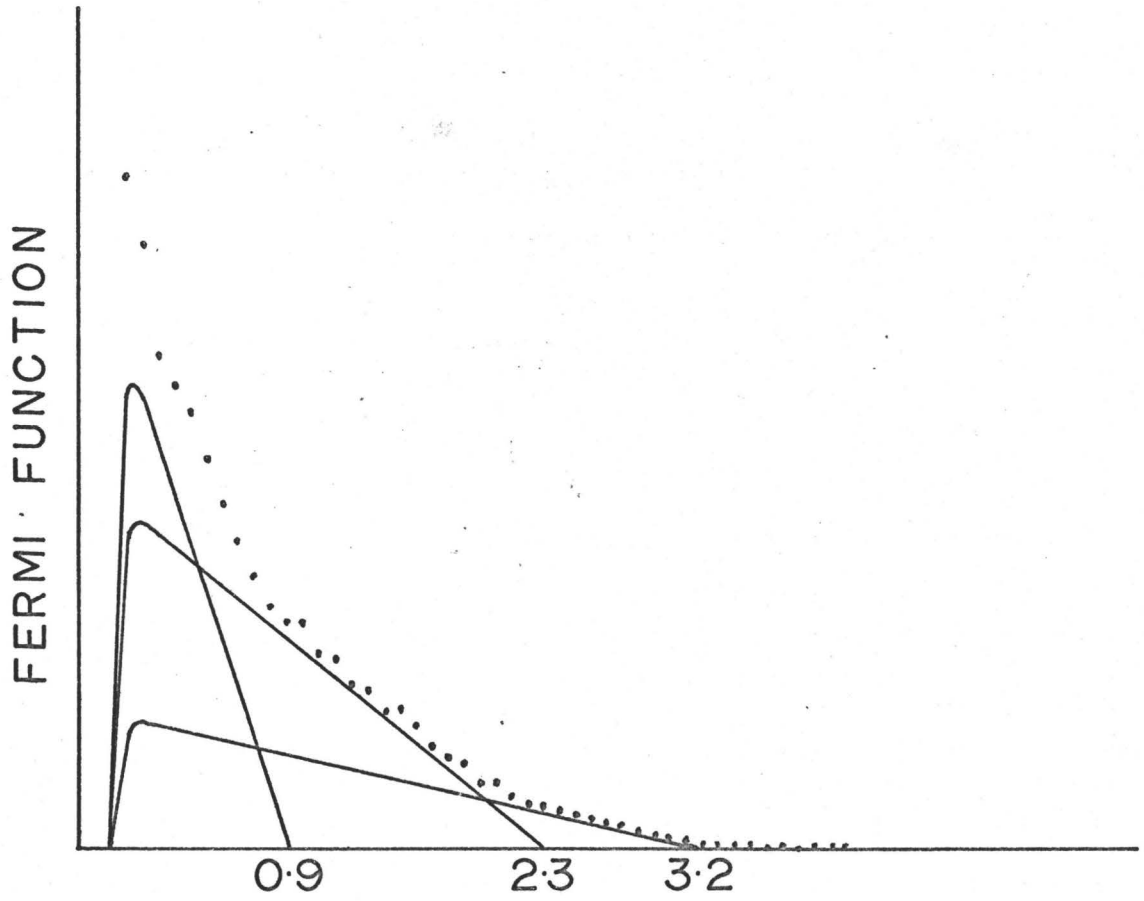

FIGURE 5-11

showed the gamma-ray response curves of the NaI(Tl) detector to the gamma-rays with which the beta groups are in coincidence. Figures 5-10 and 5-11 illustrate the beta groups in coincidence with the 898 and 1836 keV lines in ^{88}Rb respectively. The results confirmed existing assignments to the first and second excited states in ^{88}Sr but the intensities of the lower energy beta transitions were so low and the beta group end-point energies so closely spaced, that no further assignments could be made on the basis of the beta-gamma coincidence results alone.

5-3.2 Beta Analysis of ^{87}Kr

The method of isotope separation used as described in section 3-10 gave about 85% ^{87}Kr activity with the remainder being mainly ^{85}Kr and ^{88}Kr. Rubidium decay products were removed by means of a travelling charged wire. Thus spectrum recording could be and was started immediately after the sample reached the chamber. Preliminary calibration runs were made in the same manner as before in doing the beta singles on ^{88}Rb. Then several consecutive runs were recorded in series. However no attempt was made to analyze the runs for random summing contributions because of the suspected leakage of the active gas from the chamber. Following the singles runs, background and standards were run. As the total counting rate during these runs was never greater than 1500

counts per second, the random summing contributions were assumed to be negligible.

Using calibration standards and the end-point energy of the ^{88}Rb ground state group the highest energy beta group was measured as having an end-point energy of 3900±100 keV. This value agrees with the ground state beta-group energy of 3.9 MeV as obtained by Holm[47]. By a careful analysis of the high energy portion of the spectrum it was possible to establish the decay rate to the ground state of ^{87}Rb which is known to be a first forbidden transition. By averaging over four separate spectra a value of 0.40±0.05 was obtained for the ratio of the intensity of the ground state beta-ray transition to that of the transition to the first excited state. Further analysis of the spectra was done despite the presence of Compton scattering arising from the detection of high gamma-rays. The spectra were stripped down with due consideration for ^{88}Kr contamination. Figure 5-12 shows the results of the stripping-down process carried out for seven beta-group components. The low energy groups are not well defined in energy or intensity because of the close spacing of the energy end-points.

In order to carry out the beta-gamma coincidence runs on ^{87}Kr, more active sources than used for the singles analysis were produced. Two separate coincidence runs were

Figure 5-12. Beta-singles run for ^{87}Kr with seven beta components stripped off

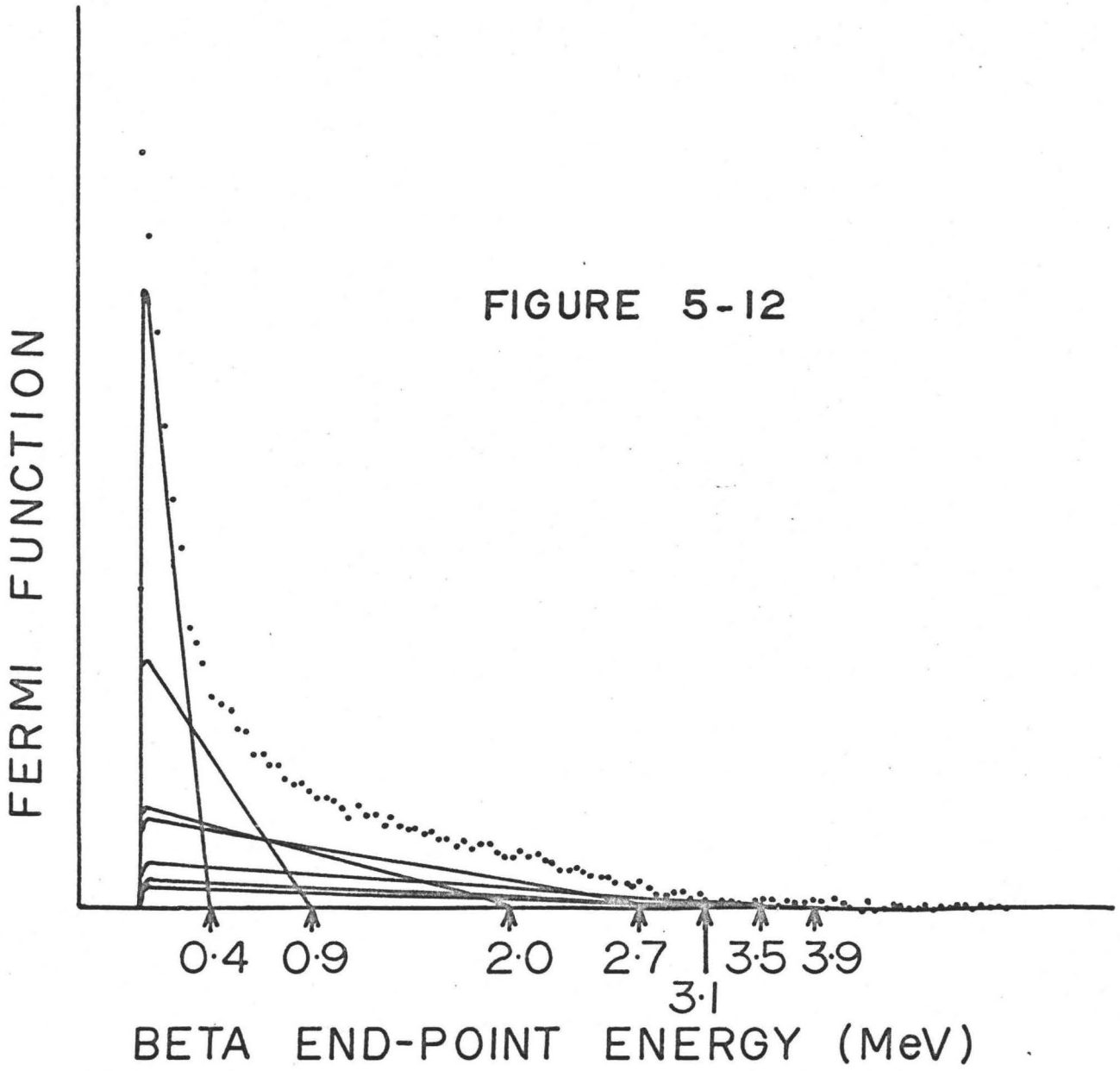

FIGURE 5-12

performed and both were recorded in a 64×64 two parameter configuration. The first run covered the entire beta spectrum in one dimension and the gamma-ray spectrum from 0.6 to 2.5 MeV in the other dimension. A total of 100,000 coincidence events were recorded in a period of 16 minutes. The second coincidence run covered the entire beta energy range again in the one dimension and the gamma energy range from 0 to 0.9 MeV in the other dimension. In a 17 minute period, 220,000 coincidence events were recorded. Both coincidence runs were kept short to reduce the amount of ^{88}Rb contamination which grew in with a half-life of 18 minutes from the ^{88}Kr activity in the sample. The removal of the rubidium activity by means of the travelling charged wire was not 100% efficient.

The chief results of these coincidence runs were as follows. The 403 keV gamma-ray is in coincidence with three major beta-ray groups as depicted in figure 5-13. The beta group with end-point energy 3.5 MeV populates the well-known energy level in ^{87}Rb at 403 keV while the beta group with end-point energy 1490 keV populates the energy level at 2415 keV. The low energy group then is interpreted as populating a level around 3.0 MeV. It was found that all three gamma-rays of energy 674, 1741 and 2012 keV were in coincidence with a beta group of end-point energy 1490 keV. A beta-group of

Figure 5-13. Beta spectrum in coincidence with 403 keV line in ^{87}Kr

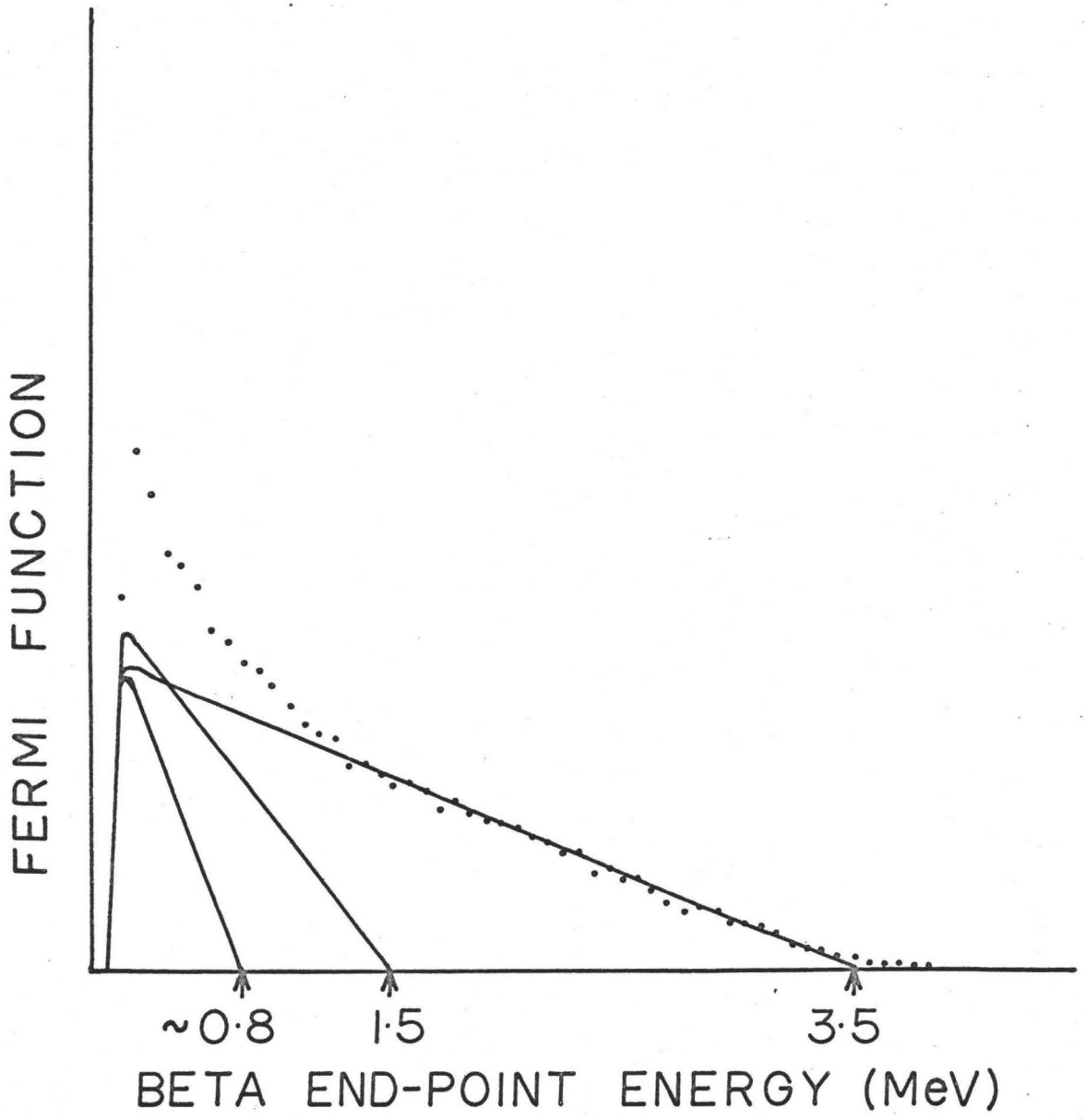

FIGURE 5-13

Figure 5-14. Beta spectrum in coincidence with 2557 keV line in ^{87}Kr

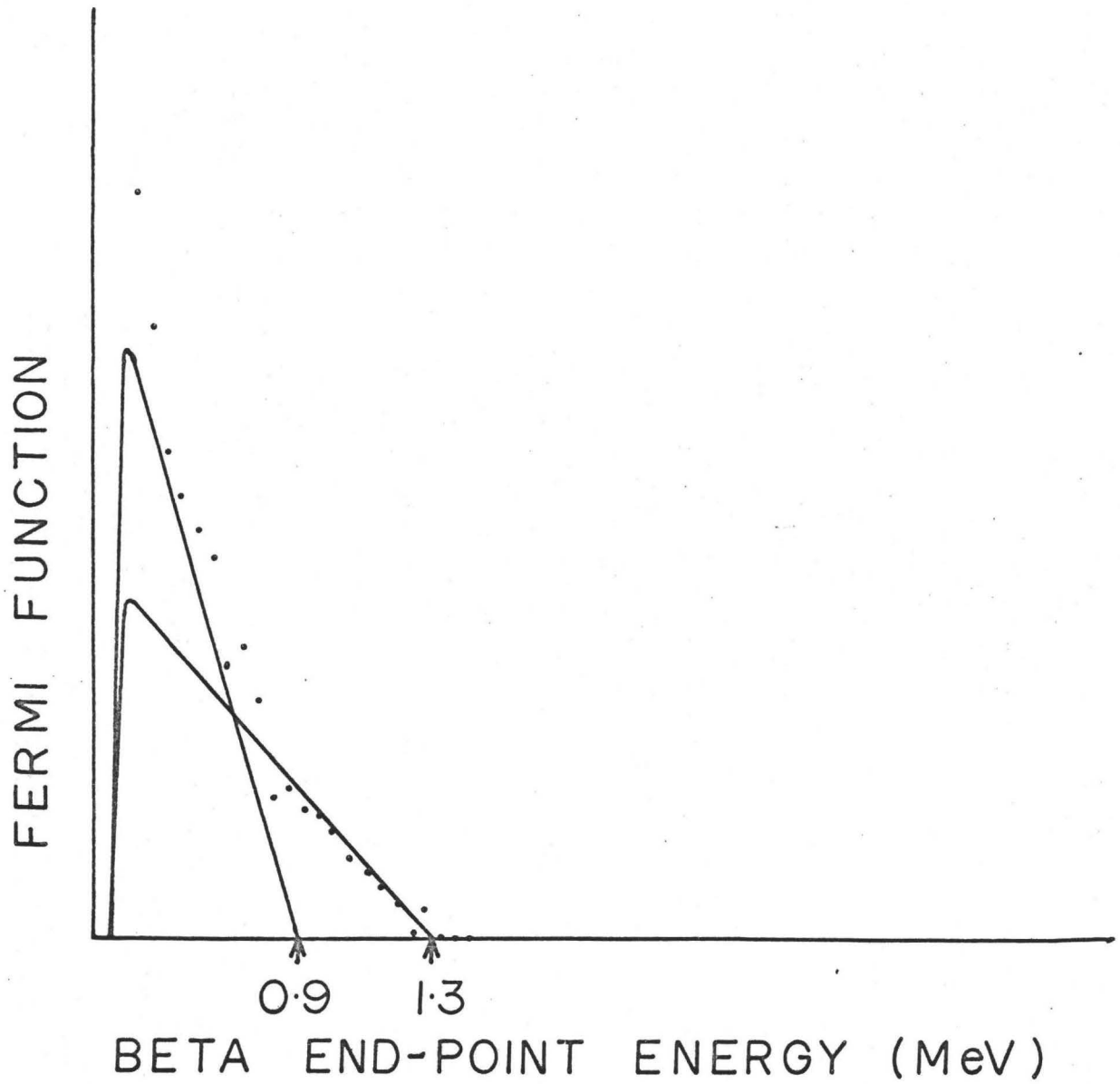

FIGURE 5-14

end point energy 3050 keV is in coincidence with the 846 keV gamma-ray line. In figure 5-14 the beta spectrum in coincidence with the 2556-2559 keV doublet has been stripped to two components with end-point energies 0.9 and 1.3 MeV. This is in contradiction with Holm's result[47] of one component of end-point energy 1300 keV in coincidence with a gamma-ray line at 2557 keV. The present results however confirm the gamma-gamma coincidence results which indicated the existence of a doublet at this energy.

5-3.3 Beta Analysis of ^{88}Kr

A sample of the ^{88}Kr isotope could not be produced without some contamination from ^{87}Kr. In order to minimize the amount of ^{87}Kr in the sample, the source produced was allowed to decay for one hour before flushing it into the counting chamber. Samples produced in this fashion had approximately 60% ^{88}Kr activity with the remainder being ^{87}Kr and ^{85}Kr.

Singles runs for ^{88}Kr followed the same procedure as for ^{87}Kr. Although the ^{88}Rb contamination did not exceed 8% of the total activity excluding background, the contribution of this contamination to the spectrum was subtracted from the total spectrum by fitting to the high energy part of the spectrum. In doing the Fermi-plot analysis it was

realized that there was a fair amount of gamma-ray interference along with the ^{87}Kr activity. A very high proportion of the ^{88}Kr beta activity was found to decay to the high energy states in ^{88}Rb. Thus there was low intensity in the high energy beta spectrum of ^{88}Kr, the part of the spectrum where there is a very large contribution from the ^{87}Kr high energy beta-ray groups. Under these conditions no judgement could be made as to the ground state beta group intensity in the decay of ^{88}Kr. However an argument can be made on the basis of spin assignments made to the low lying states by Morton and Darcey[64]. They assigned spins of 3^- and 1^- to the 28 keV and 196 keV levels respectively on the basis of (d,p) results. The ground state spin of ^{88}Rb is 2^- whereas the ground state spin of ^{88}Kr is 0^+. The beta group to the 196 keV level is then a first forbidden transition with $\Delta I=1$, yes. Since a ground state beta transition would be $\Delta I=2$, yes, it should be inhibited considerably relative to the beta-ray transition to the 196 keV level[136]. The beta singles run for ^{88}Kr is shown in figure 5-15 with the background and ^{88}Rb contamination subtracted off. The three higher energy beta groups belong to ^{87}Kr while the lower energy ones are members of the ^{88}Kr beta groups. The 2700 keV component and a strong low energy group are easily stripped off of the complex beta spectrum. It was almost

Figure 5-15. Beta singles run for ^{88}Kr with ^{88}Rb components and background subtracted

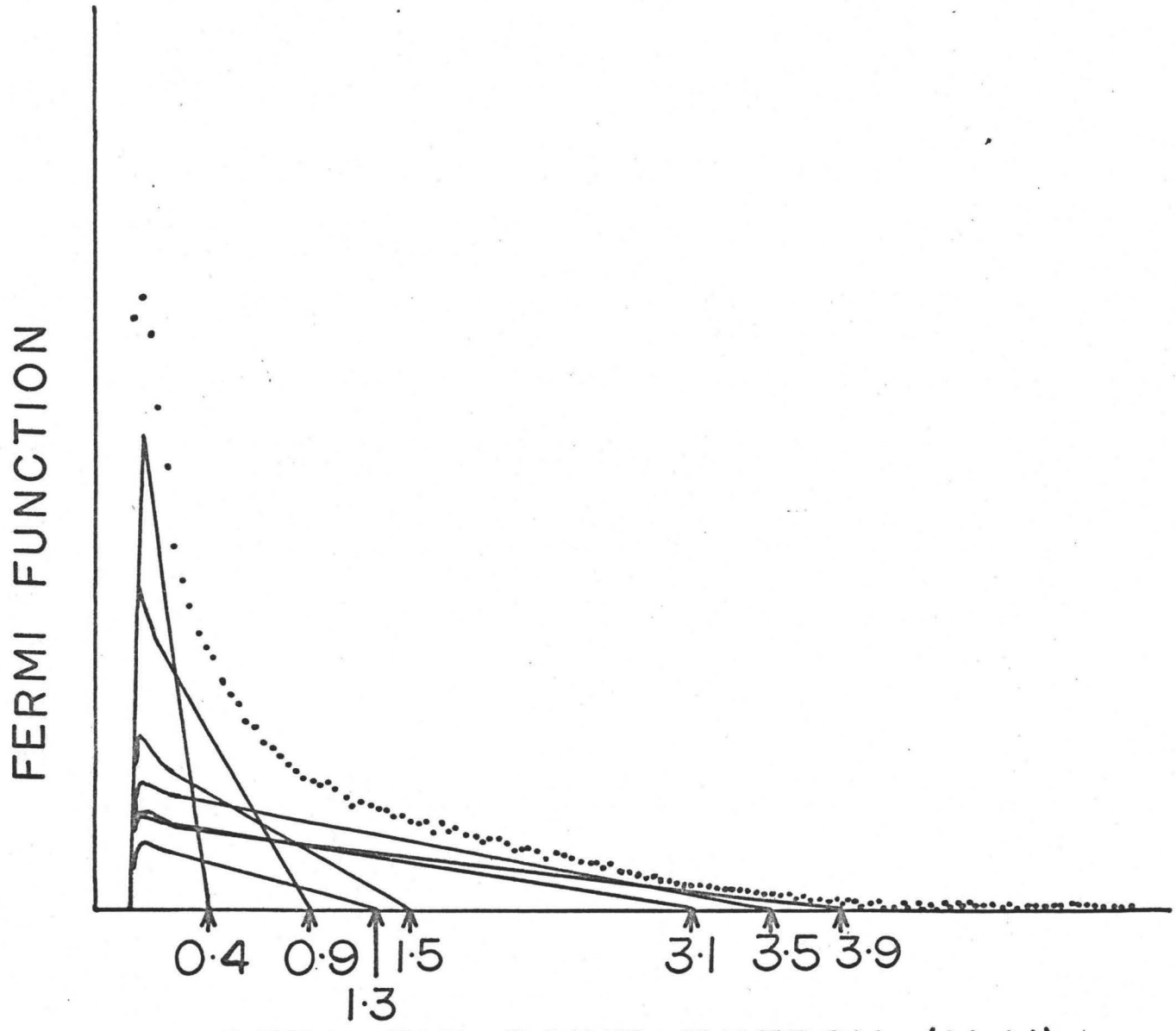

FIGURE 5-15

impossible to strip off any more groups with any reliability. Accurate measurements of the end-point energies of the beta groups were not possible from the singles spectrum. Thus the beta-gamma coincidence runs were used to determine the beta end-point energies of the ^{88}Kr beta groups.

Samples were prepared for the coincidence runs in the same manner as for the singles runs. Again two coincidence experiments were carried out using a 64×64 configuration. The first run covered the entire beta energy range in one dimension and the gamma energy range from 0.5 to 2.7 MeV in the other dimension. The second run covered the gamma-ray energy range from 0 to 1.0 MeV. In both runs the coincidence counting rate averaged about 350 events per second over a ten minute period.

Some of the important beta-gamma coincidences analyzed were as follows. One strong group with end-point energy 500 keV was detected in coincidence with the 1530, 2030, 2196 and 2392 keV gamma-ray lines. Two beta groups were detected in coincidence with the 835 keV line as shown in figure 5-16, namely the 510 and 2040 keV beta groups. The 1760 keV beta group was detected in coincidence with the 1142 keV line as was the 2700 keV group in coincidence with the 196 keV line. Any other possible coincidence spectra were too difficult to strip from the beta spectrum. Using the beta-gamma coin-

Figure 5-16. Beta spectrum in coincidence with 835 keV line in ^{88}Kr

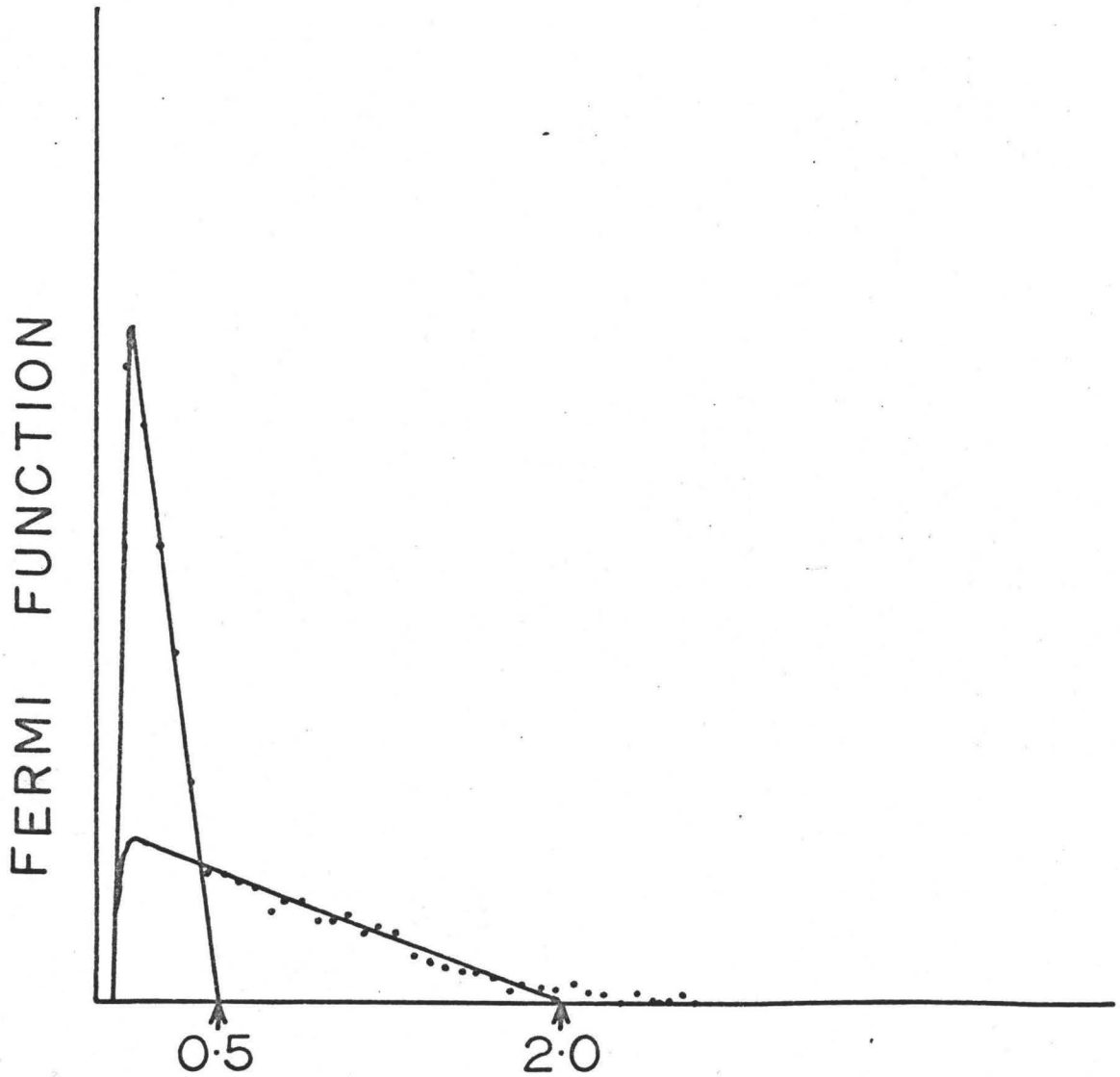

FIGURE 5-16

cidence results, a Q value of 2900±100 keV was determined for the beta decay of ^{88}Kr. This compares with 2800 keV as measured by Thulin[44].

5-4 Measurements on the 28 keV State in ^{88}Kr

In order to verify the decay scheme of ^{88}Kr as presented in section 5-5.2, a coincidence experiment was performed with the 28 keV gamma ray and all higher-energy gamma rays. The 28 keV gamma ray was detected using a 1 mm thick NaI(Tl) counter while the higher-energy gamma rays were detected using a Ge(Li) detector. The coincidence rate was very low and this was thought to be mainly due to the fact that the 28 keV line is strongly converted as would be expected for an M1 transition of this energy. However, there were definite indications that the 835 and 1530 keV lines are in coincidence with the 28 keV line . There was no indication of any coincidence of the 28 keV line with the 2196 keV line or with the 166 keV line. Thulin[46] on the other hand indicated that a coincidence had been detected between the 28 keV conversion electron and a 165 keV gamma transition.

The Weisskopf estimates of the half-life of a 28 keV state which decays by an M1 transition is of the order of one nanosecond for an unconverted transition. The K/(L+M) ratio

of 8 for the 28 keV gamma ray classifies it is an M1 transition[46]. As the line of interest is strongly converted ($\alpha_K \doteqdot 4.5$ for E_γ = 28 keV and an M1 transition) the lifetime of the state is expected to be much shorter than one nanosecond. An attempt was made to measure the lifetime of the 28 keV state using electronic timing and the centroid shift technique. Using a TAC (time-to-amplitude converter) the starting pulse was generated by gamma rays with energy greater than 800 keV detected by a fast plastic scintillator. The stop pulse was generated by the 28 keV gamma ray detected by a thin NaI counter. The only conclusion that could be drawn from this experiment was that the lifetime of the state is less than 200 ps, which is about the minimum lifetime which can be detected using the present technique. The results are consistent with a strongly converted ($\alpha_K \sim 4.5$) M1 transition.

5-5.1 Decay Scheme of ^{87}Kr

Based on the experimental results of this investigation a consistent decay scheme was constructed for the beta decay of ^{87}Kr as shown in figure 5-17. Assignment of the gamma rays in the decay scheme was based mainly on the gamma-gamma and beta-gamma coincidence results as very few levels were known in the ^{87}Rb nucleus from other reaction data. Since no coincidences were seen with the 2811 or 3310 keV gamma-ray

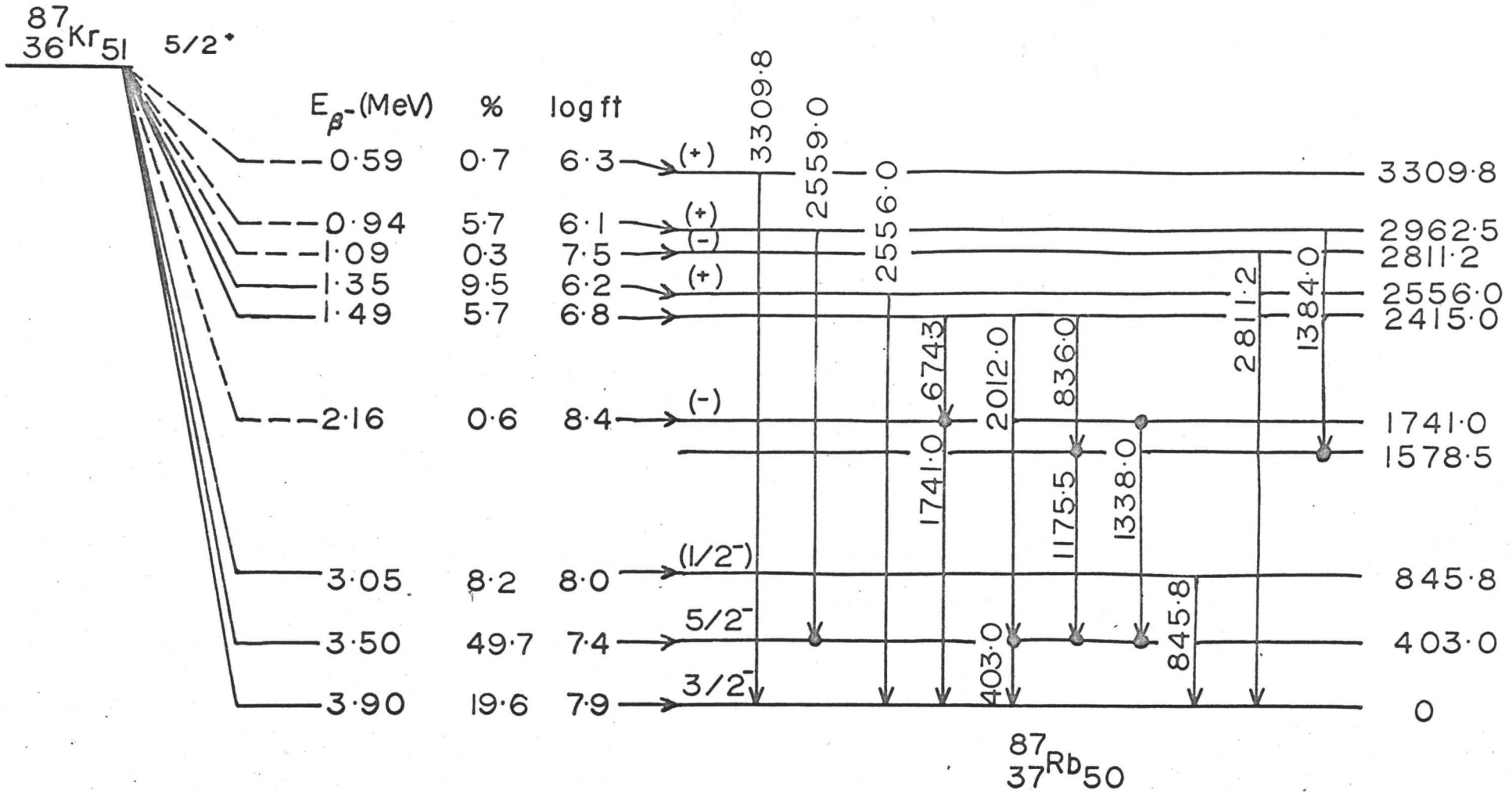
87 36Kr51 5/2+
Eβ-(MeV)
%
log ft
0·59
0·7
6·3
0·94
5·7
6·1
1·09
0·3
7·5
1·35
9·5
6·2
1·49
5·7
6·8
2·16
0·6
8·4
3·05
8·2
8·0
3·50
49·7
7·4
3·90
19·6
7·9
(+)
(+)
(-)
(+)
(-)
(1/2-)
5/2-
3/2-
3309·8
2559·0
2556·0
6743
2012·0
836·0
2811·2
1384·0
1741·0
1175·5
1338·0
845·8
403·0
3309·8
2962·5
2811·2
2556·0
2415·0
1741·0
1578·5
845·8
403·0
0
87 37Rb50

FIGURE 5-17

lines, these were assumed to be ground-state transitions. The 1384 keV line was detected in coincidence with the 403 keV line and was assigned its place in the decay scheme based on energy considerations as the sum of 1384.0+1175.5 is equal to 2559.0 keV within the errors of measurement. This also explains the coincidence of the higher energy component of the doublet at 2557 keV with the 403 keV line. The lower-energy component of the doublet was assigned as a ground-state transition on the basis of beta-gamma coincidence results. The beta-gamma coincidence results also established that the 674 keV line was in coincidence with a low-energy beta component; hence its assignment in the decay scheme. The 846 keV transition de-excites the well-known 846 keV level in ^{87}Rb.

Using this decay scheme and the fact that the intensity of the beta group to the ground state is 40% of the intensity of the beta group to the first excited state, it was possible to obtain the beta-ray branching percentages (including 19.6% to the ground state) from the relative gamma-ray intensities. The absolute gamma-ray intensities were consequently determined and are listed in Table 5-1. Log ft values have been calculated using the deduced beta-ray branching ratios and the end-point energies of the beta groups.

5-5.2 Decay Scheme of ^{88}Kr

The decay scheme shown in figure 5-18 has been constructed for ^{88}Kr using the experimental results of the preceding sections. This decay scheme has been modified from the one presented by Thulin[46] based on the better energy measurements available. In general the strong transitions listed in Table 5-2 have been placed in the decay scheme on the basis of gamma-gamma and beta-gamma results. The weaker lines were assigned in the decay scheme on the basis of the known (d,p) levels in ^{88}Rb as listed in Table 2-7. The 835 keV line has been assigned as de-exciting the 862 keV level based on its coincidence with the 28 keV line and the fact that a level was observed at 862 keV in the $^{87}Rb(d,p)^{88}Rb$ reaction. The 166 keV line was detected in coincidence with the 196 keV line and thus was assigned as shown rather than populating the 28 keV level. The energy difference between the 196 and 166 keV lines also makes the latter assignment unlikely. However Thulin[46] detected the conversion electrons of the 28 keV line in coincidence with a gamma transition of energy 165 keV. The present coincidence experiment carried out with the 28 keV line indicated a possible coincidence with a line of approximately 166 keV although it was difficult to determine positively. If the coincidence were real the line at 166 keV would have to be a doublet with

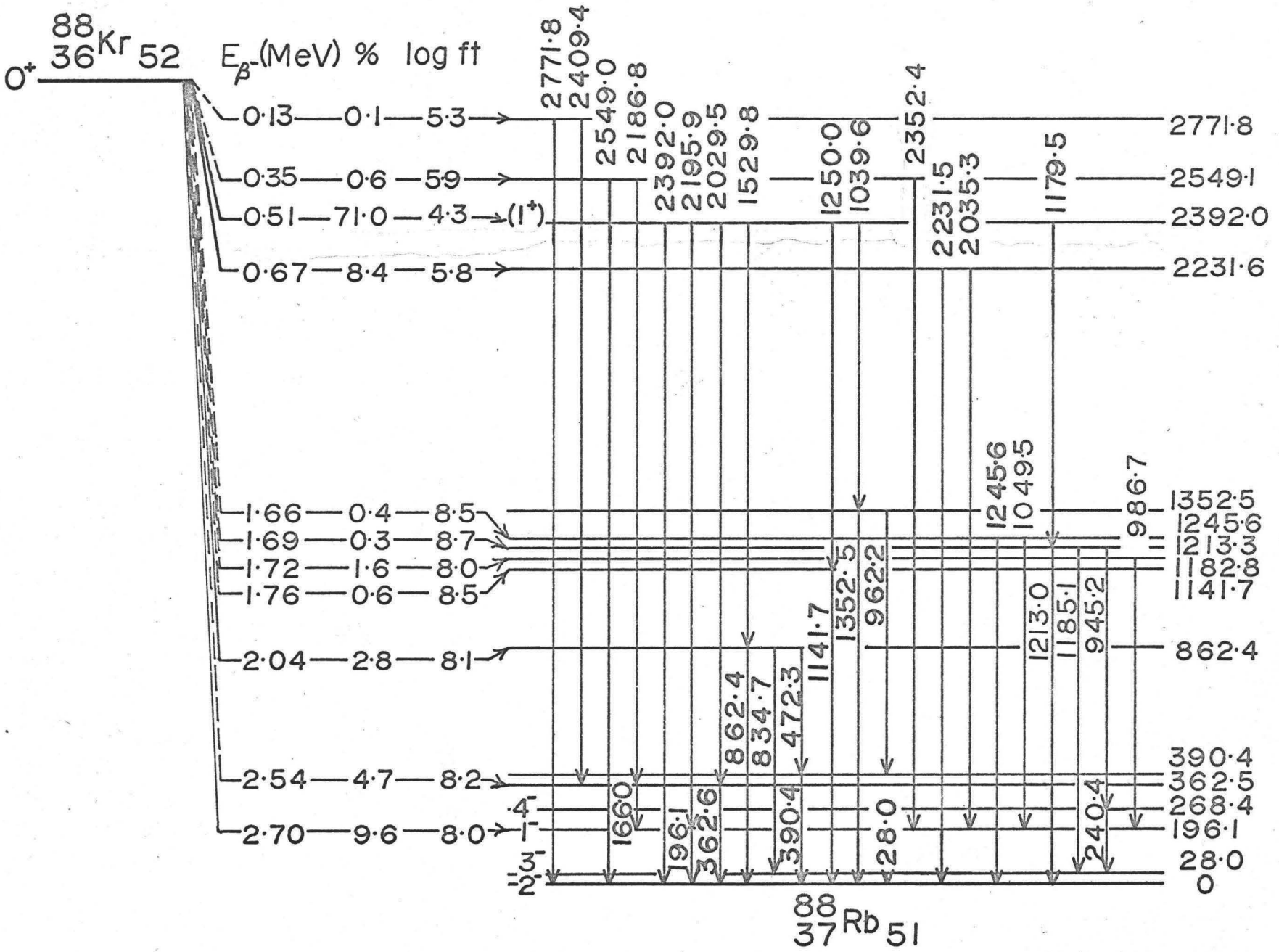
88 36Kr 52
0+
Eβ-(MeV) % log ft
0·13 — 0·1 — 5·3
0·35 — 0·6 — 5·9
0·51 — 71·0 — 4·3 → (1+)
0·67 — 8·4 — 5·8
1·66 — 0·4 — 8·5
1·69 — 0·3 — 8·7
1·72 — 1·6 — 8·0
1·76 — 0·6 — 8·5
2·04 — 2·8 — 8·1
2·54 — 4·7 — 8·2
2·70 — 9·6 — 8·0
2771·8
2409·4
2549·0
2186·8
2392·0
2195·9
2029·5
1529·8
1250·0
1039·6
2352·4
2231·5
2035·3
1179·5
1245·6
1049·5
986·7
1352·5
962·2
1141·7
1213·0
1185·1
945·2
862·4
834·7
472·3
390·4
362·5
268·4
196·1
28·0
0
1660
196·1
362·6
390·4
28·0
240·4
2771·8
2549·1
2392·0
2231·6
1352·5
1245·6
1213·3
1182·8
1141·7
862·4
390·4
362·5
268·4
196·1
28·0
0
88 37Rb 51

FIGURE 5-18

a higher energy component at 168 keV. This was not evident in the present investigation. The levels at 1142, 1213, 1246 and 1353 keV were observed in the (d,p) reaction but the level at 1183 keV was postulated on the basis of the coincidence of the 987 keV line with the 196 keV line. The strong level at 2392 keV was not populated in the (d,p) reaction although the level at 2232 keV was weakly populated. The assignment of the 2232 and 2035 keV lines was based mainly on energy considerations. The levels at 2549 and 2772 keV were postulated on the basis of ground state transitions and a transition to the 362 keV level in each case. The 2549 keV level also has a transition to the 196 keV level. The 789 and 1518 keV transitions were not assigned to the decay scheme

Based on this decay scheme and the fact that no beta rays are seen populating the ground state of ^{88}Kr, the beta-branching ratios have been calculated and hence the absolute intensities of the gamma rays are listed in Table 5-2. These calculations were done assuming no internal conversion of the 196 keV line although Thulin[46] indicated that the internal conversion coefficient was measurable but small. Another assumption was that the intensity of the 28 keV line equals the sum of the intensities of the 835, 1185 and 240 keV lines. However if there is a 168 keV line feeding the 28 keV level, the intensity of the 28 keV line would be greater. Log ft

values have been calculated for all the beta groups based on the Q value of 2900 keV and the deduced branching ratios. These are summarized in figure 5-18.

5-5.3 Decay Scheme of ^{88}Rb

A decay scheme for ^{88}Rb consistent with the experimental results has been constructed as shown in figure 5-19. the significant additions made to the decay scheme as presented by Lazar et.al.[55] are as follows. The 4.87 MeV level reported by Lazar et.al.[55] is actually a triplet consisting of levels at 4744, 4846 and 4854 keV. The members of the doublet observed in this investigation at 2112 and 2119 keV de-excite the 4846 and 4854 keV levels respectively. Two more levels are also populated at 4270 and 4414 keV. These levels are de-excited by the weak gamma-ray lines of 1535 and 2578 keV, respectively. No evidence for a level at 3691 keV was seen. Using the fact that the ^{88}Rb and ^{88}Kr spectra in figure 5-2 were collected at equilibrium, the intensities of the ^{88}Rb lines were determined relative to the intensities of the ^{88}Kr lines. The ground-state beta group intensity was calculated as 68.7% assuming that all the ^{88}Kr activity was detected. This compares with 65.5% as determined from the beta singles run. The best value for the ground-state beta intensity, however, is $\geq$ 68.7% as the effects of internal conversion in ^{88}Kr are not known.

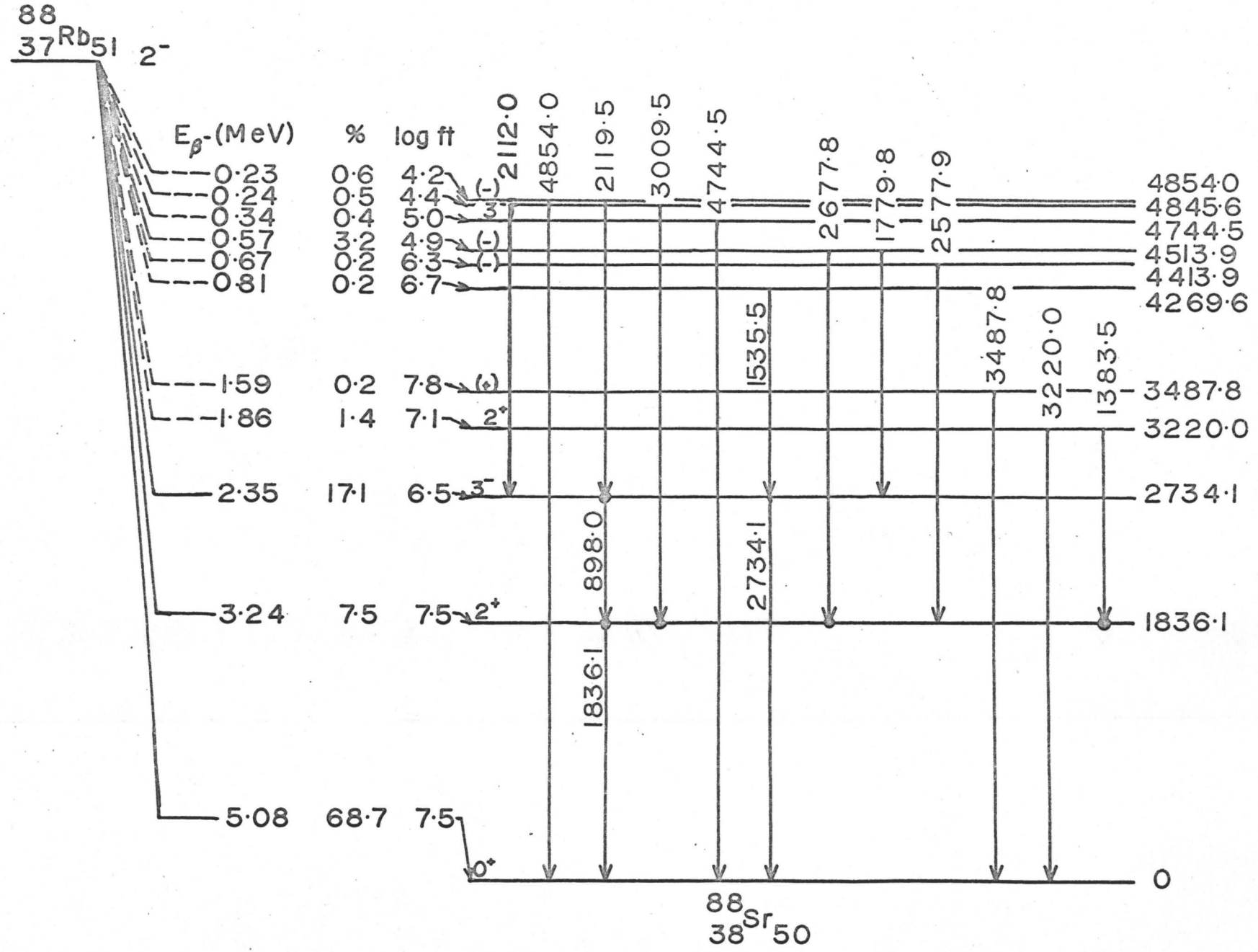
88
37Rb51 2-
Eβ-(MeV)
%
log ft
0·23
0·24
0·34
0·57
0·67
0·81
1·59
1·86
2·35
3·24
5·08
0·6
0·5
0·4
3·2
0·2
0·2
0·2
1·4
17·1
7·5
68·7
4·2
4·4
5·0
4·9
6·3
6·7
7·8
7·1
6·5
7·5
7·5
(-)
3-
(-)
(-)
(-)
(+)
2+
3-
2+
0+
2112·0
4854·0
2119·5
3009·5
4744·5
2677·8
1779·8
2577·9
1535·5
3487·8
3220·0
1383·5
898·0
2734·1
1836·1
4854·0
4845·6
4744·5
4513·9
4413·9
4269·6
3487·8
3220·0
2734·1
1836·1
0
88
38Sr50

FIGURE 5-19

CHAPTER 6

STRONTIUM THERMAL NEUTRON CAPTURE RESULTS

6-1 Singles Runs

Singles spectra were obtained using samples of natural strontium in the form of $SrCO_3$ powder. The samples were at least 99% pure with small calcium, iron and other metal impurities of the order of about .02% each. The carbon contaminant gave rise to three gamma-ray lines at 1262, 3684 and 4945 keV. Significant contributions to the capture cross-section were provided only by the $^{86}Sr(n,\gamma)^{87}Sr$ and $^{87}Sr(n,\gamma)^{88}Sr$ reactions as outlined in Table 2-2.

Various spectra were collected using both neutron irradiation facilities, two different sample holders and a variety of Ge(Li) detectors. By using both neutron irradiation facilities it was possible to eliminate certain background lines from the spectra. Background lines arising from neutron capture in the impurities in the sample, in the sample holder and in the detector chamber material were of course common to all spectra. Gamma-radiation arising from neutron capture in the sample holder was identified by using two different sample holders. One sample holder was a quartz tube which gives rise to gamma-radiation from the $^{28}Si(n,\gamma)^{29}Si$

reaction. The energies and intensities of these transitions are well known and were thus used as calibration standards[104]. A paper container was used as the second sample holder. Paper contains hydrocarbons and thus gives rise to the characteristic gamma radiation following the $H(n,\gamma)D$ and $^{12}C(n,\gamma)^{13}C$ reactions. These lines also provided good internal calibration standards in the strontium singles run.
All of the Ge(Li) detectors used were of the wrap-around configuration. The active volume of the counter determined the detection efficiency for the double-escape and photo-peak events. The difference in the relative detection efficiencies for the two types of events for the various counters used provided a means of distinguishing between photo-peaks and double-escape peaks in the energy range 1.5 to 3.0 MeV where the photo-peak and double-escape relative efficiencies are within a factor of 2 or 3 of each other.

The singles run which gave the most detailed information is depicted in figure 6-1. This spectrum was obtained in a two-day counting period using the reactor horizontal beam port facility and the strontium sample contained in a paper holder. The spectrum was recorded initially as a series of consecutive eighty minute dumps on magnetic tape. Each set of data was adjusted to have the same gain and zero parameters as those determined for the first dump. Following

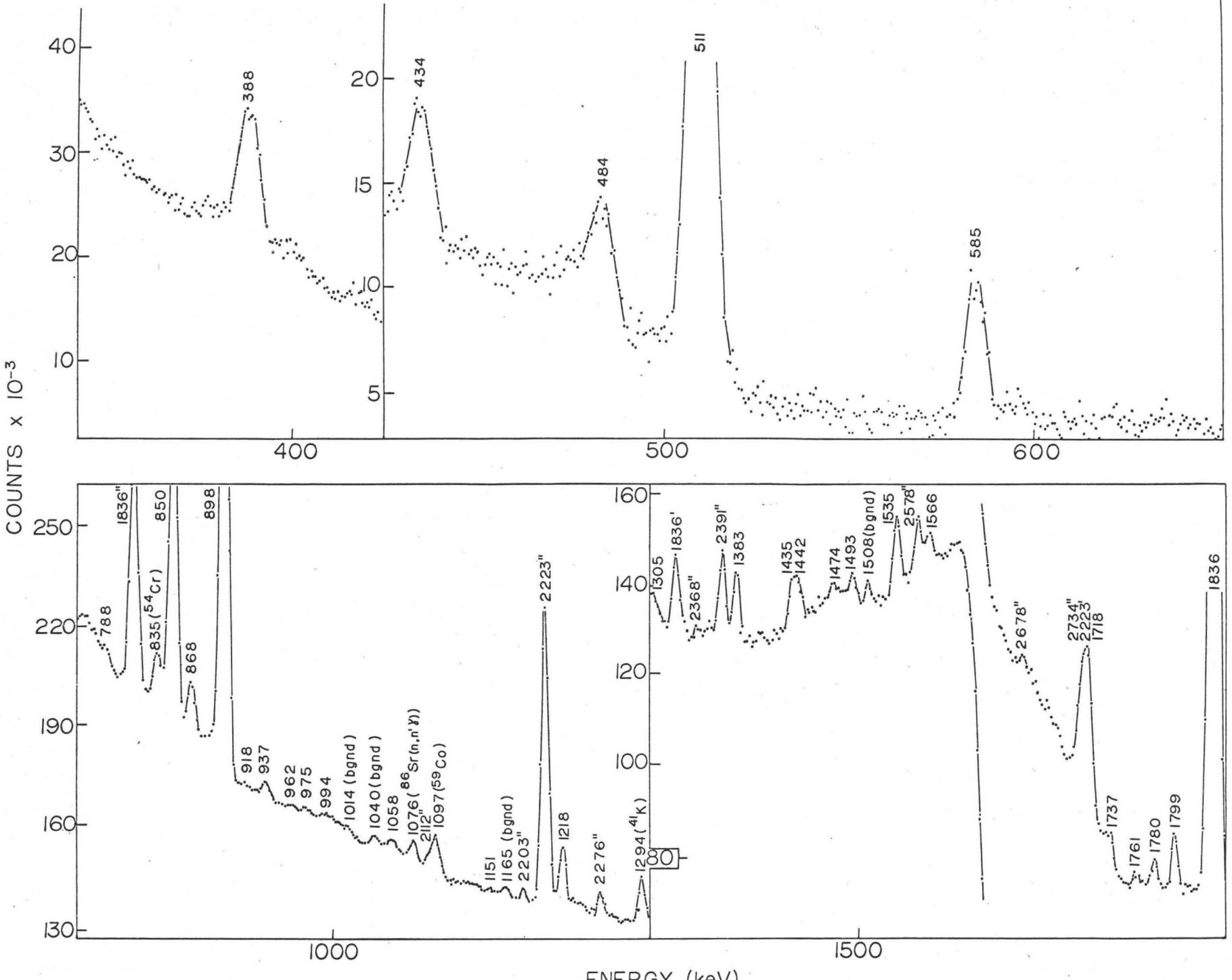
COUNTS x 10⁻³
ENERGY (keV)
388
434
484
511
585
788
836"
835(⁵⁴Cr)
850
868
898
918
937
962
975
994
1014 (bgnd)
1040 (bgnd)
1058
1076(⁸⁶Sr(n,n'γ))
1112"
1097(⁵⁹Co)
1151
1165 (bgnd)
2203"
2223"
1218
2276"
1294(⁴¹K)
1305
1836'
2368"
2391"
1383
1435
1442
1474
1493
1508(bgnd)
1535
2578"
1566
2678"
2734"
2223'
1718
1737
1761
1780
1799
1836

FIGURE 6-1a

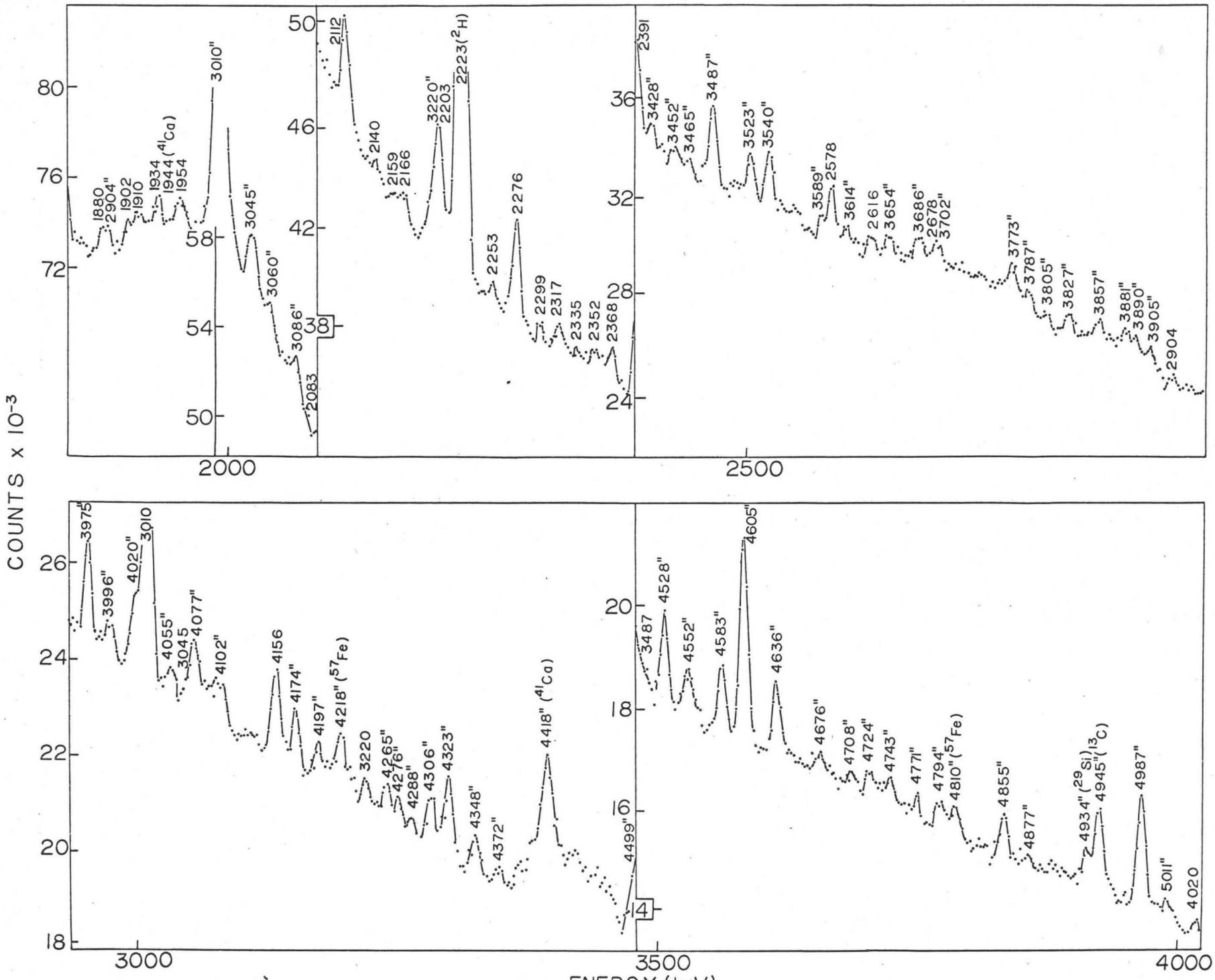
COUNTS x 10⁻³
ENERGY (keV)
1880
2904"
1902
1910
1934
1944 (41Ca)
1954
3010"
3045"
3060"
3086"
2083
2112
2140
2159
2166
3220"
2203
2223(2H)
2253
2276
2299
2317
2335
2352
2368
2391
3428"
3452"
3465"
3487"
3523"
3540"
3589"
2578
3614"
2616
3654"
3686"
2678
3702"
3773"
3787"
3805"
3827"
3857"
3881"
3890"
3905"
2904
3975"
3996"
4020"
3010
4055"
3045
4077"
4102"
4156
4174"
4197"
4218" (57Fe)
3220
4265"
4276"
4288"
4306"
4323"
4348"
4372"
4418" (41Ca)
4499"
3487
4528"
4552"
4583"
4605"
4636"
4676"
4708"
4724"
4743"
4771"
4794"
4810" (57Fe)
4855"
4877"
4934" (29Si)
4945" (13C)
4987"
5011"
4020

FIGURE 6-1b

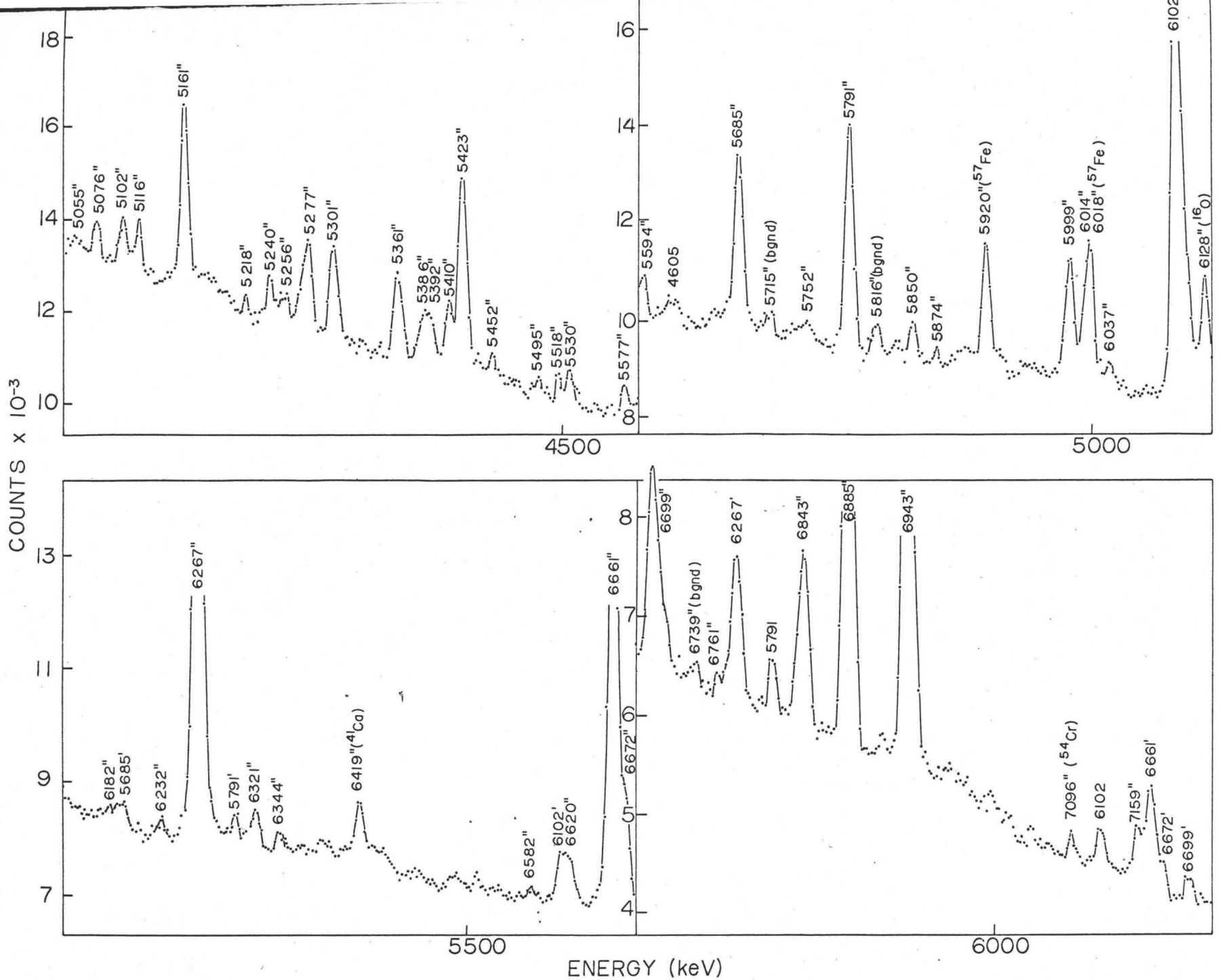
COUNTS x 10⁻³
ENERGY (keV)
4500
5000
5500
6000
5055"
5076"
5102"
5116"
5161"
5218"
5240"
5256"
5277"
5301"
5361"
5386"
5392"
5410"
5423"
5452"
5495"
5518"
5530"
5577"
5594"
4605
5685"
5715" (bgnd)
5752"
5791"
5816"(bgnd)
5850"
5874"
5920"(⁵⁷Fe)
5999"
6014"
6018"(⁵⁷Fe)
6037"
6102"
6128"(¹⁶O)
6182"
5685'
6232"
6267"
5791'
6321"
6344"
6419"(⁴¹Ca)
6582"
6102'
6620"
6661"
6672"(O)
6699"
6739"(bgnd)
6761"
6267'
5791
6843"
6885"
6943"
7096"(⁵⁴Cr)
6102
7159"
6661'
6672'
6699'

FIGURE 6 - Ic

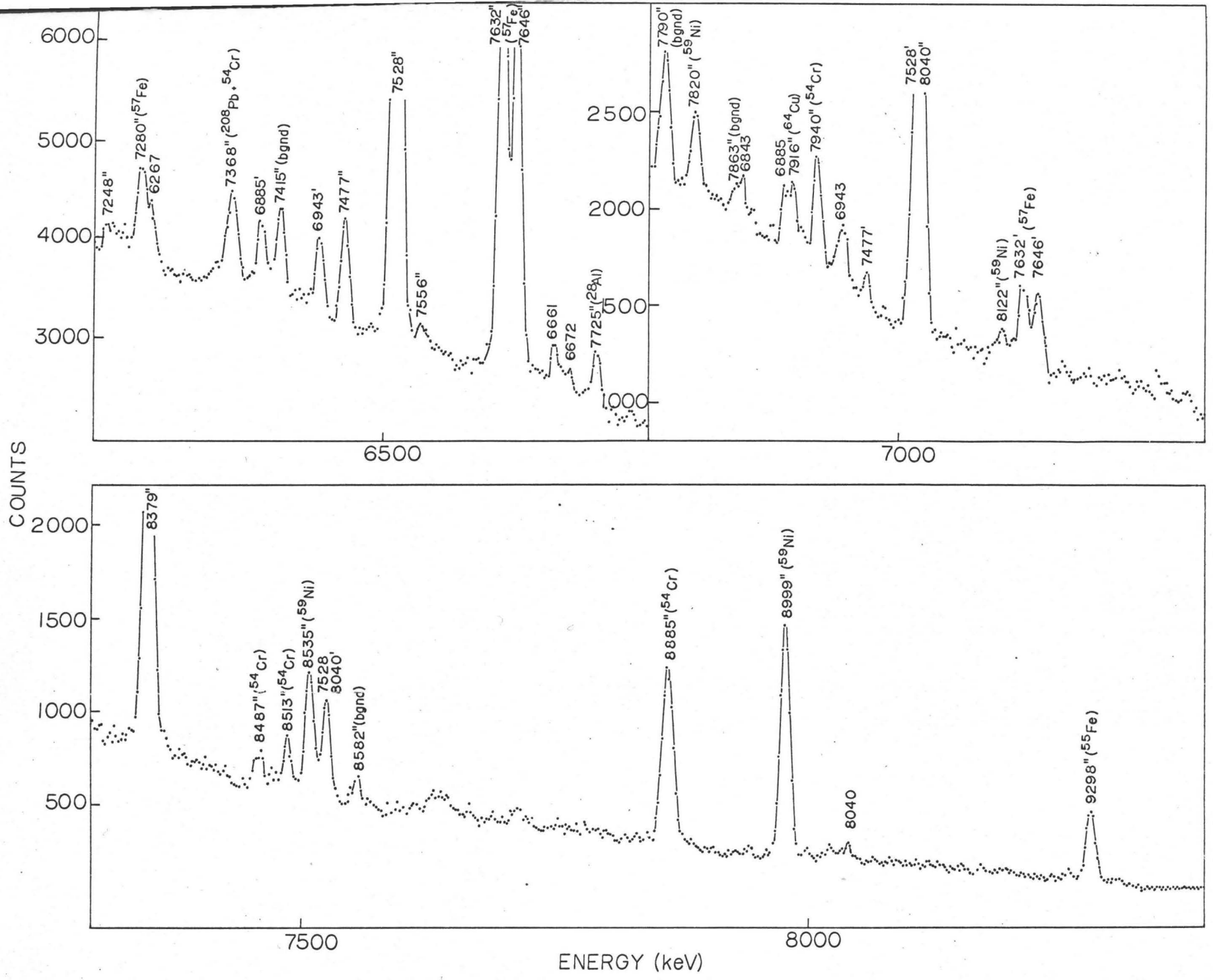
COUNTS
ENERGY (keV)
6000
5000
4000
3000
2500
2000
1500
1000
500
6500
7000
7500
8000
7248"
7280"(57Fe)
6267
7368"(208Pb+54Cr)
6885'
7415"(bgnd)
6943'
7477"
7528"
7556"
7632"
(57Fe)
7646"
6661
6672
7725"(28Al)
7790"
(bgnd)
7820"(59Ni)
7863"(bgnd)
6843
6885
7916"(64Cu)
7940"(54Cr)
6943
7477'
7528'
8040"
8122"(59Ni)
7632'
7646'(57Fe)
8379"
8487"(54Cr)
8513"(54Cr)
8535"(59Ni)
7528
8040'
8582"(bgnd)
8885"(54Cr)
8999"(59Ni)
8040
9298"(55Fe)

FIGURE 6 - Id

this adjustment the spectra were summed and a background function was calculated and subtracted from the sum. The resulting spectrum is shown in figure 6-1 with the exception of the upper portion of figure 6-1(a) which was extracted from another low energy run of the strontium thermal neutron capture reaction.

This spectrum as well as others were analyzed in detail to obtain the energies and intensities of all of the peaks. The centroid of each peak was calculated by computer where there were no overlapping peaks nearby. The positions of those peaks which overlapped were calculated either by a non-linear Gaussian fitting technique where statistics warranted or by visual estimation when a good Gaussian fit could not be achieved. The strong strontium thermal neutron capture gamma-ray lines were initially calibrated using the well-known high energy lines from the $^{28}Si(n,\gamma)^{29}Si$ reaction in a previous run with the sample in a quartz tube holder. The strong iron thermal neutron capture gamma rays were also used as calibration points as iron is a major contributor to background radiation. The deuteron and carbon capture gamma-ray lines also appear in the background and were used for calibration purposes. In all, twelve gamma-ray lines due to photo-peak, single-escape and double-escape response peaks of background lines as well as the strong low energy lines

of $^{87}Sr(n,\gamma)^{88}Sr$ were used as calibration standards. The energy values adopted for the standards are listed in Table 6-1. The average error in fitting these peaks to a para-

Table 6-1

Calibration lines for Strontium Capture Gamma-Rays

Reaction	E_γ (keV)	ΔE_γ (keV)	Reference
$^{56}Fe(n,\gamma)^{57}Fe$	7646	1	137
	7632	1	
	6018	1	
	5920	1	
$^{12}C(n,\gamma)^{13}C$	4945.4	.17	138
$H(n,\gamma)D$	2223.28	.15	117
$^{88}Y \xrightarrow{\beta^+} {}^{88}Sr$	1836.08	.07	114
	898.01	.05	

bolic function was ± 0.5 keV which is a measure of the accuracy with which the gamma-ray energies can be measured. The energies of the strong strontium thermal neutron capture gamma rays as determined from the calibration run were then used as calibration standards to determine the energies of all the strontium capture gamma rays. The calibration peaks were fitted to a parabolic function over the nearly linear

portion of the ADC gain, i.e. channels 500 to 3800. The energies of all of the gamma-ray lines are indicated in figure 6-1 to the nearest keV. The background lines are labelled as such. The gamma rays which likely originate from neutron capture in strontium are listed in Table 6-2 along with the errors in parenthesis. The gamma-ray lines observed by the other three research groups are listed for comparison. The errors associated with the energies measured by Schmidt et.al.[60] are generally a factor of three larger than the corresponding errors quoted by the other three groups including those quoted in the present work. In the column under the heading, "Comments", the contributing isotopes of some of the background lines are noted. Gamma-ray energies which may correspond to double-escape peak energies are also noted. The isotopic assignment of most of the lines is also listed as discussed in later sections of this chapter. In the case of the stronger strontium capture gamma rays, the energies listed are weighted averages of several determinations from spectra collected by different Ge(Li) detectors. In the case of the weaker lines, the energies were mainly determined from the spectrum shown in figure 6-1 as it had the greatest number of counts in the peaks of all of the runs carried out.

The intensities of the gamma-ray lines were determined from the efficiency curves (of which a typical one is

TABLE 6-2

List of Strontium Capture Gamma Rays

Line No.	Present Work		Schmidt et al(60)	Irigaray et al(56)		Rasmussen et al(57)		Comment
	E_γ	I_γ	E_γ	E_γ	I_γ	E_γ	I_γ	
			9154					
				8997	0			^{59}Ni
				8895	0.70			8379'
				8886	11.4			^{54}Cr
				8754				
				8554	1.1			
1	8378.9(1)	2.30*	8376	8381	4.6	8378.4	1.57	88***
2	8039.7(1)	2.60	8038	8040	5.1	8039.0	1.31	87
				7965				
				7912				^{64}Cu
				7691	0.9			
3	7556 (2)	0.10		7558				87
4	7528.4(1)	8.00	7527	7529	14.6	7527.7	5.08	88**
						7498.0	0.12	
5	7477.3(1)	0.68	7476			7476.5	0.46	88**
				7457	0.9			
				7422				
				7400	1.1			
						7384.9	0.14	
				7367				
						7308.1	0.24	
				7292	0.9			
			7272					
6	7248.0(2)	0.15	7247	7247				
						7235.5	0.14	
						7219.9	0.14	
				7208				
				7178	1.1			

(continued next page)

Line No.	Present Work		Schmidt et al (60)		Irigaray et al (56)		Rasmussen et al (57)		Comment
	E_γ	I_γ	E_γ	E_γ	I_γ	E_γ	I_γ	
7	7159.8(2)	0.25	7153	7162	1.1	7160.8	0.13	88
				7125	1.1	7117.6	.10	
						6963.8	.12	
8	6942.8(1)	6.65	6941	6944	11.7	6941.9	3.71	88**
9	6885.3(1)	5.18	6883	6885	9.7	6885.1	3.31	88**
10	6842.7(1)	0.85	6843	6847	1.4	6844.3	0.66	88**
11	6812.7(2)	0.25	6811	6814	0.6			(88)
				6778	3.1			
12	6760.6(2)	0.20	6766	6765	0.6			
13	6699.2(1)	1.20	6693	6704	2.3	6698.9	0.93	88**
14	6671.5(2)	1.20						
15	6661.0(1)	6.90	6658	6661	16.3	6660.6	6.05	88**
16	6620.0(2)	0.25		6619	0.9			
			6612	6609	0.9			
17	6582(2)	0.10				6585.5	0.08	
			6569					
						6544.7	0.09	
						6507.8	0.13	
						6487.0	0.10	
						6463.5	0.24	
						6417.0	0.17	^{41}Ca
						6390.3	0.26	
18	6344(2)	0.15				6343.7	0.13	
19	6319(2)	0.30		6312		6322.2	0.21	
20	6267.1(1)	8.55	6264	6267	18.8	6267.3	6.10	88**
21	6231.9(2)	0.25	6228			6230.4	0.23	
22	6182.0(2)	0.25	6188	6184	1.1			
						6136.6	0.09	
23	6101.8(1)	4.80	6101	6102	11.2	6101.9	3.88	88**
24	6037.1(2)	0.20	6040					88
25	6014.4(3)	0.35		6009	2.6	6012.9	0.15	

(continued next page)

Line No.	Present Work		Schmidt et al[60]	Iragaray et al[56]		Rasmussen et al[57]		Comment
	E_γ	I_γ	E_γ	E_γ	I_γ	E_γ	I_γ	
26	5999.3(1)	1.20	6003	5996	1.7	5999.5	0.47	88
			5927	5926	0.66			
						5906.5	0.14	
			5887					
27	5874.3(2)	0.20		5873				
28	5850.0(2)	0.35	5853	5852	0.71			88
						5823.7	0.74	
29	5790.8(1)	1.86	5791	5789	4.6	5790.4	1.71	88**
30	5749.3(2)	0.20	5744	5753		5751.7	0.09	
						5706.7	0.14	
31	5685.4(1)	1.62	5687	5686	5.1	5686.1	0.77	88**
				5669				
			5628					
						5611.1	0.10	
32	5593.8(2)	0.25	5590	5588		5593.1	0.24	88
33	5577.3(2)	0.20		5570		5579.5	0.10	88
						5559.2	0.09	
34	5529.6(2)	0.20	5538	5535				
35	5518.5(2)	0.20						
				5505				
36	5495.5(2)	0.10		5490				
37	5451.7(2)	0.10		5458				88
38	5423.3(1)	1.32	5424	5423	4.9	5424.1	0.98	88**
39	5409.9(2)	0.36				5409.9	0.13	
40	5391.8(2)	0.25				5397.5	0.09	
41	5386.1(2)	0.25	5391	5384	1.4	5386.3	0.30	
42	5361.5(1)	0.50	5366	5360	1.4	5361.6	0.38	88**
						5322.5	0.22	
43	5300.8(1)	0.70	5304	5301	2.0	5301.0	0.54	88

(continued next page)

Line No.	Present Work		Schmidt et al.(60)	Iragaray et al.(56)		Rasmussen et al.(57)		Comment
	E_γ	I_γ	E_γ	E_γ	I_γ	E_γ	I_γ	
44	5276.8(1)	0.55	5279	5277	2.6	5276.9	0.42	88
45	5256.3(2)	0.15						88
46	5240.4(2)	0.30	5245	5242	1.4	5244.0	0.27	
47	5218.2(2)	0.15						
						5200.2	0.19	
			5189					
48	5161.5(1)	1.30	5162	5161	3.7	5162.0	1.60	88**
49	5116.5(2)	0.25				5115.2	0.19	
50	5101.7(2)	0.20	5106	5104		5102.9	0.14	88
51	5076.3(2)	0.25	5074			5075.6	0.33	
52	5055.3(2)	0.15		5053		5056.1	0.11	
53	5010.8(2)	0.15				5007.3	0.28	
54	4987.6(1)	0.60	4988	4990	1.1	4988.0	0.54	88
				4980				
			4944			4945.2	0.85	^{13}C
			4918			4912.2	0.08	
				4900	1.1			
			4888					
55	4877.0(2)	0.08						
56	4854.7(2)	0.20	4855	4852		4852.5	0.25	88
			4833			4810.5	0.32	
57	4794.5(2)	0.15				4795.0	0.15	
58	4770.6(2)	0.15				4771.9	0.11	
			4752			4748.6	0.08	
59	4743(2)	0.08				4743.6	0.10	88**
				4732	0.9			
60	4724(2)	0.08						88
61	4708(2)	0.08	4712	4715				
						4700.5	0.15	
62	4676(2)	0.10	4679	4665		4671.8	0.08	Fe?

(continued next page)

Line No.	Present Work		Schmidt et al[60]	Iragaray et al[56]		Rasmussen et al[57]		Comment
	E_γ	I_γ	E_γ	E_γ	I_γ	E_γ	I_γ	
63	4636.0(1)	0.50	4642	4636		4635.8	0.26	
64	4604.8(1)	1.75	4610	4604	3.7	4605.4	1.42	88
65	4583.3(1)	0.53	4587	4581	1.1	4583.7	0.34	
66	4552.0(2)	0.30	4560	4552		4553.9	0.12	88
67	4528.5(2)	0.42	4533	4529		4529.6	0.24	
						4517.6	0.08	
68	4499.0(2)	0.36	4503	4494		4500.2	0.38	
			4476	4478				
				4439				
69	4417.7(1)	0.42	4417	4415	1.7	4416.7	0.57	(^{41}Ca)
			4403					
						4392.2	0.19	
70	4371.9(2)	0.15	4375			4371.9	0.13	
71	4348.1(2)	0.25	4350			4350.2	0.08	88
72	4323.0(2)	0.35	4324	4321		4324.7	0.17	
73	4305.8(2)	0.25	4308	4299		4306.0	0.31	
74	4287.7(2)	0.10	4295			4297.2	0.06	88
75	4276.0(2)	0.08	4281			4276.6	0.08	
76	4264.7(2)	0.15	4263	4259	1.7	4259.6	0.19	
			4241					
77	4196.8(2)	0.15	4204					
78	4174.2(2)	0.50	4182					
79	4155.7(1)	0.55	4160	4152		4157.7	0.25	
				4132		4127.8	0.21	
80	4102.1(2)	0.25	4100					
81	4077.0(1)	0.40	4074			4079.4	0.28	
82	4054.7(2)	0.20	4052					
						4036.2	0.38	
83	4020.5(2)	1.62	4025	4021	4.9	4020.4	0.22	88

(continued next page)

Line No.	Present Work		Schmidt et al (60)		Iragaray et al (56)		Rasmussen et al (57)		Comment
	E_γ	I_γ	E_γ		E_γ	I_γ	E_γ	I_γ	
84	3996.4(2)	0.15	3996						
85	3975.2(1)	0.52	3973		3975	2.3	3975.8	0.33	88
			3956		3965	2.3			
86	3904.9(2)	0.20	3907				3905.3	0.11	
87	3889.8(2)	0.15	3887				3887.9	0.12	
88	3880.8(2)	0.15	3869						88
89	3857.0(2)	0.25							
90	3826.8(2)	0.25	3827						88
91	3805.3(2)	0.20							
92	3773.0(2)	0.30	3765		3772		3770.9	0.28	88
							3756.9	0.09	
			3737				3745.5	0.21	
93	3701.7(2)	0.25					3704.5	0.30	88
94	3686.0(2)	0.25	3691						C?
					3678				
95	3654.1(2)	0.25	3656						88
							3638.8	0.27	
96	3614.1(2)	0.20	3620				3620.5	0.17	
97	3589.0(2)	0.25					3589.3	0.10	
98	3540.3(2)	0.50	3547				3542.0	0.51	88
99	3522.6(1)	0.50	3529				3524.0	0.26	88
100	3487.0(2)	1.20	3490		3488	4.6	3488.8	0.51	88**
101	3464.6(2)	0.15					3465.5	0.14	
102	3451.8(2)	0.25					3452.4	0.22	
103	3428.0(2)	0.20					3424.7	0.61	88
							3397.6	0.22	
							3385.8	0.12	
							3371.7	0.26	
							3356.7	0.20	
							3337.4	0.38	
							3318.1	0.31	
							3302.1	0.16	

(continued next page)

Line No.	Present Work		Schmidt et al[60]		Irigaray et al[56]		Rasmussen et al[57]		Comment
	E_γ	I_γ	E_γ	E_γ	I_γ	E_γ	I_γ	
104	3277.0	0.20				3277.1	0.28	88
105	3220.0(1)	0.60	3228	3224		3219.1	0.99	88**
						3189.8	0.27	
						3135.4	0.12	
						3111.5	0.44	
106	3086.3(2)	0.20				3090.8	0.14	
107	3060.5(2)	0.15				3057.1	0.14	88
108	3044.6(2)	0.50				3044.5	0.33	
						3032.3	0.32	
109	3009.5(1)	8.0	3010	3010	16.6	3009.5	5.90	88**
						3957.3	0.74	
110	2903.6(2)	0.45	2905			2902.6	0.23	88
						2828.2	0.19	
						2802.3	0.26	
111	2783.1(2)	0.70				2785.9	0.22	88
112	2758.0(2)	0.90				2766.6	0.65	88
113	2734.1(.5)	0.70	2734	2731		2736.9	1.11	88**
114	2677.7(.5)	0.42	2682	2680		2678.2	0.45	88**
						2659.9	0.84	
115	2615.7	0.70						88**
116	2577.8(.5)	1.70	2578	2579		2578.1	3.18	88**
				2571				
						2550.6	0.40	
						2542.0	0.20	
						2489.3	0.25	
						2457.9	2.90	
			2437	2443				
117	2391.4(1)	4.05	2396	2392	8.6	2391.5	5.05	88**
118	2367.6(1)	0.50	2368	2370		2363.2	0.35	88**

(Continued next page)

Line No.	Present Work		Schmidt et al[60]	Iragaray et al[56]		Rasmussen et al[57]		Comment
	E_γ	I_γ	E_γ	E_γ	I_γ	E_γ	I_γ	
119	2354.0(2)	0.50	2349	2351				
120	2335.2(2)	0.25	2332	2333	6.6	2336.9	0.41	88**
121	2316.9(2)	0.70	2320	2313		2314.9	0.23	88
122	2298.8(2)	0.60	2306	2296		2290.8	0.24	88
123	2276.4(1)	3.75	2279	2276	9.7	2276.8	3.50	88**
124	2252.5(1)	1.36	2256	2254		2251.2	0.23	88
125	2203.4(1)	2.50	2206	2202	4.9			88**
126	2166.5(2)	0.35	2167	2164		2168.9	2.48	88**
127	2159.3(2)	0.30						88
128	2140.4(2)	0.35	2148	2140		2142.6	0.48	88
			2130					
129	2111.5(1)	2.95	2113	2112	3.1	2111.0	1.47	88**
130	2082.0(2)	0.60	2082			2081.2	0.39	88
			2063					
						2053.5	0.29	
			2027					
				2012				
						1982.2	0.38	
						1969.3	0.61	
131	1953.7(1)	2.03		1955				88
132	1934.1(1)	1.52	1935	1935	1.4			88
			1920			1922.8	0.36	
133	1910.3(2)	1.0				1910.2	0.61	88
134	1902.5(2)	1.0	1902					88
135	1881.6(2)	2.0	1880	1880	0.9	1891.7	1.05	88
136	1836.1(.5)	100.	1836	1836	100.	1835.9	100.	88**
137	1799.1(1)	3.1	1799	1799	2.6	1799.8	1.66	88**
						1786.6	0.48	
138	1779.8(2)	1.5				1774.4	0.71	88**+^{28}Al
139	1761.1(2)	1.66	1766					88
140	1737.0(2)	2.1	1741	1735		1738.2	0.63	88**

(continued next Page)

Line No.	Present Work		Schmidt et al.(60)	Iragaray et al.(56)		Rasmussen et al.(57)		Comment
	E_γ	I_γ	E_γ	E_γ	I_γ	E_γ	I_γ	
141	1718.0(2)	10.0	1714	1717	10.9	1718.4	3.85	88**
				1709				
						1687.6	0.63	
142	1678.4(2)	0.8				1676.9	0.81	88
						1661.9	1.04	
				1589				
143	1566.4(2)	1.0	1559	1560	1564.3		0.79	88
144	1535.2(1)	2.5	1538	1537	1.1	1535.1	1.87	88**
145	1492.9(1)	1.0	1500	1496	1.1			88**
146	1474.4(1)	0.8	1473	1475	0.6			88
147	1442.1(1)	1.96	1443	1440	1.7			88
148	1434.9(1)	1.96						88**
			1413	1419				
				1400				
149	1383.0(1)	2.24	1388	1385	2.9	1382.4	0.93	88**
						1365.7	1.31	
			1347	1347	0.51			2368"
			1330	1324	1.1			1836'
150	1304.6(2)	1.0		1311				
151	1218.5(1)	4.64	1220	1219	4.0	1218.6	2.46	88
152	1181.0(2)	2.00						88
			1161					
153	1150.8(2)	0.25		1145				88**
154	1058.1(2)	0.62	1059					88
			1052					
155	1039.7(2)	0.20						(bgnd)
			1029					
156	993.6(2)	0.10						88
157	974.8(2)	0.10		981				88**
158	962.2(1)	0.10				960.7	0.43	(88)

(continued next page)

Line No.	Present Work E_γ	I_γ	Schmidt et al.(60) E_γ	Iragaray et al.(56) E_γ	I_γ	Rasmussen et al.(57) E_γ	I_γ	Comment
				942	0.43			
159	937.0(1)	0.40	936	936	0.43			88
160	918.1(2)	0.10						88
161	898.0(.5)	64.0	897	898	45.7	897.9	32.3	88**
162	867.6(1)	1.30	863	868		868.9	0.39	88**
163	850.5(.5)	24.6	850	851	19.2	850.4	13.90	88**
164	788.0(2)	0.4						
				727		731.6	0.51	
						723.5	0.79	
			714					
						695.5	0.69	
			685					
						666.5	0.27	
				645		650.9	5.15	
				633				
						596.0	1.04	
165	585.5(.5)	5.2	586	585	4.6	585.7	2.14	88**
						576.4	0.43	
						558.5	15.90	
166	484.0(1)	2.35	484	483	2.0	484.9	0.38	87
			464					
167	434.0(1)	2.42	434	434	1.4	434.9	2.15	88
						423.2	0.23	
						418.2	0.32	
						410.4	0.19	
						401.1	0.31	
168	388.0(1)	6.93	388	388	4.9	387.7	0.90	87
			378					

*Intensity errors are estimated to be 10% or 0.02 whichever is greater.

All intensities quoted are normalized to $I_{1836} = 100$.

***Numbers refer to strontium isotopic assignment of the gamma rays.

depicted in figure 4-3) for each detector used. Again the major spectrum used for this purpose was that shown in figure 6-1. In the case where both photo-peak and double-escape peaks were detected for a gamma ray it was possible to obtain two estimates of its intensity and take the average. To aid in distinguishing photo-peaks from double-escape peaks the ratio of photo-peak to double-escape peak areas was plotted as a function of gamma-ray energy for the counter used to obtain the spectrum in figure 6-1. This ratio is depicted in figure 6-2. The intensities listed in Table 6-2 for the gamma-ray lines are average values obtained from two spectra collected with two different detectors with different active volumes and hence different photo-peak to double-escape peak area ratios. The intensities of the weaker lines were obtained from the peak areas in figure 6-1. By comparing two spectra obtained with two different detectors it was possible to eliminate most of the ambiguities as to whether a particular peak is a photo-peak or double-escape peak but some are still listed as ambiguous as noted in Table 6-2. The intensities listed for the gamma rays were normalized to 100 for the 1836 keV line. The intensities for the lines observed by Irigaray et.al.[56] and Rasmussen et.al.[57] were renormalized to 100 for the 1836 keV line for ease of comparison. A comparison of the corresponding intensities obtained by the various re-

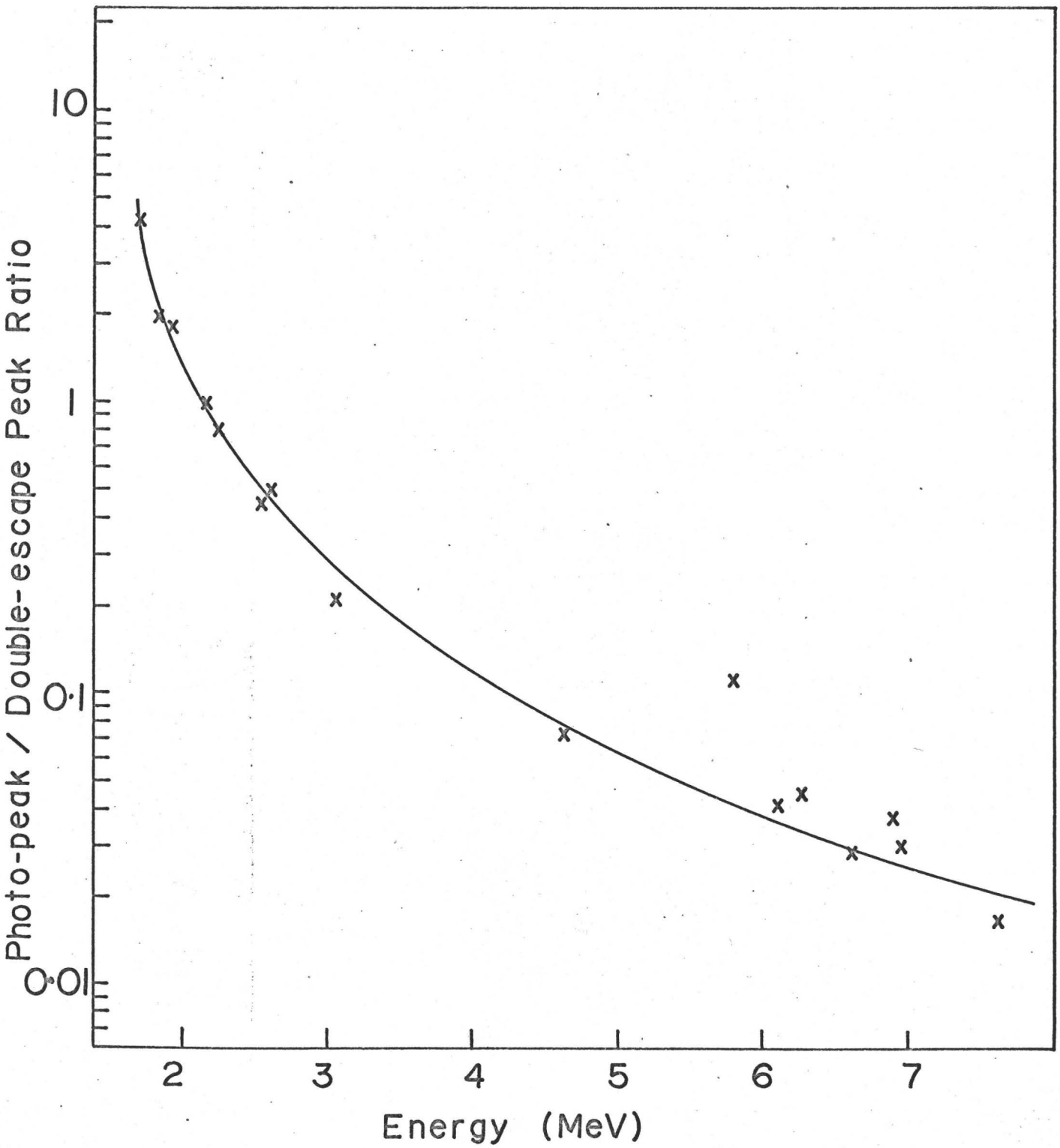
10
1
0·1
0·01
Photo-peak / Double-escape Peak Ratio
2
3
4
5
6
7
Energy (MeV)

FIGURE 6-2

search groups shows that for the high energy gamma rays the intensities obtained in the present work fall in between the values obtained by Irigaray et.al.[56] and Rasmussen et.al.[57]. However at lower energies the values obtained in this work tend to be higher than those reported by the other two groups. A study of the decay modes presented in later sections for the $^{87}Sr(n,\gamma)^{88}Sr$ reaction shows that the intensities obtained here are quite reasonable. The errors associated with the intensity measurements are of the order of ten percent.

6-2 Coincidence Results

The gamma-gamma coincidence experiment carried out on the strontium isotopes employed a NaI(Tl)-Ge(Li) configuration with the NaI(Tl) crystal covering the low energy range from 0 to 3 MeV and the Ge(Li) detector covering the total energy range from 0 to 8.5. The Ge(Li) counter used had an active volume of about 15 cc. so that it had relatively good efficiency at the high energy end. To retain the energy resolution in the NaI dimension 128 channels were found to be sufficient giving a gain of about 25 keV per channel. The minimum that could be used in the Ge(Li) dimension was 512 channels giving a gain of about 16 keV per channel. This provides only two channels per peak at the very most. The memory size required then was 64^K which is four times greater

than the analyzer memory size. Hence coincidence events were recorded as address encoded events as discussed in section 3-8.

The coincidence circuit used was found to be nearly 100% efficient at a resolving time of $2\tau = 60$ nsec. The count rate was 30 coincidence events per second with a chance rate of 15%. At this rate it took about 40 hours to fill one magnetic tape 2400 feet long written at 556 bits per inch. As soon as each tape was filled the events were sorted out in the analyzer in four passes of the magnetic tape. This required about two hours per tape. A total of 10 tapes were filled with the address encoded events over a period of three weeks of continuous running time.

The final result then was 10 runs consisting of a 128 by 512 channel coincidence array each. There were some minor gain and zero shifts in both dimensions over the three week period of data collection. However these were easily corrected for by shifting the arrays in the computer so that the gains of all runs were identical. The coincidence data were then gathered up into one two-dimensional array of 128 channels in the NaI dimension and 512 channels in the solid state dimension. Attempts were made to smooth the data and then to calculate a background function for the coincidence surface in order that Compton contributions could be removed.

However the statistics were inadequate in most regions of the surface and this technique of data treatment was found to have only limited usefulness. In general it was easier to analyse the original array in detail in order to find the coincidence relationships.

The ^{88}Sr nucleus is rather unique having a 4^+, 5^+ capture state and a ground state spin and parity of 0^+. Thus most cascades are expected to have at least three members and most gamma rays are expected to be in coincidence with the intense 1836 keV gamma ray de-exciting the first 2^+ state. The detection of a gamma ray in coincidence with the 1836 keV gamma ray actually provides a means of distinguishing between gamma rays de-exciting levels in ^{88}Sr and those de-exciting levels in ^{87}Sr. Also since about 60% of the intensity to the 1836 keV level is provided by the 898 keV gamma ray, the observance of a gamma ray in coincidence with this line also provides a method of making isotopic assignments to the gamma rays. Figures 6-3 and 6-4 show the high energy portion of the Ge(Li) spectra in coincidence with the 898 and 1836 keV gamma rays in the NaI dimension respectively. These coincidence spectra were obtained by summing up the Ge(Li) spectra over the respective peaks in the NaI dimension and subtracting from these sums an equal number of background spectra obtained from the wings of the peaks. These coincidence results were then used to assign some previously un-

Figure 6-3. Ge(Li) spectrum in coincidence with the 898 keV gamma-ray

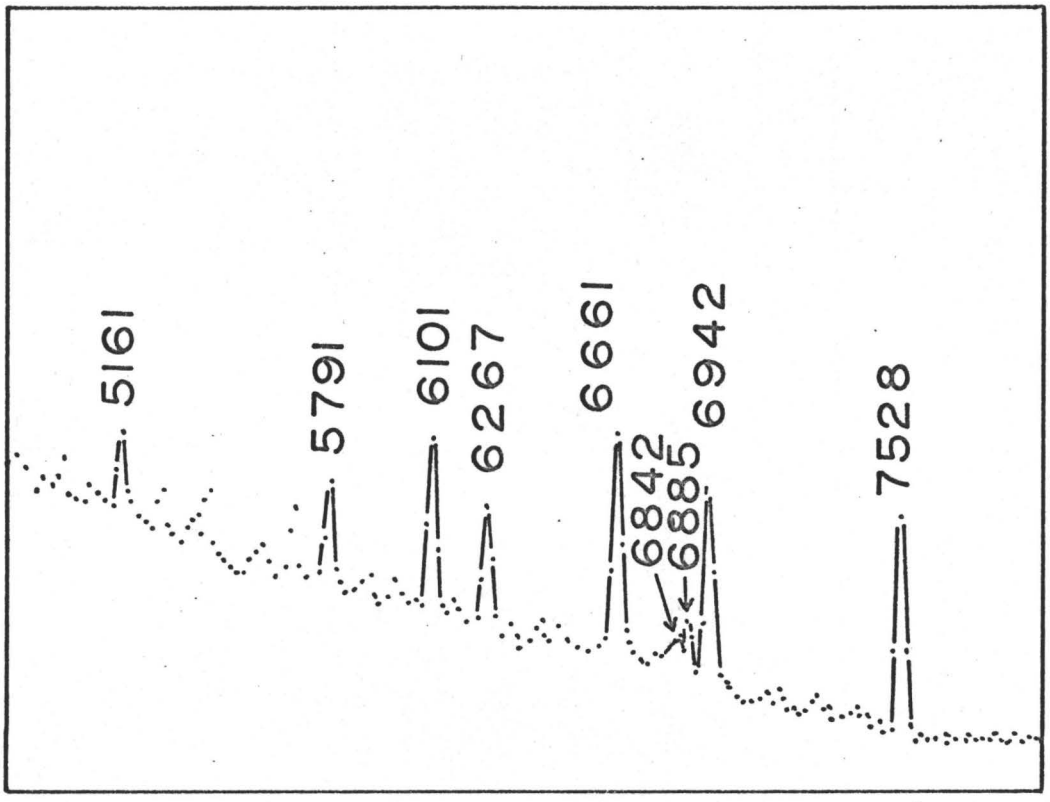

FIGURE 6-3

Sum of several spectra
in coincidence with
898 keV line

Figure 6-4. Ge(Li) spectrum in coincidence with the 1836 keV gamma-ray

FIGURE 6-4
Sum of several spectra in coincidence with 1836 keV line

assigned lines to the $^{87}Sr(n,\gamma)^{88}Sr$ decay scheme. By examining the Ge(Li) spectra in coincidence with the 511 keV gamma ray it was possible to identify many double-escape peaks in the high energy end. However most of the lines between 2 and 5 MeV are weak and it was thus impossible to distinguish the double escape peaks from the photo-peaks on the basis of coincidence with the 511 keV peak.

Many more coincidence relationships were detected. These are all listed in matrix form in figure 6-5. Some of these coincidence relationships were used to establish new levels and/or confirm new levels in ^{88}Sr as will be shown in later sections. The coincidence of the 5161 keV line with the 434 keV line is shown in figure 6-6. This established the 434 keV line as belonging to the ^{88}Sr decay scheme. Another important coincidence relationship is that of the 1218 keV line with the 898 keV line as depicted in figure 6-7. In all 73 coincidence relationships were detected. Most coincidences were observed by examining the Ge(Li) spectra in coincidence with peaks in the NaI dimension as this provided the most sensitive test for coincidence relationships.

6-3 Initial Decay Scheme Construction by Computer

The singles and coincidence results were initially used to construct a basic decay scheme for the $^{87}Sr(n,\gamma)^{88}Sr$

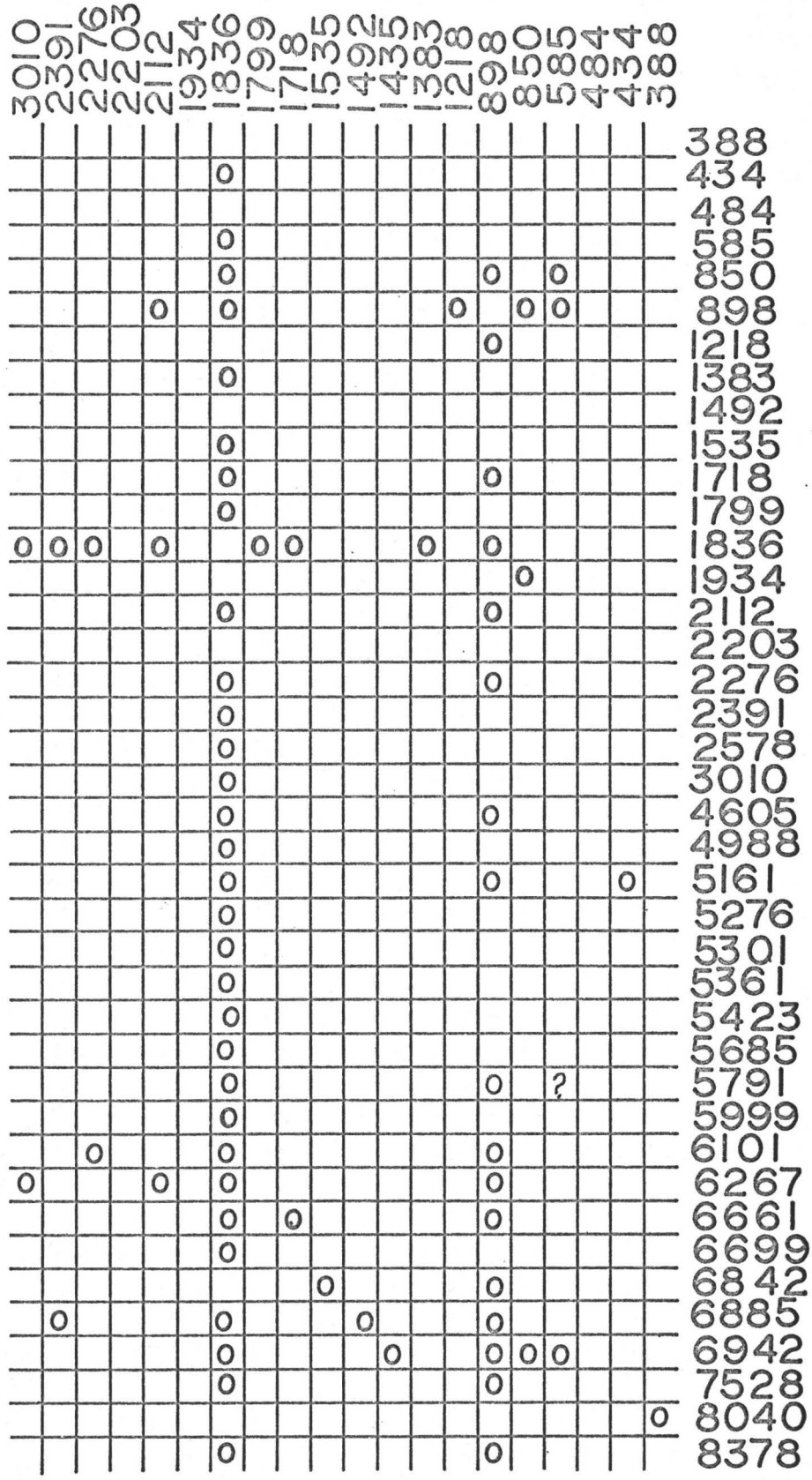

Gamma-Gamma Coincidence Matrix

FIGURE 6-5

Figure 6-6. Ge(Li) spectrum in coincidence with the 434 keV gamma-ray

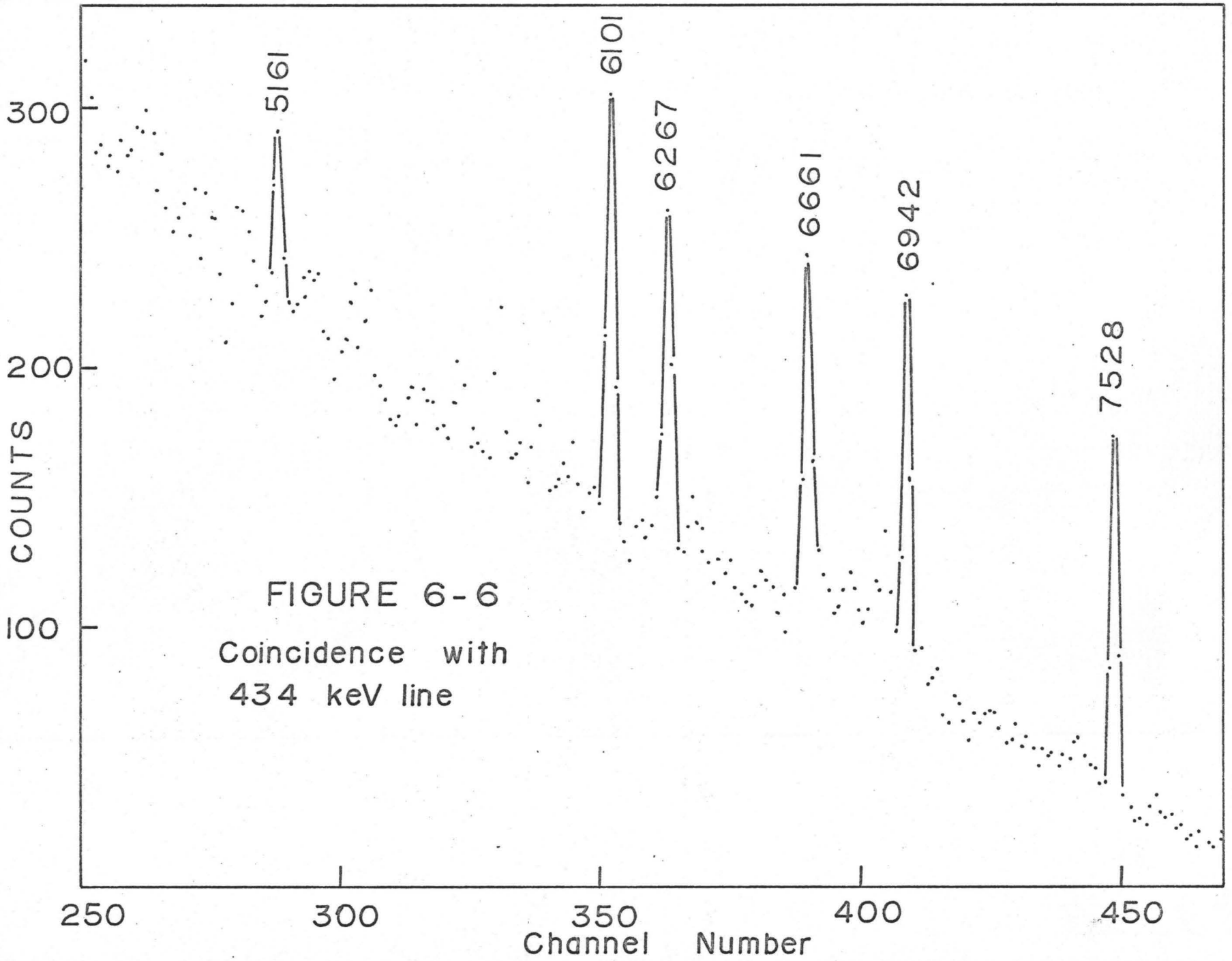

FIGURE 6-6

Coincidence with
434 keV line

Figure 6-7. Low energy Ge(Li) spectrum in coincidence with the 898 keV gamma-ray

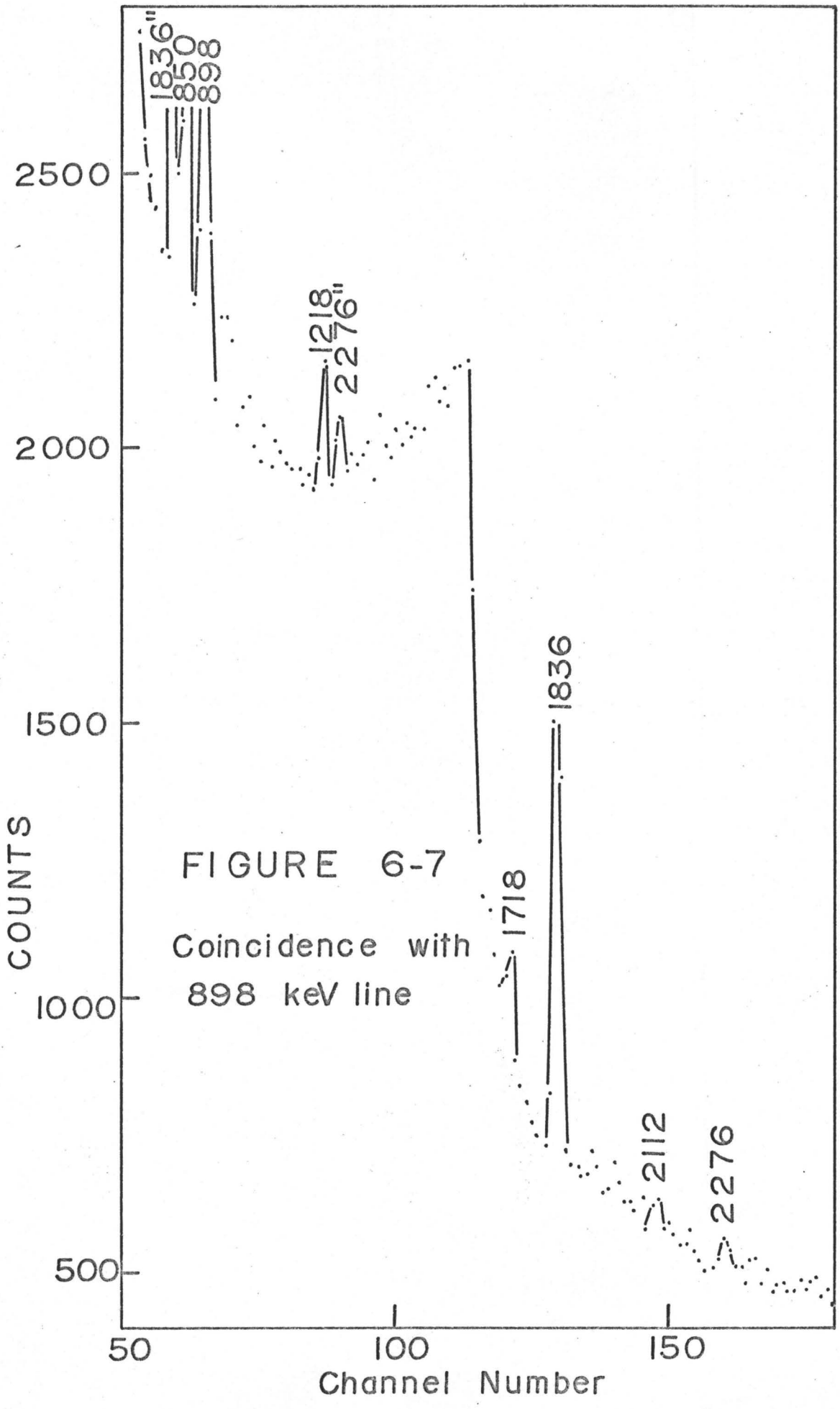

FIGURE 6-7

Coincidence with 898 keV line

reaction. For this purpose a computer program DCYSCH was coded to aid in the actual construction of the decay scheme based on levels deduced either from the beta-decay work discussed in the previous chapter or from the strong primary gamma rays observed in the (n,γ) study. The input data required for the program included the gamma-ray transition energies, errors and intensities and the level energies and errors. Four gamma-rays were initially removed from the list of 168 gamma rays in Table 6-2 because they belong to the $^{86}Sr(n,\gamma)^{87}Sr$ decay scheme. This left 164 transitions most of which are expected to fit into the $^{87}Sr(n,\gamma)^{88}Sr$ decay scheme. The output of the DCYSCH program suggests all possible fits for the gamma-ray transitions as outlined below.

A set of level differences were calculated as,

$$\{D_{\ell_j}\} = \{L_\ell - L_j\} \ , \quad j=1,\ \ell-1$$

L_ℓ being the energy of the capture state. A search was then made for all sets of gamma-ray transitions T_i and T_k satisfying the following relationship,

$$\left|(T_i+T_k)-D_{\ell_j}\right| \leq \alpha(\Delta L_\ell^2 + \Delta L_j^2 + \Delta T_i^2 + \Delta T_k^2)^{\frac{1}{2}} \ , \quad \begin{matrix} i=1,n-1 \\ k=i+1,n \\ j=1,\ell-1. \end{matrix}$$

Here α is the number of standard deviations within which the

quantity on the left hand side of the inequality is required to close. As a straightforward calculation of all the differences required by the above inequality would require the order of $n^2\ell/2$ comparisons, it was necessary to use a fast computer search algorithm to find the pairs of gamma-ray transitions satisfying this inequality. Actually for each T_i there was usually only one T_k which would satisfy the inequality. It was found that the fastest computer search algorithm was provided by arranging the gamma-ray transitions in order of increasing energy and then making a least squares fit for the gamma-ray number associated with each gamma-ray energy. Then for each T_i the search is made starting at the least squares value of k. If the average number of comparisons required for each T_i is n', then the total number of comparisons required is only of the order $nn'\ell/2$ where $n' \ll n$.

For a certain combination $T_{i'} + T_{k'}$ which fits the difference $D_{\ell_{j'}}$ within the allowed errors two possible assignments for each of the gamma rays were considered,

$$T_{i'} \quad L_\ell \rightarrow (L_{j'} + T_{k'})$$
$$(L_{j'} + T_{i'}) \rightarrow L_{j'}$$
$$T_{k'} \quad L_\ell \rightarrow (L_{j'} + T_{i'})$$
$$(L_{j'} + T_{k'}) \rightarrow L_{j'} .$$

As well as the gamma-ray transition energies, errors and intensities and the level energies and errors, the input data for the program included all transition assignments which were fixed in the decay scheme as well. For instance the

gamma-ray transition of energy 1836.1 keV was always given the fixed assignment,

1836.1 1836.1 → 0.

Thus if the transition T_i, has been given a fixed assignment and it does not correspond to one of the two assignments listed above, all four transition assignments were excluded from the final list of possible solutions. If the fixed assignment given to T_i, does correspond to one of those listed above, that assignment and the corresponding one for T_k, were treated as possible assignments provided that T_k, has not been given a fixed assignment or if it has, it corresponds to one of those listed. Also if a fixed transition has been "referenced" it is so indicated by the program output. The program output lists all the possible locations for each gamma-ray transition T_i indicating whether it has been fixed in the decay scheme, has a unique assignment or has a number of ambiguous assignments. The program described above has been coded in the subroutine FITGAM for which the complete flow chart is shown in Appendix A.

The program then performs intensity calculations in the subroutine INTENS which calculates the intensity balance across each level. For each level six parameters were calculated, namely,

(1) the sum of the intensities of the possible transitions

to the level

(2) the sum of the intensities of the fixed transitions to the level

(3) the sum of the intensities of the unique transitions to the level

(4) the sum of the intensities of the possible transitions from the level

(5) the sum of the intensities of the fixed transitions from the level , and

(6) the sum of the intensities of the unique transitions from the level.

A comparison of the corresponding intensities to and from a level gave an indication of how well the gamma-ray transition assignments were made at each step in the decay scheme fitting program. On the average however it is expected that the intensity from a given level will be greater than the intensity to this level because of the greater number of missed weak transitions expected for a statistical decay process such as discussed here. This is so since for a given level a few MeV above the ground state there are a great many more modes of population than of de-excitation. Thus the de-excitation radiation intensity is concentrated in a few strong transitions whereas the populating radiation is dispersed among

many weaker transitions making it impossible to detect the weakest transitions. Besides providing a comparison of the intensities to and from each level this subroutine also provides a list of the gamma-ray transitions to and from each level. The complete flow chart for INTENS is drawn in Appendix A.

The next step performed by the program was to check all of the transition assignments as to whether or not they proceeded between known levels. All transitions which did proceed between known levels and proceeded to a level which had a mode of de-excitation were then fixed in position. Then the subroutine FITGAM was entered again to create a new list of transition assignments consistent with the fixed assignments just generated, thus reducing the number of possible fits accordingly. The subroutine INTENS was used again to calculate intensities in and out of the levels as well as to generate the lists of transitions to and from each level. At this point changes could be made in the input data list according to the output data and information gained from other sources, and the program DCYSCH run again.

The program DCYSCH was initially tested out on the decay scheme of the $^{31}P(n,\gamma)^{32}P$ reaction which had been constructed[139] on the basis of known (d,p) levels with typical errors of ± 6 keV and using the 65 gamma-ray transi-

tions observed in the spectrum. A total of 58 levels were known from (d,p) data. When the three lowest energy gamma-ray transitions were fixed in their proper positions in the decay scheme the program managed to find the correct transition assignments for 57 of the gamma rays. The other gamma-ray transitions were then easily fit manually by ensuring proper intensity balances across the levels. A typical run of the program required 25 seconds of machine time on the CDC 6400 computer.

For the initial fit on the $^{87}Sr(n,\gamma)^{88}Sr$ decay scheme the input data included 164 gamma-ray transitions and 20 levels. The 164 gamma-ray transitions used were those listed in Table 6-2 excluding the four gamma rays which have been assigned to the $^{86}Sr(n,\gamma)^{87}Sr$ reaction on the basis of the energy levels at 388 keV and 872 keV established by a study of the positron decay of ^{87}Y.[51] These four gamma-ray transitions are shown in the decay scheme in figure 6-11. The initial 20 levels used in the input data list for the initial construction of the $^{87}Sr(n,\gamma)^{88}Sr$ decay scheme included those determined from the beta decay of ^{88}Rb as reported in the previous chapter and those populated by the stronger primary transitions. These 20 levels are marked by an × on the decay scheme in figure 6-10. Below 5 MeV the only levels used which were not populated in beta decay are the

three levels at 4170, 4227 and 4452 keV. These three levels as well as the six levels above 5 MeV are populated directly by strong primary transitions which were detected in coincidence with the 1836 keV gamma ray. The levels at 4743, 4514, 3220 and 1836 keV are not populated directly by primary transitions. The decay modes of these levels are well known from beta decay so that the gamma-ray transitions de-exciting these levels were fixed in the decay scheme for the DCYSCH program. Using the program it was possible to make 45 unique gamma-ray transition assignments involving the 20 levels, the ground state and the capture state. The transitions thus assigned are marked as 88** in the comment column of Table 6-2. These assignments include most of the assignments made by Schmidt et.al.[60] as well as 24 more, but there are some disagreements. Here the 3487 keV line is assigned as de-exciting the 3487 keV level as in the beta-decay of ^{88}Rb. This level is populated by the 2203 keV line which Schmidt et.al.[60] had postulated as de-exciting the 5426 keV level. This latter assignment is impossible based on the energy and error of the 2203 keV line. Also on the basis of energy measurements and errors it is impossible for the 5685 keV and 5423 keV lines to form a two-step cascade to the ground state. The 4418 keV line cannot de-excite the 4414 keV level as suggested by Schmidt et.al.[60]

as it was not observed in the beta-decay of ^{88}Rb. In fact the 4418 keV line is suspected as being due partly to calcium contamination in the sample. A line was observed in the singles spectrum at 4855 keV; however a line at 2119 keV was not observed. Therefore it is probable that the 4854 keV level is not populated in the neutron capture reaction $^{87}Sr(n,\gamma)^{88}Sr$.

An attempt was made to determine the significance of the number of two-step cascades to a level at energy E in the final nucleus by calculating the number of combinations N(E) satisfying the inequality,

$$|(T_i+T_k) - (L_\ell-E)| \leq \alpha(\Delta T_i^2 + \Delta T_k^2 + \Delta L_\ell^2)^{\frac{1}{2}}$$

as a function of energy. Then defining $\bar{N}$ as the average number of two-step combinations over an energy interval, the probability of there being N combinations in that interval is given by the Poisson distribution,

$$P_{\bar{N}}(N) = \frac{\bar{N}^N e^{-\bar{N}}}{N!} .$$

One can then define the probability that this number of combinations does not correspond to a real level as,

$$\sum_{i=N}^{\infty} P_{\bar{N}}(i) = 1 - \sum_{i=o}^{N-1} P_{\bar{N}}(i).$$

However the number N includes random as well as real two-step

combinations and as the number of random two-step combinations were quite significant it was in general difficult to determine the reliability of the value found for N. Also some of the real two-step combinations were no doubt missed due to the inability to detect the weaker members of the cascades. Thus the probability of a real level being found using this technique could only be relied on if most of the real two-step combinations were detected and if the number of random combinations could be reduced by means of more accurate energy measurements. It was also found that the number of chance combinations satisfying the relation,

$$T_a + T_b = T_c$$

within the allowed errors,

$$\alpha(\Delta T_a^2 + \Delta T_b^2 + \Delta T_c^2)^{\frac{1}{2}}$$

was too great to warrant a study of these relationships. In fact for the 164 gamma rays and a value of $\alpha = 0.5$, there were 411 combinations, whereas for a random set of 164 gamma rays there were 391 chance combinations.

However a study of the output of the DCYSCH program indicated a means of determining whether more gamma rays could be fitted into the decay scheme. The initial use of the program resulted in the fitting of 45 gamma rays, representing 83.5% of the total gamma intensity of the 164 lines, in the

$^{87}Sr(n,\gamma)^{88}Sr$ decay scheme. It also indicated that there were a possible 269 transition assignments for the remaining 119 unassigned gamma rays within two step cascades between the capture state and the 21 input levels including the ground state. The DCYSCH program was then run with the 45 assigned transitions as fixed and with the remaining 119 gamma-ray energies randomized. The output indicated that there were only 207 possible transition assignments for the randomized 119 gamma rays. Thus it should be possible to add about 25% of the 269 possible assignments for the remaining 119 unassigned gamma rays to the decay scheme. This indicates that it should be possible to fit about 100 gamma rays in the $^{87}Sr(n,\gamma)^{88}Sr$ decay scheme with the 20 levels defined before forming the basis of the level structure in ^{88}Sr. It was also clear from the program output that other levels must be populated in the $^{87}Sr(n,\gamma)^{88}Sr$ reaction below 6 MeV as the intensity into some levels was greater than the intensity out. A computer technique is presented in the next section to find some more levels which may be populated in the $^{87}Sr(n,\gamma)^{88}Sr$ reaction.

6-4 Computer Search For Other Levels Populated

In order to accommodate some of the other transitions which have not yet been assigned some other levels must be

populated. To find the location of these levels, a computer program COMB was coded to deal with one-step combinations with existing levels to a level at energy E. In the program a search is made for all combinations of the transitions with the known level energies to a possible level energy E satisfying the relationship,

$$||L_j - E| - T_i| \leq \alpha(\Delta L_j^2 + \Delta T_i^2) \quad , \; i=1,n \quad j=1,\ell-1.$$

The number of combinations m satisfying the above relationship for each energy E is calculated in steps of δE which are less than the minimum possible error,

$$[\alpha(\Delta L_j^2 + \Delta T_i^2)^{\frac{1}{2}}]_{min.}$$

In general it is desirable to look at the parameter m over the whole energy excitation range from the ground state to the capture state. If at a particular energy E there is a large number of combinations, this could indicate evidence for a level at this excitation energy.

It is desirable to know the significance of the number of combinations m to a certain excitation energy E. This is done using an auxiliary program RCMB which was coded to calculate the probability of obtaining a random number of combinations in a given energy region. The probability that the level L_j will combine with a gamma-ray transition

T_i to result in a level at E is defined by,

$$S_j = \frac{\alpha}{\Delta E} \sum_i (\Delta L_j^2 + \Delta T_i^2)^{\frac{1}{2}}$$

where the sum is performed over all gamma rays satisfying the relationship,

$$||E-L_j|-T_i| \leq \Delta E$$

where the energy region ΔE is sufficiently large to provide a good average. In all calculations performed with RCMB the energy interval was chosen to be 100 keV as the values of S_j obtained for ΔE = 200 did not differ significantly from those for ΔE=100. From the definition of S_j it can be seen that $(1-S_j)$ is the probability that the level L_j does not combine with any gamma-ray transition to form a level at E. Then the probability of no combinations of the ℓ levels with the gamma-ray transitions forming a level at excitation energy E is given by,

$$P(o) = \prod_{j=1}^{\ell} (1-S_j).$$

Similarly the probability that one and only one level forms a combination to energy E is given by,

$$P(1) = \sum_{j_1=1}^{\ell} [S_{j_1} \prod_{j \neq j_1}^{\ell} (1-S_j)].$$

And in general the probability that m and only m levels combine with the gamma-ray transitions to form an energy level at E is given by,

$$P(m) = \sum_{j_m=1}^{\ell-m+1} S_{j_m} \left(\sum_{j_{m-1}=j_m+1}^{\ell-m+2} S_{j_{m-1}} \times \ldots \times \left(\sum_{j_1=j_2+1}^{\ell} \left[S_{j_1} \prod_{j \neq j_1 \neq j_2 \neq \ldots \neq j_m}^{\ell} (1-S_j) \right] \ldots \right) \right)$$

To perform a calculation of these probabilities on the computer using the above formula it must be realized that the number of multiplications required varies as $\ell^m/m!$ As it took approximately 120 seconds of computing time to calculate P(5) for one value of E, using the above formula it would be impossible to calculate P(m) for values of m larger than 5 in any reasonable computing time. Fortunately the values of P(m) can be calculated in much faster time by realizing the simple recursion relationships which they obey. P(1) can be written as,

$$P(1) = P(o) \sum_{j=1}^{\ell} \left(\frac{S_j}{1-S_j} \right)$$

$$= P(o) \left[S_1^o + S_1^1 \right]$$

where $S_k^1 = \sum_{j=k+1}^{\ell} \left(\frac{S_j}{1-S_j} \right)$ and $S_k^o = \frac{S_k}{(1-S_k)}$.

Then in turn P(2) can be written as,

$$P(2) = P(o) \left[\sum_{j=1}^{\ell-1} (S_j^o * S_j^1) \right]$$

$$= P(o) \left[S_1^o * S_1^1 + S_1^2 \right]$$

where $S_1^2 = \sum_{j=2}^{\ell-1} S_j^o * S_j^1$. Then in general the probability P(m) can be written,

$$P(m) = P(o) \left[\sum_{j=1}^{\ell-m+1} S_j^o * S_j^{m-1} \right]$$

where the following recursion formula holds,

$$S_k^m = \sum_{j=k+1}^{\ell-m+1} S_j^o * S_j^{m-1} , \quad m \geq 2.$$

Using the above formula for P(m) the calculation time varies linearly with m and is no longer prohibitive. The typical computation time to calculate 5000 values of P(m) for m ranging from 0 to 10 was now only 20 seconds on the CDC 6400.

It is to be noted that the normalization condition, $\sum_{m=o}^{\infty} P(m)=1$ holds for the probabilities. A check of the computer calculations verified this condition. However the coefficients of interest are not the P(m) but rather

$$R(m) = \sum_{i=m}^{\infty} P(i) = 1 - \sum_{i=o}^{m-1} P(i),$$

which give the probability of forming m or more combinations at a certain excitation energy E. The number of occurrences of m or more random combinations in a given energy region consisting of k steps of δE is then given by,

$$N(m) = k\overline{R(m)}$$

where $\overline{R(m)}$ is the average value of R(m) in that energy region. This value of N(m) then is to be compared with M(m) the number of occurrences of m or more combinations observed in the energy region of interest by means of the program COMB. The

number of possible levels (real and random) associated with the M(m) occurrences of m or more combinations is referred to by $\mu(m)$. Then the number of random distinct levels formed by m or more combinations is given by

$$v(m) = \mu(m) \left(\frac{N(m)}{M(m)}\right).$$

Then for a random distribution of levels the probability of observing x levels is given by the Poisson distribution,

$$P_v(x) = \frac{v^x e^{-v}}{x!} .$$

The probability that all μ observed levels are random is given by,

$$P_v^{\mu} = \sum_{x=\mu}^{\infty} P_v(x) = 1 - \sum_{x=0}^{\mu-1} P_v(x)$$

while the probability that only one of the levels are random is given by,

$$P_v^1 = \sum_{x=1}^{\infty} P_v(x) = 1 - P_v(o).$$

The above formulae have been tested by using a random set of gamma-ray energies generated from the original set and found to describe the probabilities quite well quantitatively.

The programs COMB and RCMB were initially used with the 20 levels and 45 fixed transitions as determined previously by DCYSCH. The flow chart in Appendix A indicates how these programs are all combined. The remaining 119 gamma-ray transitions were allowed to combine with the 20 levels,

the ground state and the capture state to form new levels. The number of combinations was calculated as a function of excitation energy in 1 keV steps which are smaller than the minimum possible error. Figure 6-8 shows a plot of the number of combinations as a function of excitation energy for two energy regions of interest, 3800 to 4200 keV and 5200 to 5600 keV. Only combinations greater than or equal to 3 are shown.

Looking only at combinations of 4 or greater it can be seen that 6 new possible levels should be considered. However some of these levels can be eliminated by other considerations. There are no primary transitions observed to the possible levels at 5301 and 5451 keV and one of the contributors to each of the 4 combinations forming these levels is the ground state transition. Also there is no primary transition to the possible level at 4018 keV and two of the contributions are from the 434 keV gamma-ray transition to the 3584 keV level and from the 4452 keV level respectively. This leaves only the 3953, 5518 and 5537 keV levels to consider, each of which have a possible primary transition to it.

In order to ascertain the significance of the number of combinations to each level the program RCMB was run with the same input parameters as COMB. The probabalities P(m) were calculated over the whole energy excitation range in

Figure 6-8 - Number of combinations satisfying the relationship, $||E-L_j|-T_i| \leq \alpha (\Delta L_j^2 + \Delta T_i^2)^{\frac{1}{2}}$ as a function of excitation energy E for the 20 levels and 119 unassigned transitions as defined in the text. Only combinations equal to or greater than 3 are shown.

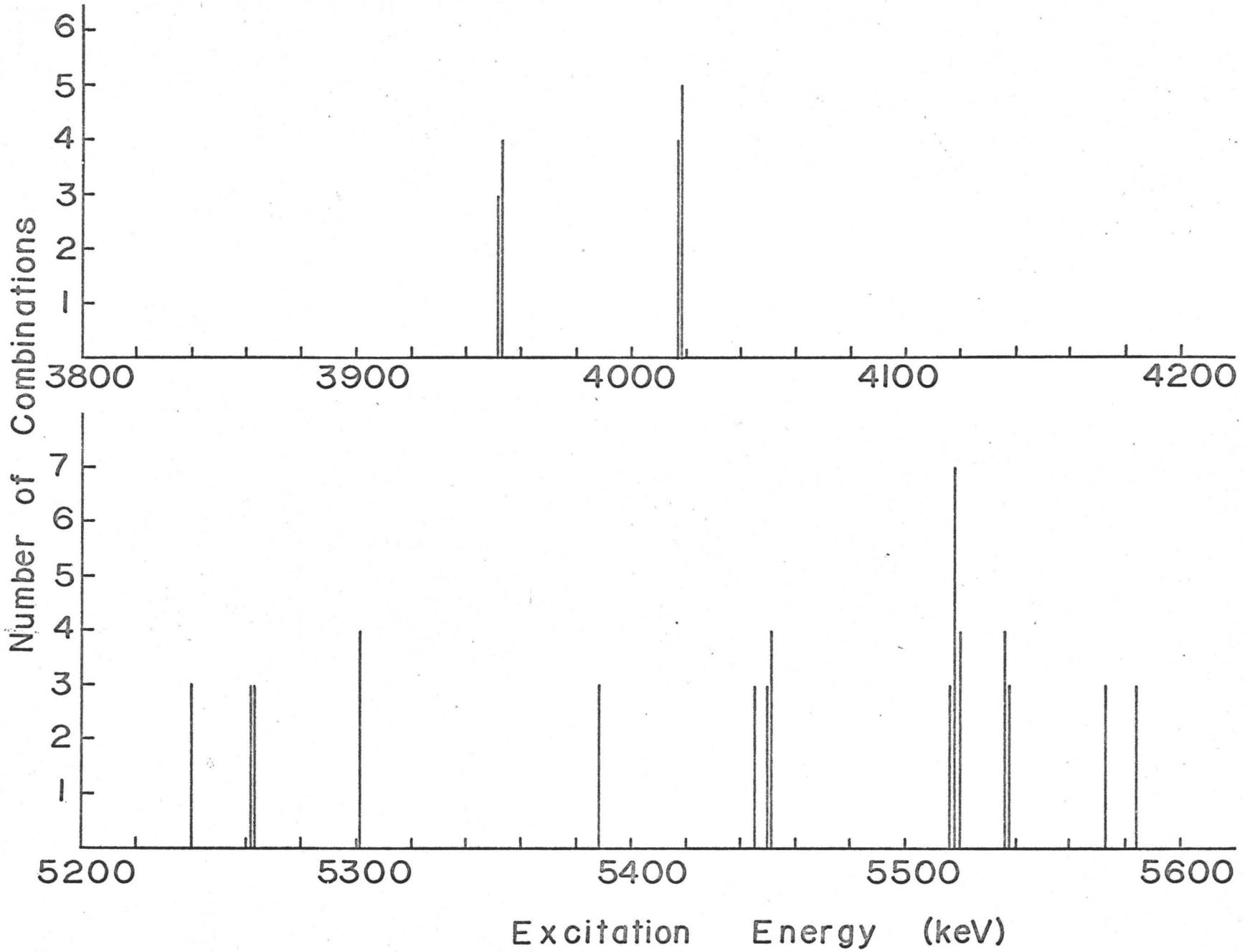
Number of Combinations
6
5
4
3
2
1
3800
3900
4000
4100
4200
7
6
5
4
3
2
1
5200
5300
5400
5500
5600
Excitation Energy (keV)

FIGURE 6-8

steps of 50 keV for values of m from 1 to 10. Figure 6-9 shows a plot of the parameters R(m) on a semi-log plot. It should be noted that the parameters vary very rapidly as a function of energy and for one value of m may differ by as much as 3 orders of magnitude over the whole energy range. The energy variation of each R(m) was also calculated for a set of 119 random gamma-ray energies and found to give about the same values for R(m) at corresponding values of m and energy E. The number of m random combinations in a certain energy region consisting of k steps of δE is given by,

$$N(m) = k\ \overline{R(m)}$$

where $\overline{R(m)}$ is the average value of R(m) in that energy region.

In the energy region 3800 to 4000 keV there is a possible new level at 3953 keV with 4 combinations. According to RCMB there should be .184 occurrences of 4 combinations in this region and thus,

$$v(4) = 1 \times \frac{.184}{1} = .184.$$

The probability of this one level being random is then,

$$P^{1}_{.184} = 1-e^{-.184} = .168, \text{ i.e. } 16.8\%.$$

On the other hand if there had been only 3 combinations forming this level the probability of the level being random would have been 63.2%. The existence of the 3953 keV level also accounts for the detection of the 1218 keV gamma ray in coinci-

Figure 6-9 - Plot of the parameters R(m) as a function of excitation energy E for the 20 levels and 119 unassigned transitions as defined in the text.

Here,

$$R(m) = \sum_{i=m}^{\infty} P(i)$$

where

$$P(m) = P(o) \left[\sum_{j=1}^{\ell-m+1} S_j^o * S_j^{m-1} \right]$$

and

$$P(o) = \prod_{j=1}^{\ell} (1-S_j)$$

and

$$S_j = \frac{\alpha}{\Delta E} \sum_i (\Delta L_j + \Delta T_i)^{\frac{1}{2}}.$$

The above sum over i is performed over all gamma rays satisfying the energy relationship,

$$||E-L_j| - T_i| \leq \Delta E.$$

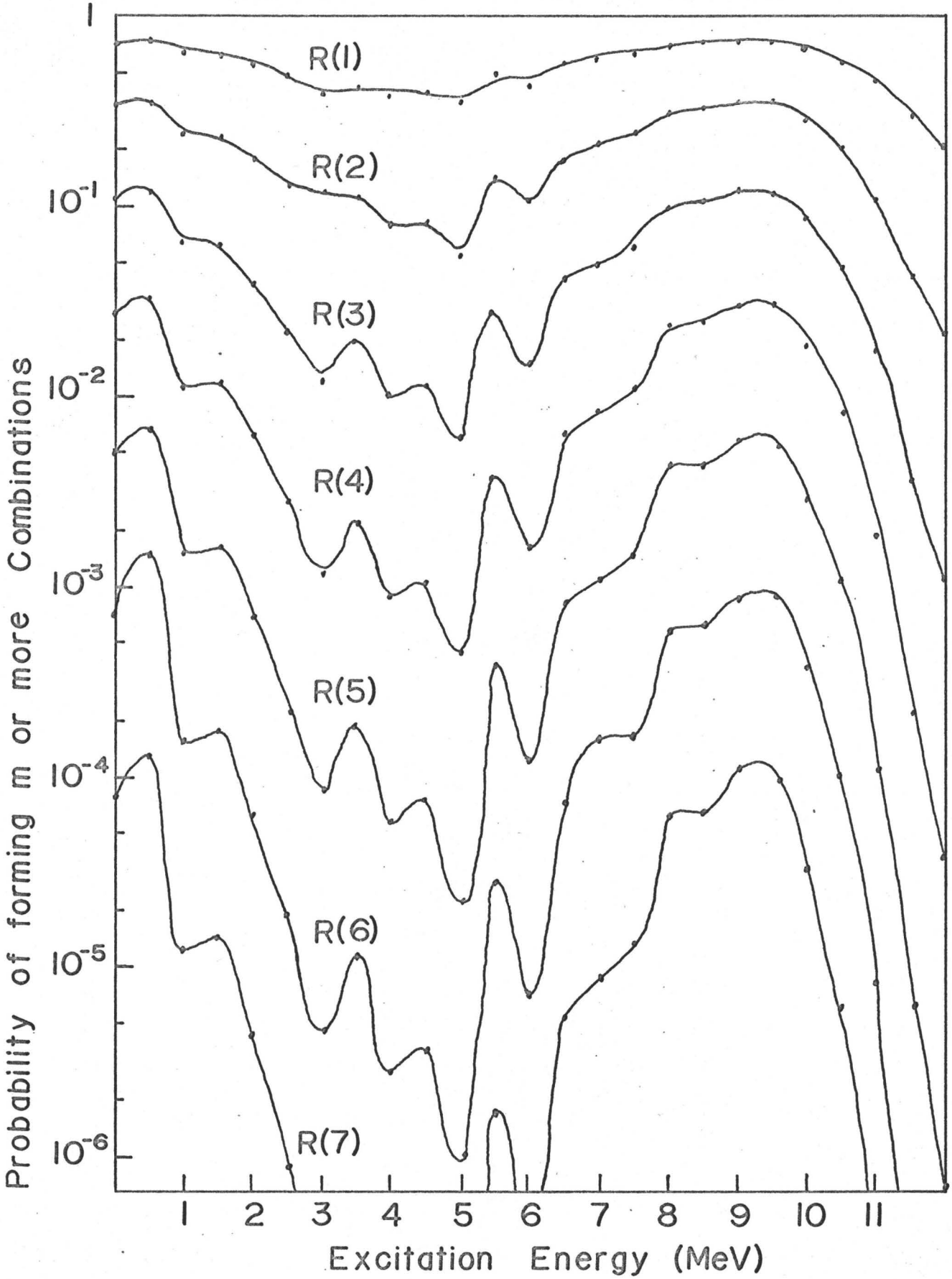
1
10^{-1}
10^{-2}
10^{-3}
10^{-4}
10^{-5}
10^{-6}
R(1)
R(2)
R(3)
R(4)
R(5)
R(6)
R(7)
Probability of forming m or more Combinations
1 2 3 4 5 6 7 8 9 10 11
Excitation Energy (MeV)

FIGURE 6-9

dence with the 898 keV transition. The strong 1218 keV transition was previously unassigned. In the energy region 4000 to 4200 keV there are 5 combinations forming a possible new level at 4018 keV with only a 1.2% probability of being random. However if the two contributions to the 5 combinations due to the 434 keV transition are not counted, there are only 3 combinations forming this possible level and the level now has an 86.4% probability of being random. This level cannot be the 2^+ level seen at 4030 keV in the (t,p) reaction[75] as it lies outside the errors and therefore will not be considered as a possible new level in ^{88}Sr.

In the energy region 5400 to 5600 keV there are 4 occurrences of 4 or more combinations forming a possible 3 new levels. The probabilities of one, two or all of the new levels being random are 39.4%, 8.9% and 0.9% respectively. Thus the probability of 2 of these levels being true levels is 91.1%. Also the level at 5518 keV has one occurrence of 7 combinations. Thus this level has only a 0.034% probability of being random.

At this point the programs COMB and RCMB were run again with the 119 unassigned gamma-rays and 22 levels this time including the two levels at 5518 keV and 5537 keV. There were then found to be 5 combinations forming a level at 3953 keV. The level then had only a 2.3% probability of

being random. Subsequently the program DCYSCH was run this time with 23 levels besides the ground state and capture state. The three levels added were those at 3953, 5518 and 5537 keV. The 45 transition assignments made before were fixed in position. Unique assignments were now found for 13 more gamma rays making a total of 58 gamma rays fit comprising 87.5% of the total intensity of the 164 gamma rays. The previously unassigned 434 keV gamma-ray transition was fit from the 5952 keV level to the 5518 keV level satisfying energy, intensity and coincidence relationships.

6-5 Final Decay Scheme Fit for $^{87}Sr(n,\gamma)^{88}Sr$

Although 58 transitions have been fit in the $^{87}Sr(n,\gamma)^{88}Sr$ decay scheme a few of the stronger transitions have not been assigned. Also the number of fits possible for the 106 remaining unassigned transitions is significantly greater than the number of fits possible for a random set of 106 gamma rays. Thus the computer programs were utilized again to find some new likely levels and hence transition assignments.

Using COMB and RCMB a possible level at 7835 keV was located with 7 combinations and only a 2% probability of being random. This level provides an assignment for the previously unassigned 5999 keV transition. Other levels were also added

TABLE 6-3

Strontium Neutron Separation Energies

(a) Neutron Separation Energy for ^{88}Sr

E_{γ_1}*	E_{γ_2}	E_{γ_3}	E_{γ_4}	E_{γ_5}	Separation Energy
8379.3	2734.1				11113.4
8379.3	898.0	1836.1			11113.4
7528.7	850.5	2734.1			11113.3
7528.7	850.5	898.0	1836.1		11113.3
7477.6	1799.1	1836.1			11112.8
7160.1	1218.5	2734.1			11112.7
7160.1	1218.5	898.0	1836.1		11112.7
6943.1	2335.2	1836.1			11114.4
6943.1	1434.9	2734.1			11112.1
6943.1	1434.9	898.0	1836.1		11112.1
6943.1	585.5	850.5	2734.1		11113.2
6943.1	585.5	850.5	898.0	1836.1	11113.2
6885.6	2391.4	1836.1			11113.1
6885.6	1492.9	2734.1			11112.6
6885.6	1492.9	898.0	1836.1		11112.6
6843.0	1535.2	2734.1			11112.3
6843.0	1535.2	898.0	1836.1		11112.3
6699.5	2577.8	1836.1			11113.4
6661.3	2615.7	1836.1			11113.1
6661.3	1718.0	2734.1			11113.4
6661.3	1718.0	898.0	1836.1		11113.4
6661.3	867.6	850.5	2734.1		11113.5

(continued next page)

E_{γ_1} *	E_{γ_2}	E_{γ_3}	E_{γ_4}	E_{γ_5}	Separation Energy
6661.3	867.6	850.5	898.0	1836.1	11113.5
6267.3	3009.5	1836.1			11112.9
6267.3	2111.5	2734.1			11112.9
6267.3	2111.5	898.0	1836.1		11112.9
6102.0	2276.4	2734.1			11112.5
6102.0	2276.4	898.0	1836.1		11112.5
6102.0	1058.1	1218.5	2734.1		11112.7
6102.0	1058.1	1218.5	898.0	1836.1	11112.7
5791.0	1737.0	850.5	2734.1		11112.6
5791.0	1737.0	850.5	898.0	1836.1	11112.6
5685.6	1474.4	1218.5	2734.1		11112.6
5685.6	1474.4	1218.5	898.0	1836.1	11112.6
5423.5	2203.4	3487.0			11113.9
5161.7	2367.6	850.5	2734.1		11113.9
5161.7	2367.6	850.5	898.0	1836.1	11113.9
5161.7	434.0	2298.8	3220.0		11114.5
5161.7	434.0	2298.8	1383.0	1836.1	11113.6

Research Group	Ave. Separation Energy
Present Work	11113.0 ± 0.6
Kinsey et.al.[36]	11140 ±50
Schmidt et.al.[60]	11111 ± 4
Irigaray et.al.[56]	11113.5 ± 1.5

(continued next page)

(b) Neutron Separation Energy for ^{87}Sr

E_{γ_1}*	E_{γ_2}	E_{γ_3}	Separation Energy
8040.1	388.0		8428.1
7556.3	484.0	388.0	8428.3

Research Group	Ave. Separation Energy
Present Work	8428.2 ± 1.0
Irigaray et.al.(56)	8428.5 ± 2.5

*All energies in keV. Recoil energies are included in the transition energies.

to the list of probable levels as follows. The level at 3523 keV was observed in the positron decay of ^{88}Y [58]. The level at 6258 keV corresponds to an $\ell=1$ level seen in the $^{87}Sr(d,p)^{88}Sr$ reaction. Levels at 5262, 5812, 5836 and 6124 were postulated on the basis of the relatively strong 5850, 5277, 5301 and 4988 keV primary transitions. The level at 7339 keV was postulated since the 4605 keV transition was detected in coincidence with the 898 keV transition. The only logical place for the 4020 keV transition to be assigned was from the capture state to a level at 7092 keV; hence the postulation of a level at this energy. A level at 7573 keV was formed by 4 combinations but has a fairly large percentage probability of being random. This gave a total of 33 levels besides the ground state and capture state. With these 33 levels and 58 fixed transitions, the DCYSCH program managed to fit a total of 89 transitions.

A run of COMB and RCMB with 33 levels and 89 fixed transitions indicated the existence of another level at 5077 keV with only a 3.8% probability of being random. Adding this level to the list of levels and fixing the corresponding transitions indicated by a run of DCYSCH, the programs COMB and RCMB were run again. This run indicated the possible existence of levels at 5662 keV and 6388 keV with 5.2% and 22% probability of being random, respectively. One more level

was postulated at 4300 on the basis of the primary 6813 keV transition and on the basis that a 4^+ level at 4301 keV was reported recently in a (p,p') study on ^{88}Sr [140]. This gave a total of 37 levels in all populated in the thermal neutron capture reaction $^{87}Sr(n,\gamma)^{88}Sr$. With another run of the program DCYSCH it was possible to fit a total of 103 gamma rays.

A subsequent run of COMB and RCMB indicated that no other levels could be postulated with a very great percentage probability of being true levels. Also the output of the final DCYSCH program indicated that there were 88 more possible fits for the remaining 61 unassigned gamma-ray transitions. A randomized list of 61 transitions had a total of 83 possible locations. As there was no significant difference between the possible fits of a real and a random set of 61 transitions, most of the transitions which could be placed with a good probability of being correct are assumed to have been assigned. Thus a total of 103 gamma-ray transitions have been placed into the $^{87}Sr(n,\gamma)^{88}Sr$ decay scheme representing 95.3% of the total gamma-ray intensity of the 164 gamma rays. The only notably strong gamma ray which has not been fit is the 6671 keV transition. The intensity balance across all levels was quite reasonable. In general there was more gamma-ray intensity out of a level than into the same level. This was to be expected as explained in section 6-3. The inten-

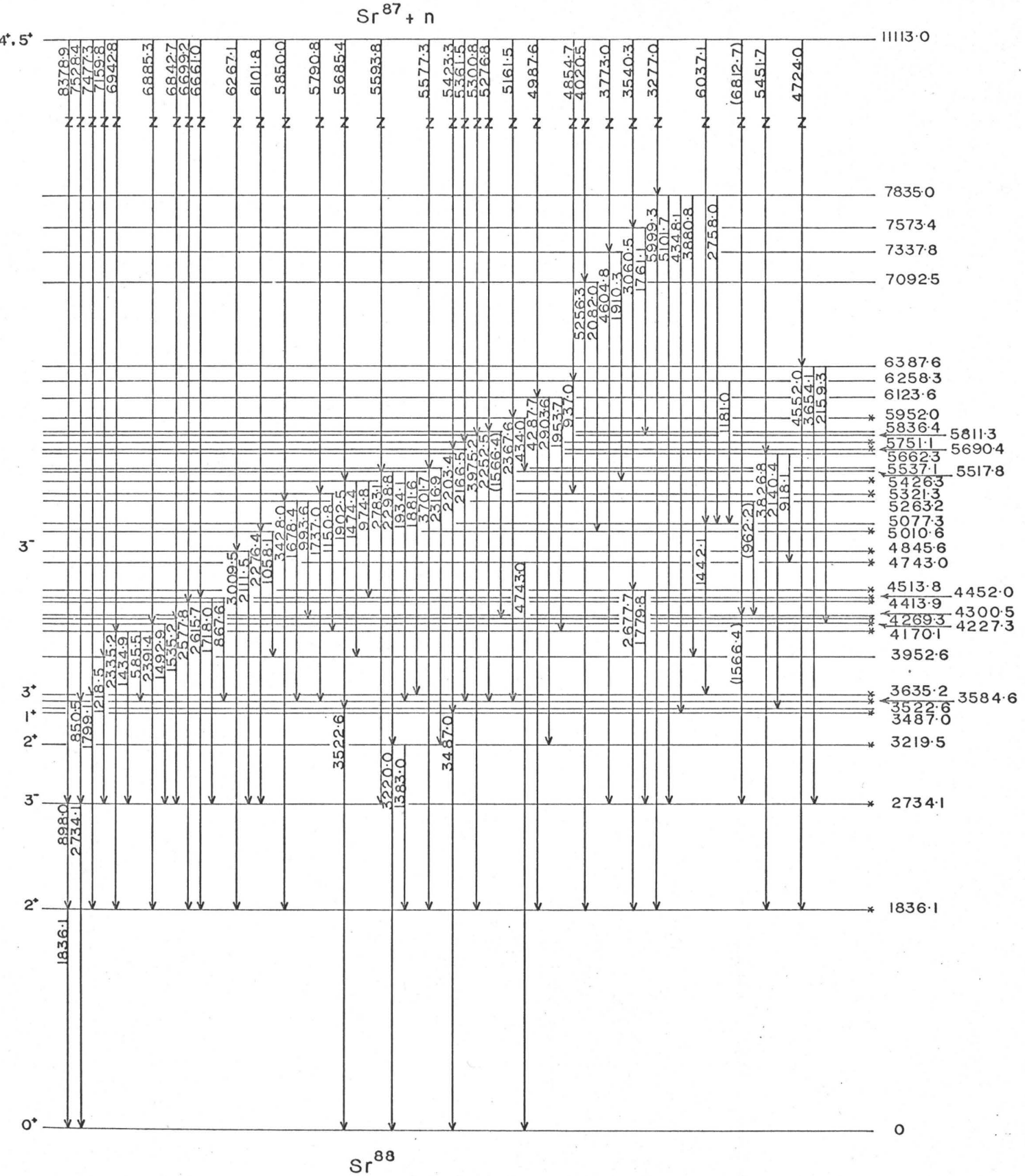
Sr87 + n
Sr88
11113·0
7835·0
7573·4
7337·8
7092·5
6387·6
6258·3
6123·6
5952·0
5836·4
5751·1
5662·3
5537·1
5426·3
5321·3
5263·2
5077·3
5010·6
4845·6
4743·0
4513·8
4413·9
4269·3
4170·1
3952·6
3635·2
3522·6
3487·0
3219·5
2734·1
1836·1
0
5811·3
5690·4
5517·8
4452·0
4300·5
4227·3
3584·6
8378·9
7528·4
7477·3
7159·8
6942·8
6885·3
6842·7
6699·2
6661·0
6267·1
6101·8
5850·0
5790·8
5685·4
5593·8
5577·3
5423·3
5361·5
5300·8
5276·8
5161·5
4987·6
4854·7
4020·5
3773·0
3540·3
3277·0
6037·1
(6812·7)
5451·7
4724·0
7758·0
5999·3
5101·7
4348·1
3880·8
1181·0
(962·2)
3826·8
2140·4
918·1
144·2·1
4552·0
3654·1
2159·3
5256·3
2082·0
4604·8
1910·3
3060·5
1761·1
937·0
1953·7
2903·6
2487·7
434·0
2367·6
(1566·4)
2252·5
3975·2
2166·5
2203·4
2316·9
3701·7
1881·6
1934·1
2298·8
2783·1
974·8
1474·4
1902·5
1150·8
1737·0
1678·4
993·6
3426·0
1058·1
2276·4
2111·5
3009·5
867·6
1718·0
2615·7
2577·8
1535·2·1
1492·9
2391·4
585·5
1434·9
2335·2
1218·5
1799·1·1
850·5·1
1836·1
2734·1
898·0
3522·6
3220·0
1383·0
3487·0
4743·0
2677·7
1779·8
(1566·4)
(962·2)
4513·8
4413·9
4269·3
4170·1
3635·2
3522·6
3487·0
3219·5
2734·1
1836·1
0
3⁻
3⁺
1⁺
2⁺
3⁻
2⁺
0⁺
4⁺, 5⁺

FIGURE 6-10

sity from the capture state was calculated to be 58.1 relative to 103.1 into the ground state.

The Q-value for the $^{87}Sr(n,\gamma)^{88}Sr$ reaction was calculated to be 11113.0 ± 0.6 keV as summarized in Table 6-3. The Q-value was calculated by taking the average value of the sum of the strongest 39 cascades taking into consideration the recoil energies associated with the gamma rays. Average values were also calculated for the energy levels by taking the average of the sum of the de-exciting cascades. The energy values are noted in figure 6-10 and are also summarized in Table 7-4 along with their associated errors.

6-6 Decay Scheme for $^{86}Sr(n,\gamma)^{87}Sr$ Reaction

Having fit most of the gamma rays in the $^{87}Sr(n,\gamma)^{88}Sr$ decay scheme, an attempt was made to find some significant gamma-ray assignments for the $^{86}Sr(n,\gamma)^{87}Sr$ decay scheme. The program DCYSCH was utilized with the 35 levels populated in the (d,p) reaction as listed in Table 2-6 as the input levels. The input gamma-ray list included the 61 gamma rays not assigned in the $^{87}Sr(n,\gamma)^{88}Sr$ decay scheme and the 4 gamma rays of energy 388, 484, 7556 and 8040 keV which were assigned to the ^{87}Sr nucleus on the basis of known levels at 388 and 872 keV. A total of 58 possible fits were found for the 61 unassigned gamma rays but none of these fits proceeded between

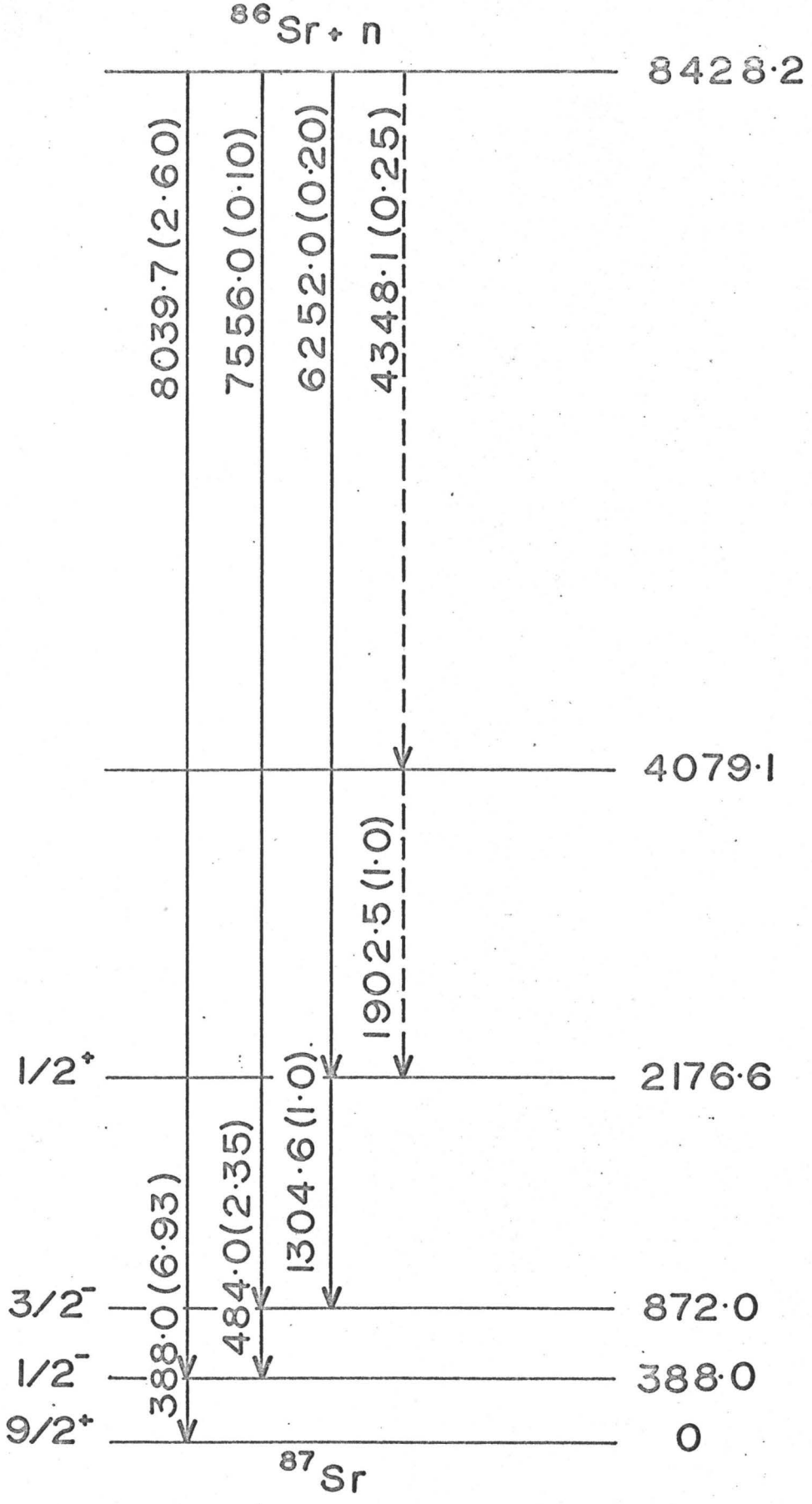
$^{86}Sr + n$
8428·2
8039·7 (2·60)
7556·0 (0·10)
6252·0 (0·20)
4348·1 (0·25)
4079·1
1902·5 (1·0)
1/2⁺
2176·6
1304·6 (1·0)
484·0 (2·35)
388·0 (6·93)
3/2⁻
872·0
1/2⁻
388·0
9/2⁺
0
^{87}Sr

FIGURE 6-11

any of the (d,p) levels. Thus it was impossible to add any further assignments to the $^{86}Sr(n,\gamma)^{87}Sr$ decay scheme with this list of input data. A second use was made of the decay scheme program, this time with the input gamma-ray list including the 119 gamma rays which were unassigned after the first 45 gamma rays were fit in the $^{87}Sr(n,\gamma)^{88}Sr$ decay scheme as well as the 4 fixed gamma rays of energy 388, 484, 7556 and 8040 keV. The program now fit three more gamma rays populating the levels at 2177 keV and 4079 keV. In fact a close scrutiny of the strontium gamma-ray spectrum revealed that the shoulder on the lower energy side of the double escape peak of the 6267 keV gamma ray may be the double escape of the 6252 keV gamma ray populating the 2177 keV level which is an $\ell_n=0$ level. No attempt was made to use COMB or RCMB as not enough levels were available as a basis. The tentative decay scheme for $^{86}Sr(n,\gamma)^{87}Sr$ is presented in figure 6-11. Gamma-ray intensities are included in brackets. The determination of the neutron separation energy for ^{87}Sr is summarized in Table 6-3.

CHAPTER 7

DISCUSSION OF RESULTS

7-1 Level structure of ^{87}Rb

The decay scheme of ^{87}Kr consistent with the experimental results outlined in chapter 5 is shown in figure 5-17. The nature of only the first few excited states in ^{87}Rb has been deduced from other reactions leading to the same final states as summarized in chapter 2. An attempt will be made here to deduce the spins and parities of some of the other levels on the basis of log ft values and gamma-decay branching ratios presented in chapter 5. The level structure of this nucleus will then be interpreted in terms of the concepts outlined in chapter 1.

In general the level structure of nuclei in the mass region where the nucleon numbers lie between 28 and 50 are more difficult to interpret than for the lighter or heavier nuclei. However ^{87}Rb is an example of a single closed shell nucleus in which the neutrons fill the N=50 major shell. According to simple shell model theory the 37^{th} proton in ^{87}Rb will be in the $2p_{3/2}$ shell and the ground state spin of ^{87}Rb should be determined by the proton hole in this shell. In fact the spin has been measured to be $3/2^-$ [41]. The nucleus ^{87}Kr has 36 protons and 51 neutrons so that its ground state spin should be determined by the 51^{st} neutron in the $d_{5/2}$

shell. The ground state spin has been determined to be 5/2+ as discussed in chapter 2 thus contradicting the 7/2+ value assumed by Thulin[46]. This changes the interpretation of the beta spectra correspondingly.

The first few levels in ^{87}Rb can be considered as good quasi-particle states. On the basis of the shell model one would expect to find the $1f_{5/2}$, $2p_{1/2}$ and $1g_{9/2}$ quasi-particle states in the low-lying level structure of ^{87}Rb along with the $2p_{3/2}$ quasi-particle ground state. The beta groups to the ground and first two excited states have high log ft values typical of first forbidden transitions. The spin assignment of 5/2- for the 403 keV state as determined by the (d,He^3) reaction to the same final state is consistent with the observed log ft value . The log ft value of 8.0 determined for the beta transition to the 846 keV level designates this transition as a possible first forbidden unique transition according to the distribution of log ft values shown in figure 1-1. This level can then be identified as the $2p_{1/2}$ quasi-particle state. The fact that no gamma coincidences were detected with the 846 keV gamma-ray transition also supports the 1/2- spin-parity assignment for this level. The spin assignment is further confirmed by the fact that there is a strong gamma-ray transition to the ground state from

this level but that no 443 keV transition was detected to the 403 keV $1f_{5/2}$ quasi-particle state. In fact on the basis of simple shell model calculations a possible 443 keV transition would be down by a factor of 2×10^4 in intensity from the measured intensity of the 846 keV transition. There is no beta intensity detected to the 1579 keV level within the experimental uncertainties. On the basis of this and the decay mode of this level it is interpreted as the $1g_{9/2}$ quasi-particle state. The beta transition to this level would then have to be a second forbidden transition with a very high log ft value and hence little intensity as observed experimentally. The 1579 keV level decays only via the 1176 keV gamma-ray transition to the 403 keV 5/2- level. The 9/2+ spin assignment for this level is supported by the fact that no transition was detected to the ground state or to the 1/2- level at 846 keV. These transitions would be E3 and M4 respectively and therefore down many orders of magnitude in intensity from the 1176 keV transition.

The interpretation of the ground state and the first three excited states in ^{87}Rb as the $2p_{3/2}$, $1f_{5/2}$, $2p_{1/2}$ and $1g_{9/2}$ quasi-particle states respectively is consistent with the experimental results. To excite another one quasi-particle state a proton would have to be excited across the gap at the N=50 major shell. This level would be at much higher

energy than the $1g_{9/2}$ quasi-particle state. Thus it is expected that it would be much easier to excite 3 quasi-particle states of the type

$$\pi[(2p_{1/2})^2(2p_{3/2})^{-1}]$$

and $$\pi[(1g_{9/2})^2(2p_{3/2})^{-1}] \ .$$

The 1741 keV level is populated by a first forbidden beta group with a log ft value of 8.4. The decay modes of this level indicate that the most probable spin assignment for this level is 5/2-. The level does not decay to the 1/2- level. The ratio of the intensities of the 1741 and 1338 keV transitions is consistent with M1 transitions to the 3/2- ground state and the 5/2- first excited state. This level is probably a 3 quasi-particle state with the proton configuration $\pi[(2p_{1/2})^2(2p_{3/2})^{-1}]_{5/2-}$.

The log ft value of the beta transition to the 2415 keV level does not indicate conclusively whether it is an allowed or first forbidden beta transition. The spin can be assigned as 7/2 with good probability of being correct because the level decays to the two 5/2- states and to the 9/2+ state but not to the 3/2- ground state or the 1/2- second excited state. The ratios of the observed intensities of the three de-exciting gamma rays agree with the single particle estimates better if a positive parity is assumed for this

level.

With the exception of the beta transition to the 2811 keV level the log ft values of the beta transitions to the higher energy states are all relatively low indicating allowed beta transitions. Thus most of the higher energy levels have positive parities and possible spins of 3/2, 5/2 or 7/2. The predominant transitions from these states are to the ground state or first excited state indicating strong E1 transitions. The 2556 and 3310 keV levels decay only directly to the ground state indicating 3/2+ or 5/2+ assignments for these levels. The 2962 keV level decays both to the 9/2+ and 5/2- states. The probable spin-parity assignment for this level is then 7/2+. A negative parity assignment for this level is inconsistent with the observed ratio of the 1384 and 2559 keV gamma-ray intensities. The 2811 keV level decays only to the ground state thus narrowing the spin possibilities to 3/2 or 5/2. A definite parity assignment cannot be made for this level. The spin and parity assignments for the levels in ^{87}Rb are summarized in Table 7-1.

The level structure of the low-lying states of ^{87}Rb, which is a single closed shell nucleus, agrees quite well with the model proposed by Kisslinger and Sorensen[20,21] as discussed in chapter 1. They treat the low-lying states of

Table 7-1

Spin-Parity Assignments for ^{87}Rb Levels

E_x(keV)	J^π	Configuration
0	3/2-	$p_{3/2}$
403.0	5/2-	$f_{5/2}$
845.8	1/2-	$p_{1/2}$
1578.5	(9/2+)	$g_{9/2}$
1741.0	(5/2-)	
2415.0	(7/2+)	
2556.0	(3/2+,5/2+)	
2811.2	(3/2±,5/2±)	
2962.5	(7/2+)	
3309.8	(3/2+,5/2+)	

spherical nuclei in terms of quasi-particle excitations. Higher energy states are treated in terms of phonon excitations and states of higher seniority. In the case of ^{87}Rb the positive parity band of the higher energy states can be interpreted as an octupole vibration built on the negative parity ground state. These positive parity states can arise from the proton configurations $\pi[(1g_{9/2})(1f_{5/2})^{-2}]$ and $\pi[(1g_{9/2})(2p_{3/2})^{-2}]$ which are seniority three quasi-particle states.

It is interesting to compare the level structure of ^{87}Rb with that of ^{89}Rb which also has 37 protons but 2 more neutrons. The levels of ^{89}Rb have been studied via the beta decay of ^{89}Kr[141]. Both ^{87}Kr and ^{89}Kr ground states have the proton configurations $\pi[(2p_{3/2})^{-2}]$ and $\pi[(1f_{5/2})^{-2}]$ coupled to the neutron configurations $\nu[(2d_{5/2})]$ and $\nu(2d_{5/2})^{3}]$ respectively as in both beta-decay processes beta groups were observed to the respective ground states as well as first excited states. However in the beta decay of ^{87}Kr the ground state beta-group branching percentage is much higher than in the corresponding decay of ^{89}Kr to the ground state of ^{89}Rb. This indicates that the $\pi[(2p_{3/2})^{-2}]$ proton configuration is much stronger in the ^{87}Kr ground state than in the ^{89}Kr ground state. It also indicates a difference in character of the ^{87}Rb and ^{89}Rb ground states. However in both cases the ground states of ^{87}Rb and ^{89}Rb can be interpreted as $2p_{3/2}$ quasi-particle states whereas the first excited states are $1f_{5/2}$ quasi-particle states. The $2p_{1/2}$ and $1g_{9/2}$ quasi-particle states have not been identified in ^{89}Rb. Above the first few excited states in ^{89}Rb the level structure is much more complex than that of ^{87}Rb because of the addition of a neutron pair beyond the N=50 major shell. In the case of ^{89}Rb the larger number of low-lying negative parity states arise from coupling of the $\pi[(2p_{3/2})^{-1}]$ and $\pi[(1f_{5/2})^{-1}]$ proton hole configurations with

the $\nu[(2d_{5/2})]$ and $\nu[(1g_{7/2})]$ as well as other low energy neutron configurations. In both ^{87}Rb and ^{89}Rb the positive parity levels are populated above about 2.4 MeV excitation energy. These positive parity states can arise from the coupling of the $\pi[(1g_{9/2})(1f_{5/2})^{-2}]$ and $\pi[(1g_{9/2})(2p_{3/2})^{-2}]$ proton configurations with the neutron states containing paired neutrons. In the case of ^{87}Rb these states are likely primarily proton states whereas for ^{89}Rb they would probably have a measureable contribution from neutron configurations as well.

7-2 Level Structure of ^{88}Rb

The decay scheme of ^{88}Kr consistent with the experimental results outlined in chapter 5 is shown in figure 5-18. The ℓ_n values for some of the states populated in the beta-decay process have been determined from the ^{87}Rb(d,p)^{88}Rb reaction as listed in Table 2-7. These ℓ_n values determine the parities of many of the low-lying levels in ^{88}Rb. The spins of these low-lying levels can be deduced in some cases from log ft values and gamma-decay branching ratios as calculated in chapter 5. The level structure of ^{88}Rb can be interpreted in terms of the concepts outlined in chapter 1.

The ground state spin of ^{88}Kr is of course 0+ with 36 protons and 52 neutrons, the last two neutrons being outside the major closed shell at N=50. The odd-odd nucleus

^{88}Rb has one neutron beyond the N=50 shell which can be associated with the $d_{5/2}$ orbital. This neutron is coupled to the $\pi[(2p_{3/2})^{-1}]$ ground state configuration of ^{87}Rb to give a ground state configuration of $\pi[(2p_{3/2})^{-1}]\nu[(2d_{5/2})]$ in ^{88}Rb. This gives rise to a multiplet of states with spins 1-, 2-, 3- and 4-. The lowest energy state which corresponds to the ground state of ^{88}Rb has been found[43] to be the 2-. The other members of this multiplet have been populated in the (d,p) reaction as well as the beta-decay process.

A beta transition with log ft = 8.0 has been observed to populate the 196 keV level. This log ft value is typical of a first-forbidden transition. No other beta transitions have been detected to this spin multiplet. The first excited level decays via the 28 keV gamma-ray and also by internal conversion. The second level at 196 keV decays only to the 2- ground state, whereas the 4- level decays only to the first excited state. The spin assignments made in the (d,p) reaction results are consistent with the beta transition to the 1- state at 196 keV and with the gamma-decay modes of these low-lying levels. Thus the first 4 levels in ^{88}Rb including the ground state can be interpreted as the multiplet of 2-, 3-, 1- and 4- arising from the coupling of the $2p_{3/2}$ proton hole state with the $2d_{5/2}$ neutron particle state.

The 362 keV level is populated by a beta transition

with a high log ft value indicating either a first forbidden or a first forbidden unique transition. The level decays both to the 1- and 2- levels indicating a spin assignment of either 1- or 2- for the 362 keV level. The 390 keV level can likely be given a spin assignment of 2- or 3- as it is not populated by a beta transition and decays only to the 2- ground state. The 862 keV level is populated by a beta transition with log ft value of 8.1. It decays to the ground state, to the 390 keV level and strongly to the 3- first excited state. A spin assignment of 2- is consistent with these results indicating that the beta transition to the 862 keV level is first forbidden unique and the decay transitions are all M1 in character. The decay modes of the 862 keV level and the gamma population modes of the 362 and 390 keV levels (to be discussed in connection with the 2392 keV level) favor spin assignments of 1- and 3- for the 362 and 390 keV states respectively. The configuration $\pi[(1f_{5/2})^{-1}]\nu[(2d_{5/2})]$ can give rise to a multiplet with spins ranging from 0- to 5-. The three states discussed here, the levels at 362, 390 and 862 keV are likely the 1-, 3- and 2- members respectively, of this multiplet. The higher spin states would not likely be populated in the beta-decay process. The ℓ_n=2 413 keV level observed in the (d,p) reaction is then quite probably the 4- member of this multiplet.

All five levels between 1140 and 1360 keV have negative parity based on the high log ft values exhibited by the first forbidden beta transitions to them. The 1142 keV level is probably a 2- spin state since the log ft value of the associated beta transition is high and gamma decay proceeds entirely to the ground state. The beta transition to the 1183 keV level has a somewhat lower log ft value and de-excitation occurs only via the 987 keV transition to the 1- 196 keV state. Thus the spin assignment may be either 1- or 2-. The 1213 keV level is an ℓ_n=0 state and is fed by a beta transition with a high log ft value. Thus its spin is likely 2-. This spin assignment is supported by the fact that this level decays to the 2-, 3- and 4- components of the ground state multiplet. On this basis the transitions to the 2- and 3- states are M1 in character while the transition to the 4- state is an enhanced E2 transition. The 1246 keV level decays both to the ground state 2- level and to the 196 keV 1- level. The high log ft value of the beta transition to this level favors a 2- assignment but a 1- assignment cannot be ruled out. The 1353 keV level is another ℓ_n=0 state allowing spin assignments of 1- or 2-. Because no beta transition is observed to this level, the 1- assignment can be ruled out. A 2- spin assignment is supported by the fact that the level decays only to the 2- ground state and the (3-) 390

keV level. This band of negative parity states must be due to higher seniority states consisting of higher phonon-excitations. The levels can be interpreted as arising from quadrupole vibrations coupled to the negative parity ground state band in ^{88}Rb. It is then a vibrational band built on quasi-particle states as illustrated in figure 1-4b. Some of the lower energy states of seniority 4 which could contribute to this band of levels are,

$$\pi[(1f_{5/2})^{-2}(2p_{1/2})]\nu[(2d_{5/2})]$$

$$\pi[(2p_{3/2})^{-2}(2p_{1/2})]\nu[(2d_{5/2})]$$

$$\pi[(1f_{5/2})^{-2}(2p_{1/2})]\nu[(1g_{7/2})]$$

$$\text{and } \pi[(2p_{3/2})^{-2}(2p_{1/2})]\nu[(1g_{7/2})].$$

Between the 1353 and 2232 keV levels there is a large gap in which no levels are populated in the beta-decay process. Some levels in this region were populated in the (d,p) reaction however. These are probably the higher spin state members consisting of the seniority 4 configurations listed above. It would be impossible to populate these levels directly in the beta-decay process. The log ft values of the beta transitions to the four highest energy levels populated in the beta decay of ^{88}Kr indicate that these beta transitions are all allowed. The possible spins of these states are then

0+ or 1+. The strong 2392 keV level is almost certainly a 1+ level because of the very low log ft value of its beta transition and the fact that the gamma radiation from this level feeds only final states of spin 1- and 2-. These transitions are then all E1 in character. Table 7-2 shows that there is

Table 7-2

Reduced Widths of gamma rays from 2392 keV level

E_γ (MeV)	I_γ	I_γ/E_γ^3*
2.392	37.8	2.09
2.196	14.9	1.06
2.030	4.8	0.43
1.530	11.3	2.38
1.250	1.1	0.43
1.179	0.75	0.34
1.040	0.4	0.27

*Normalized to $\overline{I\gamma/E_\gamma^3} = 1.0$

no more than an order of magnitude variation in the reduced gamma-ray widths of the transitions de-exciting the 2392 keV level assuming that all transitions are E1 in character. A strong case can be made for 1+ spin assignments for all of the 4 positive parity levels populated above 2 MeV in ^{88}Rb on

the basis of the low log ft values and the fact that each level de-excites only to 1- and 2- final states.

This positive parity band of levels can be interpreted in terms of an octupole vibration built on the negative parity ground state multiplet. From the point of view of collective motions, Kisslinger and Sorensen[20,21] suggested, as pointed out in chapter 1, that in this mass region of closed shells one could expect to have bands of levels resulting from the coupling of a two quasi-particle state with vibrational states. The states in this positive parity band are likely comprised of 4 quasi-particle states with the following configurations.

$$\pi[(1f_{5/2})^{-2}(1g_{9/2})]\nu[(2d_{5/2})]$$
$$\pi[(2p_{3/2})^{-2}(1g_{9/2})]\nu[(2d_{5/2})]$$
$$\pi[(1f_{5/2})^{-2}(1g_{9/2})]\nu[(1g_{7/2})]$$
$$\text{and } \pi[(2p_{3/2})^{-2}(1g_{9/2})]\nu[(1g_{9/2})]$$

The spin and parity assignments for the levels of ^{88}Rb populated in the beta-decay process are summarized in Table 7-3. The nature of these levels as discussed in this section can be summed up as follows. There are two low-lying spin multiplets due to the two quasi-particle configurations $\pi[(2p_{3/2})^{-1}]\nu[(2d_{5/2})]$ and $\pi[(1f_{5/2})^{-1}]\nu[(2d_{5/2})]$.

Table 7-3

Spin-parity assignments for ^{88}Rb levels

E_x(keV) β-decay	E_x(keV) (d,p)	ℓ_n	log ft	J^π
0	0	0+2		2-
28.0	27	2		3-
196.1	196	0+2	8.0	1-
268.4	268	2		4-
362.5	361	(2,0)	8.2	(1-,2-)
390.4	390	2		(2-,3-)
	413	2		
862.4	861	0	8.1	(2-)
1141.7	1142	0	8.5	(1-,2-)
1182.8			8.0	(1-,2-)
1213.3	1212	0	8.7	(2-)
1245.6	1245	2	8.5	(1-,2-)
1352.5	1353	0		(2-)
	1609	?		
	1665	0		
	1794			
	1860			
	1927			
	1970			
	2090			
	2170			
2231.6	(2230)		5.8	(1+)
	2257			
	2361			
2392.0			4.3	(1+)
	2452			
2549.0			5.9	(1+)
2771.8			5.3	(1+)

Above these levels there is first of all a negative parity band due to the coupling of quadrupole vibrational states to the negative parity ground state. Then there is a higher lying positive parity band due to the coupling of octupole vibrational states to the negative parity ground state.

A similar comparison of the level structure of ^{88}Rb to that of ^{90}Rb can be made as done in the case of ^{87}Rb and ^{89}Rb in section 7-1. Here again ^{90}Rb has two more neutrons outside of the closed N=50 shell than does ^{88}Rb. This is expected to complicate the level structure of ^{90}Rb somewhat compared to that of ^{88}Rb. However ^{90}Rb is expected to have low-lying states resulting from the 2 quasi-particle configurations $\pi[(2p_{3/2})^{-1}]\nu[(2d_{5/2})]$ and $\pi[(1f_{5/2})^{-1}]\nu[(2d_{5/2})]$ as in the case of ^{88}Rb. In fact an examination of the low-lying levels in ^{90}Rb as determined by Goodman et.al.[142] and modified by Mason et.al.[143] shows that such an interpretation is possible. There is no beta ground state transition likely indicating a 2- spin assignment for this state as in the case of ^{88}Rb. The relatively high log ft values for the beta transitions to the low-lying states indicate negative parity assignments for them. Between 730 keV and 1240 keV there is a large gap in which no levels are populated in the beta decay of ^{90}Kr. This corresponds to the gap at slightly higher excitation energy noted in the levels in ^{88}Rb populated

in the beta decay of ^{88}Kr. Above this gap in each nucleus there is a positive parity band strongly populated in both cases. In the ^{88}Kr decay process 71% of the beta intensity goes to the 2392 keV 1+ level in ^{88}Rb whereas in the ^{90}Kr decay 66% of the beta intensity goes to the 1780 keV 1+ level in ^{90}Rb. In both ^{88}Rb and ^{90}Rb it is expected that these positive parity states are due to the coupling of a 2 quasi-particle state with octupole vibrational states and arise from the 4 quasi-particle configurations described before. The above analysis points to the strong similarities between the ^{88}Kr and ^{90}Kr beta-decay processes and between the ^{88}Rb and ^{90}Rb level structures.

7-3 Level Structure of ^{87}Sr

The level structure of this nucleus was studied via the neutron capture reaction on natural strontium. As the capture cross-section contributing to the population of final states in this nucleus was small only a few gamma rays could be assigned to ^{87}Sr as shown in figure 6-11. Some levels in ^{87}Sr are known as a result of the (d,p) and (d,α) reactions to final states in ^{87}Sr as summarized in Table 2-6. The (d,α) reaction populates predominantly neutron hole states while the (d,p) reaction populates predominantly neutron particle states.

The ^{87}Sr nucleus has a neutron hole in the N=50 major shell indicating that some of its low-lying states can be attributed to neutron hole states. In fact the ground state and first two excited states can be interpreted as the $\nu[(1g_{9/2})^{-1}]$, $\nu[(2p_{1/2})^{-1}]$ and $\nu[(2p_{3/2})^{-1}]$ neutron hole states. As the capture state will have a spin of 1/2+ for s-wave neutrons and E1 transitions are expected to predominate over M1 transitions the two negative parity states should be and are populated in the (n,γ) reaction. The 1/2- state is populated strongly whereas the 3/2- state is populated only weakly. These two levels are the only ℓ_n=1 levels populated in the (d,p) reaction. Any M1 transitions would populate 1/2+ or 3/2+ states. It might be expected that some of the ℓ_n=0 states which have spin 1/2+ would be populated in the (n,γ) reaction. There is some indication that the 2177 keV ℓ_n=0 state is populated by a primary transition. Primary transitions to no other levels were detected except perhaps for the primary transition to the 4079 keV level as shown in figure 6-11. No ℓ_n value has been measured for the 4079 keV level. Thus it is not possible on the basis of this scanty information to indicate whether the E1 primary strength predominates over the M1 primary strength although the available data favors this premise. The 5/2+ state at 1231 keV observed in the (d,p) and (d,α) reaction is probably the $\nu[(2d_{5/2})(1g_{9/2})^{-2}]$

neutron state. The existence of the $\nu[(1f_{5/2})^{-1}]$ state could also be expected in the low energy region but it would be an $\ell_n=3$ state and as such was not observed in the (d,p) reaction or in the (n,γ) reaction. Above the 1 quasi-particle excitations the 3 quasi-particle excitations arising from the coupling of the neutron states with the $\pi[(2p_{1/2})(1f_{5/2})^{-1}]$ and $\pi[(2p_{1/2})(2p_{3/2})^{-1}]$ proton states can be expected. However no more spin assignments can be made to the ^{87}Sr levels on the basis of (n,γ) results.

A limited comparison can be made with the ^{85}Sr nucleus which has a three-neutron hole state in the N=50 shell. It has the same ground state spin as ^{87}Sr and also has a 1/2- isomeric state which is typical of nuclei in this mass region with a few neutrons less than the closed shell of N=50.

7-4 Level Structure of ^{88}Sr

The level structure of ^{88}Sr has been studied by means of a beta-decay process and a thermal neutron capture reaction. The decay scheme of ^{88}Rb shown in figure 5-19 is consistent with the experimental results as presented in chapter 5. The decay scheme corresponding to the ^{87}Sr(n,γ)^{88}Sr reaction as shown in figure 6-10 is consistent with the experimental results outlined in chapter 6. The fact that some common levels are populated in the beta-decay process and the (n,γ)

reaction below 5 MeV provides a means of determining the spins and parities of some of these levels. Levels in this energy region as well as some above 5 MeV were populated in other reactions leading to final states in ^{88}Sr as summarized in chapter 2. By knowing which reactions populate a state it is often possible to determine the nature and the configurations contributing to that state. The nature of the states in ^{88}Sr populated in the beta decay process and in the neutron capture reaction will be interpreted in terms of the concepts outlined in chapter 1.

The nature of the thermal neutron capture reaction and indeed of the capture state itself can often be inferred from the distribution of reduced widths of the primary gamma-ray transitions. It can be seen that not many of the levels populated in the (d,p) reaction were populated by primary gamma-ray transitions. Most of the levels populated in the (d,p) reaction are ℓ_n=0 or ℓ_n=2 states whereas E1 primary transitions would populate ℓ_n=1 states. Thus it is impossible to compare the intensity of primary gamma rays and of corresponding proton groups to ascertain whether the (n,γ) reaction is a direct reaction or proceeds via compound nucleus formation. It does show that the M1 strength is down considerably from the E1 strength as expected. However, according to arguments presented by Porter and Thomas[29] the distribution

of reduced gamma-ray widths obey a chi-squared distribution of one degree of freedom if capture occurs at a resonance level in the compound nucleus. Usually more than one resonance level contributes to the capture state and the distribution will consequently follow a chi-squared distribution of more than one degree of freedom (ν=1). Figure 7-1 displays the distribution of the reduced widths (I_γ/E_γ^3) for the 31 primary gamma rays from the ^{88}Sr capture state in the form of a histogram assuming that all are E1 transitions. The two solid lines show the distributions expected for chi-squared distributions with one and two degrees of freedom. It is found that the primary gamma-ray reduced widths obey a chi-squared distribution of 1.55 ± 0.55 degrees of freedom corrected for finite sample size effects[144]. The actual value of ν is probably less than 1.55 if one considers the number of small widths not detected because of resolution and efficiency effects. The small value of ν supports compound nucleus formation in the thermal neutron capture in ^{88}Sr and also points to the predominance of one spin state contributing to the capture state. An analysis of the decay modes of the capture state indicates that the 4+ spin state is the major contributor to the capture state.

^{88}Sr is an interesting nucleus to study from a theoretical point of view as it is an example of a single closed

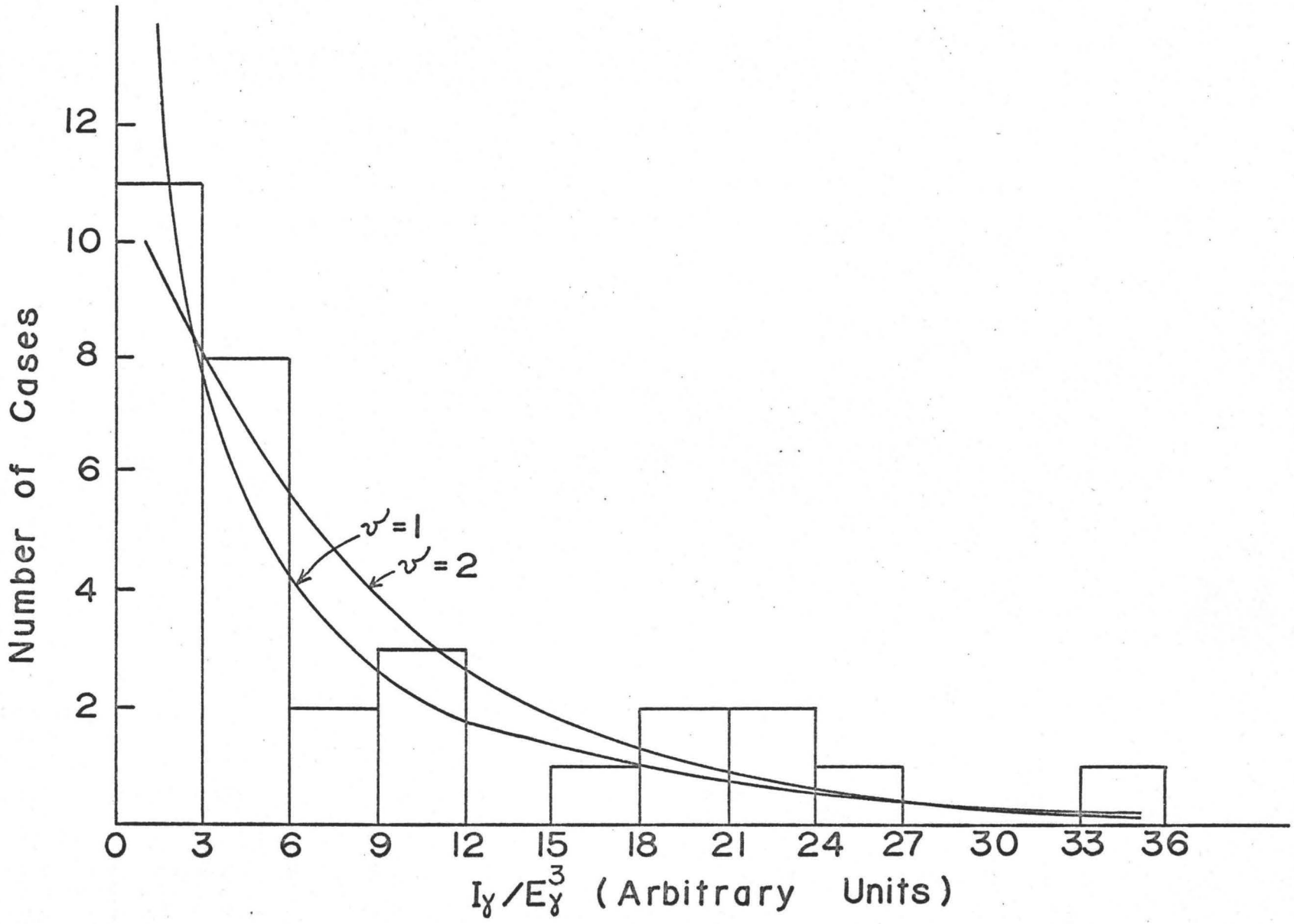
Number of Cases
12
10
8
6
4
2
0
3
6
9
12
15
18
21
24
27
30
33
36
$\nu = 1$
$\nu = 2$
I_γ / E_γ^3 (Arbitrary Units)

FIGURE 7-1

shell nucleus with the neutron shell at N=50 filled. It is in fact an even-even nucleus with the semi-major proton shell of Z=38 closed as well. The ^{88}Sr nucleus is in the region of spherical nuclei whose states can be interpreted in terms of collective vibrations consisting of one and higher phonon excitations as discussed in chapter 1. The beta decay process yields information concerning the quasi-particle nature of the states and the amount of collective character characteristic of the states. Hence it should add to the information available from the one- and two-particle stripping and pick-up reactions as summarized in chapter 2.

It is expected that the first few excited levels in ^{88}Sr will consist of proton core-excited configurations as it takes less energy to break the proton pairing energy than to excite a neutron over the major shell energy gap. The neutron core excited configurations should appear above 4 or 5 MeV in ^{88}Sr as found from the ^{87}Sr(d,p)^{88}Sr reaction results. By means of the (d,p) reaction it was possible to excite the neutron particle-hole states in ^{88}Sr built on a single $g_{9/2}$ hole in the N=50 core. The (d,p) reaction transfers a single neutron to the ^{87}Sr target with $J^{\pi} = 9/2+$. In fact most of the states in ^{88}Sr excited by the (d,p) reaction can be explained by the coupling of a $\nu[(1g_{9/2})^{-1}]$ neutron hole to the first few excited states of ^{89}Sr. The $\ell_n=0$ states arise from the $\nu[(3s_{1/2})(1g_{9/2})^{-1}]$

configuration whereas the two groups of ℓ_n=2 states arise from the $\nu[(2d_{3/2})(1g_{9/2})^{-1}]$ and $\nu[(2d_{5/2})(1g_{9/2})^{-1}]$ configurations. Only one ℓ_n=4 state beside the ground state was excited in the (d,p) reaction and this is probably a member of the $\nu[(1g_{7/2})(1g_{9/2})^{-1}]$ multiplet. Only two ℓ_n=1 states were populated in the (d,p) reaction. Actually the single-particle model predicts no excitation of ℓ_n=1 levels if the ground state of ^{87}Sr contains only the $\nu[(1g_{9/2})^{-1}]$ neutron hole configuration. The excitation of some ℓ_n=1 states can only be explained by contributions of the $\nu[(2p_{1/2})^{-1}]$ configuration to the ^{87}Sr ground state. However in the (n,γ) reaction it should be expected that mainly ℓ_n=1 states would be populated by primary transitions. Thus it is expected and observed that not many levels are populated in common by the two reactions.

For purpose of discussion of the spin and parity assignments to the levels in ^{88}Sr it will be helpful here to point out the ground state configurations of ^{87}Sr and of ^{88}Rb which are the parent nuclei in the (n,γ) reaction and beta-decay process respectively. The (d,p) data show quite conclusively that the ground state of ^{87}Sr is composed mainly of the $\nu[(g_{9/2})^{-1}]$ configuration. The ^{87}Rb(d,p)^{88}Rb reaction and the beta decay of ^{88}Kr indicate that the predominant component of the ^{88}Rb ground state is the $\pi[(2p_{3/2})^{-1}]\nu[(2d_{5/2})]$ configuration. The observed multiplet of 2-, 3-, 1- and 4- states

gives strong support to this configuration. However the observed magnetic moment of $^{88}Rb^{(43)}$ indicates a small contribution from the $\pi[(1f_{5/2})^{-1}]\nu[(2d_{5/2})]$ configuration as well to the ground state of ^{88}Rb.

The beta decay of ^{88}Rb populates low-lying states up to 5 MeV excitation energy in ^{88}Sr. These levels can have spins ranging from 1^- to 3^- for allowed beta transitions and from 0+ to 4+ for first forbidden or first forbidden unique transitions as the ground state spin of ^{88}Rb is 2-. Thermal neutron capture in ^{87}Sr leads to a ^{88}Sr capture state of spin 4+ or 5+. Hence E1 primary transitions could populate states of spin and parity 3-, 4-, 5- or 6- whereas M1 primary transitions could populate 3+, 4+, 5+ or 6+ spin states. However the latter are expected to be in the minority. Primary transitions of type E2 are not likely to be detected so that states with spin 2+ or 7+ will not be populated directly. Thus any level which is populated directly both in the beta-decay of ^{88}Rb and in the $^{87}Sr(n,\gamma)^{88}Sr$ reaction must have a spin and parity of either 3-, 3+ or 4+.

The levels populated in beta-decay and in the (n,γ) reaction as reported in chapters 5 and 6 respectively are listed in Table 7-4. These values are weighted averages and the errors indicated are obtained by applying the normal law of errors. If a level has been populated in the (d,p)

reaction as well, it is noted along with the ℓ_n value characteristic of the level. Spin and parity assignments are well known for some of the low-lying levels in ^{88}Sr and are listed as such in column 5 of Table 7-4. The spin and parity assignments made in this study are indicated in brackets. The basis of these assignments and the nature of the levels in ^{88}Sr will now be discussed.

The ground state of ^{88}Sr is of course the 0+ spin state of an even-even nucleus. The neutrons form a closed shell whereas the protons form a semi-closed shell of 38 protons. Hence the ground state configuration is expected to be well approximated by $\pi[(1f_{5/2})^6(2p_{3/2})^4]\nu[(1g_{9/2})^{10}]$. However the ground state must also have some $\pi[(2p_{1/2})^2]$ admixture as the 846 keV 1/2- level is weakly excited in the ^{88}Sr(d,He^3)^{87}Rb reaction [72]. There is of course no primary gamma-ray transition to the ground state and in fact because of the large spin difference between the capture state and the ground state most gamma-ray cascades have 3 or more members. The beta-decay branch to the ground state is of a first-forbidden unique character with a low log ft value for this type of transition indicating a relatively unhindered mode of decay. This can be regarded as consisting mainly of the single-particle decay of a $1d_{5/2}$ neutron to the $2p_{3/2}$ proton orbital.

TABLE 7-4

^{88}Sr Level Energies and Spin-Parity Assignments

E_x (keV) (n,γ)	E_x (keV) β-decay	E_x (keV) (d,p)	ℓ_n	J^π
0	0	0	4	0+
1836.1±0.5	1836.1±0.5	1839	2	2+
2734.1±0.8	2734.1±0.8	2738	ns	3-
3219.5±1.5	3219.7±2.2	3208	ns	2+
3487.0±2.0	3487.8±2.0			1+
3522.6±1.0				(2+)
3584.6±1.0		(3590)	(ns)	(4-,5-)
3635.2±1.1				3+
3952.6±1.3				(4+)
4170.1±1.1				(4-)
4227.3±1.7				(3-)
4269.3±1.3	4269.6±1.3			(3±)
4300.5±1.7				(4+)
4413.9±0.7	4413.9±1.1	4408	2	(3+)
4452.0±1.3		4450	2	(3,4-)
4513.8±2.3	4513.9±2.4	4514	2	(2-,3-)
4743.0±2.0	4744.5±3.0	4748	2	(2+)
4845.6±1.7	4845.6±1.7			(3-)
	4854.0±3.2			(2-)
5010.6±2.1				(3-,4-,5-)

(continued next page)

E_x(keV) (n,γ)	E_x(keV) β-decay	E_x(keV) (d,p)	ℓ_n	J^π
5077.3±1.5				
5263.2±1.3				
5321.3±3.0				(3-,4-,5-)
5426.3±1.8		5418	0	4+
5517.8±1.4		5506	0	4+
5537.1±3.2				(3±,4+)
5662.3±2.0		5665	(1)	(3-)
5690.4±2.2				(3-)
5751.1±2.2				(3-,4-,5-)
5811.3±1.1				
5836.4±2.8		5830	(ns)	
5952.0±2.2				(3-,4-,5-)
6123.6±1.8				
6258.3±4.0		6237	(1)	(3-→6-)
6387.6±2.0		6376	(2)	
7092.5±3.6		7088	?	
7337.8±3.0		7337		
7573.4±3.8		7561		
7835.0±1.3		7839		
11113.0±0.6				

The 1836 keV level has been well established as a 2+ quadrupole vibrational state. Again there is no primary gamma-ray transition to this level as it would have to be a E2 transition. The beta transition to this level is a first forbidden transition with a typical log ft value of 7.5 indicating that the level is not collective in nature. The inelastic electron scattering results give a value of 8.5 single particle units for the B(E2)↑ value of this level again indicating only a small amount of collective character. The lowest-lying levels of ^{88}Sr should consist mainly of proton configurations. In fact the (d,He^3) results showed that 80% of the first 2+ state was accounted for by the $\pi[(2p_{1/2})(2p_{3/2})^{-1}]$ and $\pi[(2p_{1/2})(1f_{5/2})^{-1}]$ proton configurations. The ^{87}Sr(d,p)^{88}Sr reaction results indicated that the largest fraction of the remainder of the level strength was taken up by the neutron configuration $\nu[(2d_{5/2})(1g_{9/2})^{-1}]$. The energy of this state is quite high for a first excited state but can be explained by the fact that the configuration nearest to that of a closed shell would have a high one-phonon excitation energy.

The 2734 keV level is a well-known octupole 3- state. It is populated by a strong primary El transition from the capture state and also by an allowed beta group with log ft value of 6.5 from the ^{88}Rb ground state. These excitation

modes are both consistent with a 3- spin assignment. The level is only weakly populated in the (d,p) reaction indicating weak contributions from neutron configurations to the state. A value of 25 single particle units has been measured for the B(E3)↑ value in the electron scattering reaction indicating the very strong collective character of this level. The collective nature is also shown by the relatively high log ft value for the allowed beta transition to this state. The one-particle one-hole proton configuration $\pi[(1g_{9/2})(2p_{3/2})^{-1}]$ has been shown by Shastry and Saha[145] to be the dominant part of this state's configurations. The observed branching ratio for (2734→1836)/(2734→0) was of the order 100:1 in both the beta-decay process and the (n,γ) reaction compared with a single-particle estimate of about 10^6. This indicates that the E1 transition is hindered by a large factor as might be expected for a transition from an octupole state to a quadrupole state and that the E3 transition to the ground state is enhanced.

The 3220 keV level is similar in character to that of the 1836 keV level. In fact it can be interpreted as the two-phonon state of spin 2+. It is not populated by a primary transition from the capture state as expected but it is populated in the beta-decay process by a first-forbidden transition with a log ft value of 7.1. Again the (d,He^3) reaction

results indicate that the proton configurations $\pi[(2p_{1/2})(2p_{3/2})^{-1}]$ and $\pi[(2p_{1/2})(1f_{5/2})^{-1}]$ account for 60% of the strength of this level compared with 80% for the first 2+ state. These configurations are consistent with the relatively low log ft value of the first-forbidden beta transition to this level. In contrast to the first excited state, the (d,p) results suggest that there are no particle-hole states involving a $\nu[(1g_{9/2})^{-1}]$ hole included in the composition of the wave function of the 3220 keV level. Inelastic alpha-particle scattering indicates a large proton single hole strength showing agreement with the single-particle model. According to the shell model the lowest positive parity states in ^{88}Sr should correspond to the proton configurations $\pi[(2p_{1/2})(2p_{3/2})^{-1}]$ and $\pi[(2p_{1/2})(1f_{5/2})^{-1}]$. Additional 2+ states should arise from higher energy seniority 4 configurations such as $\pi[(2p_{1/2})^2(2p_{3/2})^{-2}]$ and $\pi[(2p_{1/2})^2(1f_{5/2})^{-2}]$. The (α,α') work gives a value of $B(E2)\uparrow = 0.4$ single particle units for the 3220 keV level compared to 8.5 single particle units for the 1836 keV level as determined from (e,e') reaction results. This gives a ratio $B(E2,2_2^+\rightarrow 0^+)/B(E2,2_1^+\rightarrow 0^+)$ of $\sim$ 0.05 compared to the value of zero expected for spherical vibrations. The gamma-decay branching ratio $(2_2^+\rightarrow 0)/(2_2^+\rightarrow 2_1^+)$ should be zero for a spherical vibrator as well. However the average value of this ratio as determined from the beta-decay and neutron capture data

is 0.30. This value is still much less than the value of 12.6 expected from the single particle model for E2 transitions.

The 3488 keV level is weakly populated in the beta decay of ^{88}Rb but is not populated by a primary transition from the neutron capture state. The only de-excitation mode of this level is a ground-state transition. This confirms the spin assignment of 1^+ made by Ragaini et.al.[75] as this level is populated in the (t,α) and (d,He^3) reactions. The absence of any neutron strength in this level is indicated by the fact that it is not populated in the (d,p) or (t,p) reactions. The location of 1+ levels in single-closed shell nuclei in terms of quasi-particle excitations has been calculated by Lombard[146]. He predicted a 1+ level in ^{88}Sr at about 3.3 MeV representing the $\pi[(2p_{1/2})(2p_{3/2})^{-1}]_{1+}$ configuration. This is likely the one observed at 3488 keV as will become more evident from the following discussion. Lombard[146] also predicted a 2-hole state of spin 1+ at about 3.6 MeV excitation consisting of the $\pi[(1f_{5/2})^{-1}(2p_{3/2})^{-1}(2p_{1/2})^2]$ proton configurations. However this level was not observed in the ^{88}Sr level structure via beta decay or neutron capture. The 1+ states can be classified according to transition probabilities. The ℓ selection rule forbids M1 transitions with $\Delta\ell=2$. Thus only the spin-orbit pairs ($p_{1/2}$-$p_{3/2}$, $d_{3/2}$-

$d_{5/2}$, $f_{5/2}$-$f_{7/2}$) etc. can decay directly to the ground state. The other 1+ states must proceed by cascade. The 3488 keV state does not proceed by cascade.

The 3635 keV level is similar in character to the 3488 keV level. It is not populated in the (d,p) reaction indicating an absence of neutron strength. However it is excited in the (t,α) and (d,He^3) reactions as is the 3488 keV level indicating that proton configurations comprise both states. The configuration of this state is likely $\pi[(1f_{5/2})(2p_{1/2})^{-1}]_{3+}$. The spin 3+ of this state is verified by the neutron capture gamma-ray data as this level is populated directly from the capture state by the 7477 keV transition. This then is an M1 transition. The 3635 keV level is the highest of the five low-lying proton-hole states populated in the (d,He^3) reaction as listed in Table 2-10. All five states were populated either directly or indirectly in the (n,γ) reaction whereas only the lowest 4 states were seen in the beta decay work as outlined in chapter 5. However Ragaini et.al.[34] indicated that they observed the 3635 keV level weakly populated in beta decay. All of the spin and parity assignments made to these five levels are consistent with the results of the beta-decay and (n,γ) studies as detailed in chapters 5 and 6 respectively.

The 3953 keV level has been observed only in the

neutron capture reaction on strontium. It is populated directly by the primary 7160 keV transition and de-excites via the 1218 keV transition to the 2734 keV level. It is not populated in the beta decay of ^{88}Rb. Hence a spin-parity assignment of 4+ seems probable based partly on the fact that the primary transition is weak and may be an M1 transition. This level is interpreted as the 4+ member of the two-phonon multiplet 0+, 2+, 4+ predicted for a spherical vibrator. The 2+ member is the 3220 keV level and the 0+ member is likely the 3154 keV 0+ state observed in both the (t,α) and (t,p) reactions as noted in Table 2-11. There is no indication that this 0+ member is populated in either the beta-decay process or the (n,γ) reaction. The 3953 keV level decays to the 2734 keV 3- octupole state. Any possible transition to the 1836 keV state which might have been expected for this level is obscured by the intense 2112 keV gamma-ray. The 3953 keV level is likely a strong proton state as it is not populated in the (d,p) reaction. However without additional knowledge from other reactions leading to the same final state one can only speculate on the configurations comprising this level. The proton configuration $\pi[(1f_{7/2})^{-1}(2p_{1/2})]_{4+}$ could contribute to this level although the seniority 4 states with the configurations $\pi[(1f_{5/2})^{-2}(2p_{1/2})^{2}]$ and

$\pi[(2p_{3/2})^{-2}(2p_{1/2})^{2}]$ could also be low enough in energy to contribute to this level.

The 3523 keV level is weakly populated in the neutron capture reaction although not by a primary transition. It is not observed in the beta decay of ^{88}Rb as studied here, although Lazar et.al.[55] claim to have detected a 3.52 MeV transition in the ^{88}Rb beta-decay process with a NaI(Tl) detector. Shastry and Bhattacharyya[58] found that the 3.52 MeV level is weakly populated in the decay of ^{88}Y to ^{88}Sr. As the ground state spin of ^{88}Y is 4- the spin of this state must be $\geq$ 2. As a ground state transition is observed in neutron capture work as well as in ^{88}Y decay the most likely spin assignment for this level is 2+. This spin assignment is supported by the fact that the level is excited in the (d,d') reaction[69] as well. The level cannot be a member of the $\nu[(2d_{5/2})(1g_{9/2})^{-1}]$ multiplet as it is not populated in the (d,p) reaction. The state being low in energy likely consists primarily of proton strength.

The 3584 keV level is populated strongly in the (n,γ) reaction by the primary 7528 keV E1 gamma-ray transition giving it a negative parity assignment. It is only weakly populated in the (d,p) reaction with no stripping distribution evident. As the level is not populated in the beta-decay process its spin must be $\geq$ 4. This leaves the only spin-parity assignments possible as 4- or 5-. No

selection can be made between these two spin assignments as the level decays only via the 850 keV transition to the 2734 keV 3- level. The state is likely a member of the same proton multiplet $\pi[(2p_{3/2})^{-1}(1g_{9/2})]$ as the 2734 keV state with possible contributions from the $\pi[(1f_{5/2})^{-1}(1g_{9/2})]$ proton configuration. Then the 850 keV transition is basically a single-particle transition between the single-particle orbitals.

Below 4 MeV excitation energy, levels were populated with even parity resulting from the proton particle-hole coupling configurations $\pi[(2p_{3/2})^{-1}(2p_{1/2})]_{1+,2+}$ and $\pi[(1f_{5/2})^{-1}(2p_{1/2})]_{2+,3+}$ at slightly higher energies. A few levels also had some neutron strength due to the configuration $\nu[(1g_{9/2})^{-1}(2d_{5/2})]_{2+\to7+}$. Collective one phonon and two phonon quadrupole vibrations with spins 2+ and 0+, 2+ and 4+ respectively were also found. Above 4 MeV one could expect to populate some higher seniority positive parity states but levels of odd parity are also expected due to the excitation of the $2p_{3/2}$ or $1f_{5/2}$ protons into the $1g_{9/2}$ proton orbital. The resulting coupling could result in levels in the spin range 2- → 7-. Of these only those with spins of 3-, 4-, 5- or 6- can be populated by primary E1 transitions from the capture state.

The two energy levels at 4170 and 4227 keV are

populated by intense primary transitions whereas the level at 4269 keV is populated by a weaker gamma-ray transition from the capture state. Thus these levels are likely to have one of the spins 3-, 4-, 5- or 6-. Of these levels the only one populated in beta decay is the 4269 keV level. The beta transition to this level has a log ft value of 6.7 probably indicating an allowed transition giving the level a 3- spin assignment. However a first-forbidden transition cannot be ruled out which would indicate a 3+ spin assignment for this level. This is still consistent with the weak primary transition observed. The level could then be interpreted as arising from the proton configurations of seniority 4, $\pi[(1f_{5/2})^{-2}(2p_{1/2})^{2}]$ and $\pi[(2p_{3/2})^{-2}(2p_{1/2})^{2}]$ as discussed above. The spin assignment of the 4227 keV level is probably 3- despite the fact that it is not populated in beta decay. This assignment is based on the decay modes of this level and on the fact that a 3- level at 4234 keV has been populated in the inelastic proton scattering reaction[140]. The spin assignment of the 4170 keV level is made as 4- or 5- based on the decay modes of this level although the 4- assignment is favoured based on a weak gamma-ray transition to the 2+ 1836 keV state.

The spin and parity of the 4300 keV level is probably 4+ as suggested by (p,p') work[140]. This is consistent with

its population and decay modes as observed in the (n,γ) reaction. It is populated by a weak 6812 keV M1 primary transition and decays via the 1566 keV transition to the 3- 2734 keV level. No evidence is seen for a transition to the 1836 keV 2+ state although the response of such a transition may be obscured by the 1442 keV photo-peak. This level is not populated in the beta-decay process supporting the 4+ spin assignment of the state.

The next four energy levels at 4414, 4452, 4514 and 4743 keV are populated in the (n,γ) reaction although only two of the levels are populated by primary transitions. All levels but the 4452 keV level were populated in the beta-decay process as well. Apparently levels at nearly the same energies were populated in the (d,p) reaction as well with all proton groups showing ℓ_n=2 stripping distributions. These levels have been assigned to the $\nu[(1g_{9/2})^{-1}(2d_{5/2})]$ multiplet by Cosman et.al.[74]. However the low log ft value of the beta transitions to the 4414, 4514 and 4743 keV levels indicate that these may be allowed transitions making the parities of these three levels odd. The 4414 keV level is populated directly by a primary transition. If this is the same level as seen in the (d,p) reaction then its spin must be 3+. On the other hand the 4514 keV level is not populated by a primary transition from the capture state and the low log ft value of 4.9 indicates an allowed beta transition with

a likely spin assignment of 2- or 3-. The 2- spin assignment is to be favoured since there is no primary transition from the capture state. This then cannot be the same state as observed in the (d,p) reaction. Assuming the 4743 keV state is the same one as observed in the (d,p) reaction the spin assignment is likely 2+. The gamma-ray transition to the ground state implies a close correlation with the ground state configuration. The 4452 keV level is very unlikely the same one as seen in the (d,p) reaction as it is populated directly by a strong primary transition in the (n,γ) reaction. The ℓ_n value of the 4450 keV level populated in the (d,p) reaction could have been misinterpreted because of the small reduced width of this level. The decay modes of the level favour a 3- or 4- assignment and the absence of any beta transition to this level makes a 4- assignment more likely. The strong 1718 keV gamma-ray transition to the 3- 2734 keV level indicates a similarity between the proton configurations making up the two levels.

The level at 4846 keV is not excited in the (d,p) reaction and thus has no significant neutron configuration contribution. The level can be given an unambiguous spin-parity assignment of 3- on the basis that it is strongly populated both in the (n,γ) reaction and in the beta-decay process. In both cases the same decay modes are detected

and are consistent with the spin assignment of 3-. The level consists of strong proton configurations some of which likely include the $\pi[(2p_{3/2})^{-1}(2d_{5/2})]$ and $\pi[(1f_{5/2})^{-1}(2d_{5/2})]$ configurations as these are higher in energy than the $\pi[(2p_{3/2})^{-1}(1g_{9/2})]$ and $\pi[(1f_{5/2})^{-1}(1g_{9/2})]$ states comprising the strong 2734 and 3584 keV levels. Ragaini et.al.[75] found some evidence that the 4845 keV level is populated by the (t,p) reaction indicating some contribution from the neutron states.

There was no indication however of excitation of the 4854 keV level by the (t,p) or the (d,p) reaction indicating the absence of neutron configuration states. This level was seen only in the beta-decay process populated by a beta transition with a low log ft value indicating a negative parity state. The weak ground state transition implies a probable spin assignment of 2-. The level likely consists of some of the same proton quasi-particle states comprising the 4846 keV level.

Above 5 MeV excitation energy no levels are populated in the beta-decay process and only a few of those populated in the (n,γ) reaction are also populated by the (d,p) reaction. Very little data are available from other reactions to these final states so that any unambiguous spin assignments are almost impossible on the basis of (n,γ) results alone. In most cases only limits can be placed on the spin

values by a study of the decay modes of the levels. Above 5 MeV there is also expected to be more contribution from neutron states so that the levels will not be comprised mainly of proton particle-hole states but will likely contain significant contributions from higher seniority states of mixed proton and neutron character. Some of the lowest excited states of this type are expected to be comprised of

$$\pi[(1f_{5/2})^{-1}(1g_{9/2})]\nu[(1g_{9/2})^{-1}(2d_{5/2})],$$
$$\pi[(2p_{3/2})^{-1}(2p_{1/2})]\nu[(2p_{1/2})^{-1}(2d_{5/2})],$$
$$\pi[(2p_{3/2})^{-1}(1g_{9/2})]\nu[(1g_{9/2})^{-1}(2d_{5/2})]$$
and $$\pi[(1f_{5/2})^{-1}(2p_{1/2})]\nu[(2p_{1/2})^{-1}(2d_{5/2})]$$

configurations for the odd parity states and

$$\pi[(1f_{5/2})^{-1}(1g_{9/2})]\nu[(2p_{1/2})^{-1}(2d_{5/2})],$$
$$\pi[(2p_{3/2})^{-1}(2p_{1/2})]\nu[(1g_{9/2})^{-1}(2d_{5/2})],$$
$$\pi[(2p_{3/2})^{-1}(1g_{9/2})]\nu[(2p_{1/2})^{-1}(2d_{5/2})]$$
and $$\pi[(1f_{5/2})^{-1}(2p_{1/2})]\nu[(1g_{9/2})^{-1}(2d_{5/2})]$$

configurations for the even parity states. These are 4 quasi-particle configuration states and hence of seniority 4. There will also be some lower seniority states comprised of the neutron configurations $\nu[(3s_{1/2})(1g_{9/2})^{-1}]$ and $\nu[(2d_{3/2})(1g_{9/2})^{-1}]$ as suggested by the (d,p) results excited above 5 MeV. Proton stripping reactions such as (d,He^3) are required to pick out the proton states but it is expected that very few 2 quasi-

particle proton states would be excited above 5 MeV. Some 4 quasi-particle proton states may be populated above 5 MeV excitation energy. These would consist of the

$$\pi[(2p_{3/2})^{-2}(2p_{1/2})^{2}]$$

and

$$\pi[(1f_{5/2})^{-2}(2p_{1/2})^{2}]$$

configurations for even parity states and of the

$$\pi[(2p_{3/2})^{-2}(1g_{9/2})^{2}]$$

and

$$\pi[(1f_{5/2})^{-2}(1g_{9/2})^{2}]$$

configurations for odd parity states.

Although definite spin-parity assignments cannot be made to the levels above 5 MeV populated in the (n,γ) reaction, restrictions can be made on some of the possible assignments for the levels populated most strongly. These assignments are listed in Table 7-4 and will be discussed below. The 5537 keV level is weakly populated by a primary transition and decays only to the first two excited 2+ states. thus it is likely a higher phonon vibrational state having spin 3+ or 4+. However a 3- spin assignment cannot be ruled out. The 5426 and 5518 keV levels are likely similar in character to the 5537 keV level. Both are populated by primary transitions from the capture state and both correspond to levels populated in the (d,p) reaction with the proton groups exhibiting distributions characteristic of $\ell_n=0$ transitions. Thus spin assignments of 4+ or 5+ are possible for these levels. The 5426 keV level has decay modes to a 2+ and a 4+ level as well as to the strong 4452 keV level.

This favors a 4+ assignment for the level. The 5518 keV level decays to the 3220 keV 2+ level as well as to the strong negative parity levels at 2734 keV and 3584 keV. Again a spin assignment of 4+ is favoured for this level. However if this is not the level seen in the (d,p) reaction a spin assignment of 3- or 4- is quite probable based on the strong connections of this level to the 2734 and 3584 keV levels.

The 5690 keV level must be entirely different in character from the three levels discussed above as it is populated by a fairly strong primary transition and decays only via the 2203 keV transition to the 3488 keV 1+ level. This indicates that this level is likely a 3- spin state comprised perhaps of 4 quasi-particle proton configurations. The level directly below this one and another one at 6258 keV are notable in that they correspond closely in energy to the only two ℓ_n=1 states populated in the (d,p) reaction. This of course makes their parities negative. As the 5662 keV level has three decay modes all to 2+ spin levels the likely spin of this state is 3-. The 6258 keV level has only one decay mode and that is to the 5321 keV level. Thus no restrictions can be made on the possible spin of this state.

The 5011, 5321, 5751 and 5952 keV levels are all populated by fairly strong primary transitions and none of the levels are excited in the (d,p) reaction. The levels can all be considered to have negative parity. It is interesting to look at the decay modes of these levels as they are all similar. Table 7-5 lists the decay modes of the ten strongest negative parity levels in ^{88}Sr including six levels below 5 MeV excitation energy. The three highest energy levels all have a decay mode to the strong 3584 keV level whereas the 5011 keV level de-excites mainly via a strong gamma-ray transition to the 2734 keV 3- state. This indicates the similarity between the configurations making up these four levels. However the decay modes are not restrictive enough to make a choice between the 3-, 4- or 5- spin assignments to the four levels. Whereas the three levels above 5100 keV all have a decay mode to the 3584 keV level, all six levels below 5100 keV down to the 3584 keV level have a decay mode to the 2734 keV level. This suggests a basic difference between the configurations making up the upper three levels and those making up the lower six levels. As suggested above the lower levels can be interpreted as 2 quasi-particle states whereas those above 5100 keV can be interpreted as 4 quasi-particle states.

TABLE 7-5

Strong Decay Modes in $^{87}Sr(n,\gamma)^{88}Sr$ Decay Scheme

From Level (keV)	To Level (keV)
5952	5518
	3584
5751	3584
5321	4170
	3584
5011	3953
	2734
4846	2734
	1836
4452	3584
	2734
	1836
4227	2734
	1836
4170	3584
	2734
	1836
3584	2734
2734	1836
	0

REFERENCES

(1) W. Pauli, Noyaux Atomique, Proc. of the Solvay Congress, Brussels (1933).

(2) E. Fermi, Physik 88, 161 (1934).

(3) M. A. Preston, Chap. 15, Physics of the Nucleus, Addison Wesley Pub. Co., Reading, Massachusetts (1962).

(4) E. Segre, Nuclei and Particles, W. A. Benjamin,Inc., New York (1964).

(5) Fay Ajzenberg-Selove, Nuclear Spectroscopy, Part B, Academic Press, New York and London (1955).

(6) E. Feenberg, Shell Theory of the Nucleus, Princeton University Press (1955).

(7) L. A. Sliv and I. M. Band, Appendix 5, Alpha-, Beta- and Gamma-Ray Spectroscopy, Vol. 2 (K. Seigbahn, editor), North-Holland Publishing Company, Amsterdam (1966).

(8) J. M. Blatt and V.F. Weisskopf, Theoretical Nuclear Physics, John Wiley and Sons, New York (1952).

(9) Ibid. 7, Chap. 10.

(10) Ibid. 5, Chap. 12.

(11) K. A. Brueckner, Phys. Rev. 96, 508 (1954).

(12) A. Bohr and B. R. Mottelson, Mat. F. Medd. 27, 16 (1953).

(13) M. Mayer, Phys. Rev. 75, 1969 (1949).

(14) Ibid. 3, pg. 150, Chap. 7.

(15) K. W. Ford, Phys. Rev. 98, 1516 (1955).

(16) J. Bardeen, L. N. Cooper and R. Schrieffer, Phys. Rev. 108, 1175 (1957).

(17) A. Bohr, B. R. Mottelson and D. Pines, Phys. Rev. 110, 936 (1958).

(18) N. N. Bogoliubov, JETP 7, 41 (1958).

(19) B. L.Cohen and R. E. Price, Phys. Rev. 121, 1441 (1961).

(20) L. S. Kisslinger and R. A. Sorensen, Mat. F. Medd. 32, No. 9 (1960).

(21) L. S. Kisslinger and R. A. Sorensen, Rev. Mod. Phys. 35, 853 (1963).

(22) S. G. Nilsson, Mat. F. Medd. 29, No. 16 (1955).

(23) G. A. Bartholomew, Nuclear Spectroscopy, Part A, p.304, F. Ajzenberg-Selove (editor), Academic Press, New York (1960).

(24) A. Saplakoglu, L. M. Bollinger and R. E. Cote, Phys. Rev. 109, 1258 (1958).

(25) C. K. Bockelman, Nucl. Phys. 13, 205 (1959).

(26) A. M. Lane and J. E. Lynn, Nucl. Phys. 17, 563 (1960).

(27) A. M. Lane and J. E. Lynn, Nucl. Phys. 17, 586 (1960).

(28) G. A. Bartholomew, Ann. Rev. Nucl. Sci. 11, 259 (1961).

(29) C. E. Porter and R.G. Thomas, Phys. Rev. 104, 483 (1956).

(30) Nuclear Data Sheets (A=87 and A=88), National Research Council, Washington 25, D.C.

(31) C. M. Lederer, J. M. Hollander and I. Perlman, Table of Isotopes, Sixth Edition (John Wiley and Sons, Inc. 1967).

(32) W. B. Clarke and H. G. Thode, Can. J. Phys. 42, 213 (1964).

(33) G. A. Brinkman, A.H.W. Aten, Jr. and J. Th. Veenboer, Physica 31, 1305 (1965).

(34) R. C. Ragaini and J. D. Knight, Nucl. Phys. A125, 97 (1969).

(35) M. Bormann, E. Fretwurst, P. Schehka, G. Wrege, H. Büttner, A. Lindner and H. Meldner, Nucl. Phys. 63, 438 (1965).

(36) B.B. Kinsey and G. A. Bartholomew, Can. J. Phys. 31, 1051 (1953).

(37) L. T. Aldrich, L. F. Herzog, W. K. Holyk, F. B.Whiting and L. H. Ahrens, Phys. Rev. 89, 631 (1953).

(38) D. T. Goldman, Chart of the Nuclides, General Electric Co., Schenectady, N.Y. (1964,1965).

(39) Landolt-Börnstein, Group 1, Volume 1, Berlin-Göttingen-Heidelberg: Springer (1961).

(40) R. E. Sass, B. Rosner and E. J. Schneid, Phys. Rev. 138, B399 (1965).

(41) S.Millman and M. Fox, Phys. Rev. 50, 220 (1936).

(42) I. Lindgren, Table of Nuclear Spins and Moments, in Alpha-, Beta- and Gamma-Ray Spectroscopy, Appendix 4, Editor K. Siegbahn, Academic Press, New York (1966).

(43) P. A. VandenBout, A. Dymanus, V. J. Ehlers, M. H. Prior and H. A. Shugart, Phys. Rev. 166, 1131 (1968).

(44) S. Thulin, Arkiv Fysik 4, 363 (1962).

(45) S. Thulin, Phys. Rev. 87, 684 (1952).

(46) S. Thulin, Arkiv Fysik 9, 137 (1955).

(47) G. Holm, Arkiv Fysik 34, 433 (1968).

(48) S. Thulin, I. Moreau and H. Atterling, Arkiv Fysik 20, 41 (1961).

(49) D. G. Alkhazov, V. D. Vasil'ev, G. M. Gusinskii, I. Kh. Lemberg and V. A. Nabichvrishvili, Bull. Acad. Sci. USSR, Phys. Ser. 28, 1575 (1965).

(50) G. B. Beard and W.H. Kelly, Nucl. Phys. 28, 570 (1961).

(51) L. G. Mann and P. Axel, Phys. Rev. 84, 221 (1951).

(52) M. E. Bunker, L. M. Langer and R.J.D. Moffat, Phys. Rev. 81, 30 (1951).

(53) R. Steffen, Phys. Rev. 91, 443 (1953).

(54) J. Varma, B. L. Saraf and W. B. Todd,Jr., Phys. Rev. 91, 484 (1953).

(55) N. H. Lazar, E. Eichler and G. D. O'Kelley, Phys. Rev. 101, 727 (1956).

(56) J. L. Irigaray, G. Y. Petit, P. Carlos, B. Maier, R. Samama and H. Nifenecker, Nucl. Phys. A113, 134 (1968).

(57) N. C. Rasmussen, Y. Hakai, T. Inouye and V. J. Orphan, MIT NE-85 (1967).

(58) S. Shastry and R. Bhattacharyya, Nucl. Phys. 55, 397 (1964).

(59) BNL-325.

(60) H. Schmidt, W. Michaelis, C. Weitkamp and G. Markus, Z. Physik 194, 373 (1966).

(61) T. Inouye and N. C. Rasmussen, Trans. of the ANS 10, No. 1 (1967).

(62) S. Micheletti and J.B. Mead, Nucl. Phys. 37, 201 (1962).

(63) J. E. Kitching (Oxford, London, private communication).

(64) J. Morton and W. Darcey (private communication).

(65) A. L. Androsenko and D.L. Broder, Atomnaya Energ 7, 268 (1959).

(66) S. M. Shafroth, R. W. Jackiw and D. H. Van Patter, Bull. Am. Phys. Soc. 5, 409 (1960).

(67) D. K. McDaniels, J. S. Blair, S.W. Chen and G. W. Farwell, Nucl. Phys. 17, 614 (1960).

(68) J. Alster, D. C.Shreve and R. J. Peterson, Phys. Rev. 144, 999 (1966).

(69) E. W.Hamburger, Nucl. Phys. 39, 139 (1962).

(70) M. M. Stautberg, J. J. Kraushaar and B. W. Ridley, Phys. Rev. 157, 977 (1967).

(71) G. A. Peterson and Jonas Alster, Phys. Rev. 166,1136 (1968).

(72) C. D. Kavaloski, J. S. Lilley, D. C. Shreve and N. Stein, Phys. Rev. 161, 1107 (1967).

(73) D. C. Williams, J. D.Knight and W. T. Leland, Los Alamos Scientific Laboratory, private communication (1968).

(74) E. R. Cosman and D. C. Slater, Phys. Rev. 172, 1126 (1968).

(75) R. C. Ragaini, J. D. Knight and W. T. Leland (private communication).

(76) O. Hahn and F. Strassman, Naturwiss 27, 11 (1939).

(77) O. Hahn and F. Strassman, Naturwiss 27, 89 (1939).

(78) H. L. Anderson, E. Fermi and A. V. Grosse, Phys. Rev. 59, 52 (1941).

(79) A. C.Wahl, Paper No. SM-60/22, IAEA Symposium on Physics and Chemistry of Fission, Salzburg, Austria (1965).

(80) A. C. Wahl and N. A. Bonner, Radioactivity Applied to Chemistry, Chap. 9, John Wiley, New York (1951).

(81) N. P. Archer, Ph.D. Thesis, McMaster University (1965).

(82) R. C.Koch and G. L. Grandy, Nucleonics 18, 76 (1960).

(83) D. W. Ockenden and R. H. Tomlinson, Can. J. Chem. 40, 1594 (1962).

(84) N. P. Archer and G. L. Keech, Can. J. Phys. 44, 1823 (1966).

(85) W. Heitler, The Quantum Theory of Radiation, Chap. 3, O.U.P. London (1944).

(86) O. Klein and Y. Nishina, Z. Physik 52, 853 (1929).

(87) G. Dearnaley and D. C. Northrop, Semi-conductor Counters for Nuclear Radiations, Chap. 1, E. and F. Spon Limited, London(1963).

(88) D. Engelkemeir, Rev. Sci. Inst. 27, 589 (1956).

(89) Ibid 81, Appendix II.

(90) E. Fairstein, Rev. Sci. Inst. 27, 475 (1956).

(91) H. J. Fiedler, L.B. Hughes, T. J. Kennett, W.V. Prestwich and B.J. Wall, Nucl. Inst. and Meth. 40, 229 (1966).

(92) R. B. Day, G. Dearnaley and J. M. Palms, IEEE Trans. Nucl. Sci. NS-14, 487 (1967).

(93) M. G. Strauss, R. N. Larsen and L. L. Sifter, IEEE Trans. Nucl. Sci. NS-13, 265 (1966).

(94) V. Fano, Phys. Rev. 72, 26 (1947).

(95) H. M. Mann, Bull. Am. Phys. Soc. 11, 127 (1966).

(96) J. P. Hurley, J. M. Mathiesen and V. L. Dagragnano, Nucl. Inst. and Meth. 57, 109 (1967).

(97) A. B. Gillespie, Noise and Resolution in Nuclear Counter Amplifiers, Chap. 4, Pergamon Press, London (1953).

(98) R. L. Chase, Rev. Sci. Inst. 31, 945 (1960).

(99) E. Fairstein, T. A. Love and R. W. Peele, Proc. Sixth Tripartite Inst. Conf., Chalk River, AECL-804, 117 (1959).

(100) D.H. Wilkinson, Proc. Cambridge Phil. Soc. 46, 508 (1950).

(101) W. V. Prestwich, L. B.Hughes, T. J. Kennett and H. J. Fiedler,Phys. Rev. 43, 2086 (1965).

(102) D.D. Slavinskas, T.J. Kennett and W. V. Prestwich, Nucl. Inst. and Meth. 41, 341 (1966).

(103) A. Luukko and P. Holmberg, Nucl.Inst. and Meth. 65, 121 (1968).

(104) H. Lycklama, L. B. Hughes and T.J. Kennett, Can. J. Phys. 45, 1871 (1967).

(105) R. Gunnink , R. A. Meyer, J. B. Niday and R.P. Anderson, Nucl. Inst. and Meth. 65, 26 (1968).

(106) D. D. Slavinskas, private communication (1969).

(107) H. Lycklama and T. J. Kennett, Nucl. Inst. and Meth. 59, 56 (1968).

(108) E. N. Hatch and F. Boehm, Z. Physik 155, 609 (1959).

(109) B. Anderson, Proc. Phys. Soc. 69A, 415 (1956).

(110) C.J. Herrlander and R. L. Graham, Nucl. Phys. 58, 544 (1964).

(111) E. R.Cohen and J.W.M. DuMond, Rev. Mod. Phys. 37, 537 (1965).

(112) R. L. Graham, G. T. Ewan and J.S. Geiger, Nucl. Inst. and Meth. 9, 245 (1960).

(113) G. Murray, R. L. Graham and J. S. Geiger, Nucl. Phys. 63, 353 (1965).

(114) W. W. Black and R. L.Heath, Nucl. Phys. A90, 650 (1967).

(115) R. L. Robinson, P.H. Stelson, F. K. McGowan, J.L.C. Ford, Jr. and W. T. Milner, Nucl. Phys. 74, 281 (1965).

(116) D.H. White and D. J. Groves, Nucl. Phys. A91, 453 (1967).

(117) W. V. Prestwich, T.J. Kennett, L.B.Hughes and H. J. Fiedler, Can. J. Phys. 43, 2086 (1965).

(118) N. P. Archer, W.V. Prestwich and G. L. Keech, Nucl. Inst. and Meth. 44, 114 (1966).

(119) D. C.Hall and R. G. Albridge, Nucl. Phys. A91, 495 (1967).

(120) T. Yamazaki and J. M. Hollander, Nucl. Phys. 84, 505 (1966).

(121) J. M. Hamilton, S. R. Amtey, B. van Nooijen, A. V. Ramayya and J. J. Pinajian, Phys. Lett. 19, 682 (1966).

(122) D. C. Camp, L. M. Langer and D. R. Smith, Phys. Rev. 123, 241 (1961).

(123) J. I. Rhode, O. E. Johnson and W. G. Smith, Phys. Rev. 129, 815 (1963).

(124) T.J. Kennett, N. P. Archer and L. B.Hughes, Nucl. Phys. A96, 658 (1967).

(125) Nuclear Data Sheets (Natl. Acad. Sci. National Research Council Publ. Washington, D.C.).

(126) M. S. Freedman, T. B. Novey, F. T. Porter and F. Wagner, Jr., Rev. Sci. Inst. 27, 716 (1956).

(127) D. D. Slavinskas, T.J. Kennett and W. V.Prestwich, Nucl. Inst. and Meth. 37, 36 (1965).

(128) Ibid. 31, Appendix IV.

(129) B. Hammermesh, J. E. Monahan and R. K. Smither, Ann. Phys. 13, 284 (1961).

(130) L. V.Johnson, L. B. Hughes, T. J. Kennett and W. V. Prestwich, Nucl. Phys. 84, 113 (1966).

(131) O. I. Sumbaev, V. L. Alekseev, D. M. Kaminker, A. I. Smirnov and V. A. Shaburov, Akad. Nauk. SSSR. Bull. Phys. Ser. 29, 741 (1965).

(132) L. V. Johnson, Ph.D. Thesis, McMaster University (1969).

(133) R. G. Helmer and A. Bäcklin, Nucl. Inst. and Meth. 65, 31 (1968).

(134) J. E. Kitching and M. W. Johns, Can. J. Phys. 44, 2661 (1966).

(135) S.Y. Ambiye and R. P. Sharma, Nucl. Phys. 29, 657 (1962).

(136) Ibid. 3, p. 438.

(137) H. Lycklama, private communication (1968)

(138) W. V. Prestwich, R. E. Cote and G. E.Thomas, Phys. Rev. 161, 1080 (1967).

(139) H. Lycklama and T. J. Kennett, Can. J. Phys. 45, 3039 (1967).

(140) J. Picard, O. Beer, A. El Behay, P. Lopato, Y. Terrien, G. Vallois and R. Schaeffer, Nucl. Phys. A128, 481 (1969).

(141) J. E. Kitching and M. W. Johns, Nucl. Phys. A98, 337 (1967).

(142) R. H. Goodman, J. E. Kitching and M. W. Johns, Nucl. Phys. 54, 1 (1964).

(143) J. Mason (private communication 1969).

(144) H. Lycklama, T. J. Kennett and L. B. Hughes, Can. J. Phys. 47, 665 (1969).

(145) S. Shastry and A.K. Saha, Nucl. Phys. A97, 567 (1967).

(146) R. J. Lombard, Phys. Rev. Lett. 21, 102 (1968).

APPENDIX A

DCYSCH Program Block Diagram

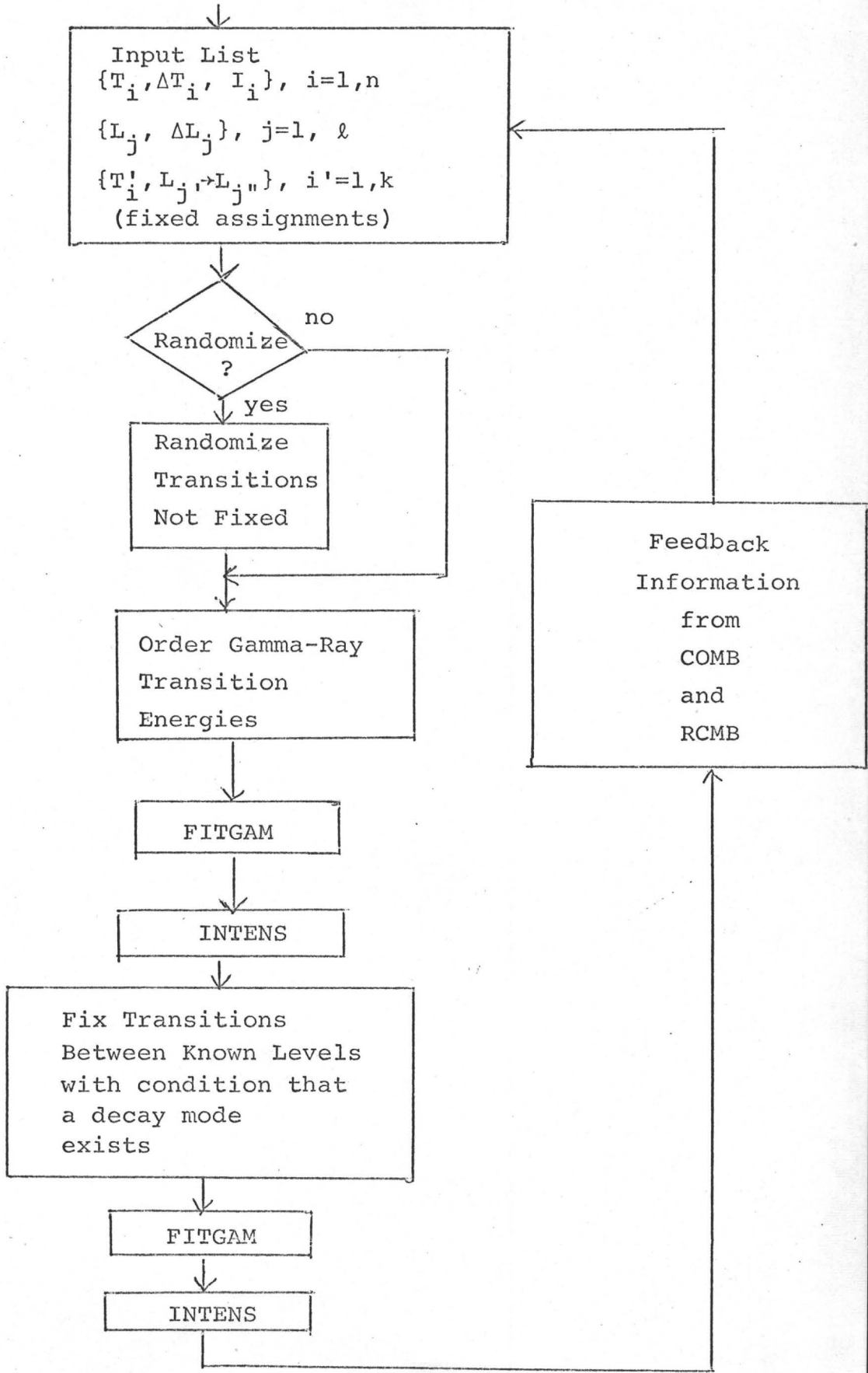

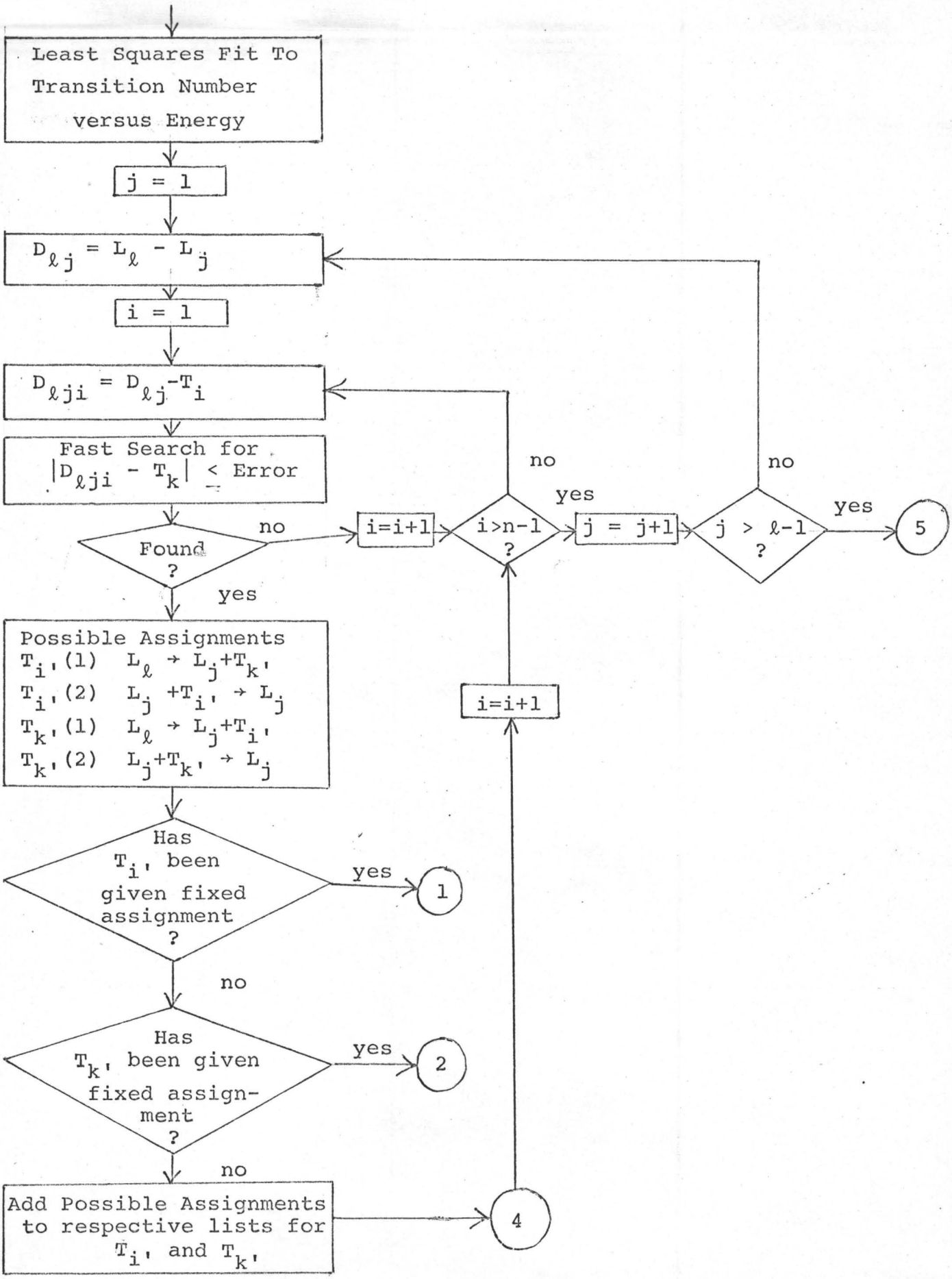
Least Squares Fit To Transition Number versus Energy
j = 1
$D_{\ell j} = L_\ell - L_j$
i = 1
$D_{\ell ji} = D_{\ell j} - T_i$
Fast Search for $|D_{\ell ji} - T_k| \leq$ Error
Found ?
no
yes
i=i+1
i>n-1 ?
no
yes
j = j+1
j > ℓ-1 ?
no
yes
5
Possible Assignments
T_i,(1) $L_\ell \rightarrow L_j + T_k$,
T_i,(2) $L_j + T_i$, $\rightarrow L_j$
T_k,(1) $L_\ell \rightarrow L_j + T_i$,
T_k,(2) $L_j + T_k$, $\rightarrow L_j$
Has T_i, been given fixed assignment ?
yes
1
no
Has T_k, been given fixed assign-ment ?
yes
2
no
Add Possible Assignments to respective lists for T_i, and T_k,
4
i=i+1

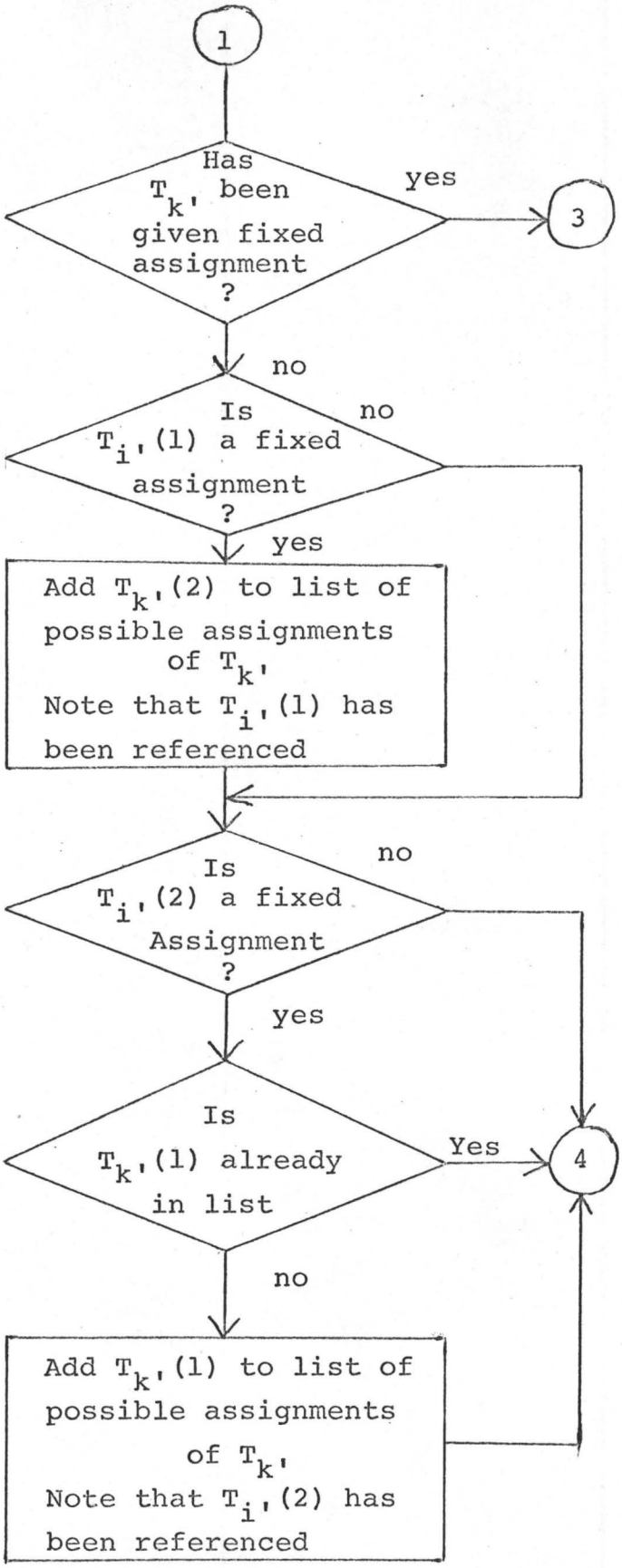
1
Has $T_{k'}$ been given fixed assignment ?
yes
3
no
Is $T_{i'}(1)$ a fixed assignment ?
no
yes
Add $T_{k'}(2)$ to list of possible assignments of $T_{k'}$ Note that $T_{i'}(1)$ has been referenced
Is $T_{i'}(2)$ a fixed Assignment ?
no
yes
Is $T_{k'}(1)$ already in list
Yes
4
no
Add $T_{k'}(1)$ to list of possible assignments of $T_{k'}$ Note that $T_{i'}(2)$ has been referenced

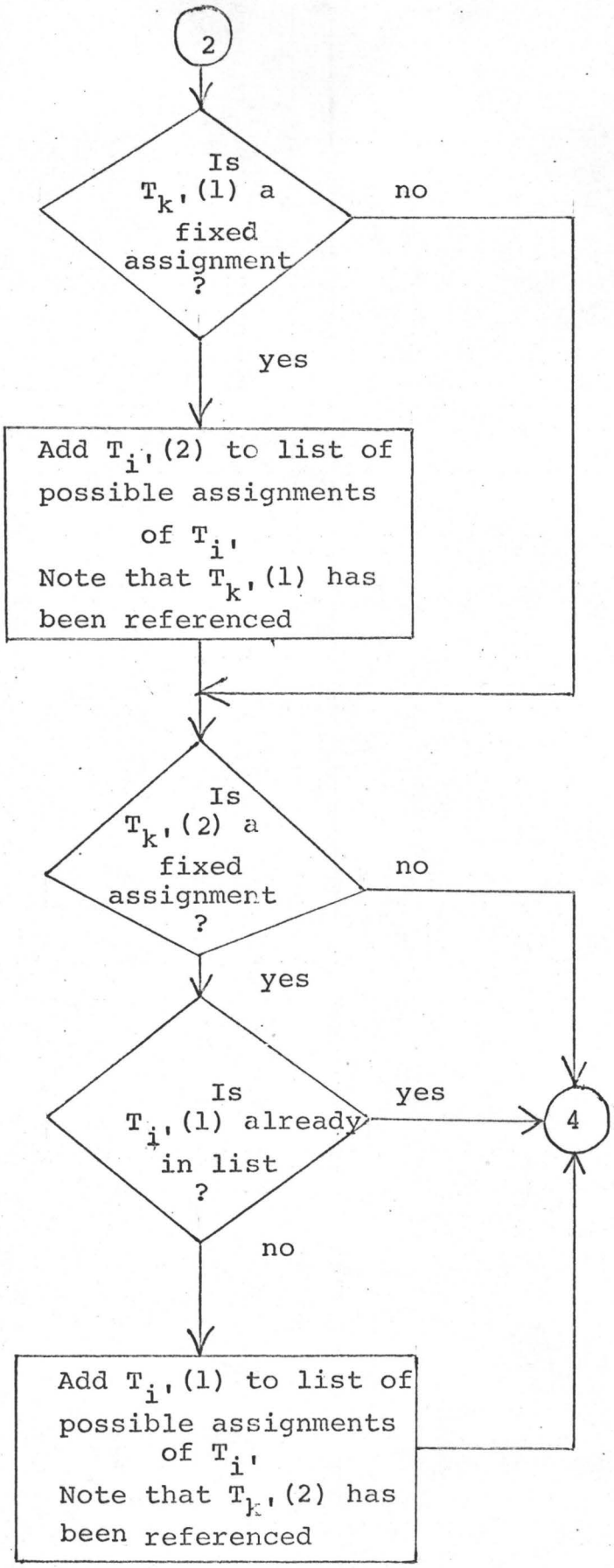
2
Is T_k,(1) a fixed assignment ?
no
yes
Add T_i,(2) to list of possible assignments of T_i, Note that T_k,(1) has been referenced
Is T_k,(2) a fixed assignment ?
no
yes
Is T_i,(1) already in list ?
yes
4
no
Add T_i,(1) to list of possible assignments of T_i, Note that T_k,(2) has been referenced

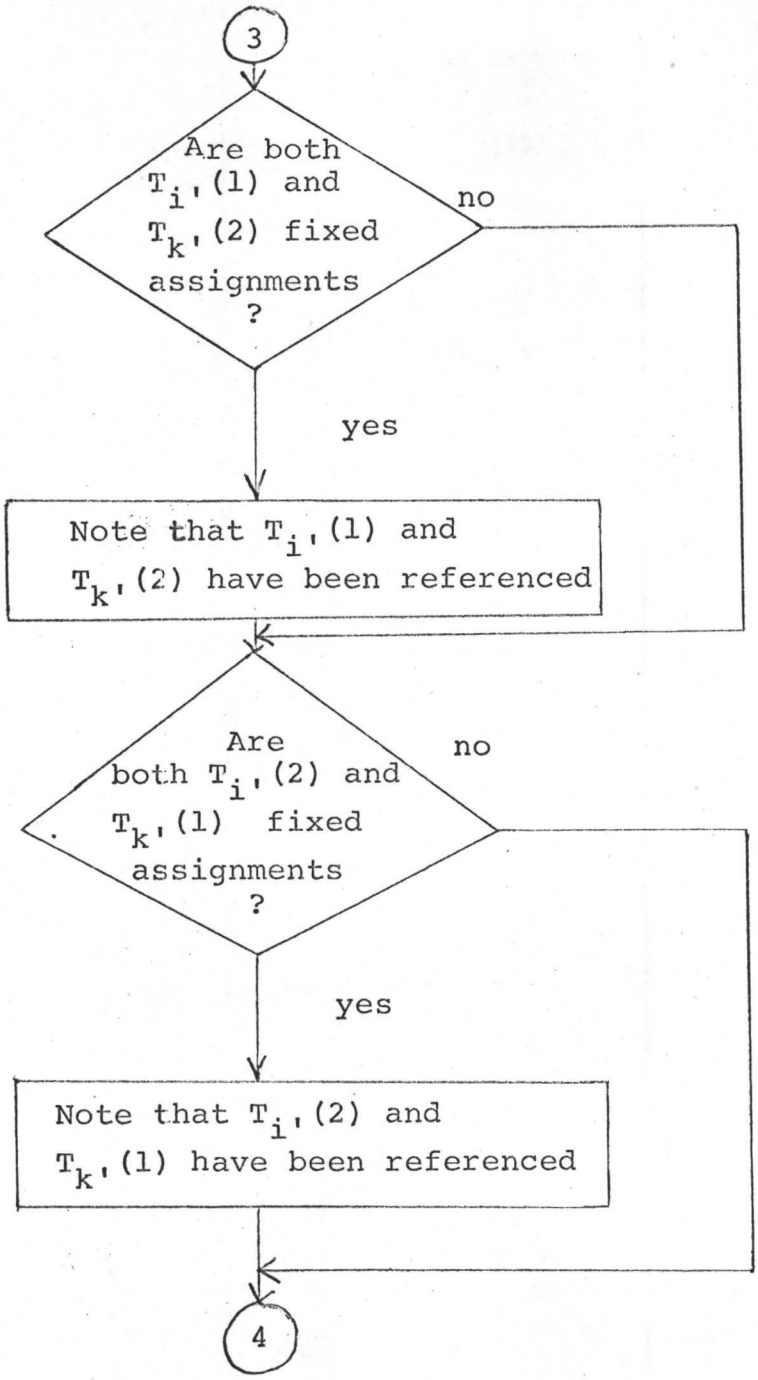
3
Are both T_i,(1) and T_k,(2) fixed assignments ?
no
yes
Note that T_i,(1) and T_k,(2) have been referenced
Are both T_i,(2) and T_k,(1) fixed assignments ?
no
yes
Note that T_i,(2) and T_k,(1) have been referenced
4

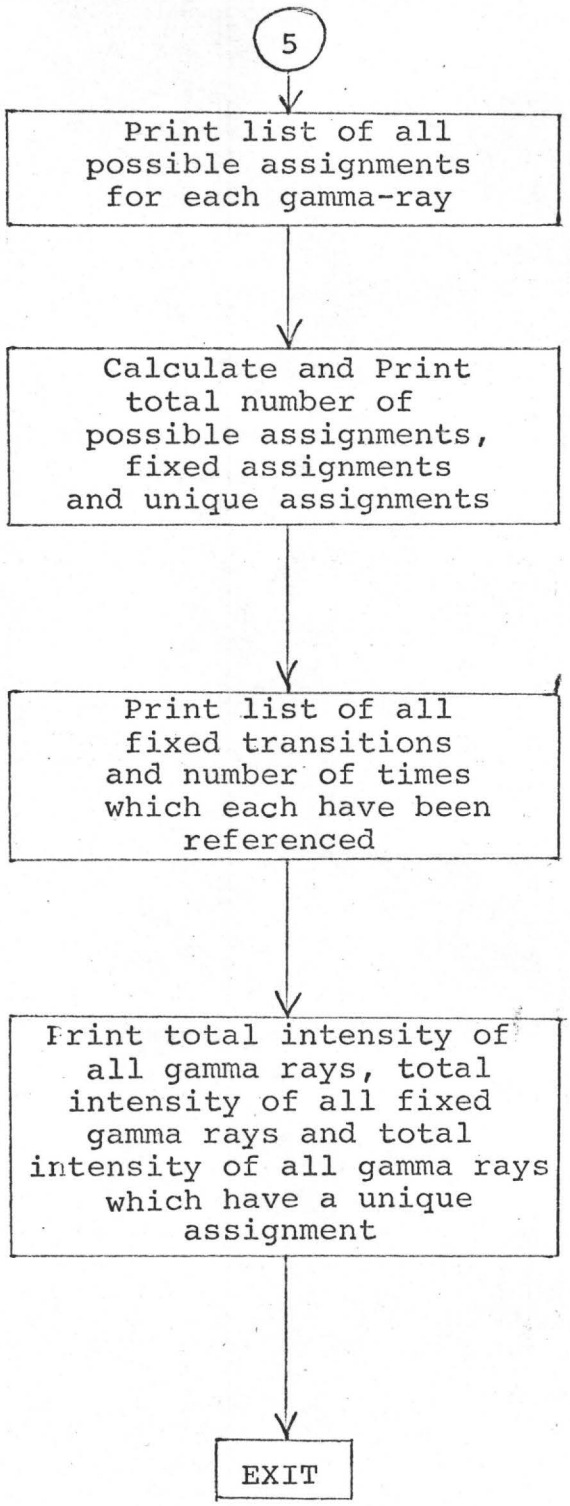
5
Print list of all possible assignments for each gamma-ray
Calculate and Print total number of possible assignments, fixed assignments and unique assignments
Print list of all fixed transitions and number of times which each have been referenced
Print total intensity of all gamma rays, total intensity of all fixed gamma rays and total intensity of all gamma rays which have a unique assignment
EXIT

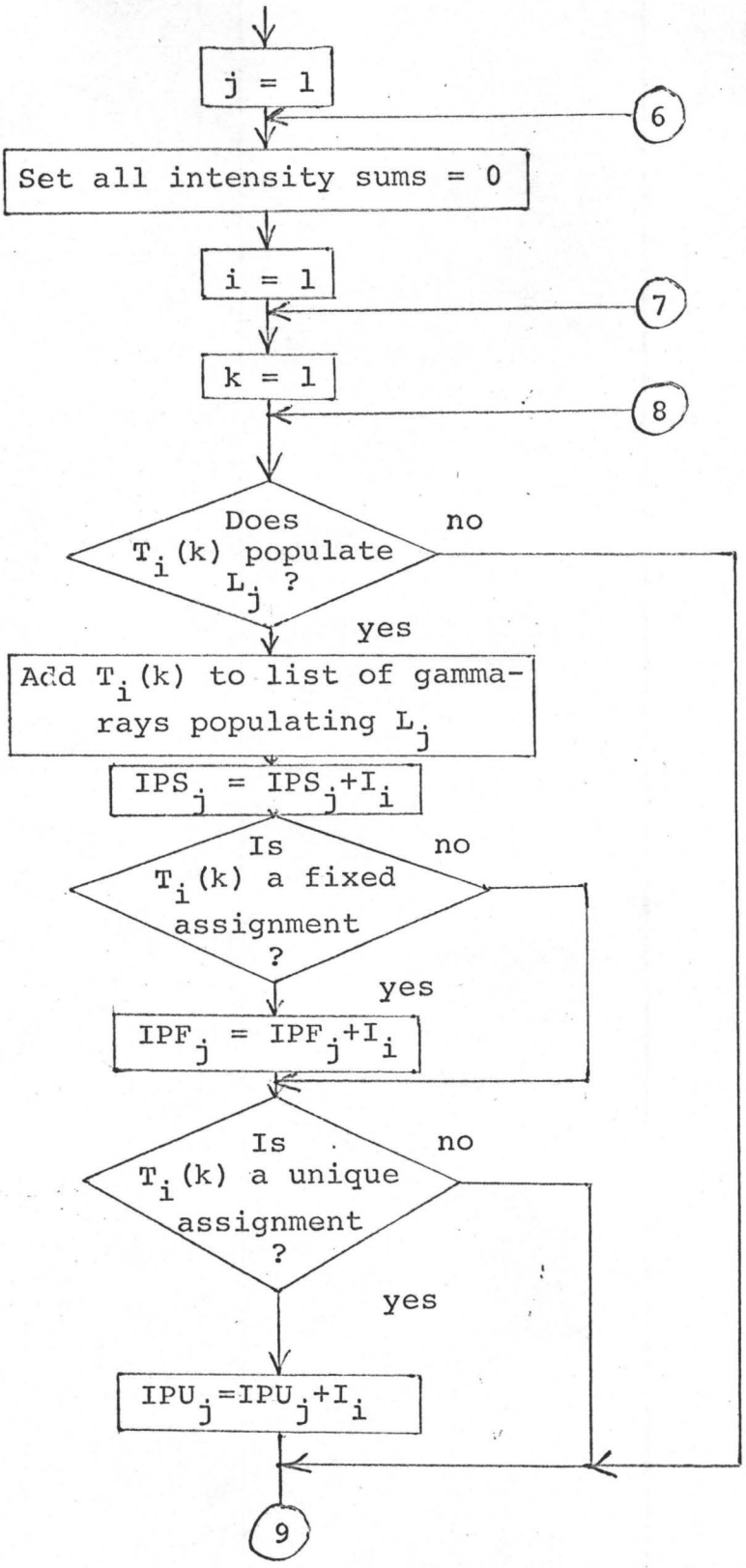
j = 1
6
Set all intensity sums = 0
i = 1
7
k = 1
8
Does $T_i(k)$ populate L_j ?
no
yes
Add $T_i(k)$ to list of gamma-rays populating L_j
$IPS_j = IPS_j + I_i$
Is $T_i(k)$ a fixed assignment ?
no
yes
$IPF_j = IPF_j + I_i$
Is $T_i(k)$ a unique assignment ?
no
yes
$IPU_j = IPU_j + I_i$
9

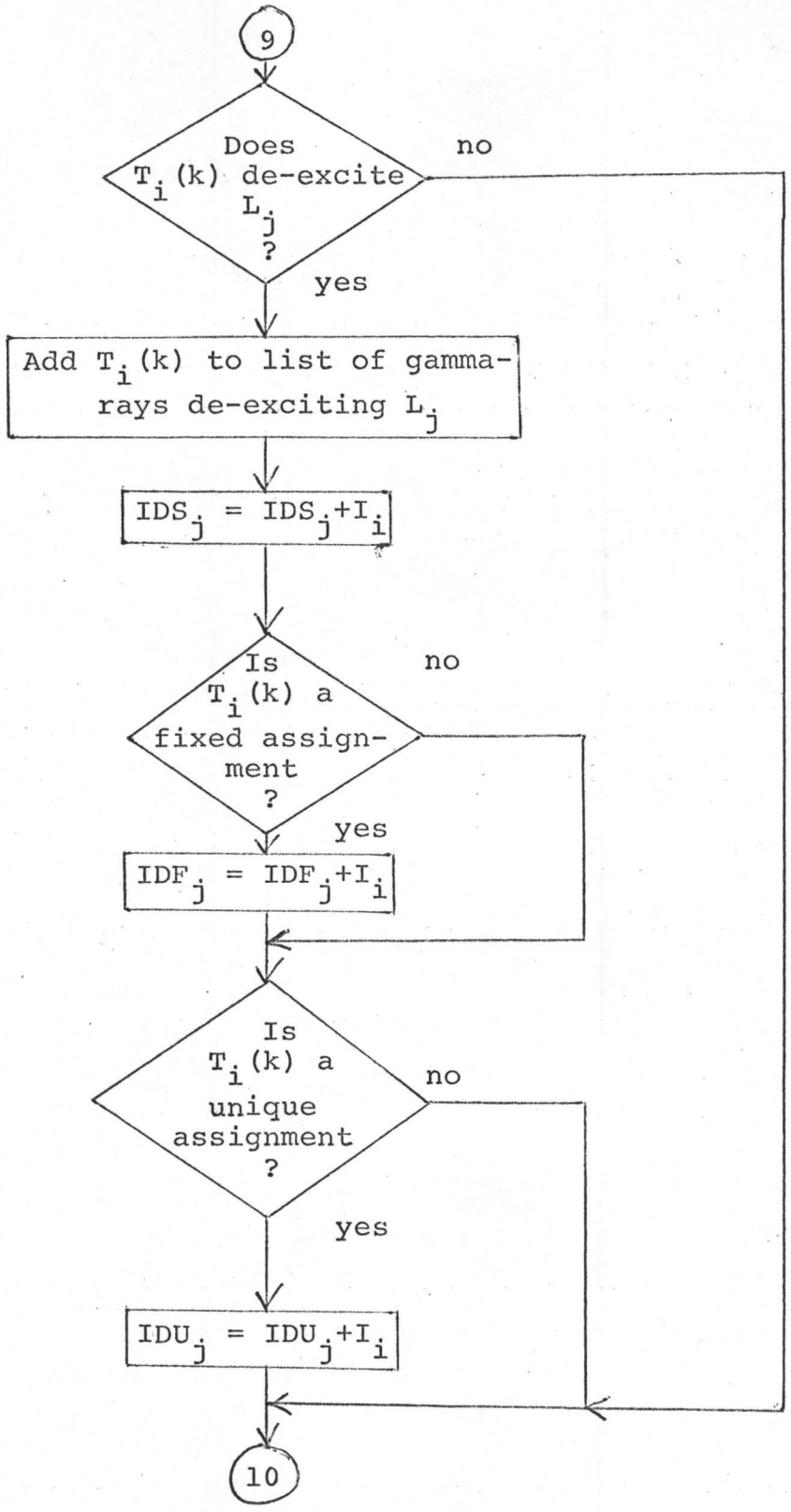
9
Does $T_i(k)$ de-excite L_j ?
no
yes
Add $T_i(k)$ to list of gamma-rays de-exciting L_j
$IDS_j = IDS_j + I_i$
Is $T_i(k)$ a fixed assign-ment ?
no
yes
$IDF_j = IDF_j + I_i$
Is $T_i(k)$ a unique assignment ?
no
yes
$IDU_j = IDU_j + I_i$
10

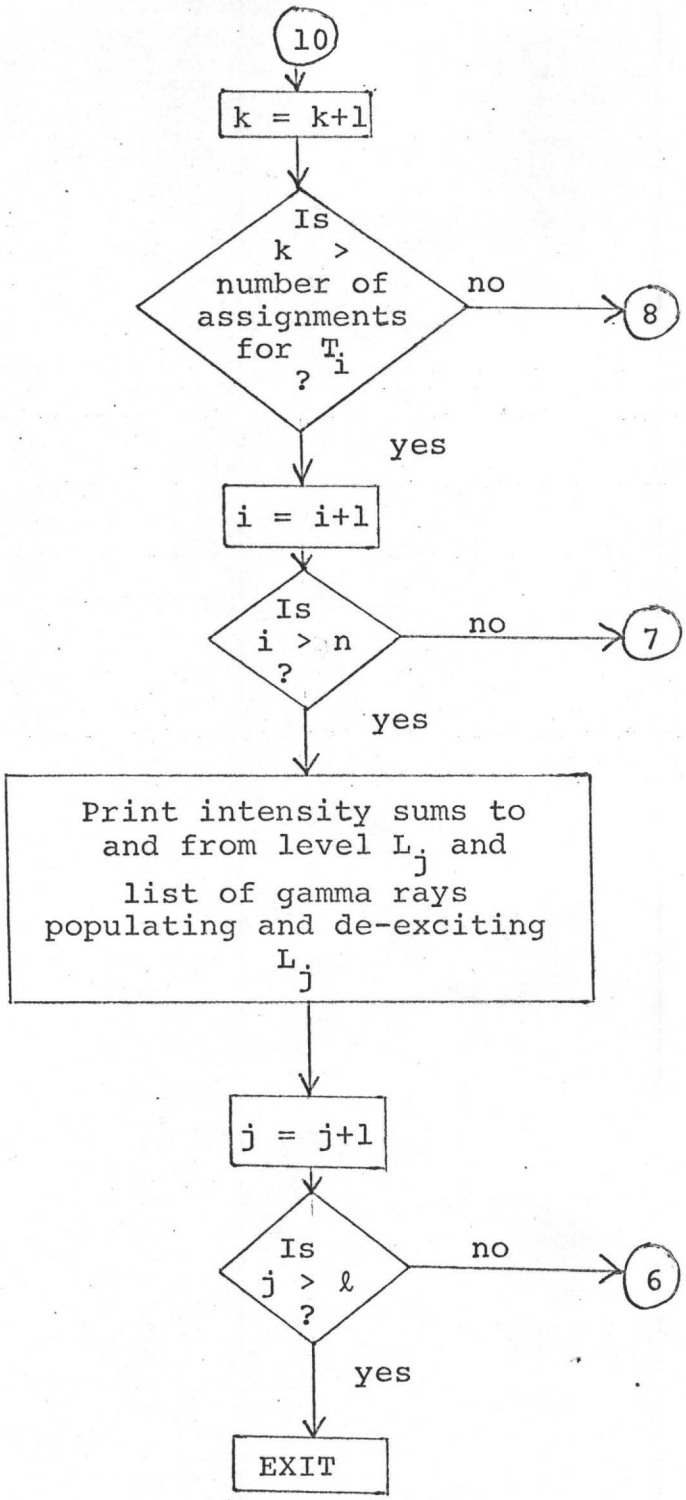
10
k = k+1
Is k > number of assignments for T_i ?
no
8
yes
i = i+1
Is i > n ?
no
7
yes
Print intensity sums to and from level L_j and list of gamma rays populating and de-exciting L_j
j = j+1
Is j > ℓ ?
no
6
yes
EXIT